Structural investigations on heme-interacting proteins.

Thesis

in partial fulfillment of the requirements for the degree of

“Doctor rerum naturalium” (Dr. rer. nat.)

submitted to the Council of the Faculty of Biological Sciences

at Friedrich Schiller University of Jena

by M.Sc. Biotechnology Amit Kumar

born on 21.02.1991 in Moradabad, Uttar Pradesh, India

Strukturelle Untersuchungen an Häm-bindenden Proteinen.

Dissertation

zur Erlangung des akademischen Grades

„Doctor rerum naturalium“ (Dr. rer. nat.)

vorgelegt dem Rat der Fakultät für Biowissenschaften

der Friedrich-Schiller-Universität Jena

Von M.Sc. Biotechnologie Amit Kumar

Geboren am 21.02.1991 in Moradabad, Uttar Pradesh, Indien

Gutachter / Reviewers:

1. Prof. Dr. Stefan H. Heinemann
Institute of Biochemistry and Biophysics, Friedrich Schiller University, Jena, Germany

2. Dr. Helmut Pospiech
Leibniz Institute on Aging – Fritz Lipmann Institute (FLI), Jena, Germany

3. Prof. Dr. Roberto Fattorussa
Department of Biological and Pharmaceutical Environmental Sciences and Technologies, University Degli Studi Della Campania Luigi Vanvitelli, Caserta, Italy

Tag der öffentlichen Verteidigung / Date of the public disputation: 17.12.2019

Dedicated

To my mentor Dr. Manish K. Thakur.

For encouraging me to pursue Ph.D. studies and being a motivator

To Dr. Ramadurai Ramachandran.

For being my continues support during my Ph.D. research and encouragement

To my family and friends

To science and humanity

Contents

List of abbreviations.....

Summary..... ..... **A**

Zusammenfassung ..... **C**

1 Introduction.....**1**

1.1 Heme..... 1

1.2 Heme homeostasis..... 2

1.2.1 Heme biosynthesis and transport 2

1.2.2 Heme catabolism and iron recycling..... 4

1.3 Regulatory Role of Heme in Biological Processes 7

1.3.1 Intrinsically disordered proteins/protein regions (IDPs/IDPRs) regulated by heme 9

1.3.2 Structured globular proteins regulated by heme..... 13

1.4 Scope of work and publication summary 15

1.4.1 Publication 1 16

1.4.2 Publication 2 18

1.4.3 Publication 3 and 4 20

2 Publications..... **23**

2.1 Heme interaction of the intrinsically disordered N-terminal peptide segment of human cystathionine-β-synthase..... 23

2.2 NMR experiments on the transient interaction of the intrinsically disordered N-terminal peptide of cystathionine-β-synthase with heme..... 42

2.3 Structural insights into heme binding to IL-36α proinflammatory cytokine 63

2.4 ^{1}H, ^{13}C, and ^{15}N resonance assignments of the cytokine interleukin-36β isoform-2..... 102

3 Further results.....**110**

3.1 HRMs investigations of IL-36β and IL-36γ.....110

3.1.1 Protein expression and purification of recombinant IL-36β and IL-36γ.....110

3.1.2 Circular Dichroism (CD) spectroscopy of IL-36β and IL-36γ..... 111

3.1.3 NMR solution structure of the IL-36β protein..... 112

3.1.4 UV/Visible spectroscopy of heme with IL-36β and IL-36γ 113

3.1.5 Resonance Raman spectroscopy of IL-36β-heme complex 114

3.1.6 NMR spectroscopy of IL-36β and IL-36γ protein (wild type and mutant proteins) with heme 115

3.1.7 IL-36β interaction with heme 115

3.1.8 IL-36γ interaction with heme 118

4 Discussion 121

4.1 N-terminus of the intrinsically disordered region (IDPR) of human cystathionine-β-synthase (CBS) (Publication 1) 121

4.1.1 Production of CBS (1-40 amino acids) protein 121

4.1.2 Heme-$_{GB1}$CBS(1-40) interaction studies 122

4.2 Development of a NMR pulse to study intrinsically disordered protein (IDP)-heme interaction (Publication 2) 124

4.3 Interleukin-36α (IL-36α) and its interaction with heme (Publication 3) 127

4.3.1 NMR spectroscopy of IL-36α-heme interaction 127

4.3.2 Docking of IL-36α structure on its cognate receptor 128

4.3.3 Negative regulation of IL-36α-mediated signal transduction 128

4.4 Interaction of heme with interleukin-36β (IL-36β) and interleukin-36γ (IL-36γ) (Publication 4 & further results) 129

4.4.1 Secondary structure elements in IL-36β and IL-36γ 130

4.4.2 NMR solution structure of the IL-36β protein 130

4.4.3 Heme interaction study of IL-36β and IL-36γ using NMR spectroscopy 131

5 Future Prospects 134

5.1 Human cystathionine-β-synthase (CBS) interaction with heme 134

5.2 Development of a NMR pulse sequence to map intrinsically disordered protein (IDP)-heme interactions 134

5.3 The Interleukin-36 family cytokine interaction with heme 134

5.4 Development of heme sensors 135

5.5 Heme induced polyreactivity in antibodies 135

6 Conclusion 136

7 References.....i

8 Declaration of honour.....xvi

9 Acknowledgement.....xvii

List of abbreviations

A° - Angstrom

ALA – 5-aminolevulinic acid

ALAS - Aminolevulinic acid synthase

bZip – Basic leucine zipper

BOXes - Bilirubin oxidation products

Z-BOX A - *Z*-2-(4-methyl-5-oxo-3-vinyl-1,5-dihydro-2H-pyrrol-2-ylidene)acetamide

Z-BOX B - *Z*-2-(3-methyl-5-oxo-4-vinyl-1,5-dihydro-2H-pyrrol-2-ylidene)acetamide

CP – Cysteine proline

CBS - cystathionine-β-synthase

IL-36 – Interleukin-36

H_2S – Hydrogen sulfide

JAK2 – Janus kinase 2

PPIX – Protoporphyrin IX

SEC – Size exclusion chromatography

HRM – Heme regulatory motif

FePPIX – Iron protoporphyrin IX

GaPPIX – Gallium protoporphyrin IX

NMR – Nuclear magnetic resonance

ROS – Reactive oxygen species

RMSD – root mean square deviation

HMOX – Heme oxygenase

CD – Circular dichroism

BOXes - Bilirubin oxidation end products

CO - Carbon monoxide

NO – Nitrous oxide

DMSO - Dimethylsulfoxide

DTT - 1,4-Dithiothreitol

E. coli - *Escherichia coli*

IRE – Iron responsive gene

EPR – Electron plasmon resonanace

HSQC – Heteronuclear single quantum correlation

NOESY – Nuclear Overhauser effect spectroscopy

IDP – Intrinsically disordered protein

IDPR – Intrinsically disordered protein regions

CAPITO – CD analysis and plotting tool

BeStSel - Beta Structure Selection

SPR – Surface plasmon resonance

PRE – Paramagnetic relaxation enhancement

Summary

Heme is a widely known cofactor molecule in many enzymes like hemoglobin, cytochromes and myoglobins. It is attached to these proteins covalently and classifies them as hemoproteins. In the last decade a growing number of reports on the regulatory role of heme in various molecular and cellular processes uncovered the signaling role of heme. Here, heme binds transiently or with low affinity to variety of proteins and regulates their function. Inspite of the number of reports on its regulatory role, they are poorly defined at structural level. Heme binds to these proteins through special amino acids called heme regulatory motifs (HRMs) such as cysteine-proline (CP), histidine and tyrosine. Studies conducted on CBS and the IL-36 cytokine family members during this project validated the heme-peptide knowledge at protein level.

Cystathionine β-synthase (CBS) is a key enzyme in the sulfur metabolism and responsible for first step of the transulfuration pathway. Dysregulation of this enzyme causes homocystinuria which leads to serious pathological conditions like neural tube defects, osteoporosis, Alzheimer's disease. CBS has a canonical heme binding site where heme binds as a cofactor along with pyridoxal-5-phosphate (PLP) and S-adenosyl-L-methionine (Adomet) and is responsible for enzyme activity. The intrinsically disordered N-terminus, a 40 amino acids peptide segment of CBS, contains a CP motif along with histidine in its vicinity which binds to heme transiently. This N-terminal segment was fused with the streptococcal protein GB1 to produce a stable CBS protein for studies. NMR along with other biophysical studies conducted on this peptide segment unravels for the first time a second heme binding site where heme binds transiently to $C_{15}P_{16}$ /H_{22} in a hexacoordinated manner and suggests a conformational change upon heme binding. Enzymatic assays done on this protein along with its mutants suggest heme binding to the N-terminal peptide segment is responsible for approximately 30% of the CBS protein activity. In addition, the data also suggests the advantages of employing the fusion protein GB1 in heme binding studies.

During the study of this N-terminal CBS peptide, which is an intrinsically disordered protein (IDPs), a new NMR pulse sequence was developed to map the heme-IDP interaction. This new HCBCACON NMR experiment was as helpful as the classical [^{1}H,^{15}N]-HSQC experiment because it allows to detect the effect of heme on side chains of a protein whilethe latter detects the effect of heme on the protein backbone. The HCBCACON experiment imparts the information either detecting ^{13}CO, called carbon detection or detecting ^{1}H$^{\alpha}$, called proton detection. Apart from detecting a range of transient interactions, this experiment can be done at physiological temperature (37 °C) and in addition delivers proline residues information which is especially crucial when studying heme interactions with a CP motif.

IL-36α is another protein used to show the translation of heme-peptide study knowledge to the protein level. IL-36α is a proinflammatory cytokine which control the expression of other cytokines (IL-6, IL-8), chemokines and antibacterial peptides. Recently it has been characterized to be involved in psoriasis, rheumatoid arthritis and with latest intervention during pregnancy. Detailed analysis using various biophysical methods suggested the existence of two heme-binding sites located on it while analysis on the atomic level performed using NMR spectroscopy revealed the structural details. NMR studies performed on full length and truncated IL-36α shows no major structural changes upon N-terminal pro-peptide truncation and that the heme binds at two sites in a penta-coordinated fashion. In addition, the NMR results also explains the reason for the necessity of N-terminal processing for a full activation at structural level. Biological tests performed on IL-36α along with other two member of this cytokine family, IL-36β and IL-36γ, on fibroblast-like synoviocyte (FLS) cells from rheumatoid arthritis (RA) patients showed the heme binding to these proteins hindered the regulation of IL-36 mediated signaling. These biological studies on IL-36β and IL-36γ along with surface plasmon resonance (SPR) data prompted us to further investigate the different heme-binding motifs involved in the IL-36 cytokine family. The initial solution NMR structure of IL-36β was determined to gain insight at structural level while site-directed mutagenesis studies coupled with spectroscopic techniques were employed to uncover the involved HRMs. The sequence similarity of IL-36β with IL-36γ and the pre-established X-ray structure of IL-36γ helped us to unravel the possible HRMs involved in IL-36γ protein. Overall, all three members of the IL-36 family display a typical β-trefoil fold and suggest two heme-binding sites or heme-regulatory motifs on each molecule. In vitro studies performed on IL-36β and IL-36γ reveal the involvement of new amino acids in heme-binding beside the canonical HRMs. These newly identified amino acids add new information to the growing class of HRMs and also add novel aspects in determination of yet unidentified transiently heme-regulated proteins.

Zusammenfassung

Häm ist ein bekannter Kofaktor in vielen enzymatischen Verbindungen wie z.B. Hämoglobin, Cytochrome und Myoglobine. Die kovalente Verknüpfung des Häms klassifiziert die Proteine dabei als Hämoproteine. In der letzten Dekade zeigten Studien, dass Häm bedeutende regulatorische Rollen in zellulären Funktionen und molekularen Signalisierungsprozessen zukommt. Hierbei bindet Häm an seine Zielproteine oft nur in transienter Form oder mit geringer Affinität und beeinflusst damit deren Funktion. Trotz der steigenden Anzahl von Berichten über die regulatorischen Eigenschaften von Häm, liegen die strukturellen Grundlagen dieser Abläufe noch im Dunkeln. Häm bindet an seine Zielproteine mittels spezieller Aminosäuren oder Aminosäuresequenzen, sogenannten Häm-regulatorischen Motiven (HRM), wie z.B. Cystein-Prolin (CP), Histidine und Tyrosin. Im Rahmen dieses Projektes konnten dazu Erkenntnisse, die im Vorfeld an Häm-Peptid-Komplexen gewonnen wurden, durch Studien an Cystathionine-β-Synthase und Proteinen der Interleukin-36 Zytokinfamilie auf Proteinebene validiert werden.

Cystathionine-β-synthase (CBS) stellt ein Schlüsselenzym im Schwefel-Metabolismus dar und ist für den ersten Schritt des Transsulfurationsmechanismus verantwortlich. Fehlregulation dieses Enzyms führen zu Homocystinurie, die mit schweren Krankheitsverläufen, wie neuronalen Tubendefekten, Osteoporose, Alzheimer, verbunden ist. CBS besitzt eine Bindungsregion in der Häm als Kofaktorzusammen mit Pyridoxal-5-phosphat (PLP) and S-adenosyl-L-Methionin (Adomet) bindet und für die Enzymfunktion verantwortlich ist. Der intrinsisch-ungeordnete N-terminale Bereich von CBS, bestehend aus 40 Aminosäuren, beinhaltet ein CP-Motiv und Histidine in dessen Umgebung. Dieses N-terminale Segment wurde zu Studienzwecken mit dem Streptokokken-Protein GB1 fusioniert. NMR-Spektroskopie zusammen mit anderen biophysikalischen Studien an diesem Segment zeigte erstmals, dass Häm transient an C15P16 /H22 in einer hexakoordinierten Form bindet und damit eine konformationelle Änderung hervorruft. Mittels enzymatischer Assays an diesem Protein und seinen Mutanten konnte zudem nachgewiesen werden, dass dieses N-terminale Segment für ca. 30% der Proteinaktivität von CBS verantwortlich ist. Zusätzlich konnte gezeigt werden, dass der GB1-Fusionsprotein-Ansatz Vorteile bei der Untersuchung der Häm-Bindung an intrinsisch-ungeordnete Peptide (IDP) aufweist. Während der Untersuchungen an diesem N-terminalen CBS-Peptid konnte damit eine neue NMR-Pulssequenz zur Kartierung der Häm-IDP-Wechselwirkung etabliert werden. Dieses neue HCBCACON NMR-Experiment erweist sich ähnlich vorteilhaft wie ein klassisches [1H,15N]-HSQC-Experiment. Jedoch erlaubt es, statt wie im letzteren nur Proteinrückgratinformationen, die evtl. noch durch chemischen Austausch nachteilig maskiert sind, direkt Informationen von interagierenden nicht-austauschenden Seitenkettenatomen zu detektieren. Das HCBCACON-Experiment erlaubt dabei, Informationen entweder über ^{13}CO-Detektion oder, in einer anderen Variante, über ^{1}H$^{\alpha}$-

Detektion zu erlangen und führt auch bei physiologischen Temperaturen (37 °C) zu auswertbaren Spektren. Nicht zuletzt liefert das Experiment Daten über Prolin-Reste, was besonders bei Studien von CP-Motiven von Vorteil ist.

IL-36α ist ein weiteres Untersuchungsobjekt, das aus Translation der Erkenntnisse von Häm-Peptid-Studien auf die Proteinebene hervorging. IL-36α stellt ein proinflammatorisches Zytokin dar, das die Expression anderer Zytokine (z.B. IL-6, IL-8), Chemokine und antibakterieller Peptide kontrolliert. In jüngerer Zeit wurde nachgewiesen, dass es mit Krankheitbildern wie Psoriasis und Rheumatoider Arthritis assoziiert ist und auch in der Immunantwort bei Schwangerschaftsprozessen eine Rolle spielt. Die Analyse mittels verschiedener biophysikalischer Methoden deutete auf die Existenz von zwei Hämbindungsstellen in IL-36α hin, deren strukturelle Details per NMR-Spektroskopie auf atomarer Ebener definiert werden konnten. Mittels NMR-Studien konnte gezeigt werden, dass das Volllängenprotein und seine N-terminal verkürzte biologisch aktive Form keine strukturellen Änderungen aufweist. Es konnte auch gezeigt werden, dass die Propeptid-Prozessierung unumgänglich ist, um die strukturellen Voraussetzungen für die Bildung eines aktiven Komplexes zu erreichen. In Bezug auf die Hämbindung wurde deutlich, dass diese an zwei Bindungstellen in Pentakoordination erfolgt. Biologische Tests mit IL-36α und den weiteren zwei Mitgliedern dieser Zytokin-Familie, IL-36β and IL-36γ, an Fibroblast-artigen Synoviocyten-Zellen von Patienten mit rheumatoider Arthritis zeigten, dass Hämbindung die Regulierung der IL-36-bedingten Signalkaskade beeinflusst. Diese und Oberflächen-Plasmon-Resonanz-Daten von IL-36β and IL-36γ stimulierten die Ausweitung unsere Untersuchungen auf andere Häm-Bindungsmotive in der IL-36-Zytokinfamilie. Die Bestimmung der initialen NMR-Lösungsstruktur von IL-36β erlaubte Einblicke auf struktureller Ebene, während via Mutagenese und spektroskopischer Untersuchungen die beteiligten HRM bestimmt werden konnten.Die Sequenzähnlichkeiten von IL-36β mit IL-36γ und die bekannte Röntgenstruktur von IL-36γ unterstützten dabei die Nutzung des Mutagenese/NMR-Ansatzes zur Aufdeckung der HRM in IL-36γ. Im Ergebnis weisen alle drei Mitglieder der IL-36-Familie eine typische β-Trefoil-Faltung mit zwei Hämbindungsstellen auf. Während in IL-36α ein CP-Motiv an der Hämbindung beteiligt ist, bindet Häm bei IL-36β und IL-36γ mittels nicht-kanonischer Wechselwirkungen. Die dabei neu identifizierten Häm-bindenden Aminosäuren erweitern die Klasse der Häm-regulatorischen Motive und eröffnen neue Perspektiven für die Aufdeckung weiterer transient hämbindender Proteine mit bioregulatorischen Funktionen.

1 Introduction

1.1 Heme

Heme (iron protoporphyrin IX) is a ubiquitous molecule present in aerobic and anerobic life from primitive prokaryotes to complex eukaryotes [1]–[3]. The term heme is derived from Greek *haima*, meaning blood. It is an organic molecule with complex structure containing four pyrrole rings, connected to a central iron atom. The four modified and connected pyrrole rings (tetrapyrrole structure) are also called porphyrin. Ultimately with the addition of iron, the system is named iron protoporphyrin-IX or heme. Usually heme is the generic term for both, the ferrous (Fe^{2+}) and the ferric (Fe^{3+}) form of iron in protoporphyrin-IX. However, strictly applied, ferrous protoporphyrin-IX refers to heme and ferric protoporphyrin-IX is represented by the term hemin. In the following studies we have used hemin but refer to it as heme [4]. Different types of heme exist in nature, e.g. heme A, heme B, heme C, heme O. They all are derivatives of each other with a basic porphyrin ring and differ by variations in the sidechains. The most abundant heme present in nature is heme B, and it is involved in many biological activities. The protoporphyrin-IX of heme B consist of four methyl groups, two vinyl groups, and two propionate side chains as well as an iron atom covalently connected to four nitrogen atoms of the respective pyrrole rings (Figure 1). This arrangement is leaving the heme iron with two free axial coordination sites for potential ligand interactions, e.g. proteins and small gas molecules (NO, CO, O_2) (Fig. 1).

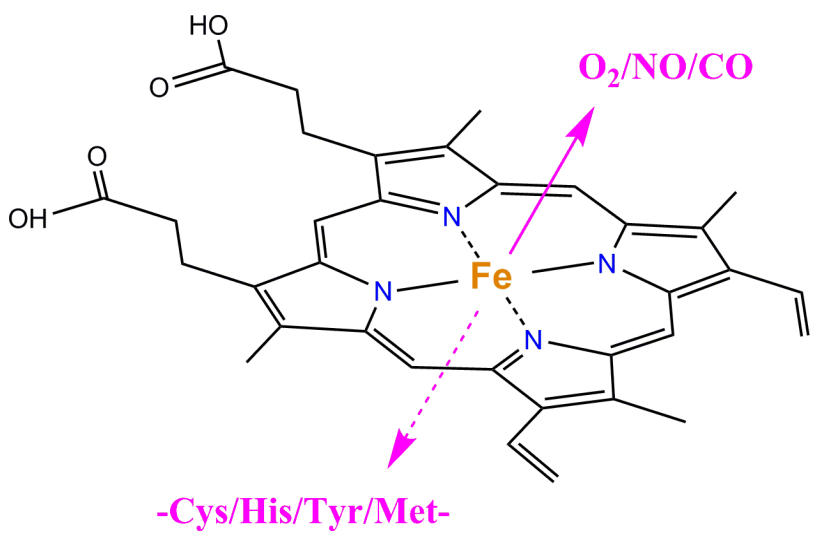

Figure 1: Structure of heme B and two co-ordination sites (arrow) shown for interaction (adapted from [4])

1.2 Heme homeostasis

1.2.1 Heme biosynthesis and transport

Cellular homeostasis of heme is governed by iron and heme transport. The toxic nature of free heme required evolution of stringent regulation in biosynthesis and degradation in all the aerobic and anaerobic life with well-developed pathways. Liver and bone marrow are the two major heme production factories in the human body. Liver produces 15% of heme, while the bone marrow makes 80% of heme in a human body [4], [5]. The heme biosynthesis pathway in mammals involves eight enzymes where three of them are present in mitochondria, while the other five are acting in the cytoplasm. This pathway can be divided in four process steps starting with formation of the pyrrole ring, converting to tetrapyrrole ring, followed by modification in side chain of the tetrapyrrole ring to form protoporphyrin IX, and ultimately the incorporation of iron ion (Figure 2).

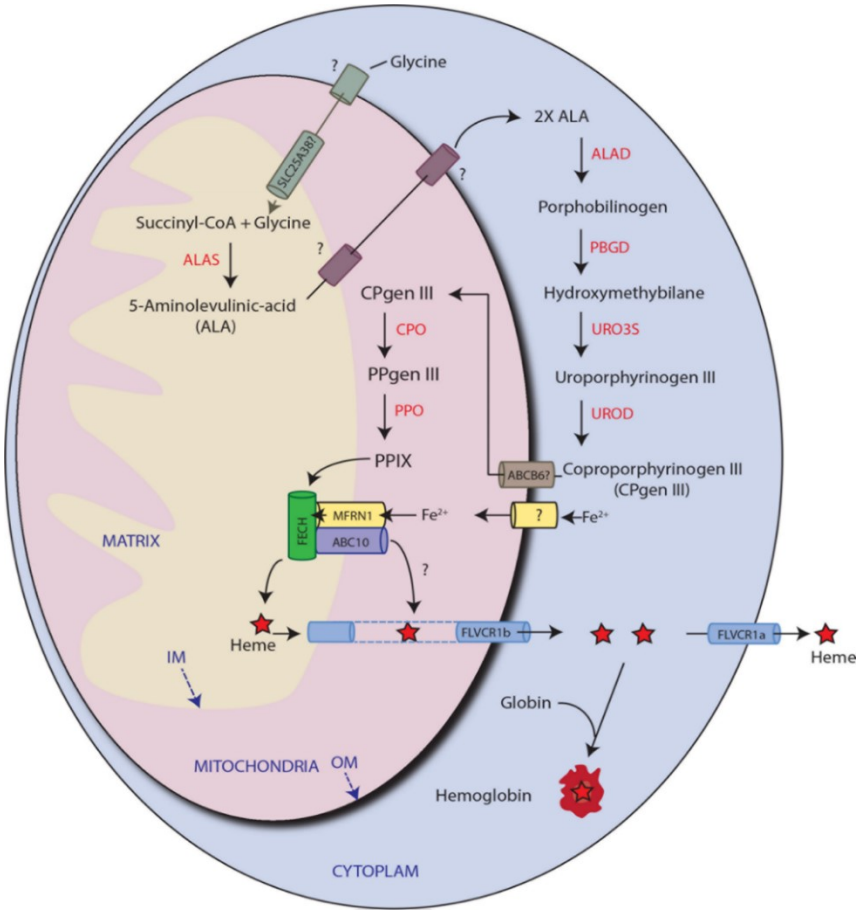

Figure 2: Biosynthesis of heme (adapted from [6]

The first step of heme biosynthesis starts in mitochondria of erythrocytes where the pyrrole formation begins with the substrates succinyl coenzyme A and glycine in presence of aminolevulinic acid synthase (ALAS), the first rate-limiting enzyme in the pathway to form 5-aminolevulinic acid as precursor for pyrrole ring formation. ALAS has two isozyme proteins, ALAS1 and ALAS2. ALAS1, also known as hepatic ALAS (ALAS-H), is ubiquitously expressed in all tissues, while the ALAS2 or ALAS-E are specifically expressed in erythrocytes cells and are located on chromosomes 3p21.1, Xp11.21, respectively. Both isozymes are regulated by heme. However, only ALAS1 expression and degradation is regulated by feedback mechanism of heme iron, while ALAS2 expression remains unaffected by heme. This negative feedback mechanism of heme is one of the processes for intracellular heme homeostasis in all cells except for red blood cells (RBCs).

The transportation of synthesized ALA in to the cytosol is currently not fully understood. In 2013, Bayeva et al. showed that knockdown of ABCB10 (inner mitochondrial membrane) in cardiac myoblasts resulted in reduced heme levels and suggests that ABCB10 might be involved in export of ALA in the cytoplasm. However, other studies in yeast on the glycine transporter Hem25 knockdown showed a decreased level of glycine and, thus, ALA. Sequence homology of Hem25 (approx. 30% amino acid similarity) suggests a similarity with the SLC25A38 gene in *Homo sapiens* and slc25a38a, slc25a38b in *Danio rerio* [7], which is further strengthened by two other studies [8], [9]. After reaching the cytosol two molecules of ALA condense to form monopyrrole porphobilinogen, catalyzed by aminolevulinate dehydratase (ALAD) [10].

The second step is the formation of uroporphyrinogen III. Starting with polymerization of four PBG molecules in presence of porphobilinogen deaminase (PBGD), an initial unstable tetrapyrrole, hydroxymethylbilane (HMB) is formed. HMB is further converted to uroporphyrinogen III by the enzyme uroporphyrinogen III synthase (URO3S) [10].

In the third step, modification of side chains (acetate and propionate chains) occurs in uroporphyrinogen III to form coproporphyrinogen III (CPG III) involving the uroporphyrinogen carboxylase enzyme. This phase is followed by CPG III conversion to protoporphyrinogen IX during localization inside the mitochondria mediated by a peripheral- type benzodiazepine receptor [11], [12] using coproporphyrinogen oxidase enzyme (CPO) located in the mitochondrial intermembrane space [10]. After import into the mitochondria, oxidation of protoporphyrinogen IX is catalyzed by the enzyme protoporphyrinogen oxidase (PPO) to form protoporphyrin IX (PPIX).

The final step is the incorporation of iron (Fe^{2+}) into protoporphyrin IX inside the inner mitochondrial membrane by an enzyme ferrochelatase (FECH) [10]. FECH is produced inside the cytosol with a leader peptide targeted to mitochondria. Subsequently, cleaving

the leader peptide produces mature FECH [13]. FECH is the second rate-limiting enzyme after ALAS in the heme biosynthesis pathway. The FECH expression level is intracellularly controlled by iron concentration through the iron-sulfur cluster located on the C-terminus [14]. Iron localization inside the mitochondria is governed by the transport protein transferrin, to which 95% of iron (Fe^{3+}) in plasma is bound. Subsequently, it delivers a major part to erythroid progenitor cells by binding to its transferrin receptor 1 (TFR 1) located on the bone marrow to form new RBCs. An estimated 80% of TFR 1 is present on the erythroid marrow of the human [15]. Per day, our body utilizes 25 mg of iron to form 200 billion new RBCs [16]. The iron (Fe^{3+})-transferrin complex is internalized through endocytosis and acidified to separate iron from transferrin. STEAP3 (six-transmembrane epithelial antigen of the prostate 3) reduces the Fe^{3+} to Fe^{2+} for the transport in the cytosol through the DMT 1 transporter [17], [18].

The final step is the transport of reduced iron (Fe^{2+}) from the cytosol in to the inner mitochondria. First, iron crosses the outer mitochondrial membrane through unknown mechanism. However, a recent study suggests iron could bind to low molecular weight ligands in the cytosol and freely diffuse into semi-permeable outer mitochondrial membrane [16]. Second, iron crosses the inner mitochondrial membrane through two known iron transporters, mitoferrin 1 (on erythroid cells, non-erythroid cells)[19] and mitoferrin 2 (on non-erythroid cells), located in the inner mitochondrial membrane, to finally reach the destination enzyme FECH where iron is inserted into the PPIX [20]. To facilitate the efficacy of iron insertion in PPIX, mitoferrin 1 forms the complex with FECH and ABCB10 proteins [21], [22] and ultimately forms iron-PPIX (heme). ABCB10 increases the stability of mitoferrin 1 and thus increases the iron transport into the mitochondria [23].

Synthesized heme can be exported out of the cell through the recently identified heme receptor/transporter system of Feline Leukemia virus subgroup C (FLvcr1). There are two isoforms of FLvcr1 present in mitochondria FLvcr1a and FLvcr1b, located on plasma membrane and mitochondrial membrane, respectively [24]. In vitro and in vivo studies supported the role of FLvcr1b in heme export, where suppression of FLvcr1b leads to mitochondrial heme accumulation and termination of erythroid differentiation, while overexpression leads to intracellular heme accumulation and erythroid differentiation [24], [25]. Multiple studies suggest their role in heme homeostasis but further research has to be done to uncover the role of these transporters.

1.2.2 Heme catabolism and iron recycling

Hemoglobin is the major source of heme, found in RBCs. Accumulation of heme in senescent RBCs and other sources is cytotoxic and must be cleared from cell. The average life of RBCs is around 120 days and after that it undergoes degradation in macrophages of liver, spleen and bone marrow, collectively called the “reticuloendothelial system” (RES)

[26]. This RES is tightly regulated in mammals and constitutes not only for heme degradation but also for biosynthesis by recycling iron. Our body daily recycles 25 mg of iron through the RES from RBCs and almost all of it returns back to the bone marrow for erythropoiesis to make a new batch of RBCs. Only 1-2 mg of iron is absorbed each day through enterocytes in the intestine in form of heme or non heme iron [16]. Heme homeostasis is regulated by two systems: 1) Scavenger proteins present in plasma like *e.g.* hemopexin bind excess free heme and transport it to macrophages of the RES [27], [28]. 2) Intracellular enzymatic degradation of heme through heme oxygenases (HMOXs), the most important enzymes responsible for the metabolism of heme, is located in the endoplasmic reticulum of the RES (Figure 3).

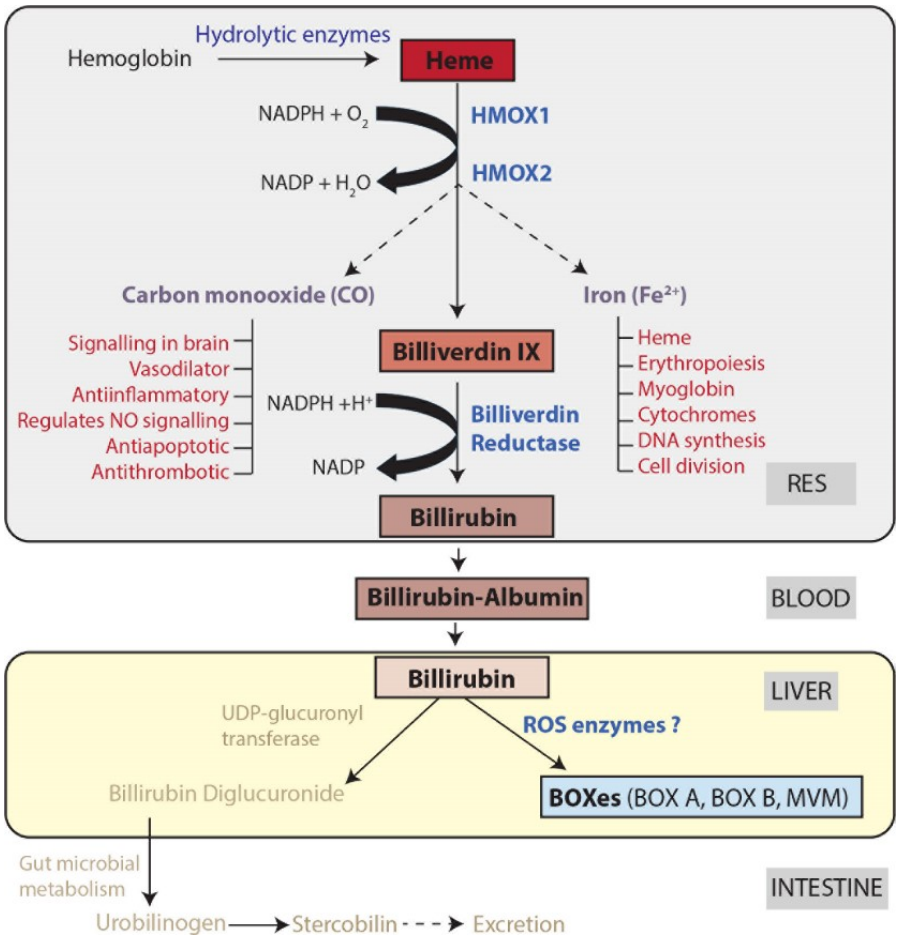

Figure 3: Schematic representation of heme degradation by HMOX enzymes

During hemolysis, free heme and hemoglobin leak into the blood circulatory system and are immediately bound to scavenger proteins like hemopexin and haptoglobin, respectively, with moderate affinity before being transferred to RES. In addition, as RBCs complete their fate, they also travel ultimately to macrophages of RES. Here, RBCs are internalized in macrophages by phagosomes, while the heme-hemopexin or hemoglobin-

haptoglobin complex is imported via the scavenger receptors LRP (or CD91) and CD163, respectively [29]–[33]. The RBC phagosome fuses with the lysosome and forms the phagolysosome, this process called as erythrophagocytosis. The phagolysosome contains hydrolytic enzymes, which degrade the hemoglobin in RBC to globin and release the heme [16]. This liberated heme undergoes the same fate as other internalized heme moieties. All the heme is exported out to the cytosol through the HRG1 transporter located on the lysosome/ endosome membrane and this HRG1 has been seen upregulated during erythrophagocytosis on the phagolysosome/endosome membrane [34]. It has been suggested that some portion of the heme is catabolized inside the phagolysosomes and released iron exported in cytosol through DMT1 homologue (NRAMP1) located on the phagolysosome membrane [35]–[37]. Heme export in the cytosol induces expression of HMOXs enzymes located on endoplasmic reticulum [38]. Higher expression of HMOXs enzymes makes macrophages more resistant to heme toxicity than endothelial cells [39]. This enzyme has two isoforms, HMOX1 and HMOX2, which perform the same function to break the heme into the first-order degradation products iron (Fe^{2+}), CO and biliverdin IX (Fig. 3). HMOX1 is an inducible enzyme present ubiquitously in almost all cells and tissues. It is highly upregulated upon heme exposure or other oxidative stress conditions and prevents the oxidative stress in cells [40]. Expression of HMOX1 is directly linked to another enzyme, namely ferritin (iron sequestering protein), which is upregulated in parallel with HMOX1 and neutralizes the pro-oxidant effect of iron by binding to it [41]. HMOX2 is a non-inducible isoform and majorly expressed in brain and testis and has been shown to protect against ischemic injuries [42], [43]. In 2005, Kemp [44] showed that HMOX2 serves as a potential oxygen sensor for a calcium-sensitive potassium (BK) channels.

Enzymatic degradation of heme can be divided into a few important steps. First heme is degraded to hydrophilic biliverdin IX via HMOXs enzymes involving NADPH, O_2 and cytochrome reductase to reduce the ferric iron from heme. This degradation also produces iron (Fe^{2+}), which is stored in ferritin (used for erythropoiesis) and CO, recently recognized as a signaling molecule (Fig. 3) [45]. Biliverdin IX is further degraded to the second-order products, hydrophobic bilirubin via biliverdin reductase using NADPH and H^+.

For further degradation an export out of the cells into the blood takes place where bilirubin binds albumin and forms a bilirubin-albumin complex. This complex reaches the liver where UDP-glucuronyl transferase, using two UDP-glucuronic acid molecules, converts it to hydrophilic bilirubin diglucuronide (BDU). Either it is excreted through the kidney or it is further degraded in the intestine by gut bacteria to urobilinogen (UB), stercobilin (SB), and eventually excreted through urine and faces [46], [47]. In 2017 [48] it was shown that bilirubin, biliverdin, and bilirubin ditaurate promote the secondary structure formation in intrinsically disordered antibacterial peptides, and bilirubin also inhibited the heme regulated inhibitor protein (HRI) [49].

Bilirubin oxidation products (BOXes) are the third or end degradation products of bilirubin. As the name suggests, these are produced after the oxidation of bilirubin during subarachnoid hemorrhage (SAH) conditions. SAH is the bleeding in the subarachnoid space and characterized by free radical formation in cerebrospinal fluid, acting upon biliverdin, bilirubin, and heme to form BOXes. In 2002, Clark et al. [50] found BOXes in cerebrospinal fluid of subarachnoid hemorrhage patients with vasospasm while searching for vasoactive compounds. Later these isomers were classified as BOX A and BOX B [51]. Recently a new Z-BOX C was identified in human bile samples which has potential relevance for liver dysfunction and cerebral vasospasms [52]. These BOXes are vasoactive in nature as shown by *in vitro* and *in vivo* models of rat brain vessels [50], [53]. They are also involved in inhibition of human Slo1 BK channels and suggested to play a role in smooth muscle regulation [54]. Because of their light-sensitive nature and low abundance, they are not well explored, but a potential therapeutic potential is proposed [55].

1.3 Regulatory Role of Heme in Biological Processes

Heme as a ubiquitous molecule in all aerobic life has been extensively studied as a prosthetic group, bound to hemoproteins. The most common roles are in oxygen binding with hemoglobin and myoglobin, in electron transport in the respiratory chain through cytochromes, or being a structural part of various proteins. In all those processes, heme is tightly bound to the proteins and called a cofactor or prosthetic group. But in the last decade heme has emerged out as a versatile signaling or regulatory molecule for many receptors, transcription factors and proteins (Table 1), thus regulating many biological processes ranging from cellular growth and survival to fundamental cellular processes like protein synthesis or localization [4]. Heme binds to these proteins through combinations of special amino acids sequences, called heme binding motifs (HBM) or heme regulatory motifs (HRM) such as the cysteine-proline (CP) motif. The term HRM was first used by Lathrop in 1993 [56], when they first identified a CP motif in the aminolevulinic acid synthase (ALAS) protein and found that heme can regulate the ALAS protein (details mentioned in section 1.3.1). CP is the most prominent motif known to date and binds directly to the central iron atom of heme. Over the last decades some other amino acid based motifs were identified which can directly bind to the heme iron like tyrosine and histidine. Heme as versatile molecule can also interact with other amino acids in proteins via its porphyrin ring or propionate side chains through electrostatic and hydrogen bonding [57], [58].

Table 1: Publications reporting transiently heme binding proteins

S.No.	Protein	Heme Binding Area	HBM/HRM	Predicted IDP content	References
1.	5-Aminolevulinate synthase 1 (ALAS1)	IDPRs	CP		[56], [59]
2.	Bach1	IDPRs	CP	50	[60]–[62]
3.	Heme oxygenase 2 (HMOX2)	Structured	CP ?	25	[63]
4.	Iron regulatory protein 2 (IRP2)		CP, H	20	[64], [65]
5.	Slo1 (BK)	IDPR	CxxCH	22	[66]
6.	Potassium channel (Kv1.4)	IDPR	CxxHx18H	26	[67]
7.	ATP-sensitive potassium channel (K_{ATP})	IDPR	CxxHx16H		[68]
8.	Rev-ErbA	IDPR	H	57	[69]
9.	Circadian clock Period 2 (PER2)	IDPR	CP ?	53	[70], [71]
10.	Microprocessor complex subunit DGCR8	IDPR	C, W	48	[72]
11.	Tumor suppressor P53	IDPR	CP	49	[73]
12.	α-Synuclein	IDP	?	52	[74]
13.	Amyloid beta peptide-40 (Aβ-40)		H	44	[75]–[77]
14.	Staniocalcinin1	Structured	CS	27	[78]
15.	Staniocalcinin2	Structured	CP	37	[79]
16.	Cystathionine-β-synthase (CBS)	IDPR	CP, H	32	[80]
17.	Janus Kinase 2 (JAK2)	Structured	CP ?	15	[81]
18.	Src kinase	Structured	CP ?	27	[82]
19.	Interleukin-36α	Structured	CP, Y	11	our lab
20.	Interleukin-36β	Structured	Q, N	14	our lab
21.	Interleukin-36γ	Structured	Q, N	23	our lab

'?' shows either contradictory publications or heme binds to protein but binding site not confirmed

The identified heme-regulated proteins can be classified into two categories based upon their structural characteristics: 1) Intrinsically disordered proteins or unstructured proteins

(IDPs) or Intrinsically disordered protein regions (IDPRs), which do not possess any secondary or tertiary structure; 2) Globular or structured proteins. Heme may bind moderately or interact transiently (in μM range) with both classes of proteins and thus regulate their functions.

1.3.1 Intrinsically disordered proteins/protein regions (IDPs/IDPRs) regulated by heme

Identification of IDPs in the last two decades challenged our understanding of the structure-function paradigm of proteins. It was believed that function of a protein is always linked to their structure and that an active enzyme/protein always has a secondary and tertiary structure. This led to theories like the 'lock and key' model. A large and growing number of reports on IDPs opened a new, 'unstructural' biology concept, where these unstructured proteins are carrying out a large variety of biological functions. According to bioinformatics predictions, these disorders are very common and can be found across all species. However, their occurrence is significantly higher in eukaryotes than in prokaryotes and there exists a strong correlation with regulatory and signaling functions [83], [84]. Approximately 10-35% of prokaryotic proteins and 15-45% of eukaryotic proteins contain a significant number of these disordered regions with a minimum length of 30 amino acids. IDPs have less hydrophobic residues and are enriched in polar and charged residues [85], [86]. IDPs can form different conformations because of their considerable flexibility and can interact with a large variety of partners, which explains why they are highly abundant in important cellular processes like transcription or signaling [87]–[89]. As reported in literature IDPs/ IDPRs can undergo a disorder to order transition upon binding to their ligands (other proteins or small molecules) (Figure 4) [80], [90].

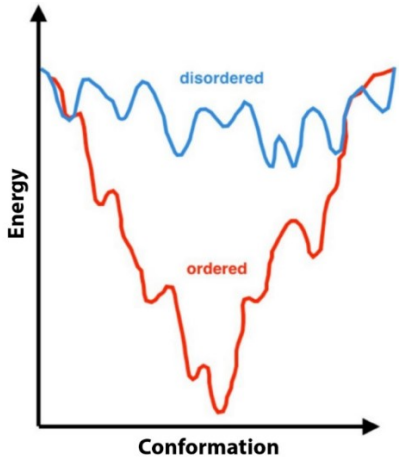

Figure 4: Schematic representation of the free-energy landscapes of ordered and disordered proteins. Structured or ordered proteins (red) have a free-energy landscape with a well-defined global minimum conformation, which can bind small molecules with lower affinities (modified from [91])

It is interesting to note that most of the identified transiently heme binding proteins either are complete IDPs or contain IDPRs in the protein sequence and that many heme binding processes take place in these disordered regions (Table 1). Here are few examples:

ALAS, aminolevulinic acid synthase, as introduced earlier, is the first rate-limiting enzyme in heme biosynthesis and has two forms: ALAS1 and ALAS2. Only the ALAS1 isoform displays a N-terminal disordered region (IDPR). ALAS1 is known to be negatively feedback regulated by heme and maintains intracellular heme levels. This negative feedback regulation is known at transcription, translation and localization of protein levels. Several studies have been done to find how heme destabilizes the ALAS1 mRNA. It is known that heme destabilizes the ALAS1 mRNA, which leads to repressed translation of ALAS1 protein, but the exact mechanism is not fully understood (Figure 5) [92], [93]. The ALAS1 precursor protein contains three cysteine-proline (CP1, CP2 and CP3) motifs heme regulatory motifs (HRM) and two of them are located in N-terminal disordered leader peptide sequences, which is responsible for ALAS1 protein localization in mitochondria. While the CP3 motif is located on the N terminus of mature ALAS1 protein and this mature protein is formed after the proteolytic cleavage of leader sequence (removing CP1, CP2 motif). Previously only CP1, CP2 were suggested to be involved in ALAS1 protein mitochondrial localization but recent studies showed the role of CP3 motif in maturation of ALAS1 protein in mitochondrial matrix [56], [94]. Maturation of ALAS1 proteins requires the proteolytic cleavage of leader peptide sequence in mitochondrial matrix. This proteolytic cleavage has been done by two ATP dependent proteases, Lon peptidase1 (LONP1) [95] and ClipX-like protein (ClpXp) [96], identified in mitochondrial matrix. Recently Kubota [97] suggested two theories for ALAS1 degradation mediating heme. The first one is that ClpXP identifies and modifies ALAS1 in the presence of heme and directly degrades ALAS1 protein. A second theory iss that LONP1 and ClpXP together mediate the ALAS1 protein degradation in the presence of heme, which was supported by Tian [98]. According to this theory, during increased intracellular heme concentration, heme binds to the CP3 motif of ALAS1 protein and induces oxidative modification of ALAS1. Modified ALAS1 protein is recognized by ClpXP protein and forms a complex with LONP1 protein triggering LONP1-mediated degradation of the ALAS1 protein. Their study suggests the possible role of both the proteases but the exact mechanism of heme-mediated degradation of ALAS1 is still not clear. CP motifs are conserved in different species of ALAS1 and ALAS2 but heme-mediated repression is only observed for ALAS1, suggesting a different mechanism of inhibition for ALAS2 in erythroid precursor cells.

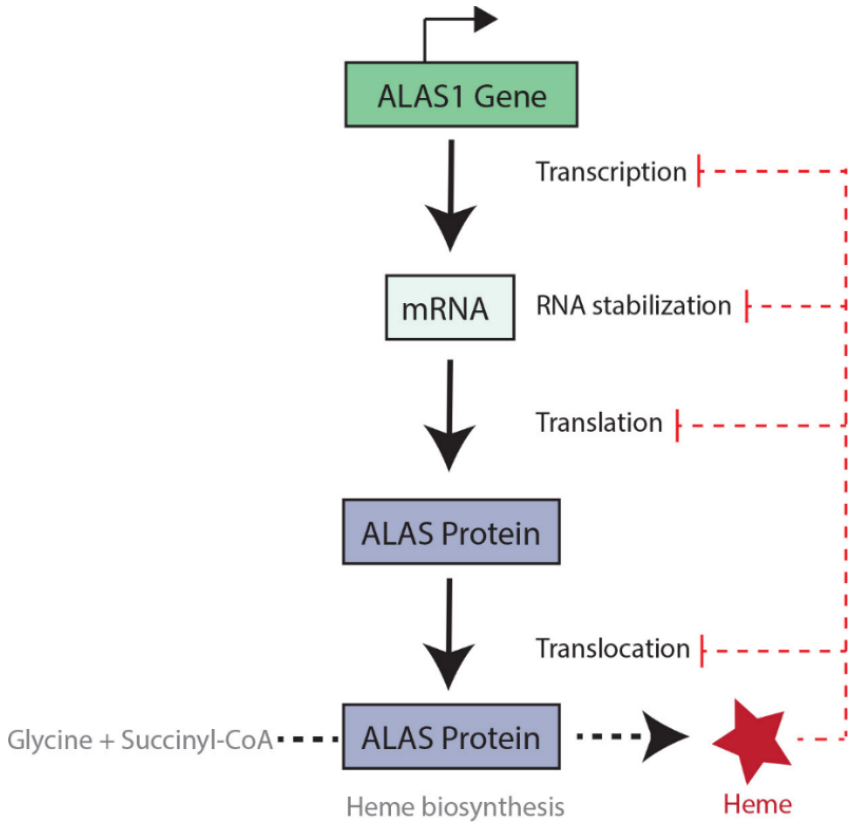

Figure 5: Heme regulates ALAS1 at different levels (Negative feedback regulation)

Similarly, **Bach1,** a transcriptional repressor which binds to the heme transiently, downregulates the expression of heme homeostasis regulating genes like HMOX1 and globin genes [61], [99]. Interestingly, Bach1 is the first identified mammalian transcription factor that binds to heme in a disordered region of the protein (IDPRs) [60]. Bach1 is a big protein (739 amino acids) containing multiple domains. There are six CP motifs located on Bach1 at different regions but only 4 or 5 CP motifs might bind to heme (Figure 6) and govern its inhibition activity upon heme binding [60], [100]. Three of these CP motifs are located proximal to the bZip (basic leucine zipper) domain and act as a DNA-binding domain. It has been suggested CP3, CP4, CP5 and CP6 motifs bind to heme and are involved in DNA binding to genes containing Maf recognition elements like HMOX1 or globin genes [101]. At low heme concentration, Bach1 and small musculoaponeurotic fibrosarcoma proteins (Maf) form a heterodimeric complex. This Bach-Maf heterodimer binds to the Maf recognition element (MARE) present on the enhancer region of HMOX1 and on the globin gene and repress their expression. Upon increased heme concentration inside the cell, the Bach1-Maf complex is detached from MARE by activators (Nrf1,2,3) and dissociates. Nrf1,2,3 activators bind small Maf proteins and form a complex which binds to the MARE region and express the genes (Figure 7). Only CP3 and CP4 are involved in the nuclear export of the Bach1 protein via the nuclear exporter Crm1 [102], [103]. In 2007 Zenke et al. showed that heme can regulate Bach1 degradation through a complex proteasome degradation

mechanism via the HOIL-1 ubiquitination protein in different cells and suggested that CP3, CP4, CP5 are involved in this process. (Figure 6). Interestingly, HOIL-1 also is involved in the degradation mechanism of another heme homeostasis protein, iron regulatory protein 2 (IRP2). Heme also binds to this protein via the CP and H motif and promotes its degradation [64].

Bach2 also binds to heme and regulates the differentiation of B-cells and T-cells [104]. Both isoforms are members of the basic leucine zipper (bZip) family of transcription factors and evolved to regulate sophisticated functions in higher eukaryotes [105].

Recent studies also indicate the regulation of ion channels by reversible heme binding such as potassium channel Kv1.4 where its intracellular disordered part binds to heme and modulates the action potential across membrane in cells [67]. Heme also induces polyreactivity in immunoglobulins (IgG, IgM, IgE etc.) which leads to a range of new antigen binding specificities [106]. In addition, in 2015 Gupta et al. demonstrated that heme induced reactivity of monoclonal IgG1 can neutralize the Japanese Encephalitis viruses. There are plenty of further examples where heme binds to IDPs/ IDPRs regions mostly with cysteine and histidine residues as shown in Table 2 across the different biological processes.

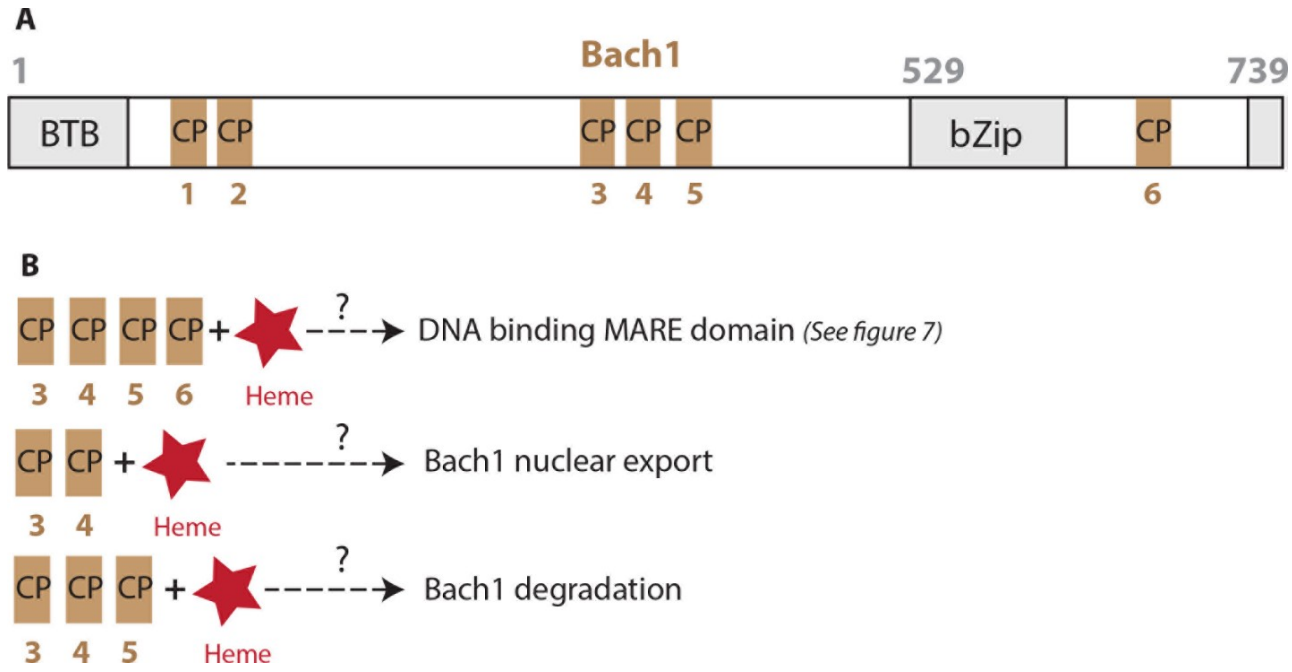

Figure 6: A) Domain structure of human Bach1 protein showing six CP motif, B) Different CP motifs involved in heme mediated regulation of Bach1 protein

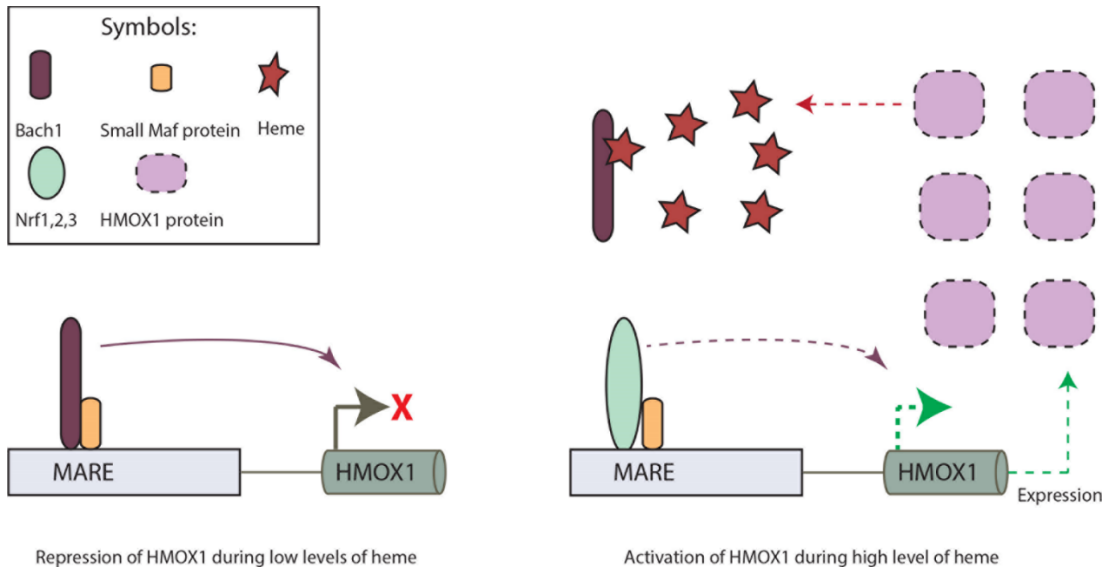

Figure 7: Diagrammatic representation showing Bach1 regulation in presence and absence of heme at transcriptional level

1.3.2 Structured globular proteins regulated by heme

Unlike IDPs, not many structured proteins that can transiently bind to heme and regulate their function are identified today. There are two structured non-receptor protein kinases known to bind heme that contain CP motifs at least. The most recent examples in this category are the interleukin-36 cytokine family members, which were identified in our lab (**Publication 3, Publication 4, Further results**).

Src kinase is the first identified oncogene and one of the extensively studied kinases [107]–[109]. It is a member of the non-receptor tyrosine kinase family. Members of this family phosphorylate at tyrosine amino acids and play a critical role in downstream signal transduction pathways of many important processes like proliferation, cell division, adhesion, survival in normal and cancer cells [110]–[121]. Usually, Src is maintained in an inactive state and only activated transiently during normal cell events like cell division or induced during abnormal events like mutation or human cancers. This kinase contains two tyrosine residues (Tyr419 and Tyr530) and maintains its activity through phosphorylation at these sites. Phosphorylation at Tyr419 is responsible for full activation of Src, while phosphorylation at Tyr530 has an inhibitory effect, which leads to an inactive conformation [110], [122]. It has been shown that heme can enhance the phosphorylation at Tyr530 and eventually inactivate this enzyme, while showing no effects on Tyr419. This heme-induced immediate phosphorylation leads to the inactive conformation of this enzyme, which has been confirmed by a protease (trypsin) based digestion sensitivity assay [82]. Interestingly, it has 3 CP motifs, which constitute potential heme interaction sites. Two of these HRMs present proximal of its tyrosine phosphorylation sites (Figure 8). However, it is not fully

understood on which site heme binds and further studies need to be performed to identify the specific heme-binding site.

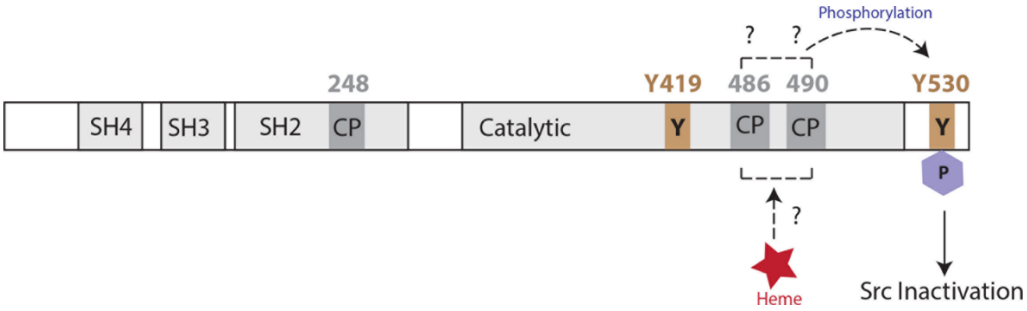

Figure 8: Domain structure of Src kinase with CP motif location and possible heme interaction sites (adapted from[4])

Janus kinase 2 (JAK2) is another structured kinase, which was identified together with the Src kinase for heme mediated phosphorylation. It is also a non-receptor tyrosine kinase, member of the Janus kinase family and plays a pivotal role in signal transduction of various processes like cell growth, histone modification, erythropoiesis, development of a cell and cytokine receptors signaling (innate and adaptive immunity). Its central role in numerous biological processes makes it a crucial connecting point for many hematopoietic diseases like myelofibrosis and myeloproliferative disorders [123]–[133]. JAK2 is a big protein of 1132 amino acids in length and contains one pseudo kinase (545-809) and one kinase (849-1124) domain. Experiments performed on the kinase (808-1132) domain reveal that heme promotes the phosphorylation at Tyr1007/1008. Phosphorylation at Tyr1007 is responsible for Jak2 activation [82]. But unlike Src kinase, where heme phosphorylates immediately, JNK2 phosphorylation takes about 12-30 hours. Like Src kinase, JAK2 also undergoes heme induced conformational changes for phosphorylation which are required for continued kinase activity [82]. This kinase domain contains one heme binding CP motif located at 1094 near to Tyr1007 (Figure 9). The binding site for heme is not specifically understood and further research needs to be done.

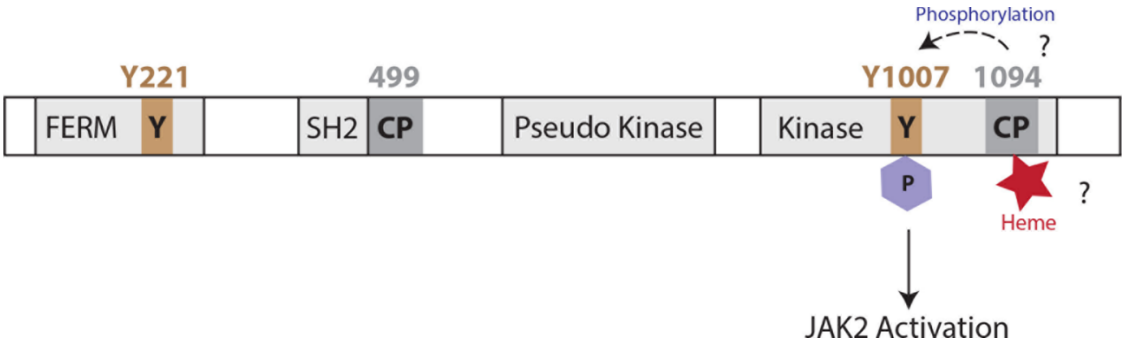

Figure 9: Domain structure of JAK2 kinase with CP motif location and possible heme interaction site (adapted from[4])

1.4 Scope of work and publication summary

This work is part of the DFG-funded researcher group (FOR 1738), a collaborative effort addressing four major subjects related to HHDPs: 1) Clinics; 2) Physiology and Cell Biology; 3) Chemistry and Biphotonics; 4) Biochemistry and Structural Biology, aiming to extend the knowledge about the functions of heme and its degradation products in biological systems. In the first funding period, heme-peptide interactions were structurally studied. Peptides were selected from a combinatorial peptide library for identifying HRMs or favorable heme-binding sequences in the lab of our collaborator and project partner Professor Diana Imhof (University of Bonn). Subsequently, the following biophysical techniques were used to characterize the heme interaction:

1) UV/ Visible spectroscopy was applied to monitor the characteristic Soret band (around 398 nm) shift of heme upon peptide binding. Heme upon binding with peptide shifts this Soret band either to 370 nm or 420 nm depending on the formation of penta or hexa co-ordination with the peptide, respectively.

2) Resonance Raman spectroscopy was proposed in collaboration with the laboratory of Dr. Ute Neugebauer (IPHT, Jena/University Hospital Jena). The resonance Raman spectra of free heme gives characteristic five bands in the spectral region between 1300 and 1700 cm^{-1}. Those five bands are obtained upon excitation of porphyrin ring in heme at 413 nm wavelength and named as ν_4, ν_3, ν_2, ν_{11}, ν_{10}. Addition of peptide or protein to heme leads to major shifts in ν_3, ν_2 bands, which shows the heme iron co-ordination pattern in the heme-peptide complex and proves their interaction.

3) Finally, NMR spectroscopy was employed to uncover the structure of peptides and to map the heme-peptide interactions. Diamagnetic gallium protoporphyrin IX was used as the substitute for paramagnetic heme (iron protoporphyrin IX), to avoid the paramagnetic effect of iron heme. This paramagnetic effect may lead to large spectral widths and severe line broadening, ultimately resulting in reduced or vanishing signals in NMR spectra. 2D NMR experiments were performed to derive the structure and dynamics of peptides and peptide-heme complexes.

Based upon above analysis, three major HRMs classes containing eight subclasses (shown in Table 2) have been classified.

Table 2: HRMs classes

Number	Classes	Sub Classes
1	Cysteine based ▪ Cysteine only	Without Histidine or Tyrosine (Class I) With Histidine or Tyrosine (Class II)
	▪ Cysteine-Proline	Without Histidine or Tyrosine (Class III) With Histidine or Tyrosine (Class IV)
2	Histidine based	Without Histidine or Tyrosine (Class V) With Histidine or Tyrosine (Class VI)
3	Tyrosine based	Without Histidine or Tyrosine (Class VII) With Histidine or Tyrosine (Class VIII)

In this work – encompassing the second funding period of 'FOR 1738' – the aim was to extend the acquired knowledge to the protein level.

Surveying the literature on transient heme-protein interaction revealed that very little information is available at the structural level describing how heme binds or interacts with certain heme-interacting motifs in proteins and regulates their functions and about the affinity of this transient or reversible interactions. To further validate the knowledge obtained from the peptide studies during the first term of the HHDP project and to translate that knowledge to the protein level in the second term of this project, we developed new methods for probing protein-heme interactions, and selected new protein targets: the uncrystallizable N-terminal region of cystathionine-β-synthase (CBS) and the interleukin-36 cytokine family.

All of the molecules were biophysically characterized and subsequently studied by NMR spectroscopy to obtain structural information at the atomic level. This also included adaptation and extension of NMR experiments for the challenging tasks to characterize the transient heme interactions and to study intrinsically disordered molecules or molecular sections.

1.4.1 Publication 1

CBS is one of the critical enzymes involved in the transsulfuration pathway. CBS possess a pivotal position in sulfur metabolism at the homocysteine intersection where it determines the fate of methionine to keep or to condense it to nontoxic cysteine (Figure 9) [134], [135]. CBS catalyzes the first reaction in the transsulfuration pathway to convert the toxic homocysteine to cystathionine utilizing serine in the process. In the second step, cystathionine gamma lyase (CGL) converts the cystathionine to cysteine. Both the enzymes also produce hydrogen sulfide (H_2S), a recently recognized gasotransmitter and vasodilator in humans [136], [137]. This produced cysteine is used intracellularly for the protein synthesis and the production of a cellular antioxidant called glutathione [138]. Abnormality

in the CBS gene causes an inborn autosomal recessive inherited impaired sulfur metabolism disease homocystinuria. Homocystinuria was first reported in 1963 in mentally retarded siblings in Northern Ireland [139]. It is characterized by increased homocysteine, reduced cysteine and cystathionine concentration in plasma [140]. Elevated levels of homocysteine affect majorly four central organ systems, the ocular, skeletal, cardiovascular and central nervous system. If left untreated, homocystinuria leads to pathological conditions like neural tube defects, dislocated eye lenses, osteoporosis, connective tissue abnormalities, atherosclerosis, and Alzheimer's disease [141].

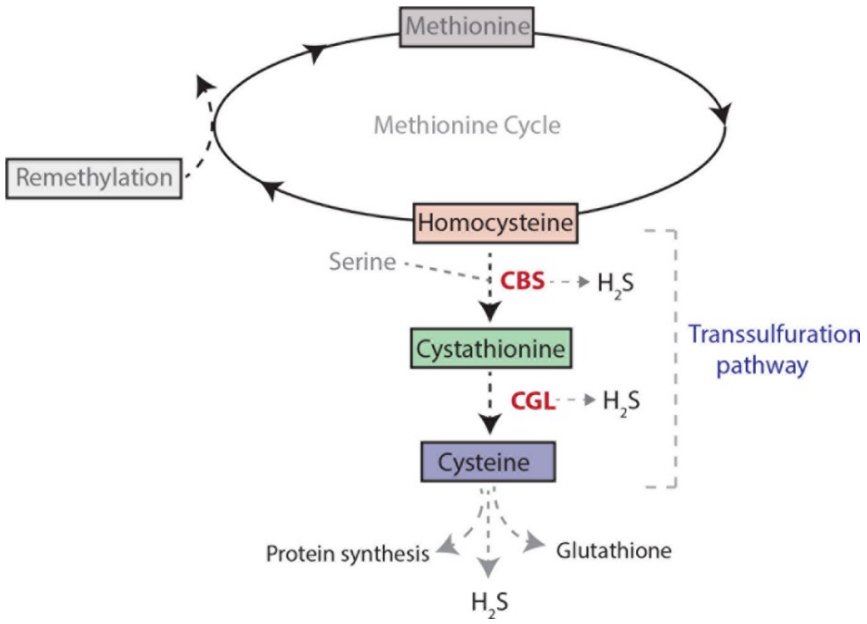

Figure 10: CBS in methionine cycle and transsulfuration pathway

CBS is a complex modular enzyme of 551 amino acids belonging to the fold type II family of the pyridoxal 5-phosphate (PLP) dependent enzymes and naturally present as homotetrameric form [134]. CBS is a unique PLP family enzyme which binds to heme and its activity is regulated by three cofactors: heme, pyridoxal 5-phosphate (PLP) and the allosteric activator S-adenosyl-L-methionine (Adomet) [135], [142]. It contains the N-terminal heme-binding domain, a central catalytic domain and a C-terminal regulatory domain. The N-terminal heme-binding domain is 70 amino acid long and contains a canonical heme binding site where heme-B binds to cysteine-52 and histidine-65 tightly in a hexa-coordinated manner [142]. The central catalytic domain binds to the cofactor PLP via a Schiff bond to the K119 residue [143]. The C-terminal regulatory domain contains two CBS domains also called as Bateman module where the allosteric activator, Adomet binds and activates the enzyme (Figure 11) [144], [145].

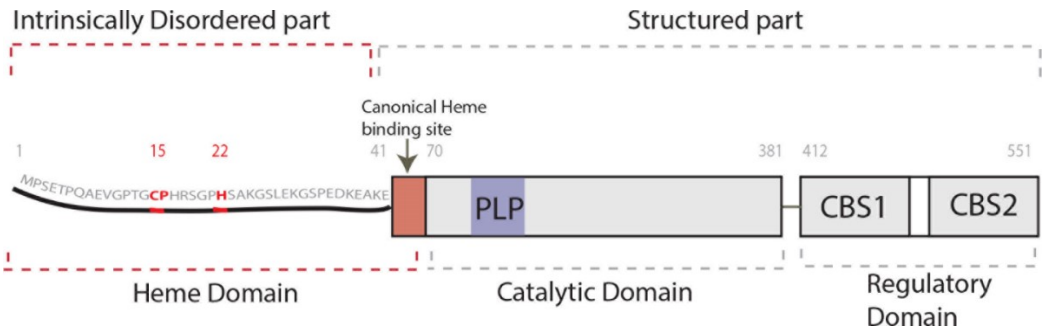

Figure 11: Domain structure of CBS showing potential heme binding site

Heme bound at position C52/H65 is suggested to be involved in redox sensing [146] and the folding of enzyme [147]. Kery et al. demonstrated that binding of heme to CBS increases the specific activity of this enzyme and suggested that heme binding can induce favorable conformational changes for PLP binding [142]. This was further confirmed by Ojha [148] where they showed that a pathogenic mutation of H65 leads to loss of heme binding affecting the catalytic activity of enzyme. In 2002, Oliveriusová conducted deletion mutagenesis studies on CBS and showed that deletion of first 1-39 residues resulted in approximately 52% of less active compared to wild-type CBS [149]. The N-terminal region of CBS is very diverse in all the species and, interestingly, X-ray structures are missing for the first 42 residues. This suggests that this molecule region to be disordered. However, this region is close to the canonical heme-binding site (C52/H65) and sequence analysis showed this region containing a CP motif with histidines (H) in its vicinity. We speculated that it could be a potential heme-binding motif because of its proximity to the canonical heme-binding motif and might be involved in enzyme activity. Additionally, sequence alignment of this protein further confirmed that the CP motif is conserved in many eukaryotic organisms. As discussed previously, CP motifs found in IDP or IDPRs can act as potential heme-binding motifs, which bind transiently and regulate the molecule function. In this context we studied this molecule as described in **Publication 1**.

1.4.2 Publication 2

The heme-protein interactions are usually studied via techniques like surface UV/Visible, surface plasmon resonance, resonance Raman and NMR spectroscopy [150], [151]. The transient nature of this heme-protein interaction makes it difficult to map it at atomic level. NMR spectroscopy has been proven a useful tool for mapping such interactions and studying specially IDPs/IDPRs.

NMR spectroscopy, a method to obtain structural information on IDPs/ IDPRs

- Considering the nature of transient interaction of heme with proteins (in the μM range), NMR is the only tool that can provide information at atomic resolution of

this interaction unlike X-ray crystallography, which can be employed for tight binding processes only.

- Homo- and hetero-nuclear multidimensional NMR experiments can deliver protein dynamics information upon heme interaction in IDPs and structured proteins while revealing the binding mode and surrounding scaffold.

- Solution-state NMR is a useful technique for structural characterization of intrinsically disordered proteins (IDPs) because X-ray crystallography does not deliver electron densities for these IDPs. The flexible nature of these IDPs or intrinsically disordered regions in proteins (IDPRs) renders them hard to crystalize, resulting in missing structural data for parts of such proteins.

During the above studies (publication 1) we found that the classical 2D [^{1}H,^{15}N]-HSQC experiment (protein finger printing spectra) has some limitations: exchange sensitivity and unability to detect all range of transient interactions. The [^{1}H,^{15}N]-HSQC experiment yields information on NH groups in a protein backbone or in other words, the effect of heme was observed at the protein backbone level. Generally, side chains are more exposed in solution than the backbone of a protein and this idea leads us to develop further NMR experimental protocols, the HCBCACON experiment for enhanced sensitivity as compared to the conventional 2D [^{1}H,^{15}N]-HSQC experiment as described in **publication 2.** Specifically, in IDPs, inter-residue $^{15}N_i{}^{13}CO_{i-1}$ chemical shift correlation spectra have a relatively higher spectral resolution as compared to intra-residue correlations [152], [153] and has been used to achieve resonance assignment. In this new experiment we were looking for the effect of heme on side chains, involving the excitation of side chain either via a coherence transfer pathway to directly detect ^{13}CO, called carbon detection, or the transfer pathway to detect $^{1}H^{\alpha}$, called proton detection (Figure 12). The HNCBCACON experiment has many advantages over the [^{1}H,^{15}N]-HSQC: it can detect ultra-transient heme interaction, studies can be done under physiological conditions in terms of temperature and pH with good signal to noise ratio. In addition, it also yields proline residue information, which is useful to monitor cysteine-proline (CP) motif interaction with heme, which was missing in conventional 2D [^{1}H,^{15}N]-HSQC experiments but can be readily seen with good signal to noise ratio.

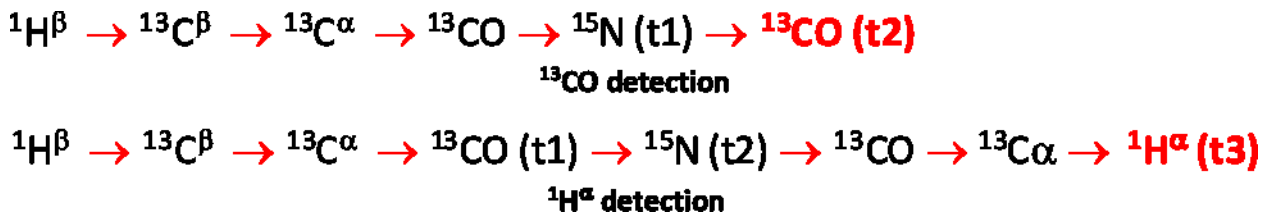

Figure 12: Transfer pathway for HCBCACON experiment

1.4.3 Publication 3 and 4

In **publication 3**, we have described our second potential heme-binding protein, interleukin-36α (IL-36α). This protein was identified during combinatorial peptide studies. IL-36α belongs to the IL-36 subfamily of the IL-1 cytokine superfamily. IL-1 is a broad cytokine family and has eleven members, IL-1α, IL-1β, IL-1Ra, IL-18, IL-33, IL-36α, IL-36β, IL-36γ, IL-36Ra, IL-37 and IL-38 [154]. This interleukin-36 subfamily was discovered more than a decade ago and has five members IL-F6, IL-F8, IL-F9, IL-F5, IL-F10, which now are known as IL-36α, IL-36β, IL-36γ, IL-36Ra (Receptor agonist) and IL-38, respectively [155], [156]. IL-36α, IL-36β, IL-36γ have pro-inflammatory activity and control the induction of other inflammatory mediators like chemokines, cytokines (IL-6, IL-8) and antimicrobial peptides [157], [158]. They all bind to the same IL36R receptor and recruit IL-1RacP (Interleukin-1 receptor associated protein), which together form a heterodimer and activate downstream NF-Kappa-B and MAP kinase pathways during pro-inflammatory response in target cells (Figure 13) [159]. IL-36α, IL-36β, IL-36γ are secretory proteins and so far no leader or signal peptide has been identified for their localization outside the cell [160]. They require proteolytic processing of their N-terminal pro-peptides for their full activation [161]. The identified neutrophil proteases are cathepsin G and elastase for IL-36α processing, again cathepsin G for IL-36β, and proteinase-3 and elastase for IL-36γ processing [162]. IL-36α processing requires truncation of the first five amino acids, while in IL-36β the first four amino acids and IL-36γ the first seventeen amino acids are removed for full activation (Figure 13). This processing can lead to an increase in IL-36 enzyme activity from 1,000-10,000 times compared to full-length proteins [161]. There is not much known about these cytokines' molecular mechanism. They are expressed in skin keratinocytes but increased expression has been seen during psoriasis condition in skin lesions [163]. Psoriasis is an autoimmune chronic disease characterized by scales and sometimes painful red patches on the skin [164]. Recently, IL-36 cytokine family members were also suggested to be involved in pregnancy complications [165].

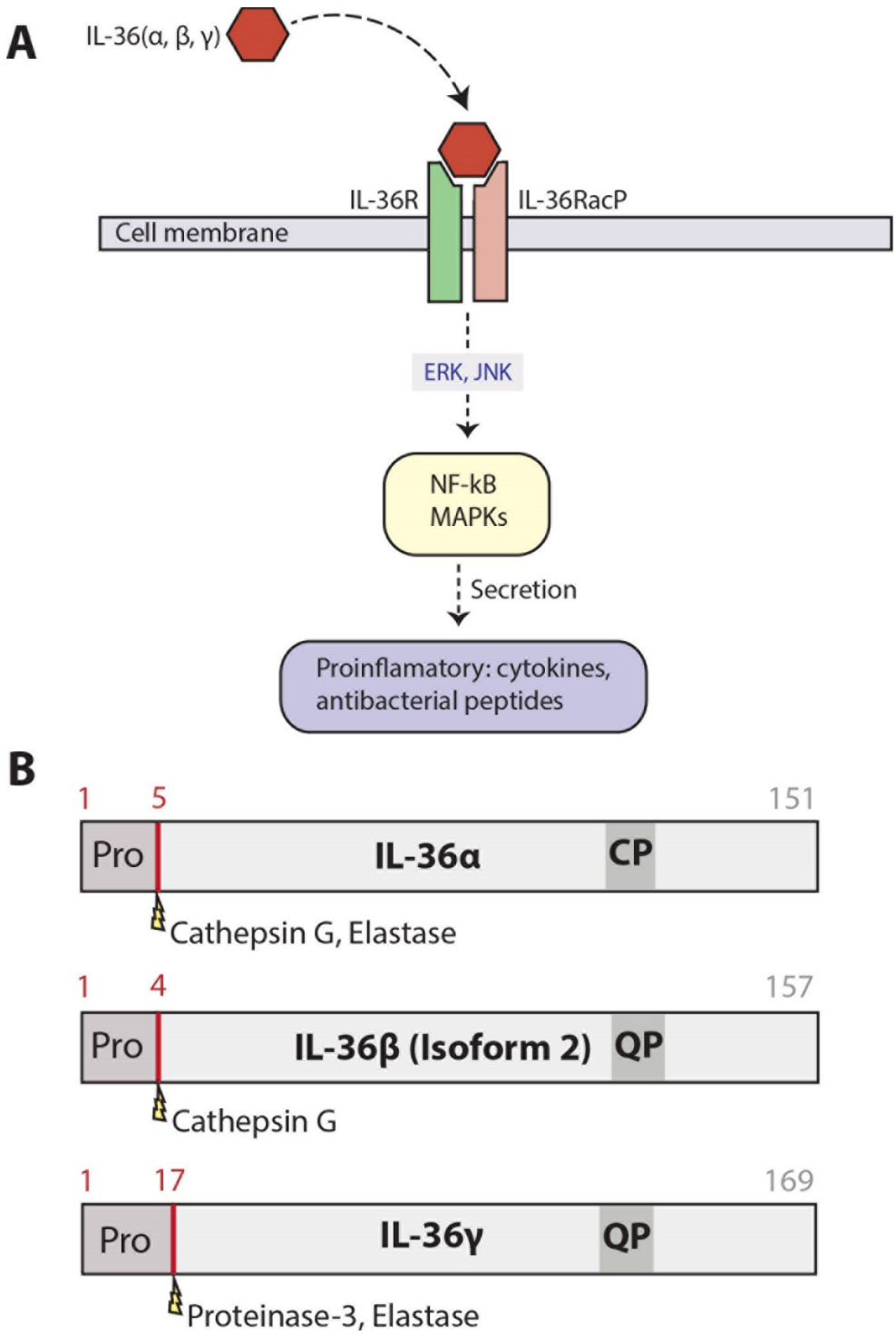

Figure 13: (A) IL-36 signaling pathway (B) Domain structure of the IL-36 family members and respective proteases responsible for truncation of the pro-peptide. Potential heme binding amino acids also highlighted.

IL-36α is a small protein of 151 amino acids and belongs to the HRM class III and IV (Table 2). The presence of a CP motif with H and Y renders it a potential heme-binding

candidate. This CP motif is also conserved in homology of several other organisms, such as mice. Multiple sequence alignment of IL-36 family members showed that the CP motif is only conserved in IL-36α and absent in IL-36β and IL-36γ. However, initial studies suggest that all three members, IL-36α, IL-36β and IL-36γ are binding to the heme. A detailed study of the IL-36α–heme interaction has been described in this paper, involving a series of biophysical techniques like UV/ Vis, Raman, SPR, NMR spectroscopy. Initial functional studies showed effects of IL-36α-heme interaction on the induction of other cytokines.

During our study we found that not only IL-36α but also IL-36β and IL-36γ can bind to heme. As mentioned above, the CP motif is only present in IL-36α, while the other two proteins have QP residues. However, they all contain H and Y residues in the vicinity. We hypothesized that heme might be interacting directly or with its propionate side chains via electrostatic interaction with other amino acids. This made us to further investigate HRMs involved in these two cytokines. We started the investigations with IL-36β because the IL-36γ structure is already available (PDB code 4IZE). In bone marrow derived dendritic cells (BMDCs) IL-36β is solely responsible for the phosphorylation of the p38MAPK activation [166], while IL-36γ activates MAPKs, JNK, ERK and p38 MAPK, as well as NF-kB and CREB transcription factors in bronchial epithelial cells [165], [167]. IL-36γ also promotes the production of interferon- γ (IFN-γ) in CD8+ T-cells and act as anti-tumor immune therapy in melanoma and lung cancer [168].

Aiming to determine the structure of IL-36β as a first step, we performed and published the chemical shift assignment of IL-36β isoform 2 (**publication 4**). Section (**further results**) shows the preliminary results of structure characterization of IL-36β using CD and NMR spectroscopy. Additionally, heme-binding studies were also performed on wild-type and mutant proteins of IL-36β and IL-36γ using UV/visible and NMR spectroscopy techniques.

2 Publications

2.1 Heme interaction of the intrinsically disordered N-terminal peptide segment of human cystathionine-β-synthase

Authors: **Amit Kumar**, Amelie Wißbrock, Nishit Goradia, Peter Bellstedt, Ramadurai Ramachandran, Diana Imhof & Oliver Ohlenschläger

Contributions: **AK contribution (80%)**
AK performed the experiments, prepared the samples, collected the NMR data, prepared figures for manuscript and RR and PB helped **AK** in NMR data analysis. RR also contributed to NMR data collection. AW helped in kD determination. OO, RR and **AK** wrote the manuscript. All the authors reviewed the manuscript. OO and DI conceived the idea.

Status: Published in Scientific Report (2018)
https://doi.org/10.1038/s41598-018-20841-z

Summary: This publication shows the transient interaction of heme with the intrinsically disordered N-terminal region (40 amino acids) of CBS. Heme interacts with this region through specific heme-binding motifs and constitutes for 30% of enzyme activity as demonstrated through an *in vitro* assay. NMR spectroscopy was employed to uncover the structural details of this region which X-ray failed to provide and revealed the second heme binding site with moderate heme binding constant.

www.nature.com/scientificreports

SCIENTIFIC REPORTS

OPEN

Heme interaction of the intrinsically disordered N-terminal peptide segment of human cystathionine-β-synthase

Received: 30 August 2017
Accepted: 23 January 2018
Published online: 06 February 2018

Amit Kumar[1], Amelie Wißbrock[2], Nishit Goradia[1], Peter Bellstedt[3], Ramadurai Ramachandran[1], Diana Imhof[2] & Oliver Ohlenschläger[1]

Cystathionine-β-synthase (CBS) belongs to a large family of pyridoxal 5′-phosphate (PLP)-dependent enzymes, responsible for the sulfur metabolism. The heme-dependent protein CBS is part of regulatory pathways also involving the gasotransmitter hydrogen sulfide. Malfunction of CBS can lead to pathologic conditions like cancer, cardiovascular and neurodegenerative disorders. Truncation of residues 1–40, absent in X-ray structures of CBS, reduces but does not abolish the activity of the enzyme. Here we report the NMR resonance assignment and heme interaction studies for the N-terminal peptide stretch of CBS. We present NMR-spectral evidence that residues 1–40 constitute an intrinsically disordered region in CBS and interact with heme *via* a cysteine-proline based motif.

Cystathionine-β-synthase (CBS) is a modular enzymatic protein of 551 amino acids. The lyase CBS acts in the transsulfuration pathway and has a central role in the mammalian sulfur metabolism by catalysing the condensation of serine and homocysteine to a cystathionine intermediate[1,2]. Mutations in CBS are responsible for an inborn autosomal recessive inherited deviation in the amino acid metabolism, homocystinuria. This rare disease results in a clinical phenotype with elevated levels of homocysteine in blood plasma affecting four central organ systems, the cardiovascular, ocular, skeletal, and central nervous system and finally manifesting e.g. in neural tube defects, cardiovascular diseases and Alzheimer's disease[3–5]. Currently, more than 150 pathogenic CBS mutations have been reported which are spread across the coding sequence[6,7]. CBS is a heme-binding protein and represents an example for a human hemoprotein that can be regulated by gases *via* their heme component[8]. Especially, besides its binding CO and NO[9], CBS is involved in cellular production of major amounts of the gasotransmitter H_2S[10]. It was shown that aberrant function of CBS may thus lead to cancer, cardiovascular and neurodegenerative diseases making it an interesting drug target[11–13].

The homotetrameric CBS, a member of the fold type II family of the pyridoxal 5′-phosphate (PLP)-dependent enzymes, is in large parts structurally well characterised[14,15]. Members of this enzyme family are of multiple evolutionary origins. CBS contains the N-terminal heme-binding domain followed by catalytic core, which is conserved in most proteins of this class of organisms, and a C-terminal regulatory domain. The N-terminal domain (residues 1–70) is sequentially diverse in many classes of organisms and absent in lower eukaryotes like yeast and mycobacterium. The canonical heme in CBS is bound *via* an axial coordination to cysteine-52 and histidine-65 in the N-terminal region of the molecule. Interestingly, this binding site is missing in the homologous yeast enzyme[14,16]. In contrast to covalent binding of heme, recent studies have shown that transient interactions of the heme moiety with proteins can act as functional triggers[17]. Here, heme-binding motifs (HBM) or heme regulatory motifs (HRM) with special amino acid combinations –among them the cysteine-proline (CP) motif– are suggested to be responsible for heme association[17–22]. However, due to moderate binding constants these motifs at the same time allow also a fast dissociation of the heme complex. Interestingly, also in the newest X-ray structures of the human CBS protein[23,24] (e.g. PDB code 4COO) the stretch from residue 516–526 and the first 42 N-terminal

[1]Leibniz Institute on Aging – Fritz Lipmann Institute, Beutenbergstr. 11, D-07745, Jena, Germany. [2]Pharmaceutical Biochemistry and Bioanalytics, Pharmaceutical Institute, University of Bonn, An der Immenburg 4, D-53121, Bonn, Germany. [3]Friedrich Schiller University, Faculty of Chemistry and Earth Sciences, Humboldtstr. 10, D-07743, Jena, Germany. Correspondence and requests for materials should be addressed to D.I. (email: dimhof@uni-bonn.de) or O.O. (email: oliver.ohlenschlaeger@leibniz-fli.de)

```
Ophiophagus_hannah     MLCDVRGTMP---SIPAETEMDTMTCTHVSVDCI
Xenopus_laevis         -------------MPAVPPTTDSAACPHIKENHV
Gallus_gallus          ----MEKLMSEKPVPVSKAKPDTNSCPHASGKYF
Bos_taurus             --------MP-FETSPADTLCRSAGCPHLSGAHL
Felis_catus            --------MP-SETP--QAETGSAGCPHLSGAHL
Macaca_fascicularis    --------MP-SETP--QAEVGPTGCPHLSGPHS
Homo_sapiens           --------MP-SETP--QAEVGPTGCPHRSGPHS
Pan_troglodytes        --------MP-SETP--QAEVGPTGCPHRSGPHS
Cricetulus_griseus     --------MP-SGTS--QCEDGSARCPQPLEVHS
Heterocephalus_glaber  --------MP-SETP--QEESGASGCPH------
```

Figure 1. Sequence alignment of the N-terminal stretches of CBS proteins from different organisms.

residues are missing. Exactly in the latter region a CP-motif is located which is followed by histidines at positions $P+2$ and $P+7$ relative to the cysteine. This region is structurally close to the canonical heme-binding site at Cys^{52}/His^{65} which allows to speculate about a scavenger-type function of the CP-motif located in this intrinsically disordered protein region to support the localisation of the heme molecule during the binding process or to act as a second independent heme-binding site. In addition, it might be of interest to note that a sequence homology analysis reveals this CPH-motif to be conserved in higher eukaryotes with secondary interacting amino acid (H, C, Y) present in vicinity (Fig. 1).

Intrinsically disordered protein regions (IDPRs) are increasingly recognised to have functional relevance for biological regulatory processes in e.g. cellular signal transduction, molecular recognition and transcription[21,25,26] making them an interesting target for drug intervention[27,28]. Bioinformatic predictions (e.g. with DISOPRED2[29]) estimate that disordered regions or segments longer than 30 residues are present in approx. 2.0% of archaean, 4.2% of eubacterial and 33.0% of eukaryotic proteins[30] and that IDPRs are highly abundant in disease-related proteins[31]. Meanwhile the aim to structurally characterise IDPRs has fostered the development of various approaches e.g. in the areas of computational prediction[30,32,33] as well as NMR spectroscopy[34–43]. Interestingly, CP-motifs are also found in intrinsically disordered regions of functional relevance in other proteins that are associated with heme binding[21].

In this context, we have expressed the CBS protein using established approaches and investigated the heme-binding domain separately from the catalytic core. Functional studies on CBS(1–413) and on mutations of the non-canonical heme-binding site (C15S) were performed to compare and analyse the heme-binding process in CBS. NMR spectroscopy was also employed to characterise the heme interaction exploiting the advantage of this technique to describe also intrinsically disordered regions at atomic level.

Results

Protein expression and purification. The recombinant CBS(1–413) and the CBS(1–413)C15S mutant were expressed and purified as per literature[44]. The N-terminal CBS peptide ($_{GB1}$CBS(1–40)), consisting of the residues 1–40 of CBS (MPSETPQAEVGPTGCPHRSGPHSAKGSLEKGSPEDKEAKE), was expressed as fusion to the B1 domain of streptococcal protein G (GB1)[45].

UV/Vis study. UV/Vis spectroscopy was employed to monitor the interaction of the proteins with heme. UV/Vis data shows the heme binding by a Soret band shift to ~421 nm (Fig. 2a). Previous studies on heme binding to peptides using UV/Vis, Raman, EPR and NMR spectroscopy revealed that a UV shift to ~420 nm may be related to a hexacoordinated complex[46–50]. Thus, this bathochromic effect is characteristic of heme binding and suggests formation of a hexacoordinated state which in CBS involves residues cysteine-15 and histidine-22. The K_D value was determined to be $2.18 \pm 0.64\,\mu M$. According to the best fit possible $_{GB1}$CBS(1–40) binds to heme with a 1:1 stoichiometry (Fig. 2b).

Enzyme activity assay. The relative activities of CBS(1–413) and of the CBS(1–413)C15S mutant were compared in an enzyme activity assay using 7-azido-4-methylcoumarin as probe as described earlier in the literature[10]. To assure reproducibility six independent measurements were performed. During expression of the two enzymes in *E. coli* heme is endogenously produced and incorporated in the CBS proteins. This is reflected in yellowish colours of the protein samples with a darker colour of the CBS(1–413) with respect to the CBS(1–413) C15S mutant (data not shown) as shown for CBS and other recombinant heme-binding molecules[51,52]. Hence, exogenous addition of heme during the assay does not lead to activity differences off to the mean from the independent measurements of both CBS(1–413) and CBS(1–413)C15S mutant. This indicates the saturation of the compounds with endogenous heme already during expression in the *E. coli* cells. Figure 3 shows that CBS(1–413) C15S was on average 32% (between 20% to 40% in the individual measurements) less active than CBS(1–413). The assay indicates that beside of its canonical binding site at Cys^{52}/His^{65} heme is also binding to the CP-motif at position 15 and involving H22. This result of the assay is consistent with an observation of a previous study[44] where truncation of amino acids M1-K39 in CBS led to a similar decrease in enzyme activity.

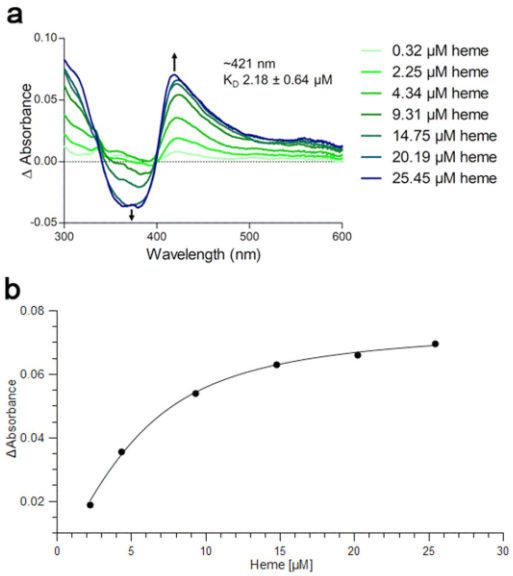

Figure 2. Heme binding to the $_{GB1}$CBS(1–40) fusion protein determined by UV/Vis spectroscopy. (**a**) The $_{GB1}$CBS(1–40) fusion protein was incubated with hemin at the concentrations indicated (5 μM protein, 0.32–25.45 μM hemin). (**b**) Titration curve observed at 421 nm.

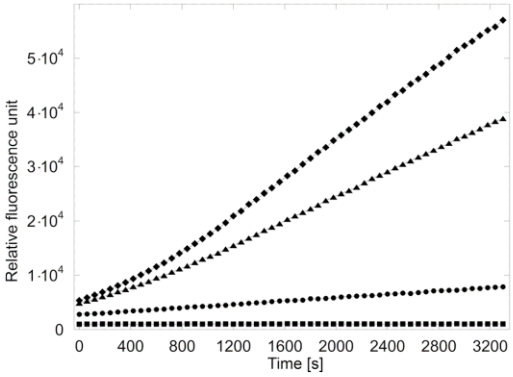

Figure 3. Fluorescence assay of CBS(1–413) and CBS(1–413)C15S. The average curve of six independent measurements is displayed. Symbols used: ♦ = CBS(1–413), ▲ = CBS(1–413)C15S, ● = blank, no protein, ■ = blank, no probe.

NMR resonance assignment of the CBS N-terminal peptide. Sequence specific resonance assignments for $_{GB1}$CBS(1–40) (Supplementary Table 1) were derived by a set of triple resonance 3D NMR spectra e.g. including well established experiments such as HNCA, HNCOCA, HNCO, HNCACO, HNCACB and HNN. Figure 4 shows the [^{1}H,^{15}N]-HSQC spectrum of the $_{GB1}$CBS(1–40) fusion protein including the assignments for the 40 N-terminal residues of CBS. The INEPT-based HNN experiment employed in this study essentially leads to the filtering out of signals from the structured part of the GB1 fusion protein due to significant relaxation losses, as shown in Supplementary Figure S1 which gives the [^{1}H,^{15}N]-projections from the 3D HNCA and HNN experiments. This considerably simplified the data analysis of the $_{GB1}$CBS(1–40) fusion protein. Representative strips indicating the sequential connectivities established are given in the Supplementary Material (Supplementary Figure S2). The calculation of the chemical shift index based on the obtained resonance assignment indicates an intrinsically disordered peptide which is supported by the prediction of the web server (IUPRED[53]) using the primary sequence as sole input.

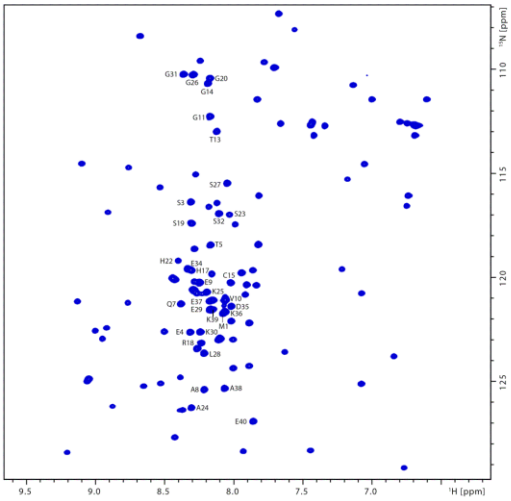

Figure 4. [^{1}H,^{15}N]-HSQC spectrum of the $_{GB1}$CBS(1–40) fusion protein. Cross peak assignments for the forty $_{GB1}$CBS(1–40) peptide residues are indicated.

NMR study of the heme interaction with the CBS N-terminal peptide (1–40). Employing 100 μM samples of ^{15}N, ^{15}N and ^{13}C-labelled GB1-fusion peptides, [^{1}H,^{15}N]-HSQC ligand titration experiments were first carried out using paramagnetic heme samples. As the ligand concentration was varied over a range of 0 to 100 μM, neither chemical shift changes were observed nor new additional peaks with increasing intensities were seen as the concentration of the heme ligand was increased (Supplementary Figure S3). Only a reduction in the intensities of few peaks (T13, G14, C15, H17, R18, S19, H22, S23) was observed, with the reduction in the intensity being maximal near C15 (Fig. 5a). This indicates the spatial proximity of these residues to the paramagnetic center and is consistent with the observation of the Soret band near 420 nm in the UV/Vis spectra (Fig. 2a) of the heme complex which resembles the situation found for transient heme binding by histidine-containing peptides[46,49]. A Soret band near 420 nm is typically associated with the occurrence of a hexacoordinated heme[21,22]. It is worth mentioning, that as with the paramagnetic Fe-PPIX, similar intensity reductions in the [^{1}H,^{15}N]-HSQC spectrum were also seen with diamagnetic Ga-PPIX (Fig. 5b). This suggests that in addition to the paramagnetic relaxation enhancement (PRE) effect[54,55] there is also an exchange contribution to the reduction in the intensities observed with the paramagnetic Fe-PPIX. We also observed that the single mutation C15S (Fig. 5c) essentially leads to no effect on the relative intensities of the cross peaks in the HSQC spectra upon heme addition. This indicates that mutation of this residue leads to no heme binding and is consistent with the UV/Vis data of this mutant which shows no sharp Soret peak (Supplementary Figure S5) either at ~420 nm (hexacoordination) or at ~370 nm (pentacoordination). It is also apparent that C15 is involved in the transient heme interaction forming a hexacoordinated complex with H22 forming the other axial ligand (H17 as second coordination site can be excluded due to steric reasons). The role of both amino acids as axial ligands is further supported by the [^{1}H,^{13}C]-HSQC spectral data recorded with and without heme (Fig. 6, Supplementary Figure S4). Spectral cross sections taken at the C^β positions corresponding to the C15 and H17/H22 residues show a similar variation of the intensity indicating the proximity of these nuclei to the heme central ions. Consistent with this, similar intensity variations in the aromatic HSQC spectral cross sections taken at the histidine $^{13}C^\varepsilon$ and $^{13}C^\delta$ positions (Supplementary Figure S6) were also observed.

In addition to the C15 mutation we have also mutated the H22 site. Although the UV/Vis spectra of this H22L mutant (Supplementary Figure S5) show a Soret peak at ~369 nm, possibly corresponding to pentacoordination at C15, the [^{1}H,^{15}N]-HSQC spectra carried out without and in presence of heme display no significant intensity variations of the cross peaks (Fig. 5d). This implies that either the heme-peptide interaction is much weaker and/or the rate of exchange between the heme-bound and the free peptide is not in the favorable range on the PRE timescale[54,55].

Viewed in totality, the results reported here suggest that the wild-type N-terminal CBS peptide upon heme binding undergoes a conformational change to a hexacoordinated complex with cysteine-15 and histidine-22 as ligands that is sparsely populated and is in exchange with a highly populated free peptide.

Discussion

Heme binding to the N-terminal stretch of CBS was confirmed by a combined UV/Vis and NMR study. In this study we decided for a fusion approach with the streptococcal protein GB1 since it is known to improve the solubility of the target protein without interfering with its fusion partner because of its inert nature. In addition,

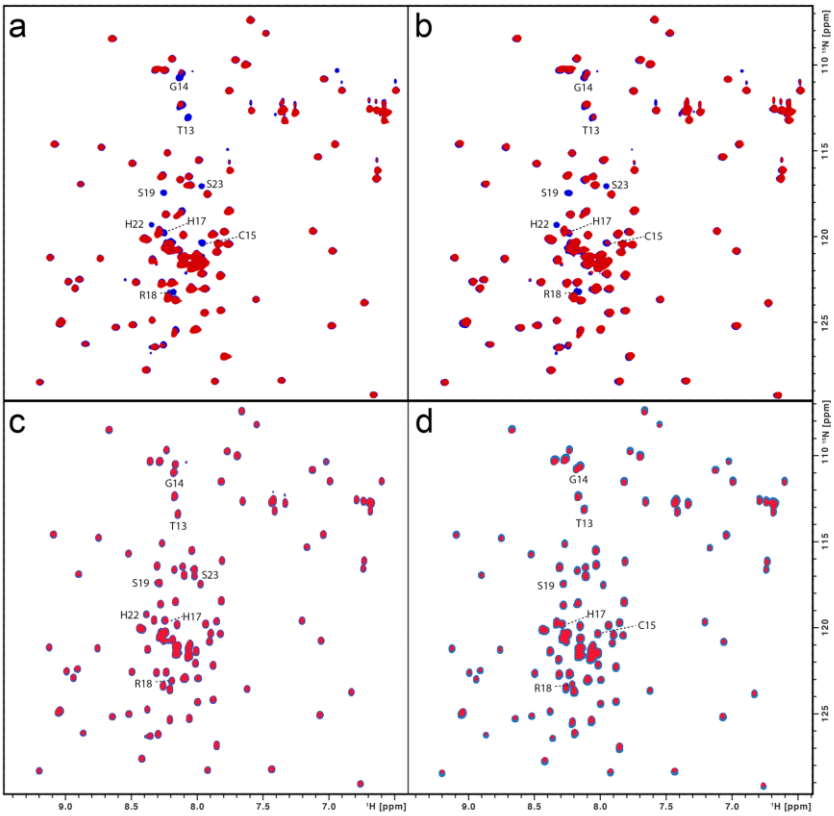

Figure 5. (**a**) Superimposition of the [^{1}H,^{15}N]-HSQC spectra of the $_{GB1}$CBS(1–40) fusion protein (100 μM) without (blue) and with hemin (50 μM; red). Interacting residues are indicated. (**b**) Superimposition of the [^{1}H,^{15}N]-HSQC spectra of the $_{GB1}$CBS(1–40) fusion protein (100 μM) without (blue) and with Ga-PPIX (100 μM; red). Interacting residues are indicated. (**c**) Superimposition of the [^{1}H,^{15}N]-HSQC spectra of the C15S mutant fusion protein (100 μM) without (blue) and with hemin (50 μM; red). (**d**) Superimposition of the [^{1}H,^{15}N]-HSQC spectra of the H22L mutant fusion protein (100 μM) without (blue) and with hemin (50 μM; red).

GB1 allows usage of easy purification protocols and is characterised with respect to structure and chemical shift assignments[45,56,57]. This fusion approach was also selected since the amino acid sequence of GB1 does not contain further cysteine or histidine residues which constitute classical heme-binding residues. In addition, NMR experiments performed solely on the GB1 protein with heme revealed no interaction between the components (data not shown). The results obtained indicate that the resonance assignments of the intrinsically disordered peptide (IDP) can be conveniently carried out in GB1-fusion since the GB1 signals can be essentially filtered out from the IDP signals. Thus, spectral overlap problems can be minimised without the need for unlabelling approaches[58,59] or ^{13}C-detected experiments[34]. NMR spectroscopy revealed that the forty N-terminal residues constitute an intrinsically disordered region of the protein cystathionine-β-synthase. This is in accordance with the observation that all available X-ray studies did not deliver a structural description of this molecular stretch. In addition, this study demonstrates for the first time that the disordered N-terminal region of CBS contributes heme-binding capacities *via* a second binding site, the CP-based motif at cysteine-15 and a histidine residue at position 22. The functional assay reveals that this heme-binding site at cysteine-15 and histidine-22 as second axial heme ligand increases the efficacy of the enzyme by approx. 30%. The intrinsically disordered N-terminal peptide of CBS is thus involved in transient heme interactions leading to a hexacoordinated complex. Transient binding was observed in both situations, with heme carrying the paramagnetic iron center as well as its diamagnetic substitute, Ga-PPIX. This also stresses the utility of both the Fe^{3+}/Ga^{3+} compounds in heme binding studies. The results on $_{GB1}$CBS(1–40) also imply the caveat that a complete functional description of molecules has to carefully consider also regions truncated to facilitate crystallisation for X-ray studies which are often intrinsically disordered, highly dynamic protein regions potentially serving as interaction sites[21,51,60].

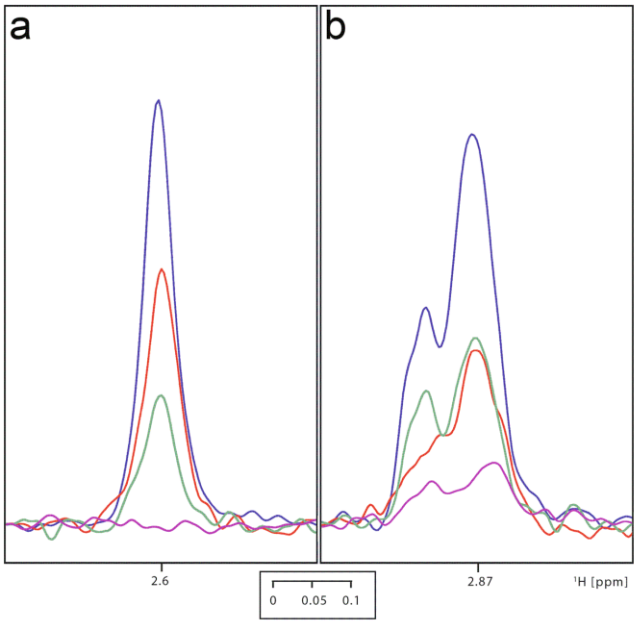

Figure 6. Superimposition of the spectral cross sections from [^{1}H,^{13}C]-HSQC spectra of $_{GB1}$CBS(1–40) (100 μM) taken at C$^{\beta}$ positions corresponding to the C15 (**a**) and H17/H22 (**b**) residues in the free (blue), Ga-PPIX (100 μM; red), Fe-PPIX (50 μM; green) and Fe-PPIX (100 μM; pink) exposed states.

Amino acid sequence comparison of the human and naked mole-rat CBS shows a deletion of the second heme-coordinating residue (histidine-22 in the human IDPR) in the latter species which occurred during evolution from a common ancestor. This might be explained by a lower need for CBS efficacy in sulfur metabolism induced by lower H_2S levels arising from a reduced dietary uptake of methionine in naked mole-rats[61]. As higher H_2S levels are connected e.g. to cancer[12], this could be one reason for the cancer resistance and longevity of naked mole-rats. However, human diet is rich in methionine, thus, evolutionary a contribution of a second heme-binding site might have become necessary to achieve the required efficacy for sulfur processing and to prevent pathological conditions. Hence, the second heme-binding site in CBS described in this study might become an attractive target for drug intervention to prevent pathological conditions without losing the complete biological functions of CBS, thus possibly preventing negative effects on the organism as observed for CBS gene deactivating mutations[6,62].

Methods

Protein expression and purification. CBS(1–413) protein was produced based upon the published protocol[44]. The sample of the CBS(1–413)C15S mutant was generated using site-directed primers, expressed, purified as described below for $_{GB1}$CBS(1–40) except no GB1 tag was used. Superdex 75 10/300 GL column (GE Healthcare, Freiburg, Germany) was used for size exclusion chromatography of CBS (1–413) and its mutant. To study the CBS(1–40) region, $_{GB1}$CBS(1–40) was expressed *via* a fusion protein approach with the streptococcal protein GB1. It was cloned in pET28a vector with GB1 domain attached to N-terminal of CBS(1–40) with flexible linker (TEV protease site - ENLYFQG) to avoid proteolytic cleavage of CBS(1–40) and additionally increasing the yield with stability. $_{GB1}$CBS(1–40) was expressed in *E. coli* BL21(DE3) cells which were grown up to an $OD_{600\,nm}$ of 0.7 in the LB medium. Cells were pelleted and transferred to M9 media containing $^{15}NH_4Cl$ and $^{13}C_6$-glucose that will result in labelled $_{GB1}$CBS(1–40). Protein expression was induced at OD_{600} of 0.7 by 0.3 mM IPTG for 18 h at 18 °C. Cells were resuspended in lysis buffer (50 mM Tris/HCl, 300 mM NaCl, 5 mM imidazole, 2 mM β-mercaptoethanol (pH 7.5)) followed by french press to lyse the cells and centrifuged at 10000 × g to collect the supernatant cell lysate. Ni-NTA agarose resin was used to capture the His_6-tagged $_{GB1}$CBS(1–40) protein followed by wash and elution with 10 mM and 250 mM imidazole, respectively. The His-tag was cleaved from the protein in overnight dialysis buffer (20 mM Tris/HCl, 150 mM NaCl, 2 mM DTT (pH 7.5)) by the addition of 5 U/mg of thrombin (Sigma-Aldrich, Taufkirchen, Germany) at 4 °C. The cleaved protein was concentrated to 1 mL using a 3-kDa Sartorius vivaspin filter and injected onto a 16/60 Hiload S75 size exclusion chromatography column (GE Healthcare, Freiburg, Germany) pre-equilibrated with 20 mM Tris/HCl, pH 6.9, 150 mM NaCl, 2 mM DTT to achive the highest purity. The fractions containing the $_{GB1}$CBS(1–40) were pooled together, concentrated, buffer

exchanged into 20 mM sodium phosphate buffer, pH 6.9 and the concentration measured at OD_{280} using UV/Vis spectroscopy. Samples were lyophilised or directly used for the biophysical and NMR experiments.

UV/Vis spectroscopy. A Multiskan GO microplate spectro-photometer (Thermo Scientific, Dreieich, Germany) was employed for UV/Vis measurements. The hemin solution was prepared by dissolving 1 mM hemin in 30 mM NaOH followed by incubation in the dark for 30 minutes on ice. Subsequently, the hemin solution was diluted with the respective buffer to the concentrations used. $_{GB1}$CBS(1–40) (5 µM) protein was incubated in the dark with different concentration of hemin (0.2–30 µM) for 60 minutes before measuring at 300–600 nm. HEPES-buffer (100 mM, pH 7.0) was used for dissolving protein and hemin.

Enzyme activity assay and protein concentration. The enzyme activity assay was performed on CBS(1–413) and the CBS(1–413)C15S mutant using established protocols[10]. Fluorescence was read at 450 nm with excitation at 365 nm using an Infinite M1000 microplate reader (Tecan, Männedorf, Switzerland). The protein concentration was determined by UV/Vis spectroscopy.

NMR spectroscopy. Solution NMR experiments were performed on a Bruker Avance III spectrometers with proton frequencies of 600 MHz at a temperature of 283 K. Data were acquired, processed and analyzed with Topspin (Bruker, Rheinstetten, Germany). The resonance assignment was performed using a combination of experiments such as HNN, HNCO/HNCACO, HNCA/HNCOCA, HCN, HBCBCGCDHD, HNCACB, HBHANH, [^{1}H,^{15}N]-HSQC, [^{1}H,^{13}C]-HSQC etc. experiments with $_{GB1}$CBS(1–40) dissolved at concentrations of 700 µM. [^{1}H,^{13}C]-HSQC spectra of the $_{GB1}$CBS(1–40) were recorded in the free, Ga(III)-protoporphyrin IX (Ga-PPIX) and hemin (Fe-PPIX) exposed state at concentrations of 100 µM and 50 µM, respectively. Ga(III)-protoporphyrin IX chloride and hemin were used as obtained from Frontier Scientific (Logan, USA). Unless otherwise stated, the $_{GB1}$CBS(1–40) and CBS samples were dissolved in 20 mM phosphate buffer and 5% D_2O.

Third-party methods. IUPred. Version 1.0 with default parameters was used.

Data availability. The authors declare that all data supporting the findings of this study are available within the article and its Supplementary Information files, or are available from the corresponding author upon request. The chemical shift assignments of CBS(1-40) have been deposited in the Biological Magnetic Resonance Data Bank (BMRB) under accession code 27351.

References

1. Miles, E. W. & Kraus, J. P. Cystathionine beta-synthase: structure, function, regulation, and location of homocystinuria-causing mutations. *J. Biol. Chem.* **279**, 29871–4 (2004).
2. Banerjee, R. & Zou, C. G. Redox regulation and reaction mechanism of human cystathionine-beta-synthase: a PLP-dependent hemesensor protein. *Arch. Biochem. Biophys.* **433**, 144–56 (2005).
3. Refsum, H., Ueland, P. M., Nygard, O. & Vollset, S. E. Homocysteine and cardiovascular disease. *Annu. Rev. Med.* **49**, 31–62 (1998).
4. Mills, J. L. *et al.* Homocysteine metabolism in pregnancies complicated by neural-tube defects. *Lancet* **345**, 149–51 (1995).
5. Clarke, R. *et al.* Folate, vitamin B12, and serum total homocysteine levels in confirmed Alzheimer disease. *Arch. Neurol.* **55**, 1449–55 (1998).
6. Kraus, J. P. *et al.* Cystathionine beta-synthase mutations in homocystinuria. *Hum. Mutat.* **13**, 362–75 (1999).
7. Kraus, J.P. CBS mutation database. http://cbs.lf1.cuni.cz.
8. Evande, R., Ojha, S. & Banerjee, R. Visualization of PLP-bound intermediates in hemeless variants of human cystathionine beta-synthase: evidence that lysine 119 is a general base. *Arch. Biochem. Biophys.* **427**, 188–96 (2004).
9. Taoka, S. & Banerjee, R. Characterization of NO binding to human cystathionine beta-synthase: possible implications of the effects of CO and NO binding to the human enzyme. *J. Inorg. Biochem.* **87**, 245–51 (2001).
10. Thorson, M. K., Majtan, T., Kraus, J. P. & Barrios, A. M. Identification of cystathionine beta-synthase inhibitors using a hydrogen sulfide selective probe. *Angew. Chem. Int. Ed. Engl.* **52**, 4641–4 (2013).
11. Wallace, J. L. & Wang, R. Hydrogen sulfide-based therapeutics: exploiting a unique but ubiquitous gasotransmitter. *Nat. Rev. Drug Discov.* **14**, 329–45 (2015).
12. Hellmich, M. R., Coletta, C., Chao, C. & Szabo, C. The therapeutic potential of cystathionine beta-synthetase/hydrogen sulfide inhibition in cancer. *Antioxid. Redox Signal.* **22**, 424–48 (2015).
13. Hellmich, M. R. & Szabo, C. Hydrogen Sulfide and Cancer. *Handb. Exp. Pharmacol.* **230**, 233–41 (2015).
14. Meier, M., Janosik, M., Kery, V., Kraus, J. P. & Burkhard, P. Structure of human cystathionine beta-synthase: a unique pyridoxal 5'-phosphate-dependent heme protein. *EMBO J.* **20**, 3910–6 (2001).
15. Ereno-Orbea, J., Majtan, T., Oyenarte, I., Kraus, J. P. & Martinez-Cruz, L. A. Structural basis of regulation and oligomerization of human cystathionine beta-synthase, the central enzyme of transsulfuration. *Proc. Natl. Acad. Sci. USA* **110**, E3790–9 (2013).
16. Ojha, S., Wu, J., LoBrutto, R. & Banerjee, R. Effects of heme ligand mutations including a pathogenic variant, H65R, on the properties of human cystathionine beta-synthase. *Biochemistry* **41**, 4649–54 (2002).
17. Kuhl, T. & Imhof, D. Regulatory Fe(II/III) heme: the reconstruction of a molecule's biography. *ChemBioChem* **15**, 2024–35 (2014).
18. Zhang, L. & Guarente, L. Heme binds to a short sequence that serves a regulatory function in diverse proteins. *EMBO J.* **14**, 313–20 (1995).
19. Zhang, L. In *Heme Biology: The Secret Life of Heme in Regulating Diverse Biological Processes* (ed. Zhang, L.), (World Scientific, Singapore, 2011).
20. Hira, S., Tomita, T., Matsui, T., Igarashi, K. & Ikeda-Saito, M. Bach1, a heme-dependent transcription factor, reveals presence of multiple heme binding sites with distinct coordination structure. *IUBMB Life* **59**, 542–51 (2007).
21. Watanabe-Matsui, M. *et al.* Heme binds to an intrinsically disordered region of Bach2 and alters its conformation. *Arch. Biochem. Biophys.* **565**, 25–31 (2015).
22. Suenaga, T. *et al.* Charge-state-distribution analysis of Bach2 intrinsically disordered heme binding region. *J. Biochem.* **160**, 291–298 (2016).
23. McCorvie, T. J. *et al.* Inter-domain communication of human cystathionine beta-synthase: structural basis of S-adenosyl-L-methionine activation. *J. Biol. Chem.* **289**, 36018–30 (2014).

24. Vicente, J. B. *et al.* A Clinically Relevant Variant of the Human Hydrogen Sulfide-Synthesizing Enzyme Cystathionine beta-Synthase: Increased CO Reactivity as a Novel Molecular Mechanism of Pathogenicity? *Oxid. Med. Cell. Longev.* **2017**, 8940321 (2017).
25. Dyson, H. J. & Wright, P. E. Intrinsically unstructured proteins and their functions. *Nat. Rev. Mol. Cell Biol.* **6**, 197–208 (2005).
26. Dunker, A. K., Brown, C. J., Lawson, J. D., Iakoucheva, L. M. & Obradovic, Z. Intrinsic disorder and protein function. *Biochemistry* **41**, 6573–82 (2002).
27. Rezaei-Ghaleh, N., Blackledge, M. & Zweckstetter, M. Intrinsically disordered proteins: from sequence and conformational properties toward drug discovery. *ChemBioChem* **13**, 930–50 (2012).
28. Uversky, V. N. Proteins without unique 3D structures: biotechnological applications of intrinsically unstable/disordered proteins. *Biotechnol. J.* **10**, 356–66 (2015).
29. Ward, J. J., McGuffin, L. J., Bryson, K., Buxton, B. F. & Jones, D. T. The DISOPRED server for the prediction of protein disorder. *Bioinformatics* **20**, 2138–9 (2004).
30. Ward, J. J., Sodhi, J. S., McGuffin, L. J., Buxton, B. F. & Jones, D. T. Prediction and functional analysis of native disorder in proteins from the three kingdoms of life. *J. Mol. Biol.* **337**, 635–45 (2004).
31. Uversky, V. N., Oldfield, C. J. & Dunker, A. K. Intrinsically disordered proteins in human diseases: introducing the D2 concept. *Annu. Rev. Biophys.* **37**, 215–46 (2008).
32. He, B. *et al.* Predicting intrinsic disorder in proteins: an overview. *Cell Res.* **19**, 929–49 (2009).
33. Deng, X., Eickholt, J. & Cheng, J. A comprehensive overview of computational protein disorder prediction methods. *Mol. Biosyst.* **8**, 114–21 (2012).
34. Gray, F. L., Murai, M. J., Grembecka, J. & Cierpicki, T. Detection of disordered regions in globular proteins using (13)C-detected NMR. *Protein Sci.* **21**, 1954–60 (2012).
35. Mantylahti, S., Hellman, M. & Permi, P. Extension of the HA-detection based approach: (HCA)CON(CA)H and (HCA)NCO(CA)H experiments for the main-chain assignment of intrinsically disordered proteins. *J. Biomol. NMR* **49**, 99–109 (2011).
36. Felli, I. C. & Pierattelli, R. Recent progress in NMR spectroscopy: toward the study of intrinsically disordered proteins of increasing size and complexity. *IUBMB Life* **64**, 473–81 (2012).
37. Wiedemann, C. *et al.* A Set of Efficient nD NMR Protocols for Resonance Assignments of Intrinsically Disordered Proteins. *ChemPhysChem* **17**, 1961–8 (2016).
38. Wiedemann, C. *et al.* HN-NCA heteronuclear TOCSY-NH experiment for (1)H(N) and (15)N sequential correlations in ((13)C, (15)N) labelled intrinsically disordered proteins. *J. Biomol. NMR* **63**, 201–12 (2015).
39. Goradia, N. *et al.* An approach to NMR assignment of intrinsically disordered proteins. *ChemPhysChem* **16**, 739–46 (2015).
40. Narayanan, R. L. *et al.* Automatic assignment of the intrinsically disordered protein Tau with 441-residues. *J. Am. Chem. Soc.* **132**, 11906–7 (2010).
41. Novacek, J., Zidek, L. & Sklenar, V. Toward optimal-resolution NMR of intrinsically disordered proteins. *J. Magn. Reson.* **241**, 41–52 (2014).
42. Felli, I.C., Pierattelli, R. & Tompa, P. Intrinsically Disordered Proteins. In *NMR of Biomolecules: Towards Mechanistic Systems Biology* (eds. Bertini, I., McGreevy, K. S. & Parigi, G.) 137–152 (Wiley-VCH Verlag & Co. KGaA, Weinheim, 2012).
43. Gibbs, E. B., Cook, E. C. & Showalter, S. A. Application of NMR to studies of intrinsically disordered proteins. *Arch. Biochem. Biophys.* **628**, 57–70 (2017).
44. Oliveriusova, J., Kery, V., Maclean, K. N. & Kraus, J. P. Deletion mutagenesis of human cystathionine beta-synthase. Impact on activity, oligomeric status, and S-adenosylmethionine regulation. *J. Biol. Chem.* **277**, 48386–94 (2002).
45. Gronenborn, A. M. *et al.* A novel, highly stable fold of the immunoglobulin binding domain of streptococcal protein G. *Science* **253**, 657–61 (1991).
46. Brewitz, H. H. *et al.* Role of the Chemical Environment beyond the Coordination Site: Structural Insight into Fe(III) Protoporphyrin Binding to Cysteine-Based Heme-Regulatory Protein Motifs. *ChemBioChem* **16**, 2216–24 (2015).
47. Kuhl, T. *et al.* Analysis of Fe(III) heme binding to cysteine-containing heme-regulatory motifs in proteins. *ACS Chem. Biol.* **8**, 1785–93 (2013).
48. Schubert, E. *et al.* Spectroscopic studies on peptides and proteins with cysteine-containing heme regulatory motifs (HRM). *J. Inorg. Biochem.* **148**, 49–56 (2015).
49. Brewitz, H. H. *et al.* Heme interacts with histidine- and tyrosine-based protein motifs and inhibits enzymatic activity of chloramphenicol acetyltransferase from Escherichia coli. *Biochim. Biophys. Acta* **1860**, 1343–53 (2016).
50. Shimizu, T. Binding of cysteine thiolate to the Fe(III) heme complex is critical for the function of heme sensor proteins. *J. Inorg. Biochem.* **108**, 171–7 (2012).
51. Sahoo, N. *et al.* Heme impairs the ball-and-chain inactivation of potassium channels. *Proc. Natl. Acad. Sci. USA* **110**, E4036–44 (2013).
52. Dimster-Denk, D., Tripp, K. W., Marini, N. J., Marqusee, S. & Rine, J. Mono and dual cofactor dependence of human cystathionine beta-synthase enzyme variants *in vivo* and *in vitro*. *G3 (Bethesda)* **3**, 1619–28 (2013).
53. Dosztanyi, Z., Csizmok, V., Tompa, P. & Simon, I. IUPred: web server for the prediction of intrinsically unstructured regions of proteins based on estimated energy content. *Bioinformatics* **21**, 3433–4 (2005).
54. Anthis, N. J. & Clore, G. M. Visualizing transient dark states by NMR spectroscopy. *Q. Rev. Biophys.* **48**, 35–116 (2015).
55. Clore, G. M. Seeing the invisible by paramagnetic and diamagnetic NMR. *Biochem. Soc. Trans.* **41**, 1343–54 (2013).
56. Sommer, L. A., Meier, M. A. & Dames, S. A. A fast and simple method for probing the interaction of peptides and proteins with lipids and membrane-mimetics using GB1 fusion proteins and NMR spectroscopy. *Protein Sci.* **21**, 1566–70 (2012).
57. Wilton, D. J., Tunnicliffe, R. B., Kamatari, Y. O., Akasaka, K. & Williamson, M. P. Pressure-induced changes in the solution structure of the GB1 domain of protein G. *Proteins* **71**, 1432–40 (2008).
58. Zhou, P. & Wagner, G. Overcoming the solubility limit with solubility-enhancement tags: successful applications in biomolecular NMR studies. *J. Biomol. NMR* **46**, 23–31 (2010).
59. Kobayashi, H. *et al.* Segmental isotope labeling of proteins for NMR structural study using a protein S tag for higher expression and solubility. *J. Biomol. NMR* **52**, 303–13 (2012).
60. Uversky, V. N. The multifaceted roles of intrinsic disorder in protein complexes. *FEBS Lett.* **589**, 2498–506 (2015).
61. Dziegelewska, M. *et al.* Low sulfide levels and a high degree of cystathionine beta-synthase (CBS) activation by S-adenosylmethionine (SAM) in the long-lived naked mole-rat. *Redox Biol.* **8**, 192–8 (2016).
62. de Franchis, R., Kraus, E., Kozich, V., Sebastio, G. & Kraus, J. P. Four novel mutations in the cystathionine beta-synthase gene: effect of a second linked mutation on the severity of the homocystinuric phenotype. *Hum. Mutat.* **13**, 453–7 (1999).

Acknowledgements

We thank Dr. Klaus Huse, Dr. Karol Szafranski and Maja Dziegelewska (FLI) for helpful discussions. Financial support by the Deutsche Forschungsgemeinschaft (DFG) within FOR 1738 (to D.I. and O.O.) is gratefully acknowledged. The FLI is a member of the Leibniz Association (WGL) and is financially supported by the Federal Government of Germany and the State of Thuringia.

Author Contributions

O.O. and D.I. designed the research; A.K., A.W., N.G., P.B. and R.R. performed the experiments; A.K., R.R. and O.O. analysed the data; A.K., R.R. and O.O. wrote the paper, all authors reviewed the manuscript.

Additional Information

Supplementary information accompanies this paper at https://doi.org/10.1038/s41598-018-20841-z.

Competing Interests: The authors declare that they have no competing interests.

Publisher's note: Springer Nature remains neutral with regard to jurisdictional claims in published maps and institutional affiliations.

Open Access This article is licensed under a Creative Commons Attribution 4.0 International License, which permits use, sharing, adaptation, distribution and reproduction in any medium or format, as long as you give appropriate credit to the original author(s) and the source, provide a link to the Creative Commons license, and indicate if changes were made. The images or other third party material in this article are included in the article's Creative Commons license, unless indicated otherwise in a credit line to the material. If material is not included in the article's Creative Commons license and your intended use is not permitted by statutory regulation or exceeds the permitted use, you will need to obtain permission directly from the copyright holder. To view a copy of this license, visit http://creativecommons.org/licenses/by/4.0/.

© The Author(s) 2018

Supplementary Information

Heme interaction of the intrinsically disordered N-terminal peptide segment of human cystathionine-β-synthase

Amit Kumar[1], Amelie Wißbrock[2], Nishit Goradia[1], Peter Bellstedt[3], Ramadurai Ramachandran[1], Diana Imhof[2*] and Oliver Ohlenschläger[1*]

[1]Leibniz Institute on Aging – Fritz Lipmann Institute, Beutenbergstr. 11, D-07745 Jena, Germany.
[2]Pharmaceutical Biochemistry and Bioanalytics, Pharmaceutical Institute, University of Bonn, An der Immenburg 4, D-53121 Bonn, Germany.
[3]Friedrich Schiller University, Faculty of Chemistry and Earth Sciences, Humboldtstr. 10, D-07743 Jena, Germany.

*Correspondence and requests for materials should be addressed to O.O. (email: oliver.ohlenschlaeger@leibniz-fli.de) or D.I. (email: dimhof@uni-bonn.de)

Supporting information contains 6 Figures (S1-S6), and 1 Table (S1).

Figure S1. Superposition of the [^{1}H,^{15}N]-projection from the 3D HNN experiment of the $_{GB1}$CBS(1-40) fusion protein (red) with the HNCA spectrum (blue). Cross peaks arising from the linker between GB1 and CBS(1-40) are annotated.

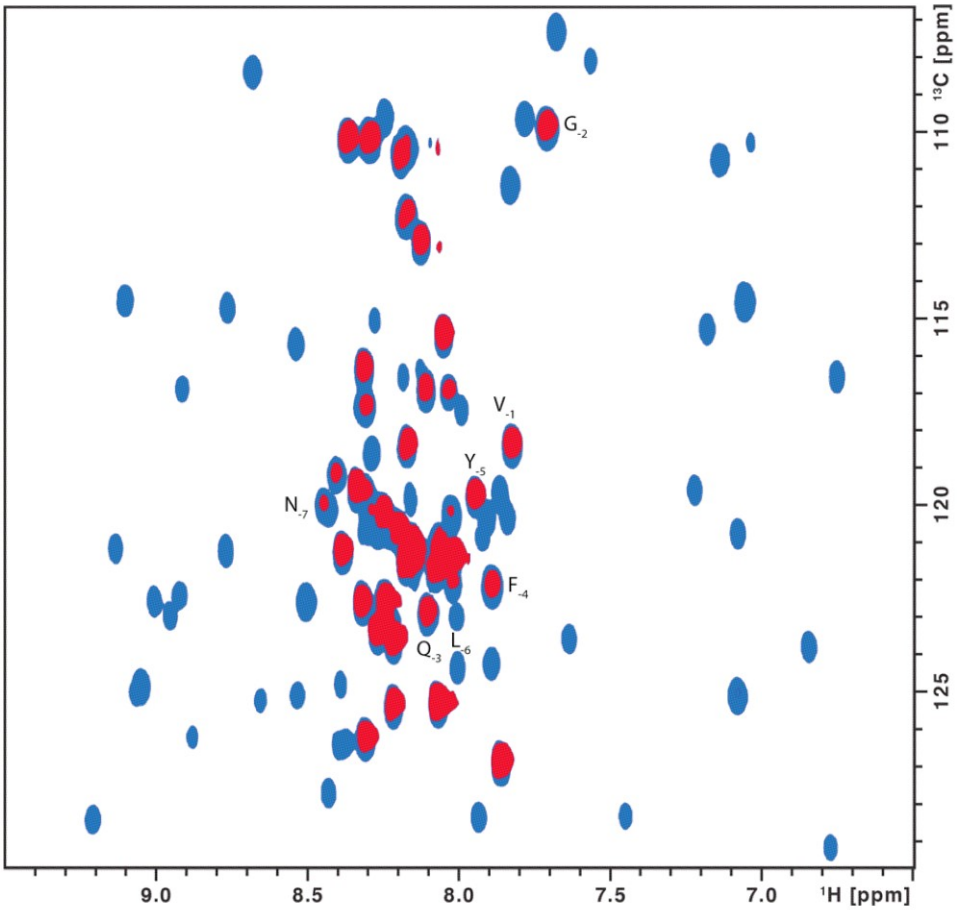

Figure S2. Representative strips from the HNN spectrum of $_{GB1}$CBS(1-40). The sequential connectivities are indicated by arrows.

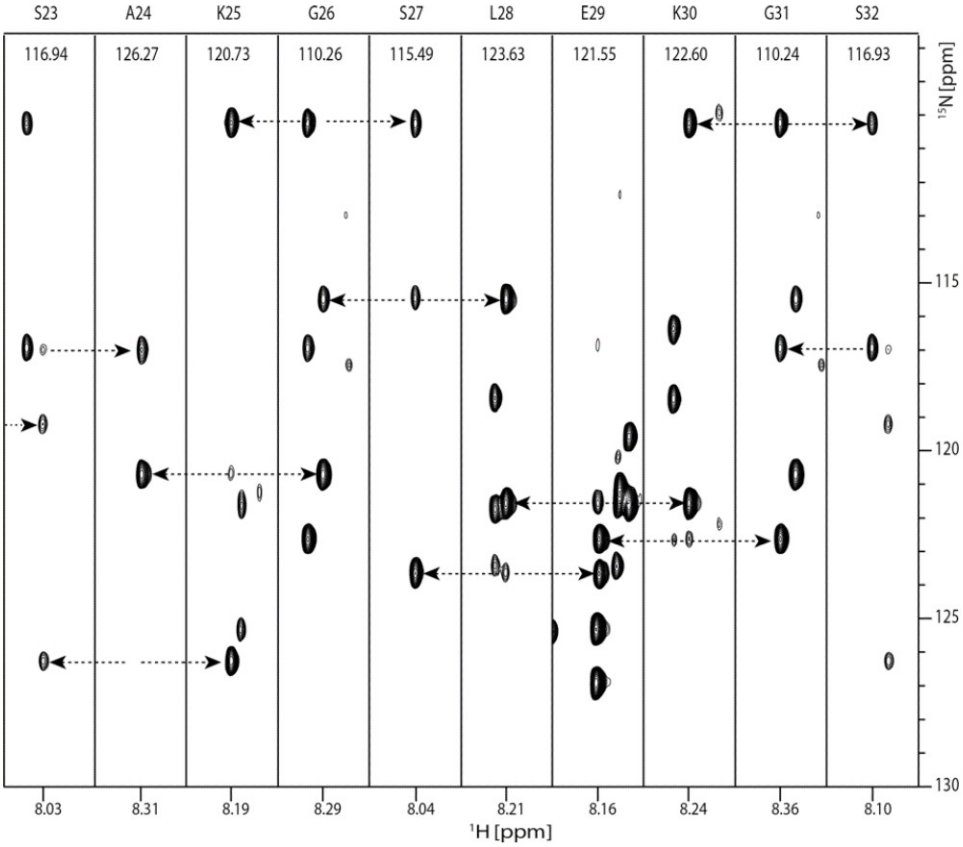

Figure S3A. Spectral cross sections from the [^{1}H,^{15}N]-HSQC spectra of the $_{GB1}$CBS(1-40) fusion protein (100 μM) without and with hemin taken at ^{15}N chemical shift positions corresponding to the amino acid residues indicated (blue – no hemin; red – Ga-PPIX, green – Fe-PPIX). The hemin and Ga-PPIX concentrations used are indicated at the bottom of the panels.

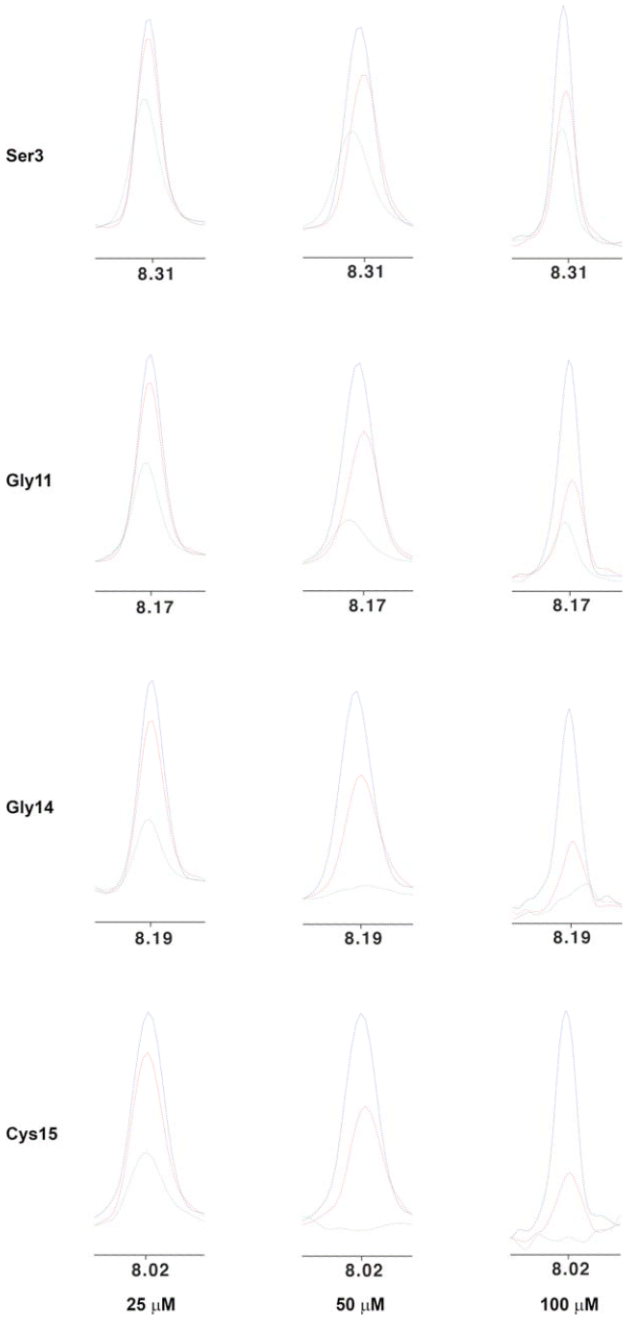

Figure S3B. Spectral cross sections from the [^{1}H,^{15}N]-HSQC spectra of the $_{GB1}$CBS(1-40) fusion protein (100 μM) without and with hemin taken at ^{15}N chemical shift positions corresponding to the amino acid residues indicated (blue – no hemin; red – Ga-PPIX, green – Fe-PPIX). The hemin and Ga-PPIX concentrations used are indicated at the bottom of the panels.

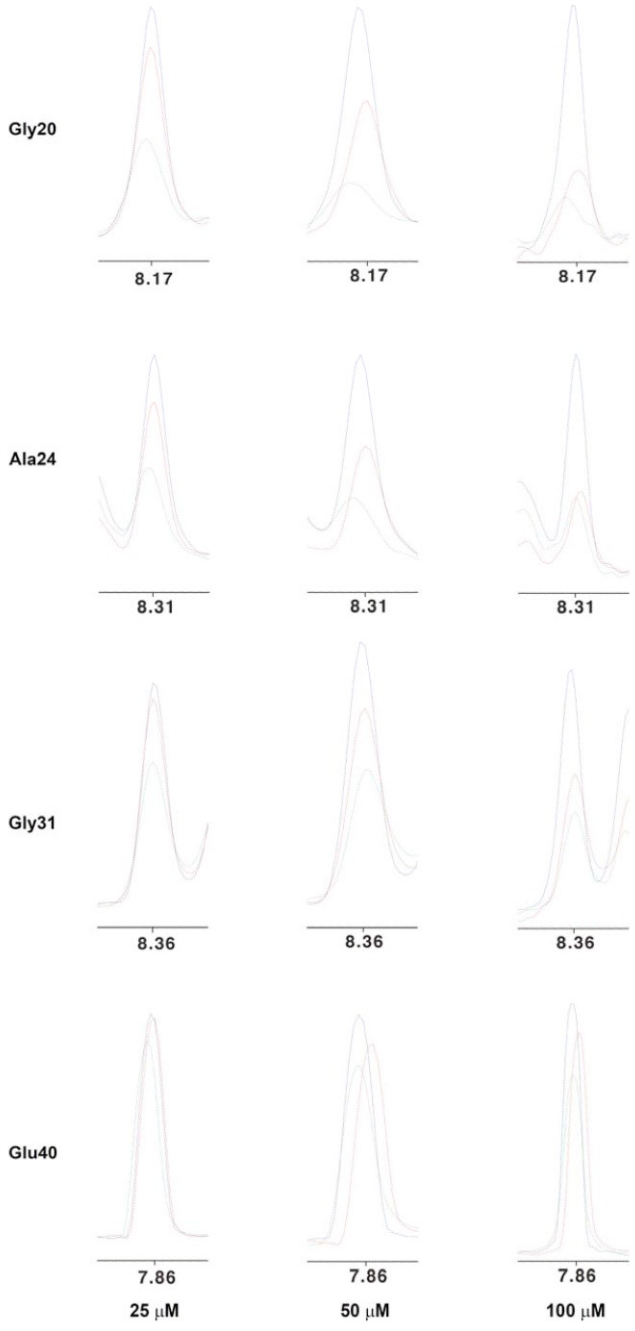

Figure S4. Constant-time [^{1}H,^{13}C]-HSQC spectrum (zoomed plot) of $_{GB1}$CBS(1-40) without heme.

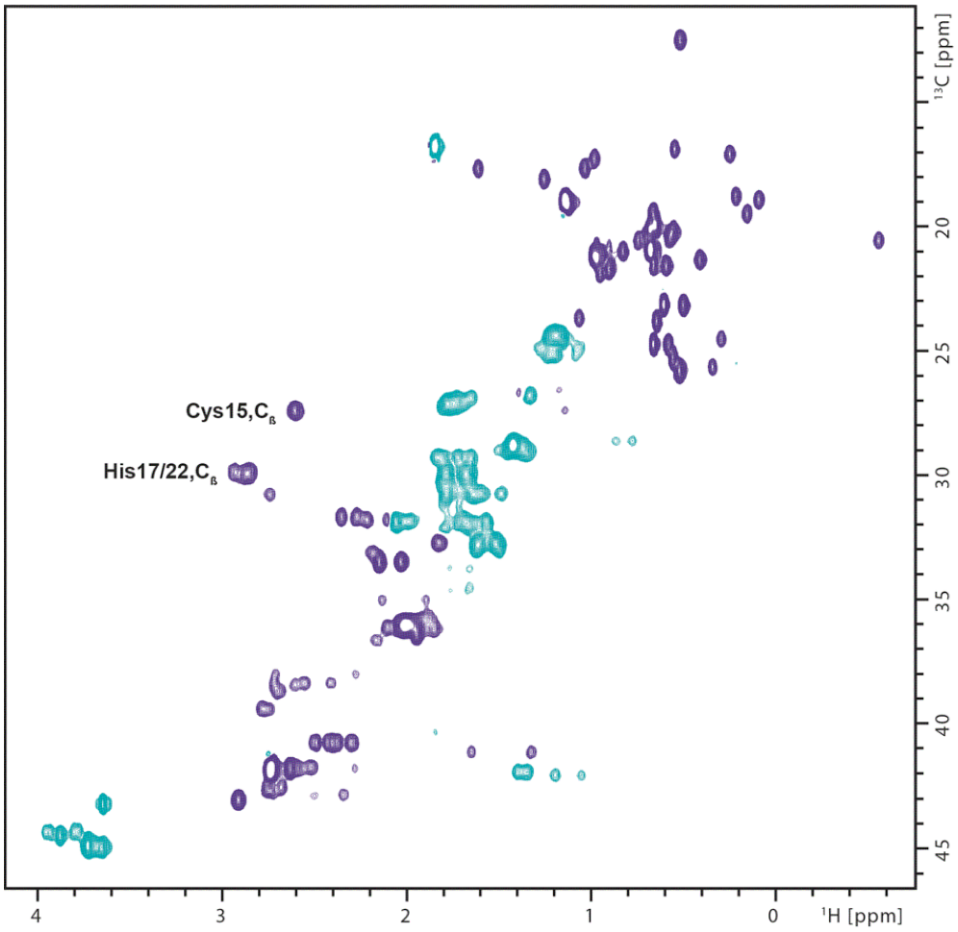

Figure S5. UV/Vis spectra for the $_{GB1}$CBS(1-40)C15S (A) and $_{GB1}$CBS(1-40)H22L (B) mutants. The fusion protein (20 μM protein) was incubated with hemin at concentrations of 2 (blue), 10 (red) and 15 μM hemin (green).

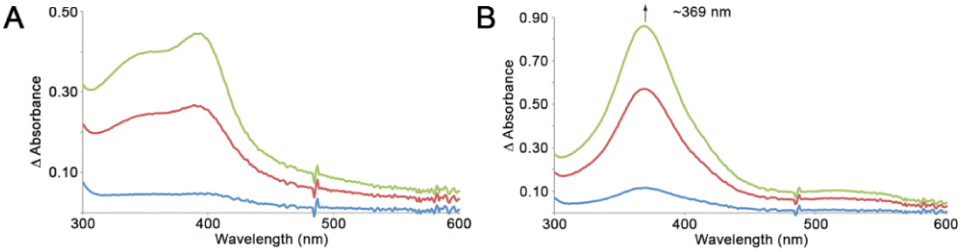

Figure S6. 2D Chemical shift correlation spectra (Figure S6A and S6B) generated via a 3D HCN experiment indicating the ($^{13}C^{\delta}$,$^{1}H^{\delta}$) and ($^{13}C^{\varepsilon}$,$^{1}H^{\varepsilon}$) cross-peaks of His17 and His22 of CBS40. ^{1}H cross-sections taken at the $^{13}C^{\delta}$ and $^{13}C^{\varepsilon}$ positions (cf. Fig. S6B 1-4) in the aromatic [^{1}H,^{13}C]-HSQC spectra generated without (blue) and with (red) the addition of hemin (Fe^{3+}) are given in S6C. Cross peaks 1 and 4 in Fig. S6B/C arise from the thrombin site at the N-terminus of GB1 and serve as indicator for the general solvent PRE effect in Fig. S6C.

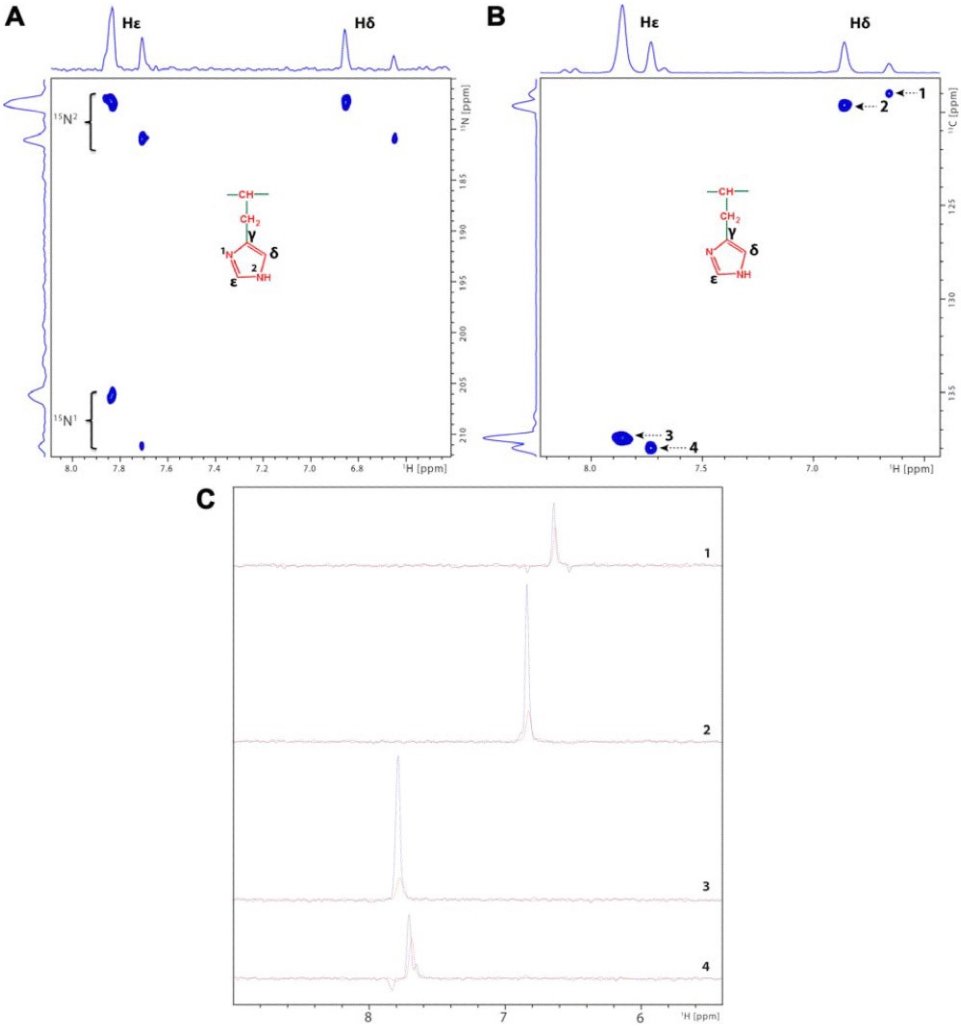

Table S1. Chemical shift assignment of $_{GB1}$CBS(1-40)

		H'	N'	H^{α}	H^{β}	C'	C^{α}	C^{β}	C^{γ}	C^{δ}	C^{ε}
-8	Glu	8.50	122.60	3.97	1.70	175.43	56.42	30.28	36.05	-	-
-7	Asn	8.44	120.05	4.37	2.40,2.55	174.72	52.86	38.26	-	-	-
-6	Leu	8.01	122.10	3.94	1.05,1.20	176.79	55.32	41.86	26.50	24.53,23.40	-
-5	Tyr	7.94	119.77	4.27	2.60,2.71	175.16	57.48	38.41	-	-	-
-4	Phe	7.88	122.19	4.26	2.79,2.75	174.99	57.73	39.38	-	-	-
-3	Gln	8.10	122.95	3.99	1.80,1.64	175.65	55.74	29.23	-	-	-
-2	Gly	7.71	109.91	3.65	-	173.62	44.99	-	-	-	-
-1	Val	7.82	118.42	3.90	1.83	175.52	61.68	32.62	20.81,19.86	-	-
0	Asp	8.26	123.42	4.33	2.41,2.30	175.45	54.17	40.77	-	-	-
1	Met	8.07	121.70	4.53	1.64	-	52.80	32.73	-	-	-
2	Pro	-	-	3.39	1.66,2.06	176.74	64.89	31.82	27.20	50.43	-
3	Ser	8.31	116.39	4.16	3.61	174.40	58.07	63.58	-	-	-
4	Glu	8.31	122.63	4.12	1.67,1.80	176.12	56.09	30.06	36.04	-	-
5	Thr	8.17	118.44	4.31	3.85	-	59.79	69.45	-	-	-
6	Pro	-	-	4.16	1.62,2.05	176.71	63.19	31.92	27.22	50.91	-
7	Gln	8.38	121.25	3.99	1.83,1.70	175.61	55.66	29.22	33.75	-	-
8	Ala	8.21	125.41	4.03	1.12	177.44	52.31	19.04	-	-	-
9	Glu	8.24	120.22	4.05	1.78,1.67	176.22	56.03	30.07	35.97	-	-
10	Val	8.06	121.07	3.91	1.81	176.13	61.78	32.63	19.75,20.71	-	-
11	Gly	8.17	112.27	3.79	-	-	44.38	-	-	-	-
12	Pro	-	-	4.24	1.72,2.05	177.50	63.25	31.85	26.96	49.62	-
13	Thr	8.12	113.00	4.11	4.01	175.10	61.71	69.35	21.24	-	-
14	Gly	8.19	110.69	3.70	-	173.43	44.93	-	-	-	-
15	Cys	8.02	120.25	4.53	2.61	-	56.12	27.32	-	-	-
16	Pro	-	-	4.15	1.57,1.99	176.40	63.11	31.81	27.03	50.58	-
17	His	8.30	119.68	4.37	2.87	174.90	55.91	30.05	-	-	-
18	Arg	8.23	123.16	4.12	1.49	175.81	55.92	30.78	26.79	43.12	-
19	Ser	8.30	117.39	4.26	3.62	174.27	58.01	63.78	-	-	-
20	Gly	8.17	110.42	3.88	-	-	44.60	-	-	-	-
21	Pro	-	-	4.15	1.56,1.97	176.92	63.35	31.70	26.81	49.48	-
22	His	8.40	119.19	4.42	2.94,2.87	174.98	56.01	29.94	-	-	-
23	Ser	8.03	116.98	4.14	3.56	174.01	58.07	63.62	-	-	-
24	Ala	8.31	126.25	4.09	1.14	177.68	52.37	18.94	-	-	-
25	Lys	8.19	120.71	4.03	1.53,1.60	177.11	56.31	32.64	24.44	28.84	41.78
26	Gly	8.29	110.26	3.72	-	173.99	44.98	-	-	-	-
27	Ser	8.04	115.48	4.17	3.61	174.59	58.16	63.52	-	-	-
28	Leu	8.21	123.64	4.11	1.40,1.36	177.26	55.02	41.85	26.62	24.47,23.36	-
29	Glu	8.16	121.55	3.99	1.64,1.77	176.34	56.20	29.89	35.88	-	-
30	Lys	8.24	122.62	4.04	1.52,1.62	176.96	56.12	32.72	24.42	28.73	41.87
31	Gly	8.36	110.24	3.73	-	173.54	44.86	-	-	-	-
32	Ser	8.10	116.93	4.55	3.64	-	56.14	63.19	-	-	-
33	Pro	-	-	4.16	2.06	177.06	63.30	31.71	27.19	50.34	-
34	Glu	8.33	119.57	3.95	1.78,1.67	176.23	56.63	29.87	36.25	-	-
35	Asp	8.01	121.38	4.32	2.38,2.50	176.16	54.23	40.78	-	-	-
36	Lys	8.06	121.63	4.03	1.63,1.51	176.52	56.15	32.60	24.34	28.71	41.73
37	Glu	8.15	121.07	3.98	1.78,1.68	176.00	56.12	29.84	36.07	-	-
38	Ala	8.06	125.34	4.04	1.13	177.29	52.24	18.85	-	-	-
39	Lys	8.17	121.55	4.09	1.62,1.50	175.51	55.85	33.00	24.43	28.78	42.07
40	Glu	7.86	126.91	3.85	1.78,1.64	-	57.75	30.71	-	-	-

2.2 NMR experiments on the transient interaction of the intrinsically disordered N-terminal peptide of cystathionine-β-synthase with heme

Authors: **Amit Kumar**, Peter Bellstedt, Christoph Wiedemann, Amelie Wißbrock, Diana Imhof, Ramadurai Ramachandran & Oliver Ohlenschläger

Contributions: **AK contribution (70%)**
AK performed the experiments, prepared the samples, prepared the figures for the manuscript. RR helped in NMR data collection and its analysis. OO and RR wrote the manuscript. All the authors reviewed the manuscript. RR conceived the idea.

Status: Submitted to Journal of Magnetic Resonance (Under revision)

Summary: This paper describes the new NMR pulse development for probing heme-IDP interactions and assignment of IDPs. This experiment detects the effect of heme on the side chains of proteins unlike the [^{1}H,^{15}N]-HSQC experiment which shows the effect only on the protein backbone. This technique makes it more sensitive over the conventional [^{1}H,^{15}N]-HSQC experiment to map the heme-IDP interactions and in addition, can also be performed at physiological temperature. It can be employed as a complementary powerful experiment for probing heme-protein interactions to other conventional methods.

NMR experiments on the transient interaction of the intrinsically disordered N-terminal peptide of cystathionine-β-synthase with heme

Amit Kumar[a], Peter Bellstedt[b], Christoph Wiedemann[c], Amelie Wißbrock[d], Diana Imhof[d], Ramadurai Ramachandran[a], Oliver Ohlenschläger[a*]

[a]Leibniz Institute on Aging – Fritz Lipmann Institute, Beutenbergstr. 11, D-07745 Jena, Germany;

[b]Institute for Organic Chemistry and Macromolecular Chemistry, Friedrich Schiller University, Humboldtstr. 10, D-07743 Jena, Germany;

[c]Institute of Biochemistry and Biotechnology, Martin Luther University Halle-Wittenberg, Kurt-Mothes-Str. 3a, D-06120 Halle, Germany;

[d]Pharmaceutical Institute, University of Bonn, An der Immenburg 4, D-53121 Bonn, Germany.

Correspondence

Oliver Ohlenschläger, Beutenbergstr. 11, D-07745 Jena, Germany.

Email: oliver.ohlenschlaeger@leibniz-fli.de, Phone: +49-(0)3641-656219

ORCID Oliver Ohlenschläger: 0000-0002-6428-4423

Compliance with ethical standards

Funding: This work was supported by the Deutsche Forschungsgemeinschaft (DFG) [grant number: FOR 1738 (Oh 86/3-2)].

Declarations of interest: none.

Keywords

human cystathionine-β-synthase, cystinuria, heteronuclear NMR spectroscopy, HCBCACON experiment, mapping, transient binding, heme

Abstract

The N-terminal segment of human cystathionine-β-synthase (CBS(1-40)) constitutes an intrinsically disordered protein stretch that transiently interacts with heme. We illustrate that the HCBCACON experimental protocol provides an efficient alternative approach for probing transient interactions of intrinsically disordered proteins with heme in situations where the applicability of the conventional [^{1}H,^{15}N]-HSQC experiment may be limited. This experiment starting with the excitation of protein side chain protons delivers information about the proline residues and thereby makes it possible to use these residues in interaction mapping experiments. Employing this approach in conjunction with site-specific mutation we show that transient heme binding is mediated by the Cys^{15}-Pro^{16} motif of CBS(1-40).

1. Introduction

Intrinsically disordered proteins (IDP) and protein regions (IDPR) attached to folded protein domains have been found to be implicated in critical biological functions and in neurodegenerative and other diseases [1-5]. In contrast to covalent binding, as in many metalloproteins, IDPs have been shown to be involved in functionally important transient interactions. In many cases, heme-binding (HBM) or heme-regulatory motifs (HRM) with special amino acid combinations such as CxxHx$_{18}$H, CxxHx$_{16}$H and cysteine-proline (CP) in small sequence stretches are responsible for the heme association with moderate binding constants [6-10]. Coupled with mutagenesis, the heme-protein interaction studies are often carried out via techniques such as resonance Raman, surface plasmon resonance, NMR and UV-Vis spectroscopy [11, 12]. Such studies demonstrated the possibility for the IDPR to undergo conformational changes upon heme binding, e.g. due to hexa-coordination of the iron moiety in the iron-porphyrin complex with cysteine and histidine residues located at different positions in the protein sequence, leading to a reduction in the flexibility of the polypeptide chain [8-10]. A variety of techniques like chemical shift perturbation, relaxation dispersion spectroscopy and paramagnetic relaxation enhancement have been demonstrated for studies of protein-ligand interactions [13-17] and [^{1}H,^{15}N]-HSQC experiments are often employed to map the interaction interface. However, in experimental situations leading to fast amide proton exchange with water molecules, e.g. at physiological temperature and pH, its applicability may be limited [18]. Thus, the required protocol strongly depends on the given experimental situation.

Many IDPs are involved in regulatory interactions with heme, with Cys-Pro (CP) motifs often playing an important role [8-10]. The proline residue in the CP motif assists the coordination of cysteine thiolate to the Fe(III) heme complex [12, 19]. We are currently investigating the N-terminal peptide stretch (1-40) of human cystathionine-β-synthase (CBS, 551 a.a.; UniProtKB P35520) in the context of heme-IDP interaction [20-22]. In the enzyme CBS heme is bound as a cofactor via an axial coordination to cysteine-52 and histidine-65. However, NMR and UV/Vis studies [23] have shown that the

disordered N-terminal region of CBS also contributes heme-binding capacities via a second binding site, the CP-based motif around cysteine-15 possibly extending to histidine-22. Functional assays revealed that this second heme-binding site increases the efficacy of the enzyme by ~30%.

Taking into consideration these factors, we aimed at a further robust strategy for probing the transient interaction of the N-terminal peptide stretch of human cystathionine-β-synthase (CBS(1-40)) with heme.

2. Materials and Methods

CBS(1-40) (0.6 mM) was expressed via a fusion protein approach with the streptococcal protein GB1. The sample preparation followed protocols described earlier [24]. Heme was dissolved 1 mM in 20 mM NaOH and incubated for 30 minutes. NMR measurements on CBS(1-40) were performed in sodium phosphate buffer pH 6.9 and carried out on a Bruker 600 MHz narrow-bore Avance III NMR spectrometer equipped with pulse field gradient accessories, pulse shaping units and triple resonance cryo-probe with the sample temperature kept at 283 K and 310 K. The States procedure was used for phase-sensitive detection in the indirect dimensions [25]. DSS was used for direct ^{1}H chemical shift referencing and ^{13}C and ^{15}N chemical shifts were indirectly referenced. The non-uniformly sampled multidimensional data sets were collected and processed as in our recent studies [26, 27] employing the Bruker Topspin version 3.5 software.

3. Results

Initial heme-binding studies were carried out via [^{1}H,^{15}N]-HSQC experiments. To improve the solubility of the target protein, make use of easy purification protocols, and minimize proteolytic degradations, GB1 fusion peptide samples of the N-terminal (1-40) of CBS (wild type and mutants) were employed in these investigations, and it is seen that the N-terminal peptide upon heme binding undergoes a conformational change to a complex that is sparsely populated and in exchange with the free peptide. Although NMR investigations could be successfully performed at 283 K, studies at the physiologically relevant temperature of 310 K could not be carried out due to considerable signal intensity losses arising from fast amide proton exchange with the solvent molecules. Another limitation in using the [^{1}H,^{15}N]-HSQC experimental protocol is that information about the proline residues is lost. In this context, using CBS(1-40) as a model system, it is demonstrated here that the HCBCACON [28-30] experimental protocol, starting with the excitation of protein side chain protons, provides a convenient alternative approach for investigations of proline-containing sequences (e.g. CP, poly-proline or proline-rich sequence motifs).

Generation of chemical shift correlation spectra with good spectral resolution is one prerequisite for undertaking any NMR based investigation of protein-ligand interactions. Typically, in the case of IDPs, inter-residue $^{15}N_i$-$^{13}CO_{i-1}$ chemical shift correlations involving the backbone nuclei lead to spectra

with relatively better spectral dispersion compared to intra-residue correlations [31, 32], and this has been exploited for achieving resonance assignments. The $^{15}N_i$-$^{13}CO_{i-1}$ correlation spectrum can be generated via the HCBCACON experiment (Figure S1) employing either the coherence transfer pathway $^{1}H^{\beta} \rightarrow {}^{13}C^{\beta} \rightarrow {}^{13}C^{\alpha} \rightarrow {}^{13}CO \rightarrow {}^{15}N$ (t1) $\rightarrow {}^{13}CO$ (t2) involving direct ^{13}CO detection or the transfer pathway $^{1}H^{\beta} \rightarrow {}^{13}C^{\beta} \rightarrow {}^{13}C^{\alpha} \rightarrow {}^{13}CO$ (t1) $\rightarrow {}^{15}N$ (t2) $\rightarrow {}^{13}CO \rightarrow {}^{13}C^{\alpha} \rightarrow {}^{1}H^{\alpha}$ (t3) involving $^{1}H^{\alpha}$ detection. The advantage with the direct ^{13}CO detection approach is that the generation of $^{15}N_i$-$^{13}CO_{i-1}$ correlation spectrum involves only a simple 2D data acquisition, and the efficacy of this protocol was first tested at 283 K using only a 250 μM IDP sample.

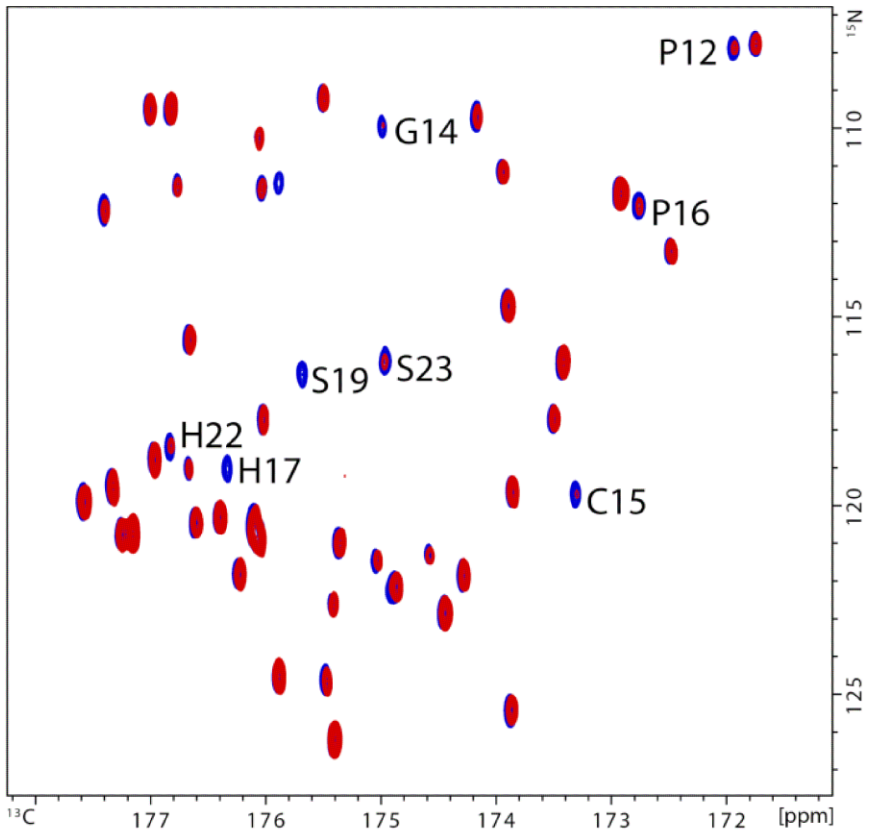

Figure 1. Superposition of the 2D $^{15}N_i$-$^{13}CO_{i-1}$ correlation spectra of CBS(1-40) (250 μM; pH 6.9) collected via the (HCBCA)CON experiment at 273 K in D_2O without (blue) and with heme (red). Amino acids ($^{15}N_i$) involved in the interaction with heme are labeled.

Consistent with the conclusions reached via heme titration studies employing [^{1}H,^{15}N]-HSQC spectra, the ^{15}N-^{13}CO correlation spectrum (Figure 1) recorded with the addition of ~100 μM heme (Fe^{3+}) shows significant reduction in the intensity of peaks involving the amino acid residues P12, G14, C15, P16, H17, S19, H22, and S23, reflecting the spatial proximity of these residues to the paramagnetic center of the heme. The fact that the cross-peaks involving P16 and P12 are affected significantly

provides additional confirmation for the involvement of C15 in heme binding. In spite of the low protein concentration, it is seen that a triple resonance cryo-probe tailored for ^{1}H detection allows to collect ^{15}N-^{13}CO correlation spectra of good quality within a reasonable amount of time. An additional advantage in carrying out IDP-heme interaction studies via ^{15}N-^{13}CO correlations is that in cases where the IDP system is investigated as a fusion peptide, as in our case a GB1 fusion, the HCBCACON protocol at 283 K leads to spectra in which signals from the GB1 domain are largely eliminated, in contrast to the situation with the conventional [^{1}H,^{15}N]-HSQC experiment (Figure S2). This leads to spectra with less overlap and the convenient mapping of the protein-heme interaction interface. Although these studies can also be carried out via other experimental schemes such as HCBCACO [33], Figure S3, good spectral resolution observed in the ^{15}N-^{13}CO correlation makes the ^{13}CO-detected HCBCACON experiment an attractive approach for the study of heme-protein interactions.

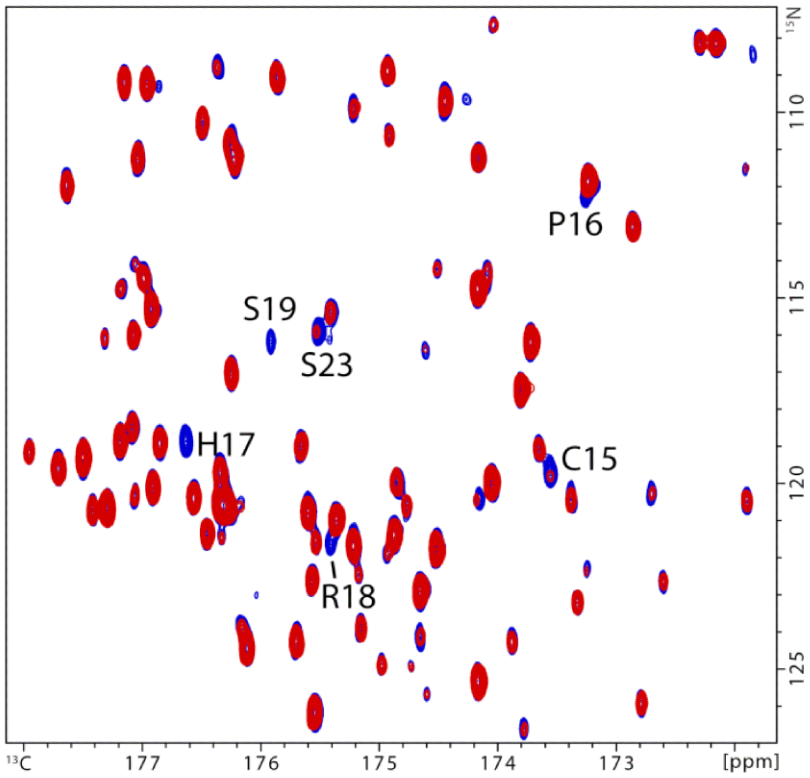

Figure 2. Superposition of the 2D ^{15}N$_i$-^{13}CO$_{i-1}$ correlation spectra of CBS(1-40) (250 µM) collected via the (HCBCA)CON experiment at 310 K in D_2O without (blue) and with heme (red). Relevant residues (^{15}N$_i$) involved in interaction with heme are labeled.

While sensitivity considerations limited the applicability of [^{1}H,^{15}N]-HSQCs at 310 K, 2D ^{15}N-^{13}CO correlation data could be conveniently collected, without and with the addition of heme. Significant variations (Figure 2) in the intensity of many of the peaks corresponding to the amino acid residues that were found to be involved in heme interaction at 283 K clearly reveal the presence of

transient heme binding even at the elevated and physiologically relevant temperature. However, unlike the situation at 283 K, cross-peaks originating from the folded GB1 domain are also seen with considerable signal intensities (Figure 2) leading to spectral crowding in the 2D ^{15}N-^{13}CO correlation spectrum. Spectral overlaps can also be expected when one deals with IDP systems of much larger size. It is also important to mention that these studies typically employ low protein concentrations (~250 μM) so as to minimize the concentration of the heme required and thereby heme aggregation and high solvent PREs. Hence, it will be difficult to carry out the ^{13}CO detection-based measurements using conventional room-temperature NMR probes optimized for ^{1}H detection.

It is conceivable that heme-protein interaction studies would require experimental protocols with good sensitivity facilitating the collection of higher dimensional data sets within a reasonable amount of time. Thanks to the introduction of powerful non-uniform data sampling and processing procedures and to better sensitivity provided by direct proton detection, this can be realized via the HCBCACON protocol using $^{1}H^{\alpha}$ detection (see above). Figure S4 shows ω_{12} spectral projections from a 3D HCBCACON experiment carried out in absence and in presence of heme at 310 K (see Figure S5 for other spectral projections). Improved spectral resolution achieved via 3D data acquisition is demonstrated by a few representative ω_{13} spectral cross-sections given in Figure 3.

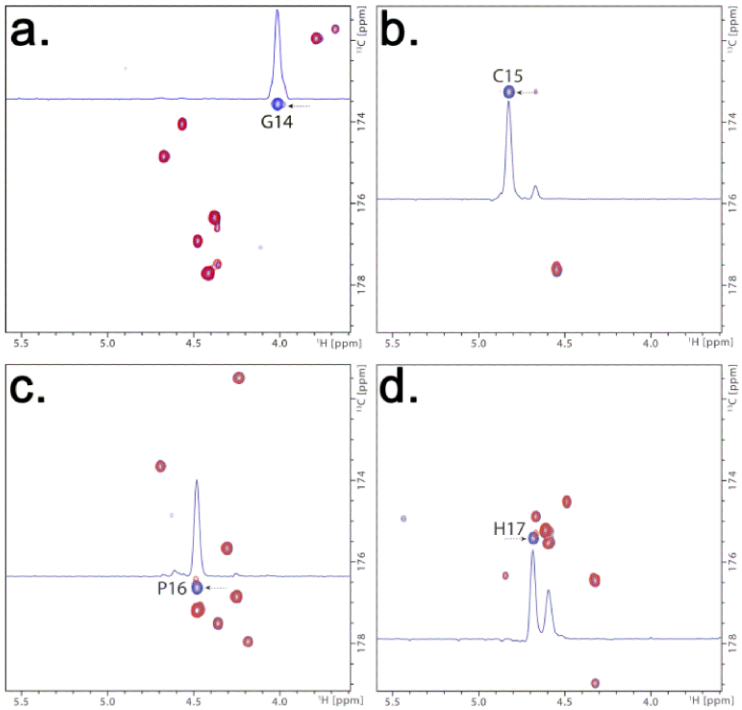

Figure 3. Superposition of the 2D $^{1}H^{\alpha}_{i-1}$-$^{13}CO_{i-1}$ cross-sections from 3D HCBCACON spectra of CBS(1-40) (250 μM) at 310 K in D_2O generated without using linear prediction in the indirect dimensions and collected without (blue) and with heme (red, 100 μM). Other experimental details are as given in Figure caption S4. The cross-sections were taken at the $^{15}N_i$ positions corresponding to the amino-acid residues

of C15 (a), P16 (b), H17 (c) and R18 (d). 1D cross-sections taken from the spectrum collected without heme and at the positions indicated by the arrow are also given to indicate spectral quality.

This data also confirms transient heme interactions at the physiological temperature and clearly illustrate the potential of 3D HCBCACON experiments for protein-ligand interaction studies. It is worth mentioning that: 1. While the [^{1}H,^{15}N]-HSQC protocol may become difficult at 310 K due to fast amide proton exchange with water, elevated temperatures are ideally suited for carrying out the HCBCACON experiment as faster molecular tumbling leads to reduction in relaxation losses and thereby to improved signal intensities. 2. In situations where the H^{α}_{i-1}-$^{15}N_i$ and $^{13}CO_{i-1}$-$^{1}H^{\alpha}_{i-1}$ correlation data have sufficient spectral resolution it is not necessary to carry out the HCBCACON experiment in the 3D mode and simple 2D data collections realizable in a few hours could be good enough to map the protein-ligand interface (Figure S6).

Our initial heme interaction studies via the [^{1}H,^{15}N]-HSQC protocol were carried out using both the wild-type and CBS(1-40) mutants. NMR data were consistent with UV/Vis that indicated heme binding to wild-type CBS(1-40), possibly forming a hexa-coordinated heme-protein complex as indicated by a shift of the Soret band to 420 nm, and no heme binding to the C15S mutant.

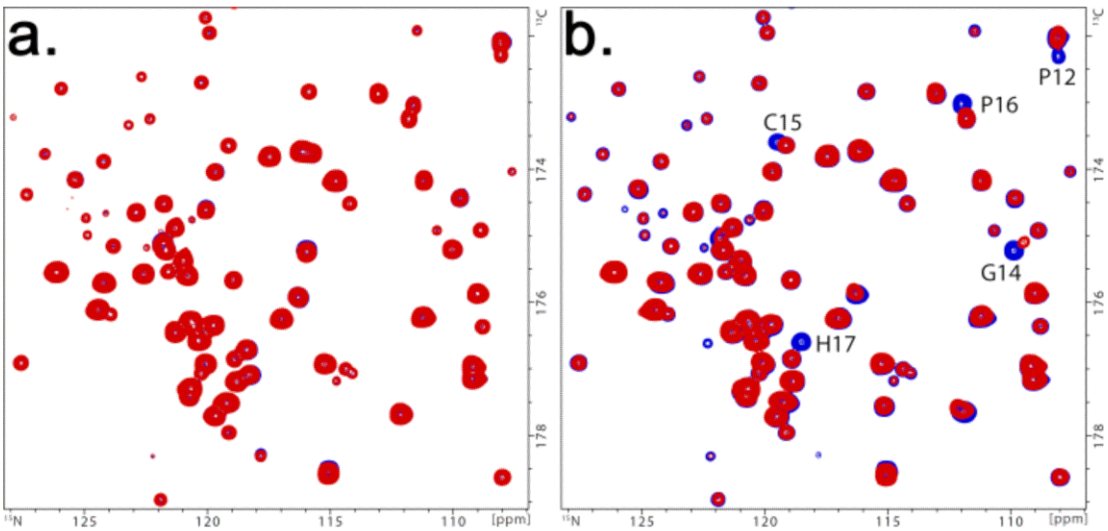

Figure 4. Superposition of the 2D $^{15}N_i$-$^{13}CO_{i-1}$ projections from 3D HCBCACON spectra of CBS(1-40) (250 μM) mutants C15S (a) and H22L (b) generated without using linear prediction in the indirect dimensions at 310 K in D_2O and collected without (blue) and with heme (red, 100 μM) employing 16 transients per t1 increment. Relevant amino acid residues ($^{15}N_i$) involved in interaction with heme are indicated.

Results from the 3D HCBCACON experiment at 310 K with the C15S mutant are in agreement with these data. Unlike the case with the wild-type, the ^{15}N-^{13}CO spectral projections obtained without

and with the addition of ~100 μM heme (Fe^{3+}) show no significant variations in the intensity of the correlation peaks (Figure 4a). Thus, heme binding is abolished in the C15S mutant.

UV/Vis data of the heme-incubated H22L mutant indicated the presence of a penta-coordinated heme-IDP complex as suggested by a maximum at 370 nm, as earlier shown for heme-coordinated CP motifs [8, 12, 19, 23]. The [^{1}H,^{15}N]-HSQC experiments carried out at 283 K on the H22L mutant of CBS(1-40) showed no effect on the relative intensities of the cross-peaks upon heme addition, possibly the binding was too weak to be detected by the experimental protocol or the exchange rate between the heme bound and free IDP was not in the favorable range on the PRE timescale. However, the ^{15}N-^{13}CO spectral projections of the HCBCACON with H^{α} detection (as well as the data employing ^{13}CO-direct detection, Figure S7) obtained without and with the addition of ~100 μM heme (Fe^{3+}) showed significant intensity variations of the correlation peaks, e.g. for residues P12, G14, C15, P16, H17 (Figure 4b) consistent with the heme-IDP interaction detected by UV/Vis.

4. Discussion and Conclusions

The objective of this study was to evaluate the heme-binding of the non-crystallizable N-terminal peptide stretch (1-40) of human cystathionine-β-synthase, an intrinsically disordered protein region. As the conventional approach via [^{1}H,^{15}N]-HSQC interaction mapping experiments was hampered by fast HN exchange, the HCBCACON protocol was adapted as an alternative strategy. This experiment has the combined advantages of being HN exchange-independent and of adding proline correlations as additional probe for the interaction mapping. Such an approach was of particular interest as CP motifs were described as preferential heme interaction sites [8-10] and in the case of CBS(1-40) the supposed heme binding could involve the $C^{15}P^{16}$ motif of the intrinsically disordered N-terminal peptide stretch. The data using site-specific mutants unambiguously showed that H22L still binds heme while heme binding is abolished in the C15S mutant. Thus, in CBS(1-40) the heme interacts with the $C^{15}P^{16}$ motif resulting in a penta-coordinated heme-IDP complex as the contribution of H17 in formation of a hexa-coordinated complex can be excluded by steric considerations. The data presented might contribute to antagonize pathological CBS conditions via therapeutic intervention at this less-well studied molecular region.

Considering that interactions leading to hexa- or penta-coordinated heme-protein complexes frequently involve the side chains of His and Cys residues, this study demonstrated that the HCBCACON protocol starting with the excitation of side-chain atoms and involving either ^{13}CO detection [34] or H^{α} detection can be effectively used in heme-IDP interaction studies as a powerful complementary procedure to the conventional [^{1}H,^{15}N]-HSQC experiment, especially at elevated temperatures with limited applicability of the canonical mapping approach. Thus, the presented approach can be used for protein-ligand or drug-screening studies and allows also for heme-IDP

investigations under cell-like crowded environment. Initial results (data not shown) indicate that CBS(1-40) is still disordered and its transient interactions with heme at 310 K stay intact under molecular crowding effected by 200 g/l of PEG-3500 and 150 g/l of Ficoll-70.

Acknowledgments

We thank S. Häfner (CS Protein production, FLI) for technical support. Financial support by the Deutsche Forschungsgemeinschaft (DFG) within FOR 1738 (to D.I. and O.O.) is gratefully acknowledged. The FLI is a member of the Leibniz Association (WGL) and is financially supported by the Federal Government of Germany and the State of Thuringia.

Appendix A. Supplementary material

Supplementary data to this article can be found online.

FIGURE S1 2D HCBCACON pulse sequence.

FIGURE S2 Superposition of the [^{1}H,^{15}N]-HSQC spectra of the GB1 fusion peptide CBS(1-40) (100 μM) without (blue) and with heme (100 μM, red). Interacting residues are indicated.

FIGURE S3 Superposition of the 2D $^{13}C^{\alpha,\beta}_{i}$-$^{13}CO_{i}$ correlation spectra (zoomed plot) of CBS(1-40) (250 μM) in 90% H_2O and 10% D_2O collected at 283 K *via* the (HCBCA)CO experimental protocol without (blue, 35 increments in the ^{13}C indirect dimension with a spectral width of 61 ppm, 112 transients per increment, recycle time of 1.0 s and a ^{13}CO acquisition time of 125 ms) and with heme (100 μM, 35 increments in the ^{13}C indirect dimension with a spectral width of 61 ppm, 400 transients per increment, recycle time of 1.0 s and a ^{13}CO acquisition time of 125 ms). Interacting residues are indicated.

FIGURE S4 Superposition of the 2D $^{15}N_{i}$-$^{13}CO_{i-1}$ spectral projections from 3D HCBCACON spectra of CBS(1-40) (250 μM) at 310 K in D_2O collected without (blue) and with heme (100 μM) employing 61 increments in the ^{15}N dimension with a spectral width of 26 ppm, 42 increments in the ^{13}CO dimension with a spectral width of 8 ppm, 32 transients per t1 increment, recycle time of 1.0 s, $^{1}H^{\alpha}$ acquisition time of 100 ms, 20% non-uniform sampling in the indirect dimensions, and using linear prediction in the indirect dimensions for improved spectral resolution. Relevant amino acid residues ($^{15}N_{i}$) involved in interaction with heme are indicated.

FIGURE S5 Superposition of the 2D $^{13}CO_{i-1}$-$^{1}H^{\alpha}_{i-1}$ (a) and $^{15}N_{i}$-$^{1}H^{\alpha}_{i-1}$ (b) spectral projections from 3D HCBCACON spectra of CBS(1-40) (250 μM) at 310 K in D_2O collected without (blue) and with heme (100 μM) employing 61 increments in the ^{15}N dimension with a spectral width of 26 ppm, 42 increments in the ^{13}CO dimension with a spectral width of 8 ppm, 32 transients per t1 increment, recycle time of 1.0 s, $^{1}H^{\alpha}$ acquisition time of 100 ms, 20% non-uniform sampling in the indirect dimensions and using

linear prediction in the indirect dimensions for improved spectral resolution. Relevant amino acid residues corresponding to $^{13}CO_{i-1}$-$^{1}H^{\alpha}_{i-1}$ (A) and $^{15}N_i$ (B) involved in interaction with heme are indicated.

FIGURE S6 Superposition of the 2D $^{15}N_i$-$^{1}H^{\alpha}_{i-1}$ spectra generated *via* the 3D HCBCACON sequence using CBS(1-40) (250 μM). These spectra were collected at 310 K in D_2O without (blue) and with heme (100 μM) employing 100 increments in the ^{15}N dimension, with a spectral width of 26 ppm, 16 transients per increment, recycle time of 1.0 s, $^{1}H^{\alpha}$ acquisition time of 100 ms. Relevant amino acid residues ($^{15}N_i$) involved in interaction with heme are indicated.

FIGURE S7 Superposition of the 2D $^{15}N_i$-$^{13}CO_{i-1}$ correlation spectra of CBS(1-40) (250 μM) mutant H22L collected *via* the (HCBCA)CON experimental protocol at 310 K in D_2O without (blue, 50 increments in the ^{15}N dimension with a spectral width of 26 ppm, 160 transients per increment, recycle time of 1.0 s and a ^{13}CO acquisition time of 125 ms) and with heme (100 μM, 50 increments in the ^{15}N dimension with a spectral width of 26 ppm, 160 transients per increment, recycle time of 1.0 s and a ^{13}CO acquisition time of 125 ms). Relevant amino acid residues ($^{15}N_i$) involved in the interaction with heme are indicated.

References

[1] P. Tompa, Unstructural biology coming of age, Curr Opin Struct Biol, 21 (2011) 419-425.
[2] C. Schulenburg, D. Hilvert, Protein conformational disorder and enzyme catalysis, Top Curr Chem, 337 (2013) 41-67.
[3] P. Tompa, Intrinsically disordered proteins: a 10-year recap, Trends Biochem Sci, 37 (2012) 509-516.
[4] R. Skrabana, J. Sevcik, M. Novak, Intrinsically disordered proteins in the neurodegenerative processes: formation of tau protein paired helical filaments and their analysis, Cell Mol Neurobiol, 26 (2006) 1085-1097.
[5] V.N. Uversky, C.J. Oldfield, U. Midic, H. Xie, B. Xue, S. Vucetic, L.M. Iakoucheva, Z. Obradovic, A.K. Dunker, Unfoldomics of human diseases: linking protein intrinsic disorder with diseases, BMC Genomics, 10 Suppl 1 (2009) S7.
[6] N. Sahoo, N. Goradia, O. Ohlenschlager, R. Schonherr, M. Friedrich, W. Plass, R. Kappl, T. Hoshi, S.H. Heinemann, Heme impairs the ball-and-chain inactivation of potassium channels, Proc Natl Acad Sci U S A, 110 (2013) E4036-4044.
[7] M.J. Burton, S.M. Kapetanaki, T. Chernova, A.G. Jamieson, P. Dorlet, J. Santolini, P.C. Moody, J.S. Mitcheson, N.W. Davies, R. Schmid, E.L. Raven, N.M. Storey, A heme-binding domain controls regulation of ATP-dependent potassium channels, Proc Natl Acad Sci U S A, 113 (2016) 3785-3790.
[8] T. Shimizu, Binding of cysteine thiolate to the Fe(III) heme complex is critical for the function of heme sensor proteins, J Inorg Biochem, 108 (2012) 171-177.
[9] M. Watanabe-Matsui, T. Matsumoto, T. Matsui, M. Ikeda-Saito, A. Muto, K. Murayama, K. Igarashi, Heme binds to an intrinsically disordered region of Bach2 and alters its conformation, Arch Biochem Biophys, 565 (2015) 25-31.
[10] T. Suenaga, M. Watanabe-Matsui, T. Uejima, H. Shima, T. Matsui, M. Ikeda-Saito, M. Shirouzu, K. Igarashi, K. Murayama, Charge-state-distribution analysis of Bach2 intrinsically disordered heme binding region, J Biochem, 160 (2016) 291-298.
[11] H.H. Brewitz, N. Goradia, E. Schubert, K. Galler, T. Kuhl, B. Syllwasschy, J. Popp, U. Neugebauer, G. Hagelueken, O. Schiemann, O. Ohlenschlager, D. Imhof, Heme interacts with histidine-

and tyrosine-based protein motifs and inhibits enzymatic activity of chloramphenicol acetyltransferase from Escherichia coli, Biochim Biophys Acta, 1860 (2016) 1343-1353.
[12] T. Kuhl, A. Wissbrock, N. Goradia, N. Sahoo, K. Galler, U. Neugebauer, J. Popp, S.H. Heinemann, O. Ohlenschlager, D. Imhof, Analysis of Fe(III) heme binding to cysteine-containing heme-regulatory motifs in proteins, ACS Chem Biol, 8 (2013) 1785-1793.
[13] M.P. Williamson, Using chemical shift perturbation to characterise ligand binding, Prog Nucl Magn Reson Spectrosc, 73 (2013) 1-16.
[14] N.J. Anthis, G.M. Clore, Visualizing transient dark states by NMR spectroscopy, Q Rev Biophys, 48 (2015) 35-116.
[15] A.J. Baldwin, L.E. Kay, NMR spectroscopy brings invisible protein states into focus, Nat Chem Biol, 5 (2009) 808-814.
[16] P. Neudecker, P. Lundstrom, L.E. Kay, Relaxation dispersion NMR spectroscopy as a tool for detailed studies of protein folding, Biophys J, 96 (2009) 2045-2054.
[17] A. Sekhar, L.E. Kay, NMR paves the way for atomic level descriptions of sparsely populated, transiently formed biomolecular conformers, Proc Natl Acad Sci U S A, 110 (2013) 12867-12874.
[18] S.P. Graether, Troubleshooting Guide to Expressing Intrinsically Disordered Proteins for Use in NMR Experiments, Frontiers in Molecular Biosciences, 5 (2019) 118.
[19] H.H. Brewitz, T. Kuhl, N. Goradia, K. Galler, J. Popp, U. Neugebauer, O. Ohlenschlager, D. Imhof, Role of the Chemical Environment beyond the Coordination Site: Structural Insight into Fe(III) Protoporphyrin Binding to Cysteine-Based Heme-Regulatory Protein Motifs, Chembiochem, 16 (2015) 2216-2224.
[20] E.W. Miles, J.P. Kraus, Cystathionine beta-synthase: structure, function, regulation, and location of homocystinuria-causing mutations, J Biol Chem, 279 (2004) 29871-29874.
[21] R. Banerjee, C.G. Zou, Redox regulation and reaction mechanism of human cystathionine-beta-synthase: a PLP-dependent hemesensor protein, Arch Biochem Biophys, 433 (2005) 144-156.
[22] M. Meier, M. Janosik, V. Kery, J.P. Kraus, P. Burkhard, Structure of human cystathionine beta-synthase: a unique pyridoxal 5'-phosphate-dependent heme protein, EMBO J, 20 (2001) 3910-3916.
[23] A. Kumar, A. Wissbrock, N. Goradia, P. Bellstedt, R. Ramachandran, D. Imhof, O. Ohlenschlager, Heme interaction of the intrinsically disordered N-terminal peptide segment of human cystathionine-β-synthase, Sci Rep, (2018).
[24] A.M. Gronenborn, D.R. Filpula, N.Z. Essig, A. Achari, M. Whitlow, P.T. Wingfield, G.M. Clore, A novel, highly stable fold of the immunoglobulin binding domain of streptococcal protein G, Science, 253 (1991) 657-661.
[25] D.J. States, R.A. Haberkorn, D.J. Ruben, A two-dimensional nuclear overhauser experiment with pure absorption phase in four quadrants, J Magn Reson, 48 (1982) 286-292.
[26] C. Wiedemann, N. Goradia, S. Hafner, C. Herbst, M. Gorlach, O. Ohlenschlager, R. Ramachandran, HN-NCA heteronuclear TOCSY-NH experiment for (1)H(N) and (15)N sequential correlations in ((13)C, (15)N) labelled intrinsically disordered proteins, J Biomol NMR, 63 (2015) 201-212.
[27] C. Wiedemann, P. Bellstedt, S. Hafner, C. Herbst, F. Bordusa, M. Gorlach, O. Ohlenschlager, R. Ramachandran, A Set of Efficient nD NMR Protocols for Resonance Assignments of Intrinsically Disordered Proteins, Chemphyschem, 17 (2016) 1961-1968.
[28] W. Bermel, I. Bertini, I.C. Felli, R. Kummerle, R. Pierattelli, Novel 13C direct detection experiments, including extension to the third dimension, to perform the complete assignment of proteins, J Magn Reson, 178 (2006) 56-64.
[29] W. Bermel, I. Bertini, I.C. Felli, R. Pierattelli, Speeding up (13)C direct detection biomolecular NMR spectroscopy, J Am Chem Soc, 131 (2009) 15339-15345.
[30] W. Bermel, I. Bertini, I.C. Felli, L. Gonnelli, W. Kozminski, A. Piai, R. Pierattelli, J. Stanek, Speeding up sequence specific assignment of IDPs, J Biomol NMR, 53 (2012) 293-301.
[31] J. Novacek, L. Zidek, V. Sklenar, Toward optimal-resolution NMR of intrinsically disordered proteins, J Magn Reson, 241 (2014) 41-52.
[32] W. Bermel, M. Bruix, I.C. Felli, M.V.V. Kumar, R. Pierattelli, S. Serrano, Improving the chemical shift dispersion of multidimensional NMR spectra of intrinsically disordered proteins, J Biomol NMR, 55 (2013) 231-237.

[33] T. Madl, I.C. Felli, I. Bertini, M. Sattler, Structural analysis of protein interfaces from 13C direct-detected paramagnetic relaxation enhancements, J Am Chem Soc, 132 (2010) 7285-7287.
[34] J. Lopez, R. Schneider, F.X. Cantrelle, I. Huvent, G. Lippens, Studying Intrinsically Disordered Proteins under True In Vivo Conditions by Combined Cross-Polarization and Carbonyl-Detection NMR Spectroscopy, Angew Chem Int Ed Engl, 55 (2016) 7418-7422.

Supplementary Material

Journal of Magnetic Resonance

NMR experiments on the transient interaction of the intrinsically disordered N-terminal peptide of cystathionine-β-synthase with heme

Amit Kumar[a], Peter Bellstedt[b], Christoph Wiedemann[c], Amelie Wißbrock[d], Diana Imhof[d], Ramadurai Ramachandran[a], and Oliver Ohlenschläger[a*]

[a]Leibniz Institute on Aging – Fritz Lipmann Institute, Beutenbergstr. 11, D-07745 Jena, Germany.
[b]Institute for Organic Chemistry and Macromolecular Chemistry, Friedrich Schiller University, Humboldtstr. 10, D-07743 Jena, Germany.
[c]Institute of Biochemistry and Biotechnology, Martin Luther University Halle-Wittenberg, Kurt-Mothes-Str. 3a, D-06120 Halle, Germany.
[d]Pharmaceutical Institute, University of Bonn, An der Immenburg 4, D-53121 Bonn, Germany.

[*]to whom correspondence should be addressed:
Oliver Ohlenschläger
oliver.ohlenschlaeger@leibniz-fli.de

Supplementary material contains 7 Figures (S1-S7).

Figure S1. 2D HCBCACON pulse sequence.

The delays are: Δ_0=1.7 ms, Δ_1=1.1 ms, Δ_2=4 ms, Δ_3=4 ms, Δ_4=4.5 ms, Δ_5=12.5 ms, Δ_6=6.25 ms, Δ_7=4.5 ms, Δ_8=8 ms, Δ_9=12.5 ms.
The phase cycle is: ϕ_1=y,y,-y,-y; ϕ_2=x,-x; ϕ_3=x,x,x,x,x,x,x,x,-x,-x,-x,-x,-x,-x,-x,-x; $\phi_{IPAP(IP)}$=x; $\phi_{IPAP(AP)}$=-y; ϕ_R=x,-x,-x,x,x,-x,-x,x,-x,x,x,-x,-x,x,x,-x.
Gradients with a sine-bell amplitude profile were used. Durations and strength (with respect to the maximum strength of 50 G/cm) are: $G_{1,2}$=1 ms (50%), 1 ms (30%).
The shaped pulse shaded red is a broadband adiabatic 180° pulse.

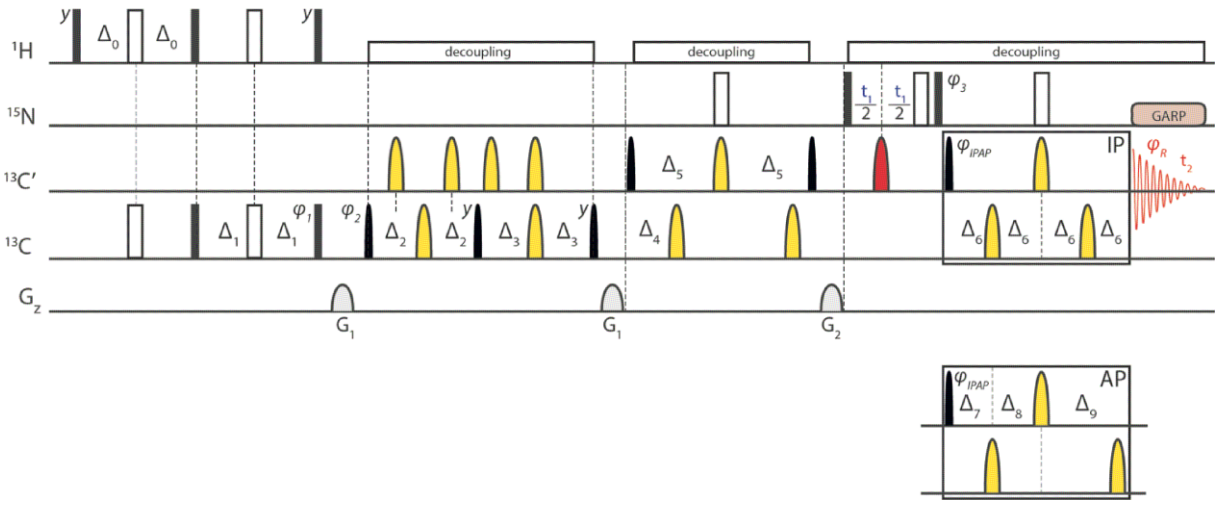

Figure S2. Superposition of the [^{1}H,^{15}N]-HSQC spectra of the GB1 fusion peptide CBS(1-40) (100 µM) without (blue) and with heme (100 µM, red). Interacting residues are indicated.

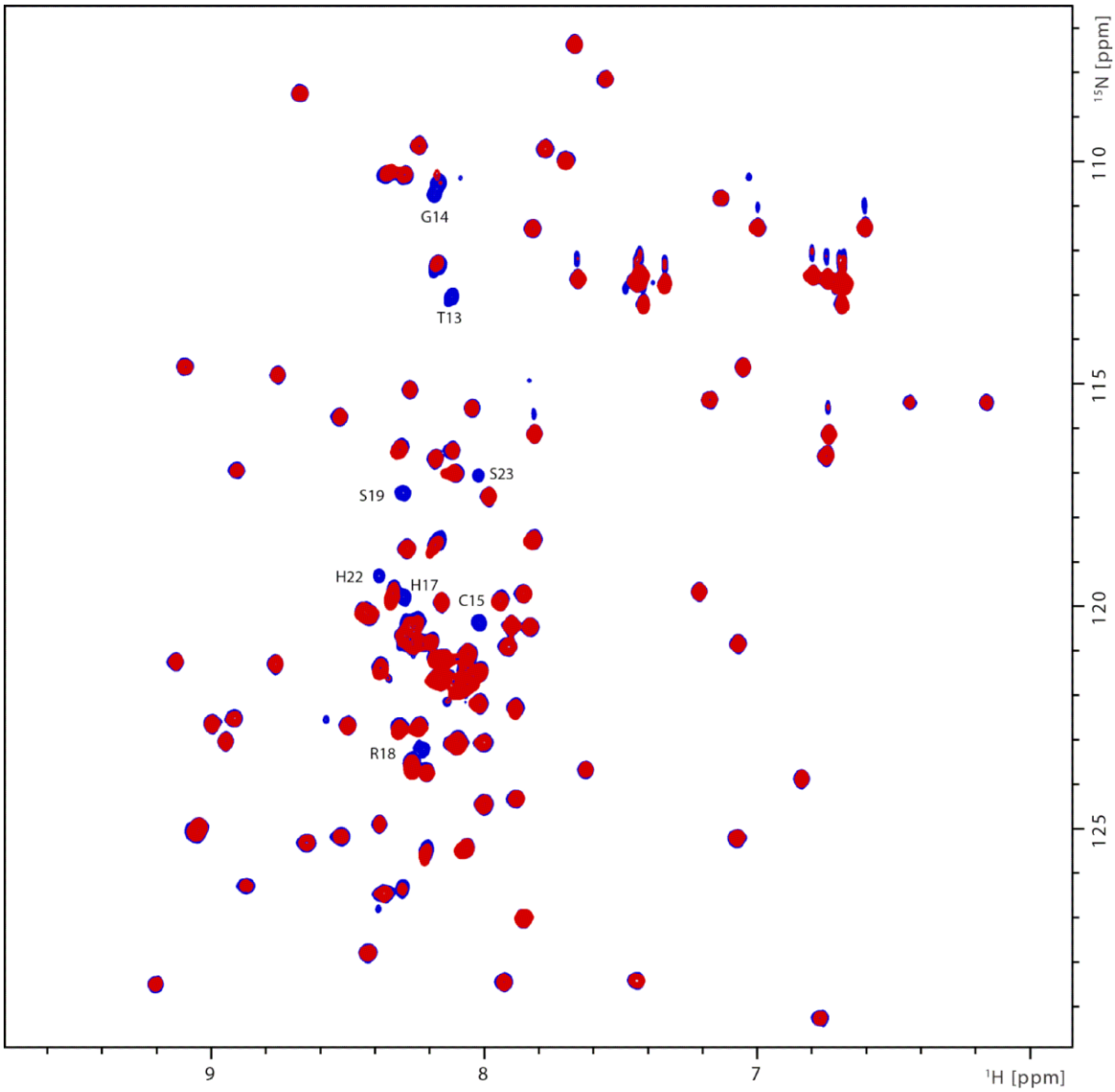

Figure S3. Superposition of the 2D $^{13}C^{\alpha,\beta}_{i}$-$^{13}CO_{i}$ correlation spectra (zoomed plot) of CBS(1-40) (250 μM) in 90% H_2O and 10% D_2O collected at 283 K *via* the (HCBCA)CO experimental protocol without (blue, 35 increments in the ^{13}C indirect dimension with a spectral width of 61 ppm, 112 transients per increment, recycle time of 1.0 s and a ^{13}CO acquisition time of 125 ms) and with heme (100 μM, 35 increments in the ^{13}C indirect dimension with a spectral width of 61 ppm, 400 transients per increment, recycle time of 1.0 s and a ^{13}CO acquisition time of 125 ms). Interacting residues are indicated.

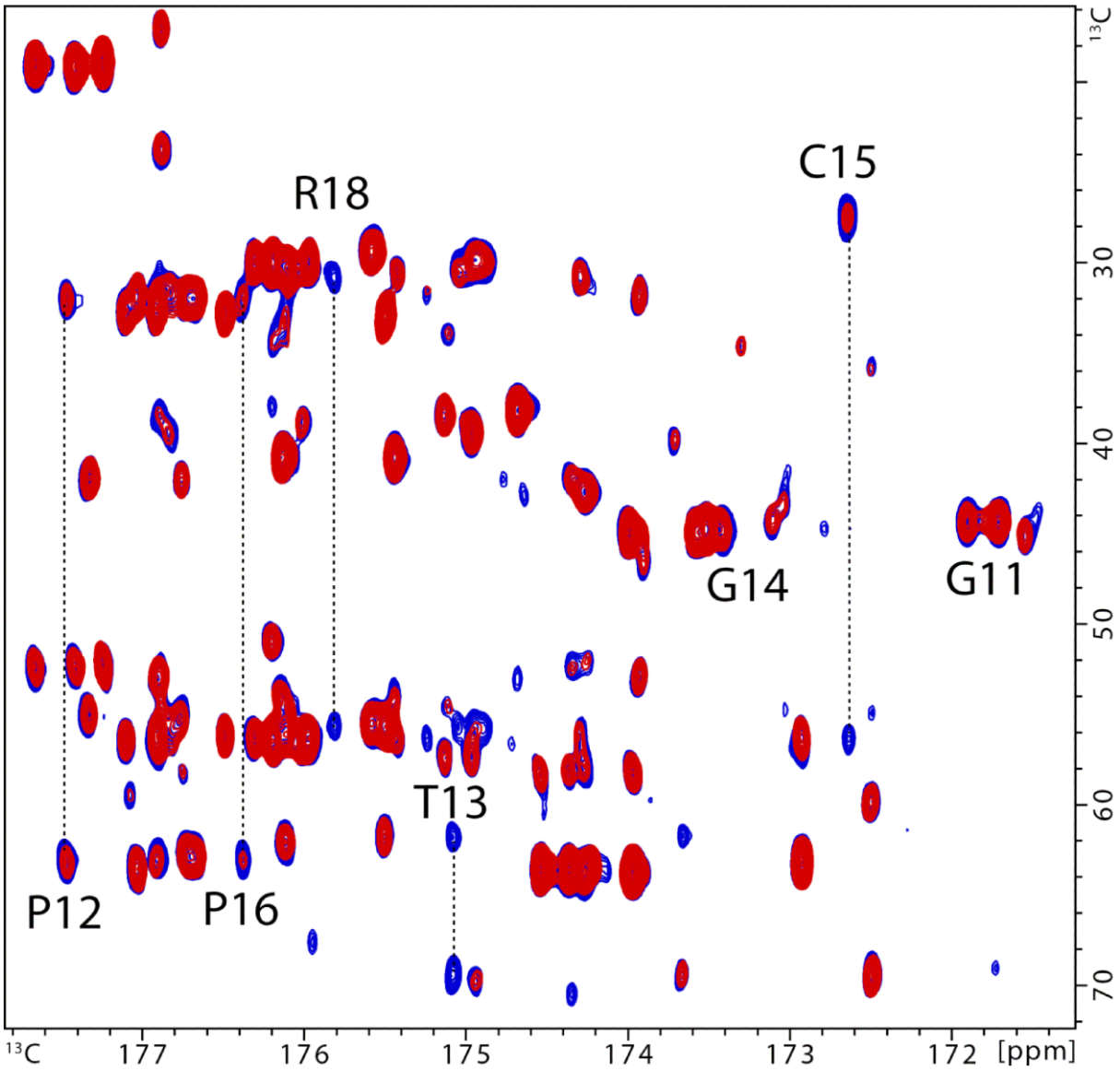

Figure S4. Superposition of the 2D $^{15}N_i$-$^{13}CO_{i-1}$ spectral projections from 3D HCBCACON spectra of CBS(1-40) (250 μM) at 310 K in D_2O collected without (blue) and with heme (100 μM) employing 61 increments in the ^{15}N dimension with a spectral width of 26 ppm, 42 increments in the ^{13}CO dimension with a spectral width of 8 ppm, 32 transients per t1 increment, recycle time of 1.0 s, $^{1}H^{\alpha}$ acquisition time of 100 ms, 20% non-uniform sampling in the indirect dimensions, and using linear prediction in the indirect dimensions for improved spectral resolution. Relevant amino acid residues ($^{15}N_i$) involved in interaction with heme are indicated.

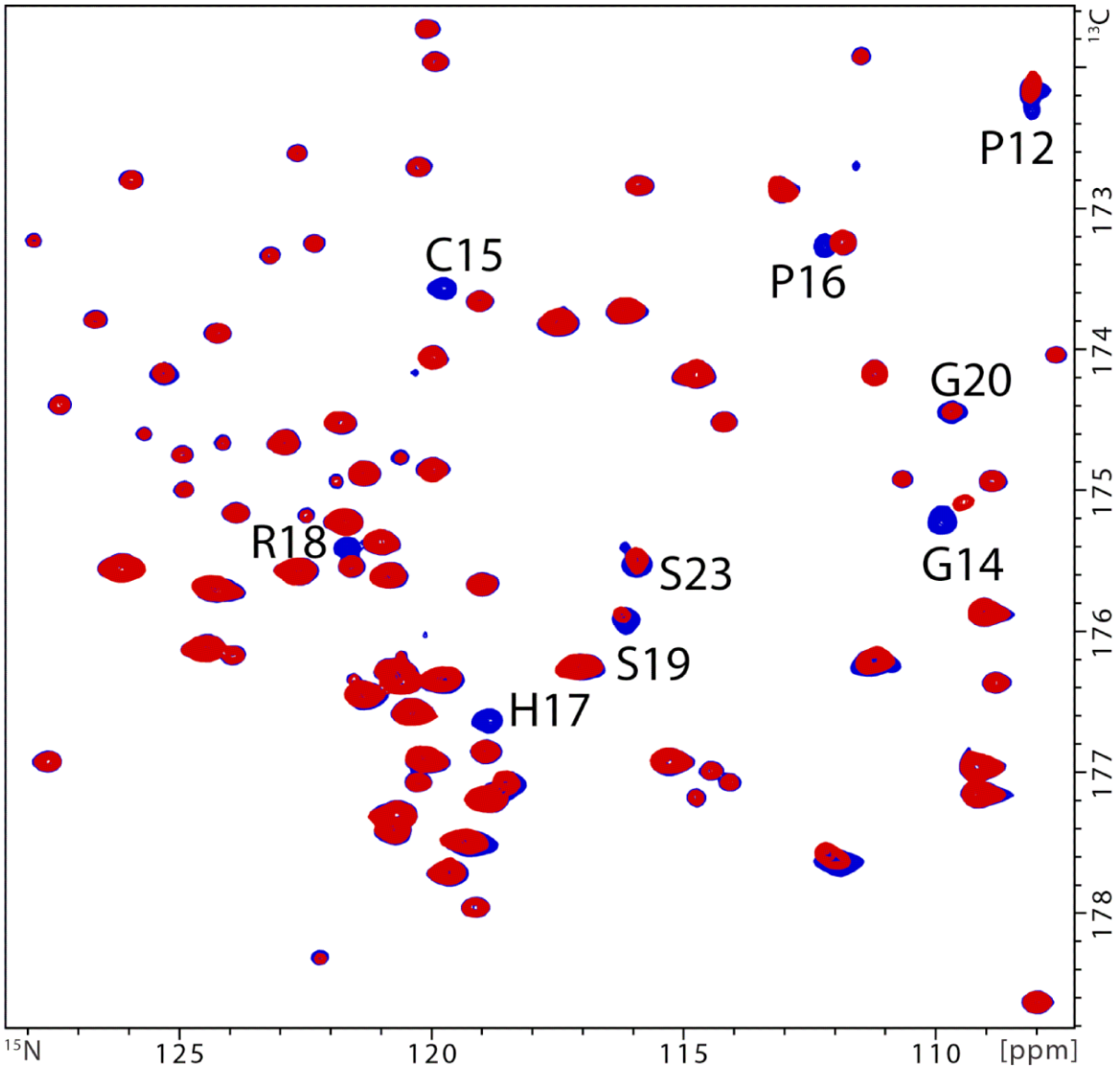

Figure S5. Superposition of the 2D $^{13}CO_{i-1}$-$^{1}H^{\alpha}_{i-1}$ (a) and $^{15}N_i$-$^{1}H^{\alpha}_{i-1}$ (b) spectral projections from 3D HCBCACON spectra of CBS(1-40) (250 µM) at 310 K in D_2O collected without (blue) and with heme (100 µM) employing 61 increments in the ^{15}N dimension with a spectral width of 26 ppm, 42 increments in the ^{13}CO dimension with a spectral width of 8 ppm, 32 transients per t1 increment, recycle time of 1.0 s, $^{1}H^{\alpha}$ acquisition time of 100 ms, 20% non-uniform sampling in the indirect dimensions and using linear prediction in the indirect dimensions for improved spectral resolution. Relevant amino acid residues corresponding to $^{13}CO_{i-1}$-$^{1}H^{\alpha}_{i-1}$ (A) and $^{15}N_i$ (B) involved in interaction with heme are indicated.

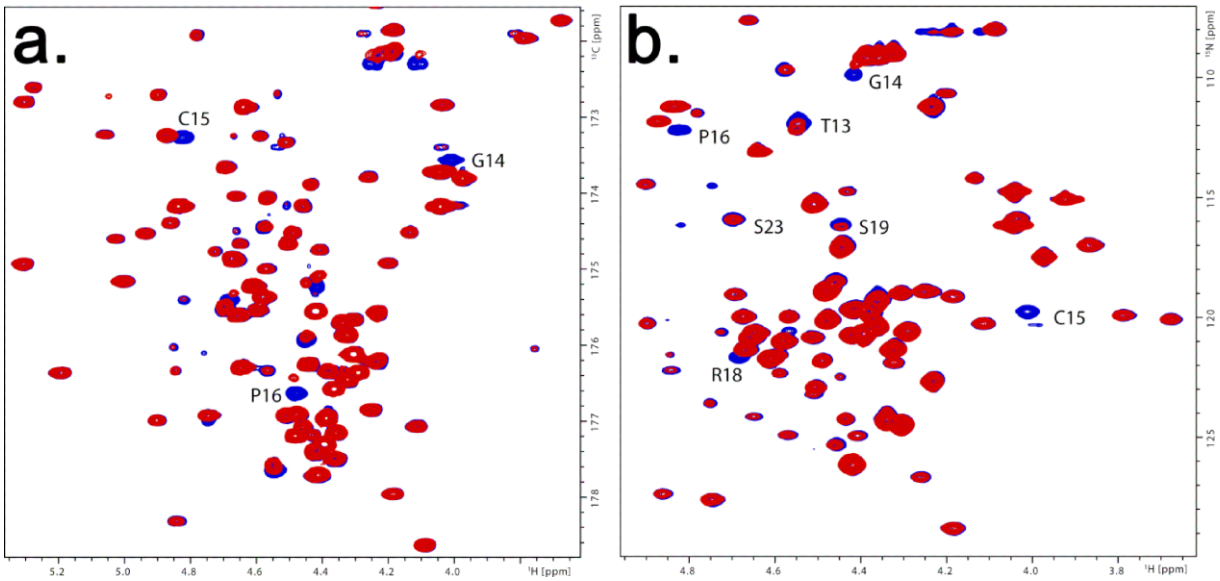

Figure S6. Superposition of the 2D $^{15}N_i$-$^{1}H^{\alpha}_{i-1}$ spectra generated *via* the 3D HCBCACON sequence using CBS(1-40) (250 µM). These spectra were collected at 310 K in D_2O without (blue) and with heme (100 µM) employing 100 increments in the ^{15}N dimension, with a spectral width of 26 ppm, 16 transients per increment, recycle time of 1.0 s, $^{1}H^{\alpha}$ acquisition time of 100 ms. Relevant amino acid residues ($^{15}N_i$) involved in interaction with heme are indicated.

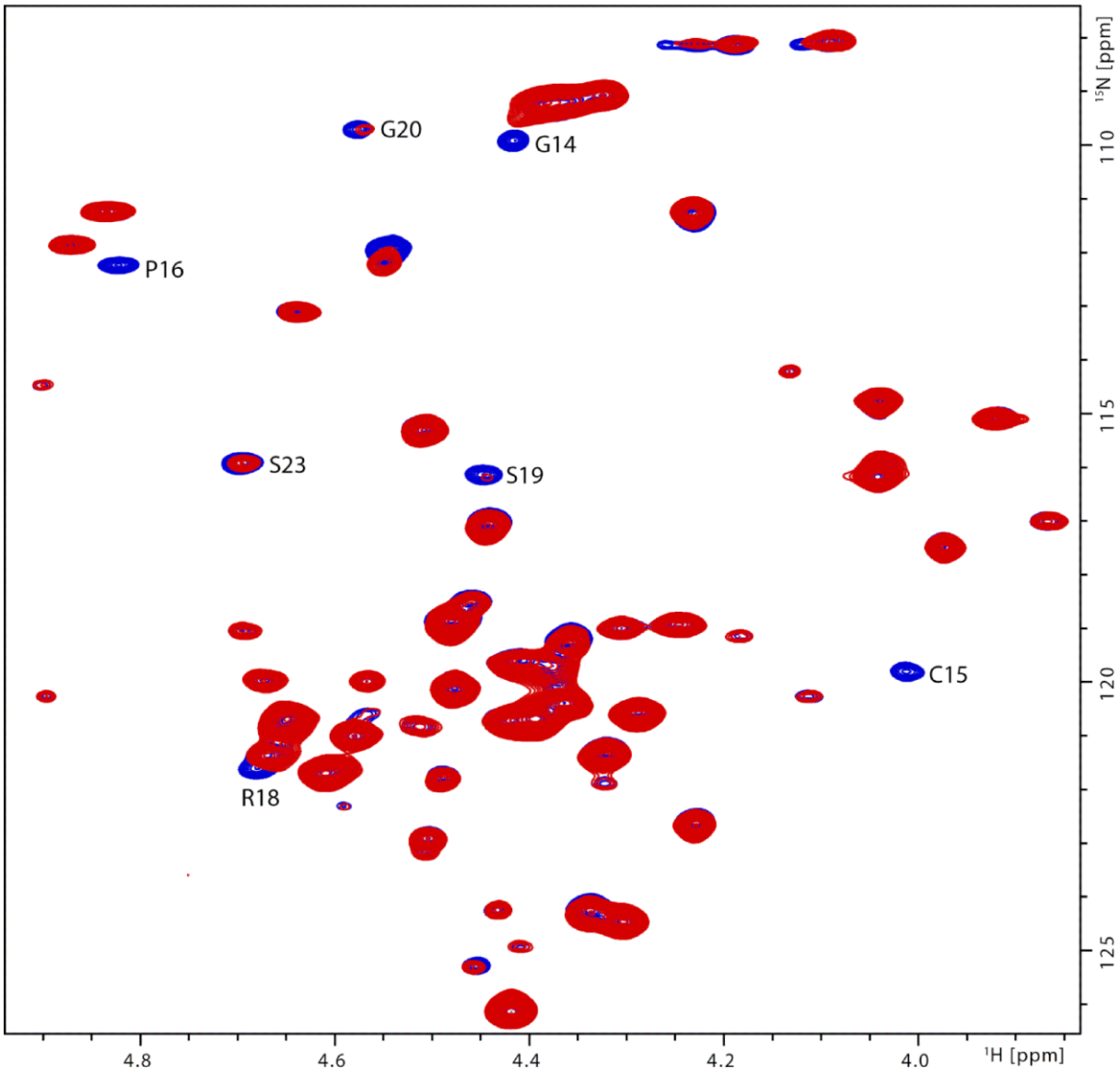

Figure S7. Superposition of the 2D $^{15}N_i$-$^{13}CO_{i-1}$ correlation spectra of CBS(1-40) (250 μM) mutant H22L collected *via* the (HCBCA)CON experimental protocol at 310 K in D_2O without (blue, 50 increments in the ^{15}N dimension with a spectral width of 26 ppm, 160 transients per increment, recycle time of 1.0 s and a ^{13}CO acquisition time of 125 ms) and with heme (100 μM, 50 increments in the ^{15}N dimension with a spectral width of 26 ppm, 160 transients per increment, recycle time of 1.0 s and a ^{13}CO acquisition time of 125 ms). Relevant amino acid residues ($^{15}N_i$) involved in the interaction with heme are indicated.

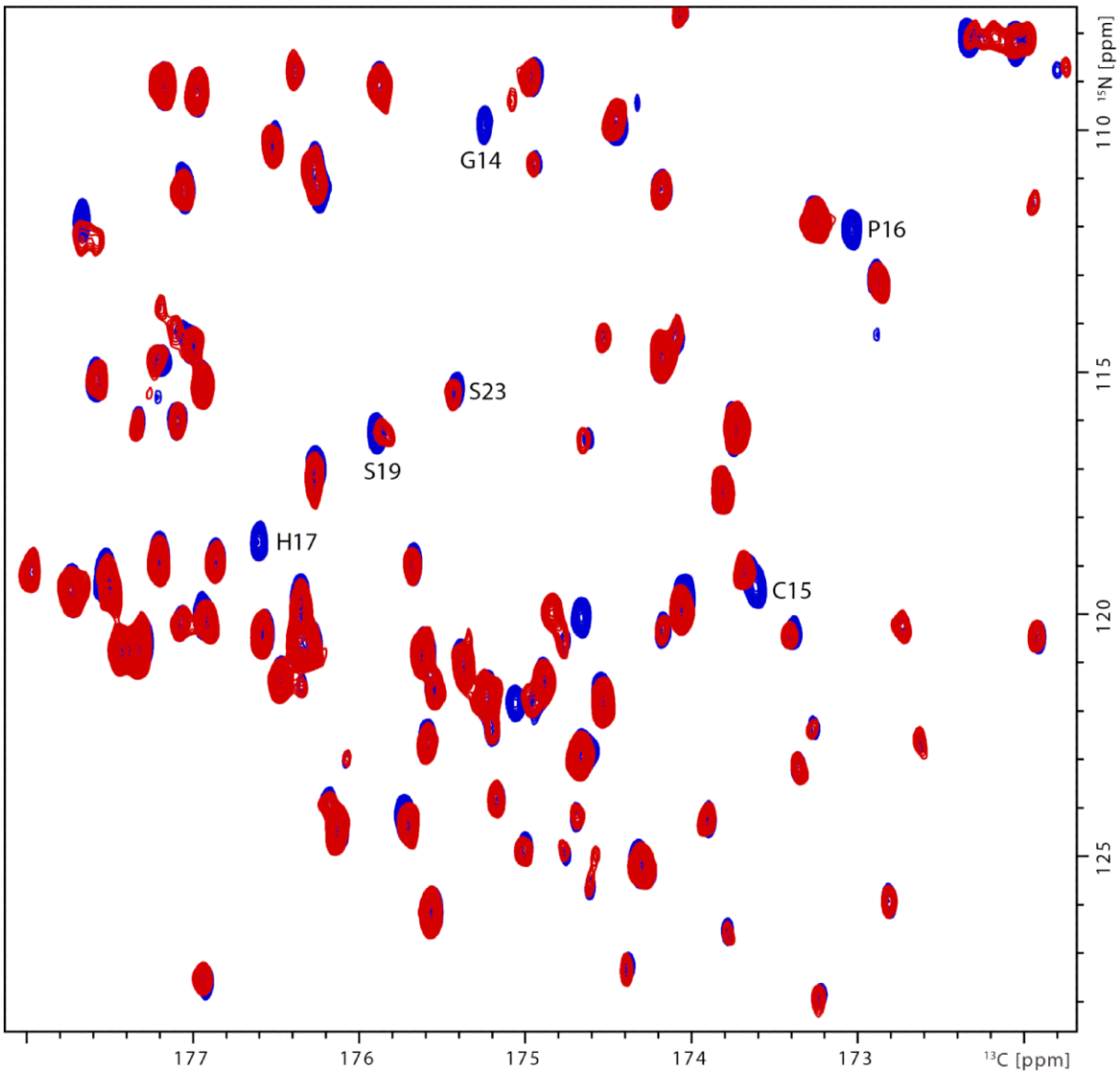

2.3 Structural insights into heme binding to IL-36α proinflammatory cytokine

Authors: Amelie Wißbrock, Nishit B. Goradia, **Amit Kumar**, Ajay Abisheck Paul George, Toni Kühl, Peter Bellstedt, Ramadurai Ramachandran, Patrick Hoffmann, Kerstin Galler, Jürgen Popp, Ute Neugebauer, Kornelia Hampel, Bastian Zimmermann, Susanne Adam, Maximilian Wiendl, Gerhard Krönke, Iqbal Hamza, Stefan H. Heinemann, Silke Frey, Axel J. Hueber, Oliver Ohlenschläger, Diana Imhof

Contributions: **AK contribution (25%)**
AW, NBG, **AK**, AAPG, PH, performed the research and analyzed the data. All the authors reviewed the manuscript. AW, DI, OO wrote the manuscript. DI and OO conceived the idea.

Status: Submitted to Scientific Report

Summary: This study reports for the first time heme regulation of interleukin-36 family members with the detailed experiments on interleukin-36α (IL-36α) protein. This manuscript describes the NMR solution structure of the IL-36α protein and structural binding details with its receptor. This paper also presents heme binding studies using NMR, UV/Vis, Raman spectroscopy to uncover the involved heme-regulatory motifs along with biological test to demonstrate the negative regulation of IL-36 mediated signaling by heme.

Structural insights into heme binding to IL-36α proinflammatory cytokine

Amelie Wißbrock[a,1], Nishit B. Goradia[b,1,2], Amit Kumar[b], Ajay Abisheck Paul George[a], Toni Kühl[a], Peter Bellstedt[c], Ramadurai Ramachandran[b], Patrick Hoffmann[d,e], Kerstin Galler[d,e], Jürgen Popp[e,f], Ute Neugebauer[d,e,f], Kornelia Hampel[g], Bastian Zimmermann[g], Susanne Adam[h], Maximilian Wiendl[h], Gerhard Krönke[h], Iqbal Hamza[i,j], Stefan H. Heinemann[k], Silke Frey[h], Axel J. Hueber[h], Oliver Ohlenschläger[b,*], and Diana Imhof[a,*,]

[a]Pharmaceutical Biochemistry and Bioanalytics, Pharmaceutical Institute, University of Bonn, D-53121 Bonn, Germany;
[b]CS Protein Production, Leibniz Institute on Aging/Fritz Lipmann Institute, D-07745 Jena, Germany;
[c]Institute of Organic and Macromolecular Chemistry (IOMC), Friedrich Schiller University Jena, D-07743 Jena, Germany;
[d]Center for Sepsis Control and Care (CSCC), Jena University Hospital, D-07747 Jena, Germany;
[e]Leibniz Institute of Photonic Technology (Leibniz IPHT), D-07745 Jena, Germany;
[f]Institute of Physical Chemistry and Abbe Center of Photonics, Friedrich Schiller University Jena, D-07743 Jena, Germany;
[g]Biaffin GmbH & Co KG, D-34132 Kassel, Germany;
[h]Department of Internal Medicine 3 – Rheumatology and Immunology, University of Erlangen-Nürnberg (FAU) and University Hospital Erlangen, D-91054 Erlangen, Germany;
[i]Department of Animal & Avian Sciences, University of Maryland, College Park, MD 20742;
[j]Department of Cell Biology & Molecular Genetics, University of Maryland, College Park, MD 20742;
[k]Center for Molecular Biomedicine, Department of Biophysics, Friedrich Schiller University Jena and Jena University Hospital, D-07745 Jena, Germany;
[1]These authors contributed equally.
[2]Current address: European Molecular Biology Laboratory, D-22607 Hamburg, Germany.
*Correspondence: dimhof@uni-bonn.de, oliver.ohlenschlaeger@leibniz-fli.de

Corresponding authors:
Diana Imhof, Pharmaceutical Biochemistry and Bioanalytics, Pharmaceutical Institute, University of Bonn, D-53121 Bonn, Germany, Phone: +49 228 735254, Email: dimhof@uni-bonn.de, ORCID: 0000-0003-4163-7334
Oliver Ohlenschläger, CS Protein Production, Leibniz Institute on Aging/Fritz Lipmann Institute, D-07745 Jena, Germany, Phone: +49 3641 656219, Email: oliver.ohlenschlaeger@leibniz-fli.de, ORCID: 0000-0002-6428-4423

Keywords: heme; interleukin; heme-binding protein; heme-regulatory motif

SUMMARY
Cytokines of the interleukin (IL)-1 family regulate immune and inflammatory responses. The recently discovered IL-36 group is involved in psoriasis, rheumatoid arthritis, and pulmonary diseases. We suggest heme interaction and regulation of IL-36 proteins, with a focus on IL-36α, based on in-depth analysis using various spectroscopic methods. We describe two heme-binding sites in IL-36α, which associate with heme in a pentacoordinated fashion. Solution NMR analysis reveals insight into structural features of the cytokine and the heme-cytokine complex. In addition, the structural determinants for receptor binding are traced back to N-terminal truncation of the proteins which is essential for biological activity of IL-36 members. Finally, we find that heme negatively regulates IL-36-mediated signal transduction in primary human patient fibroblasts. The present study substantially contributes to our understanding of the multiple functions of heme by providing structural insight into heme-binding proteins as well as by adding IL-1 cytokines to the group of potentially heme-regulated proteins.

INTRODUCTION

Regulatory heme is critical for physiological and pathological processes including neurodegenerative diseases and inflammation[1–6]. In fact, several processes including ion channel modulation[3] and transcriptional regulation[7] are influenced by transient heme interactions[2]. So-called heme-binding motifs (HBM) or heme-regulatory motifs (HRM) are responsible for heme association and allow for a fast dissociation of the effector due to moderate binding affinities[8–11]. Although the number of heme-regulated proteins is permanently increasing structural data is rare. Detailed functional and structural analysis of a plethora of HRM-containing peptides and proteins was performed in earlier studies. These investigations confirmed the specific role of cysteine residues for heme binding in the context of Cys-Pro dipeptide motifs (CP motifs)[9,10]. In silico analysis and database search for CP-motif-containing proteins[9] revealed a CP-motif in interleukin (IL)-36α, a member of the IL-1 superfamily. Sequence alignment and evaluation of the IL-36 family disclosed potential HRMs in all agonistic IL-36 cytokines with the CP motif being unique for IL-36α.

The IL-1 superfamily is a group of cytokines that act as key mediators of inflammatory responses explaining their pivotal role in chronic inflammatory diseases including rheumatoid arthritis (RA) and psoriasis[12]. IL-36 cytokines, namely IL-36α, IL-36β, IL-36γ, and the natural antagonist IL-36Ra, are members of the IL-1 family, which signal through the heterodimeric receptor complex IL-36R/IL-1RacP, mediating a pathway involving the activation of NF-κB and MAP kinases. Specific N-terminal proteolytic truncation of all IL-36 family members is required to generate the active cytokine species (trIL-36)[13,14]. Ultimately, IL-36 signaling leads to the production of proinflammatory cytokines, e.g. IL-6 and IL-8[15–17]. Since all three IL-36 cytokines signal through the same receptor complex, the occurrence, the level of cytokine production, and the activation mechanisms are discussed as critical differences between the individual family members[15]. Over the past decade, a pivotal role of IL-36 cytokines in inflammatory diseases has been described, in particular in psoriasis, a chronic, multifactorial skin disease[15–18]. An anti-IL-36R antibody (ANB019, ANAPTYSBIO) for generalized pustular psoriasis (GPP) treatment is currently under investigation and has reached in-human clinical trials[19]. However, effectors and regulatory mechanisms of IL-36 cytokines in both physiological and pathophysiological conditions remain largely unknown hampering the development of specific therapies[15].

We here demonstrate that IL-36-mediated signaling is significantly reduced upon heme association in human fibroblast-like synoviocytes from RA patients as detected by decreased p38 activation and diminished mRNA levels of IL-6 and IL-8. A substantiated structural analysis of the IL-36α-heme complex was performed using spectroscopic methods including SPR, UV/Vis-, resonance Raman- and 3D NMR spectroscopy. We present the binding characteristics and the solution NMR structure of IL-36α in complex with heme based on our recently published assignment of the free protein[20]. The findings presented herein extend the field of alternative heme functions by providing structural data on a potentially heme-regulated protein in complex with heme as well as revealing and classifying the network of hitherto unexploited heme effects.

RESULTS

Human agonistic IL-36 family members bind heme. There is raising evidence for tissue-dependent IL-36 expression but only little information on molecular regulation mechanisms of IL-36-mediated signaling[15]. IL-36 sequence evaluation revealed potential heme-binding sites raising the question whether heme acts as an IL-36 effector. Indeed, surface plasmon resonance (SPR) analysis revealed heme binding to the biologically active (truncated, tr) cytokines trIL-36α (aa 6-158), trIL-36β (aa 5-157), and trIL-36γ (aa 18-169) (Figure 1A). Bovine serum albumin (BSA) and lysozyme served as positive and negative controls, respectively, as reported earlier[6] (Supplementary Figure S1A). Sensograms of BSA and IL-36

proteins interacting with heme showed a complex biphasic binding profile and kinetic data were not fitted well by a 1:1 Langmuir binding model. A global heterogeneous ligand model, assuming the presence of two independent heme-binding sites, yielded better data fits. The data obtained did not allow for the conclusion of a distinct binding mode, such as cooperative binding of two heme molecules. All three trIL-36 proteins showed heme binding with comparable K_D values (Supplementary Table S1*)*. A similar binding behavior was observed for full-length IL-36α and trIL-36α, with a slightly faster ligand association to trIL-36α (Figure 1A, Supplementary Figure S1A). K_D values for both proteins were in the range of 3 to 4 μM for the interaction of the first heme molecule, and 9 to 13 μM for the second binding event. In addition, the binding kinetics of the heme-IL36 interaction can be distinguished into a faster and a slower binding event.

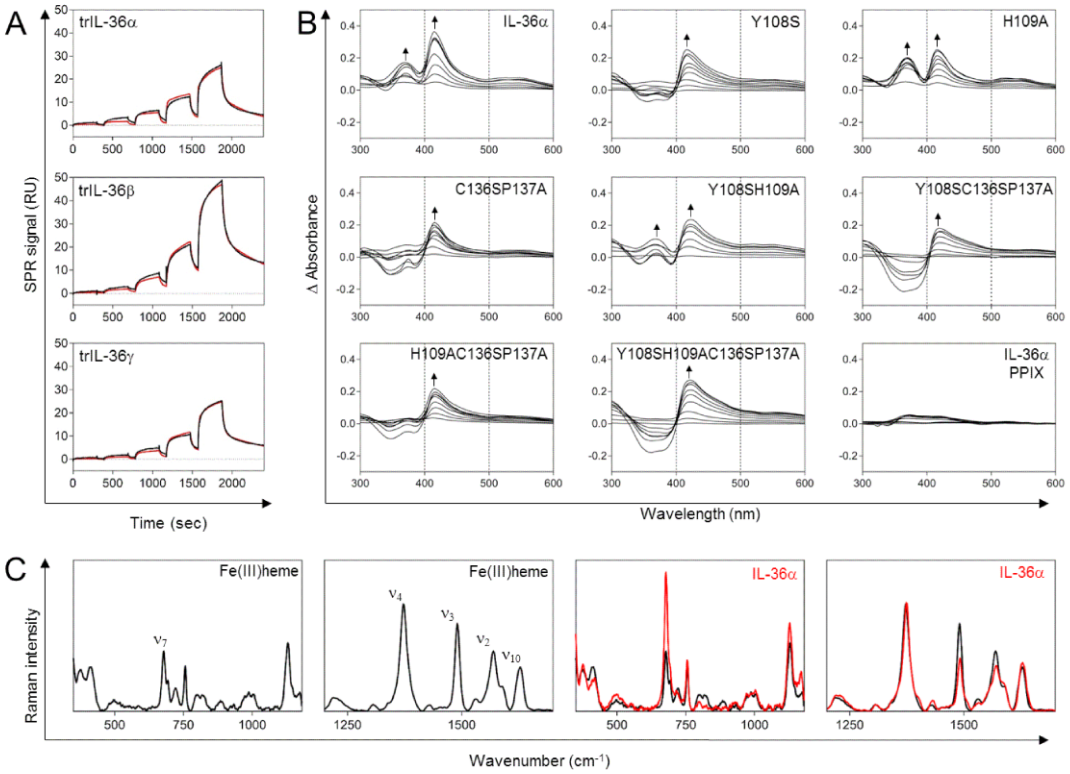

Figure 1. Spectroscopic studies on heme binding to agonistic IL-36 family members and IL-36α protein mutants. (A) SPR signal (RU) of trIL-36α, β and γ with five consecutive heme injections of increasing heme concentrations (80 nM to 20 μM) using the single-cycle kinetics method (fit is displayed in red).
(B) UV/Vis differential spectra of heme-incubated IL-36α and protein mutants. Arrows denote UV/Vis maxima whereas dashed lines at 400 and 500 nm indicate UV/Vis band width to illustrate band broadening as earlier found for unspecific heme binding [21].
(C) Raman spectra of heme (in black), and pentacoordinated wild-type IL-36α (in red) including wavenumber fingerprint region with assignment of prominent normal-mode frequencies ν_7 (681 cm^{-1}), ν_4 (1374 cm^{-1}), ν_3 (1492 cm^{-1}), ν_2 (1571 cm^{-1}) and ν_{10} (1628 cm^{-1}) for heme.

Next, sequence alignment was performed using Clustal Omega[22] in order to evaluate potential HRMs for a 2:1 (heme:protein) binding process (Supplementary Figure S1B, Table S2). Potential HRMs based on His, Tyr, and Cys as the axial ligands were found in all three cytokines, including both isoforms of IL-36β and γ. A CP motif was found in IL-36α (SEGG**C**136**P**137LIL), whereas other amino acids were identified in IL-36β (isoform 1: K136S137, isoform 2: Q135P136), and IL-36γ (isoform 1: Q147P148, isoform 2: Q112P113)

at the same position. The sequence of IL-36α (158 aa) contains ten potential heme-coordination sites (**m1-10**, Supplementary Figure S1B, Table S2*)* considering His (3 motifs), Tyr (3 motifs), and Cys (4 motifs) as axial ligand. From the ten potential HRMs, several motifs can be excluded due to their location and/or negative net charge as was earlier defined (Supplementary Table S2)[10,11]. Beside the aforementioned CP motif (**C**136**P**137), a promising Tyr-His (YH)-based HRM (**m8**/**m9**, FLF**Y**108**H**109SQSG) was selected. Further analysis was performed employing nonapeptides (**1-7**) including alanine mutants as model systems (Supplementary Table S3). Heme binding to the proposed 9mer CP-motif SEGG**CP**LIL revealed a UV shift to ~366 nm with a binding affinity of 3.75 ± 0.77 μM[9]. Alanine mutants of Cys and Pro confirmed the essential role of Cys for binding and a reduction of binding affinity upon Pro mutation[9] (Supplementary Figure S1C, Table S4). For the YH-based HRM a K_D of 4.48 ± 2.20 μM (~415 nm) was determined. Surprisingly, mutation of His and/or Tyr, i.e. YA and AH mutants, indicated heme interaction via tyrosine (Supplementary Figure S1C, Table S4), although binding to His-based motifs generally revealed higher binding affinities compared to Tyr-based ones in earlier studies[11]. The same approach applied to IL-36α also revealed potential HRMs in IL-36β and γ (Supplementary Figure S1B, Table S2), yet IL-36α was chosen for in-depth spectroscopic and structural studies due to the unique presence of the heme-binding CP motif.

Protein material was obtained by overexpressing IL-36α/ΔN5-truncated trIL-36α in *Escherichia coli* (Supplementary Figure S1D). Heme binding to the expressed IL-36 wild-type proteins (IL-36α, trIL-36α) was initially confirmed by SPR analysis (see above) and a fluorescence-based approach (Supplementary Figure S1E).

To investigate the heme-binding mode in more detail, UV/Vis measurements were performed using the experimental set-up established earlier (Figure 1B)[8,9]. BSA and lysozyme were again included as controls (Supplementary Figure S1F). Upon heme application to IL-36α the differential spectra exhibited absorbance maxima at ~369 nm and ~416 nm. A hypsochromic UV/Vis shift to ~370 nm is characteristic for heme binding via a CP motif in a pentacoordinated fashion [9,10,23]. The second absorbance maximum at ~416 nm is indicative of an additional interaction site involving another coordinating residue. The K_D values of the heme-IL-36α interactions were calculated to be 3.63 ± 2.67 μM (~369 nm) and 11.50 ± 3.06 μM (~416 nm), respectively. This indicated an interaction with two heme molecules per protein as suggested by SPR. No effect was observed when protoporphyrin IX (PPIX) was applied to IL-36α, proofing the essential role of the heme iron (Figure 1B). In order to examine the relevance of the two proposed HRMs, seven IL-36α protein mutants were produced as full-length and truncated forms in *E. coli*, i.e. Y108S, H109A, Y108SH109A, C136SP137A, Y108SC136SP137A, H109AC136SP137A and Y108SH109AC136SP137A (Supplementary Figure S1D). The UV/Vis differential spectra obtained for the protein mutants suggested altered heme binding compared to wild-type IL-36α in all cases (Figure 1B, Supplementary Figure S1*)*. Mutation of Y108 led to a significant decrease of binding affinity from 11.50 ± 3.06 μM (wild-type) to 30.69 ± 7.49 μM (Y108S) and to a loss of the UV/Vis shift to ~369 nm. The spectrum suggested a significant role of Y108 for heme binding to wild-type IL-36α. In contrast, the differential spectra of H109A was rather similar to the wild-type protein and displayed a shift to ~369 nm (K_D 0.77 ± 0.53 μM) and to ~416 nm (K_D 10.35 ± 3.16 μM), indicating that H109 has only a minor impact on heme binding. The differential spectra of the Y108SH109A mutant showed a less pronounced maximum at ~368 nm compared to wild-type IL-36α. Here determination of the binding affinity was not possible. In addition, a maximum at ~420 nm appeared (K_D 13.64 ± 4.69 μM). For the C136SP137A mutant a loss of the ~370 nm shift was observed suggesting that the CP motif is participating in heme binding to IL-36α (Figure 1B), which could be further confirmed by the mutants Y108SC136SP137A, H109AC136SP137A and Y108SH109AC136SP137A. The only exception is mutant Y108S for which no unambiguous conclusion could be reached thus far. A

UV/Vis shift to ~420 nm was found for mutant proteins Y108SC136SP137A (~419 nm, K_D 15.17 ± 4.35 μM), H109AC136SP137A (~417 nm, K_D 13.29 ± 3.12 μM), and Y108SH109AC136SP137A (~421 nm, K_D 14.23 ± 3.82 μM). It is worth noting that a striking broadening of the UV/Vis band at ~415-420 nm occurred in all Y108S protein mutants. This phenomenon was earlier found to be characteristic for a less specific or unspecific heme-protein interaction[21]. Therefore, it can be hypothesized that the Y108 mutation in IL-36α results in a loss of heme-binding specificity. Taking the peptide-based measurements into consideration, these observations indicate that the YH motif serves as heme ligand with Y108 representing the coordinating residue, and H109 supporting heme association. Thus, involvement of the suggested HRMs (C136P137, Y108H109) was successfully verified with different protein mutants. It was recognized, however, that additional residues might be involved in heme binding, yet in an unspecific fashion. In order to gain further insight into the complex geometry resonance Raman spectroscopy was applied.

Raman spectroscopy revealed a pentacoordinated IL-36α-heme complex. Resonance Raman spectroscopy with an excitation wavelength of 413 nm was conducted to selectively enhance characteristic vibrations of the heme moiety[10,11,24–26]. This provided insight into the geometry of heme complexes with IL-36α proteins and derived peptides (Figure 1C, Supplementary Figure S2, Table S1, S4). Spectral features obtained for the IL-36α-heme complexes are not as pronounced as usually found for peptide-heme complexes[9–11]. Wild-type IL-36α predominantly forms a pentacoordinated heme-complex as the coordination marker band ν_3 is still found around 1492 cm^{-1}, despite a neglectable shoulder around 1508 cm^{-1} and a slightly increased intensity of the ν_7 band (Figure 1C). The IL-36α H109A variant shows pentacoordination, and of all variants the highest similarity with the wild-type IL36α-heme complex (Supplementary Figure S2A). This is in agreement with the UV/Vis studies and supports the assumption that loss of H109 has the least effect on heme binding. Upon Y108S mutation, the ν_2 and the ν_3 bands reduce. The same spectral changes can be observed in the Y108SH109A variant, indicating that heme binding to this motif occurs via Y108. This is in accordance with resonance Raman data of the corresponding peptide-heme complexes and the aforementioned binding studies for the protein complexes (Supplementary Figure S2, Table S1, S4).
Mutations in the second heme-binding site suggested, i.e. C136SP137A (Supplementary Figure S2A, Table S1), led to the formation of a weak shoulder around 1504 cm^{-1} at the long wavelength side of the coordination-state sensitive ν_3 band. Furthermore, a decrease in intensities of the ν_3 and ν_2 bands and considerably increased intensities of the prominent vibrational modes ν_7 (around 681 cm^{-1}) as well as the oxidation state marker band ν_4 (around 1374 cm^{-1} for Fe(III)) might indicate the negligible formation of a hexacoordinated heme-complex despite the major presence of a pentacoordinated complex (Supplementary Figure S2A, Table S1)[27]. However, this behavior was neither present in all four mutants of the CP motif nor occurred it to the same extent, and thus should be interpreted with caution.

Full-length IL-36α and truncated IL-36α bind heme in a similar manner. To determine the solution structure of IL-36α we performed heteronuclear 3D NMR spectroscopy on the basis of previously derived NMR resonance assignments[20]. The conformers were calculated based on 4107 NOE constraints (Supplementary Table S5). The structure of IL-36α (Figure 2A, 2B) consists of 14 β-strands in three different β-sheets (XIV-I-IV-V-VI-VII-X-XI-XII-XIII, II-III, VIII-IX) composed in a canonical β–trefoil fold[28] as typical for cytokines of the IL-1 family[29]. These are supplemented by one short α-helix (I92-N97) of approximately 1.5 turns and two short 3_{10}- helical elements composed of three residues each. Five of the eleven loops (P34-M39 (loop 3), K79-Q82 (loop 6), S112-N115 (loop 8), E133-G135 (loop

10), L144-A147 (loop 11); Figure 3B) connecting the different β-strands exhibit higher structural disorder due to increased dynamics as also supported by the heteronuclear NOE data. This also includes loop 10 between strands VII and VIII of β-sheet 1, which directly precedes one of the potential heme-binding residues: Cys136. Superimposition with the X-ray structure of IL-36γ (sequence homology 67% at 57% identity; PDB code 4IZE; Supplementary Figure S6) results in a root-mean-square deviation (r.m.s.d.) of 1.63 Å for the backbone atoms of the ordered stretch P10-F158 excluding the loops.

The $\{^{15}N,^{1}H\}$-heteronuclear NOE data demonstrate that IL-36α with exception of the first ten N-terminal residues, i.e. including the residues cleaved by N-terminal processing, behaves as a rigid molecule (Supplementary Figure S3B). CD analysis confirmed the secondary structure elements of IL-36α obtained from the NMR studies by revealing a content of β-sheet fold between 20 and 35% (Supplementary Table S6, Figure S3A). Comparison of the $[^{1}H,^{15}N]$-HSQC spectra of IL-36α and trIL-36α (Supplementary Figure S3C) revealed - with exception of the missing cross peaks for the cleaved five amino acids - no major changes in the NMR fingerprint indicating that the truncation did not affect the 3D structural fold of the protein. In addition, the suggested HRMs (Y108H109, C136P137) are located at the C-terminus, while sequence truncation occurs at the N-terminus. Therefore, no significant change of the heme-binding behavior was expected. As aforementioned, binding studies with both proteins incubated with heme verified that heme binding occurred in a similar manner (Figure 1A, Supplementary Figure S1).

The NMR spectra of the IL-36α-heme complex indicated no change in the structural scaffold upon heme binding. In addition to the NMR experiments with Fe(III)-heme, SPR and NMR measurements were performed with Ga(III)-protoporphyrin as previously used[10,11,30,31]. The data suggested a similar interaction as observed for Fe(III)-heme. Variations in $[^{1}H,^{15}N]$-HSQC NMR cross peak intensities upon addition of heme to IL-36α (100 µM) were used to map the interaction interface. The superposition of the $[^{1}H,^{15}N]$-HSQC spectra of trIL-36α in the free and heme-bound state revealed a decrease in signal intensities for residues N19, R21, V22, I44, H51, T54, N61, Y108, H109, G113, R114, C136, D151, F152 (Supplementary Figure S3D). Thus, the NMR data of IL-36α-heme suggested that the CP motif functions as coordination site (Figure 2C-E). Moreover, the spectrum showed that at the given threshold the signal of H109 vanishes as a consequence of heme coordination to Y108, thereby supporting the attributed function of the YH site as second binding platform for heme beside of C136 (Supplementary Figure 2C-E).

Based on the NMR solution structure of IL-36α, we studied the possible binding mode of IL-36α and IL-36α-heme to its cognate receptor. Employing the coordinates of the ternary complex interleukin-1 receptor type-2 (IL-1RII)/interleukin-1 receptor accessory protein (IL-1RAcP)/interleukin-1β (IL-1β; PDB 3O4O)[32], we first superimposed the IL-36α structure onto the IL-1β moiety in the complex (cf. Supplementary Figure S3E for sequence alignment). The r.m.s.d. of 2.15 Å (IL-36α residues 10-15, 20-28, 29-34, 42-49, 60-87, 101-143, 149-158) indicates a good agreement of the backbone folds when neglecting loop areas (Supplementary Figure S6). Supplementary figure S6 shows the modeled IL-36α-IL-36R complex structure. The sequence mismatch between IL-1β and residues around K57-D58-R59 in IL-36α leads to a shortened loop conformation and thereby to a steric decompression of the molecular interaction area. Superposition revealed two major steric clashes (cf. Supplementary Figures S6A, C). Although flexible, the N-terminal residues M1-L5 cannot be accommodated in the V-shaped cleft between two β-sheet elements near residues W260 and G280 of IL-1RII. However, binding of truncated trIL-36α is not hindered because the remaining flexible amino acids K6-T9 are positioned in the upper and opened part of this V-shape. This might explain why for full activation of the IL-36α function N-terminal processing is required. In the superposition, the flexible loop K36-M39 clashes with the

stretch H21-R24 of receptor domain-I. However, domain-I is linked to receptor domain-II by a short bent linker element (E114-T116). A rotation centered at this linker element allows for repositioning domain-I to avoid disruptive van der Waals interactions between the receptor and IL-36α. The X-ray structure of the complex reveals that domain-I of the IL-1RII displays only one stabilizing hydrogen bond to domain-II (R27Hη12/22-Y125Oη), which would be perished by the domain reorientation. In contrast, no major domain movement is necessary to accommodate IL-36α at domain-III. Heme binding to trIL-36α before complex formation increases the gross shape of the molecule and leads to further steric impacts especially in the linker region between domains II and III of IL-1RAcP which may diminish the functional efficacy of the receptor complex.

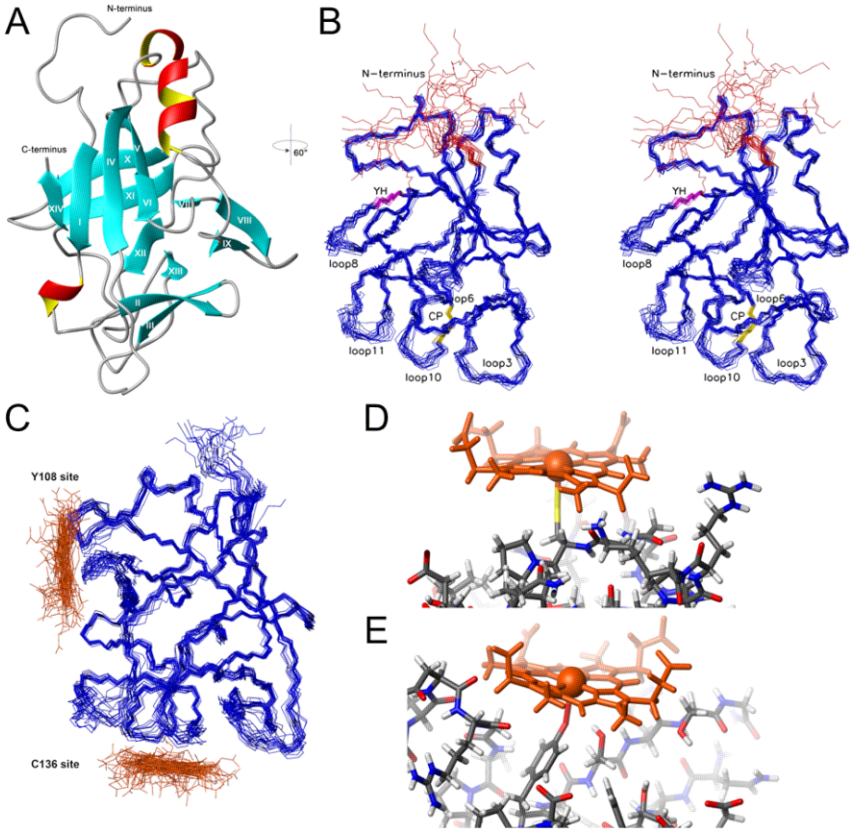

Figure 2. Structural analysis of IL-36α.
(A) NMR structure of IL-36α with numbered β-sheet elements indicated by cyan arrows, α-helical elements in red/yellow and loop regions in grey.
(B) Stereoview of the 20 best energy minimized conformers. Flexible loops are indicated and the flexible N-terminal residues, the C136P137 and Y108H109 sites are colored (Met1-Thr9 – red, Cys136Pro137 – gold, Tyr108His109 – magenta).
(C, D and E) Bundle of the IL-36α-heme complex (IL-36α backbone in blue, heme in orange) (C). Detailed view of the heme coordination at Cys136 (D) and Tyr108 (E).

Computational studies support experimental results for heme binding to IL-36α. The availability of NMR solution structures of free and heme-bound IL-36α facilitated investigations of heme binding to the protein by employing molecular docking and molecular dynamics (MD) simulations. The NMR structures also formed the basis for creating *in silico* structure models of the seven IL-36α mutant proteins (Figure 3, Supplementary Figure S4). Heme binding predicted by the Vina [33] docking algorithm helped to determine optimal conformations of the heme-protein interactions. Heme coordination to wild-type IL-36α was

found to occur via C136 and Y108 according to the top two complexes from the docking run, which is in agreement with the experimental data (Figure 3, Supplementary Movie S1, S2). The docked pose for binding via C136 was established by the heme iron placed at a proximity of 2.72 Å from the sulfur atom of C136. The docked pose was further characterized by stabilizing interactions of the surrounding residues namely T29, I31, A32, V33, P34, S132, E133, G134, G135, P137, L138, I139 and N148 (Figure 3A, B). The docked pose of heme bound via Y108 had the iron ion placed 2.32 Å from the oxygen atom of Y108. This pose was supported by additional surrounding residues, namely D58, R59, H109, S110, S112, T117 and F127 (Figure 3, Supplementary Movie S1, S2).

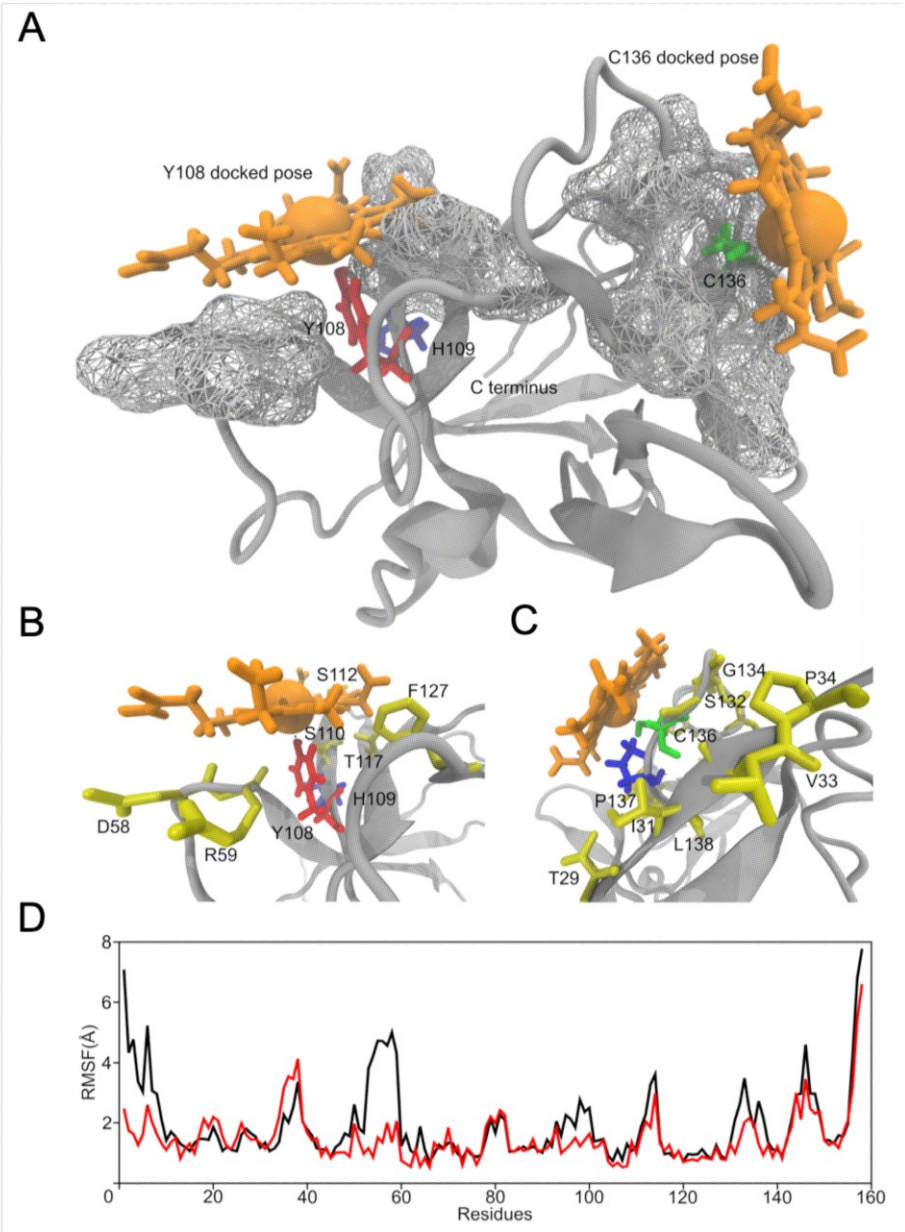

Figure 3. Heme binding to IL-36α and its effects on the protein supported by molecular docking and MD simulation studies.
(A, B and C) The structure of wild-type IL-36α (grey) with two heme molecules (orange) docked at C136 (green) and Y108 (red), respectively (H109, blue). Wireframe surfaces drawn around both binding sites (C136, Y108) represent surfaces of IL-36α residues that make contact with the heme molecule as predicted by the

docking algorithm (A). A zoom up at Y108 (B) (Y108, red; H109, blue) and C136 (C) (C136, green; P137, blue). Residues that stabilize the heme-bound conformation (yellow) are labeled.
(D) Comparative residue wise root mean squared fluctuation (RMSF) profiles of the heme bound (red) and the free states (black) of the protein. The RMSF profiles were generated from 200 ns equilibration MD simulations of the free protein and the protein-heme complex. Clear reduction of fluctuations from their mean position is noticed for several amino acids in the heme-bound state indicating the effect of heme binding to the protein.

Heme negatively regulates IL-36-mediated signal transduction in primary human patient fibroblasts. IL-36α induces expression of proinflammatory mediators such as IL-6 and IL-8 in synovial fibroblast-like synoviocytes (FLS) from RA patients[16]. Since heme binds to IL-36α, the question arises whether this interaction has an effect on IL-36α-induced activation of FLS. Human FLS were thus treated for 24 hours with different ratios of IL-36α in complex with heme.

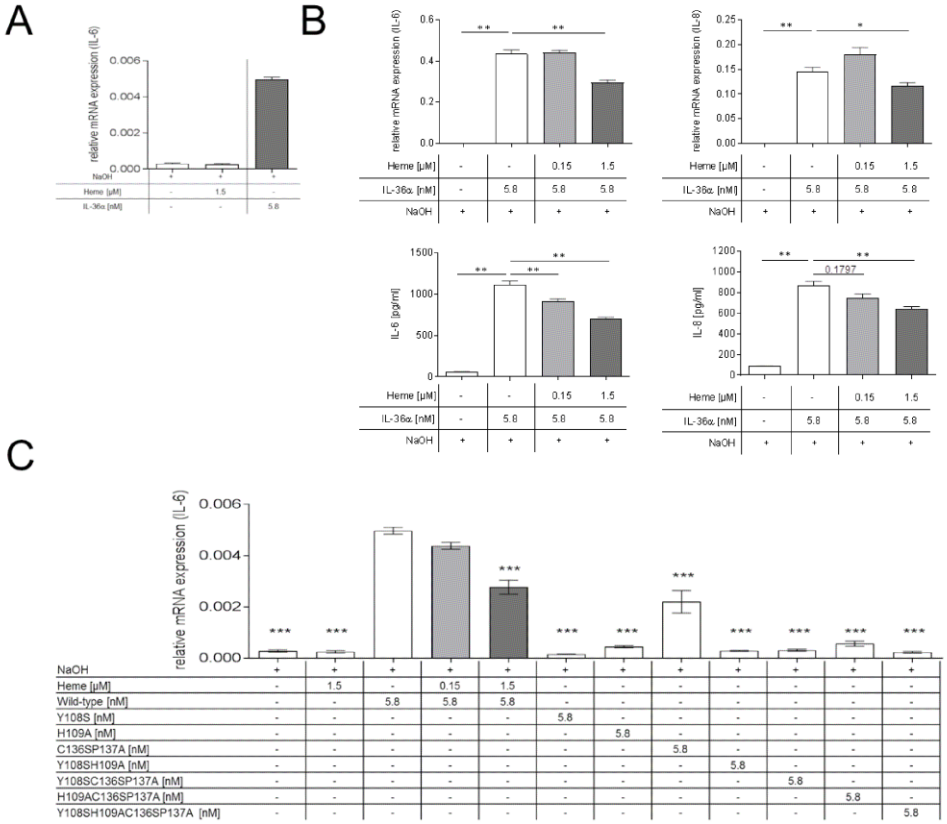

Figure 4. Heme impairs IL-36-mediated signal transduction in human patient FLS.
(A and B) FLS from RA patients were treated with heme (A) or two ratios of heme-IL-36α (B) for 24 h. Relative mRNA expression of IL-6 and IL-8, normalized to GAPDH, was analyzed by quantitative real time PCR (top) and concentration of cytokines in the cell culture supernatant was measured by ELISA (bottom). Values are means + SEM. One representative experiment (n=6) of two independent experiments is shown. Statistical analysis was performed using Mann-Whitney Test Bonferroni corrected with *$p < 0.05$ and **$p < 0.01$.
(C) Induction of IL-6 expression is impaired for IL-36α variants with altered heme-binding sites. FLS from RA patients were treated with varying ratios of IL-36α or IL-36α mutants to heme for 24 h (light and dark grey bars). Relative mRNA expression of IL-6, normalized to GAPDH, was analyzed by quantitative real-time PCR. Values are means + SEM of one experiment (n=3). Statistical analysis was performed using One-Way Anova Test Dunnet corrected, with *$p < 0.05$ and **$p < 0.01$ and ***$p < 0.0001$ for comparisons with recombinant trIL-36α.

Cytotoxicity was determined to exclude the components triggering a significant reduction of cell viability (Supplementary Figure S5A). IL-36α (5.8 nM) alone induced expression in FLS

of both, IL-6 and IL-8 mRNA, whereas heme did not have an effect on the expression levels of IL-6 and IL-8. Stimulation with the IL-36α-heme complex at two ratios (26:1 and 260:1) corresponding to 0.15 and 1.5 μM of heme resulted in significantly decreased expression of IL-6 and IL-8 compared to the controls (Figure 4A, 4B). The heme concentration was chosen according to earlier studies considering the scavenging effect of unspecific heme binding to BSA[34]. In addition to the aforementioned, the treatment with IL-36α-heme led to a significant reduction of IL-6 and IL-8 release in the supernatant (Figure 4B, lower panels). Finally, heme impaired IL-36α-mediated signaling in FLS, showing decreased activation of p38 (Supplementary Figure S5B). Similar results were observed for IL-36 family members IL-36β and γ (Supplementary Figure S4C). This confirms heme binding to all agonistic IL-36 family members as was shown by SPR. In summary, IL-36-heme interaction led to a reduced expression of IL-6 and IL-8 in human patient-derived FLS.
The IL-36α protein mutants earlier introduced were investigated using the same experimental set up to test the impact of the individual heme-binding motifs. IL-6 expression was significantly reduced in all IL-36α-mutant-treated FLS compared to IL-36α (Figure 5C). Abrogation of IL-6 expression suggests that mutations in the heme-binding motifs of IL-36α impact the protein's functionality. On the one hand, the mutations may have a major impact on protein folding, structure and consequently biological activity. On the other hand, the mutated residues might be pivotal for receptor binding. In support of this, the only protein mutant with a non-mutated YH motif (mutant C136SP137A) showed biological activity, even if reduced with respect to wild-type IL-36α. This suggests a crucial role of the YH motif and surrounding amino acids for the IL-36α receptor interplay.

IL-36α-heme complex does not exhibit peroxidase-like activity. A peroxidase-like activity of heme-peptide/protein complexes has been discussed to be critical due to cytotoxic ROS formation [4,35–37]. We thus tested the peroxidase-like activity of IL-36α-heme-complexes in two different ratios (1:1 and 1:2, protein:heme) as well as of both heme-binding motifs (CP, YH) on the peptide level (Supplementary Figure S5D). No significant increase of the heme's peroxidase activity (100%) was observed upon complex formation with proteins and peptide, respectively, which is in agreement with the results obtained for the CP-based HRM on peptide level in previous studies (Wißbrock et al., 2017). The activity of the amyloid-beta(40)-heme complex in the same TMB-based system was 550%[37]. The observation that all complexes did not show a significant effect upon heme binding indicates that the YH motif in IL-36α is not mediating a peroxidase-like activity as was earlier found for the YXXHH-motif in e.g. amyloid beta[35–38].

DISCUSSION

We show that heme interacts with the agonistic IL-36 family members α, β, and γ. Heme-IL-36 complex formation impairs IL-36 signaling and leads to a decreased production of the proinflammatory cytokines IL-6 and IL-8 *in vitro* (Figure 5). Further studies are required to clarify the *in vivo* situation. It is worth noting that in case of severe hemolysis concentrations of unbound heme in the range of 20 to 350 μM have been described[39–41].
Two heme molecules bind to one protein molecule in *in vitro* studies, one with a higher and the second with a lower binding affinity. Based on experimental and computational studies, there is strong evidence that the proposed C136P137 motif is responsible for the association with one heme molecule. For the second binding event a significant role of Y108 as heme axial ligand is proposed, while H109 acts as an assisting residue for the neighbor. A closer look revealed that wild-type IL-36α forms a pentacoordinated complex with heme as demonstrated by *resonance* Raman and 3D NMR spectroscopy. According to earlier studies, CP motifs strongly tend to form pentacoordinated complexes, supporting heme binding to the C136P137 motif. Predominantly pentacoordination was also found for Y-based HRMs,

supporting that the second heme is bound in a pentacoordinated fashion to Y108H109 in IL-36α, too.

Structural investigation of full-length and trIL-36α revealed that there is no major structural change upon N-terminal cleavage that is required for full biological activity. This supports the notion that the significantly reduced activity of full-length IL-36α is due to a very flexible region at the N-terminus that blocks necessary association sites for IL-36α-receptor binding. Indeed, modeling of the NMR structure of IL-36α into the X-ray structure of the receptor complex (Figure 5A, Supplementary Figure S6) revealed steric clashes with the IL-1RII domain-III that can be minimized by the N-terminal truncation. Heme binding to IL-36α further increases the steric demand in areas close to the IL-1RII domain-I and the linker between IL-1RAcP domains-II and -III (Figure 5A). Whether the IL-36α-heme complex is not able to interact with the receptor IL-36R at all, or IL-1RacP recruitment is inhibited by the complex remains to be clarified (Figure 5B). However, it was shown that the interaction between heme and IL-36α leads to a decreased IL-36-mediated signal transduction *in vitro* and would consequently evoke an anti-inflammatory effect in the body. Except for the C136P137A mutant, none of the other IL-36α variants exhibited biological activity impeding a functional investigation of the role of the two binding sites. The Y108H109 motif, however, appears to be of great importance with regard to the protein's functionality. In fact, point mutations in IL-36 cytokines were shown to have a significant impact on the protein function, including an alteration of agonistic/antagonistic properties as well as loss of function[29].

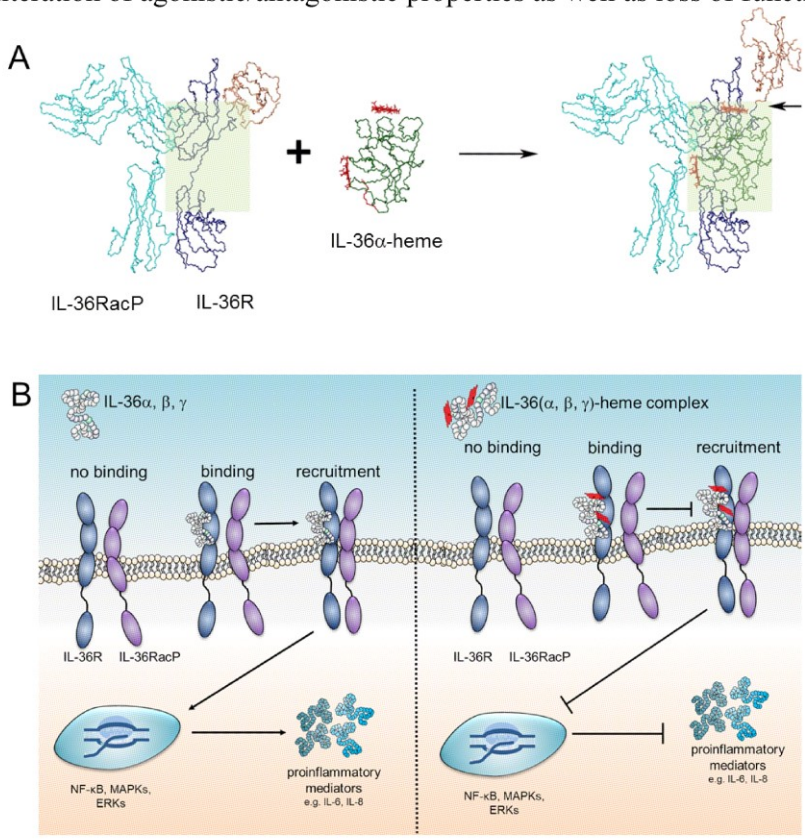

Figure 5. Potential physiological scenarios of IL-36-heme complex formation.
(A) IL-36α-heme binding to the receptor IL-36R may lead to steric clashes (indicated by an arrow) as identified by docking of the complex into the X-ray structure of the IL-1RII receptor complex (PDB: 3040,[32]).
(B) Different scenarios are conceivable that explain decreased IL-36-mediated signaling upon heme binding, either ligand binding is completely diminished or recruitment of the accessory protein (IL-36RacP) is impaired.

In the context of pathophysiological functions of heme[1], our findings seem to deviate at first sight. However, heme has been shown earlier to inhibit the classical complement pathway mediated by C-reactive protein and immune complexes via interaction with C1q[42] as an endogenous negative-feedback regulator. With respect to cellular damage where heme is released in high concentration, heme was suggested to support an anti-inflammatory event as part of a rescue system[42]. The role of IL-36 cytokines in such high heme-releasing conditions (e.g. trauma, malaria) is yet unclear. In addition, contributions of other interleukins in such scenarios are unknown so far. A sequence analysis of e.g. IL-1 family members and other interleukins revealed potential HRMs, too. CP motifs as such are present, for example, in IL-1Ra and IL-33. In addition, other motifs may also be appropriate, e.g. a sequence stretch around H54 in IL-1β or H76 in IL-33, while heme binding to other interleukins such as IL-18 seem less likely considering an in-house evaluation for potential HRMs.
To the best of our knowledge, this study is the first report on a direct heme-interleukin interaction, a comprehensive structural investigation of IL-36α, its complex formation with heme as a potential physiological regulator and biological consequences resulting from it. This adds further human proteins to the list of possible candidates regulated by heme and, in turn, increases knowledge in the field of "hemeostasis". Furthermore, our study provides a deeper insight into structural reasons for the lack of biological activity of the full-length IL-36 protein due to disabled interaction with the receptor. We thus anticipate that the emerging IL-36 research will gain momentum, in particular with regard to the biological relevance of IL-36 regulation in physiological and pathophysiological conditions.

AUTHOR CONTRIBUTION
Research was designed by D.I. and O.O.. A.W., N.G., A.K., A.A.P.G., P.B., R.R., T.K., P.H., K.G., K.H., S.A., and M.W. performed experiments. Data analysis and interpretation was performed by B.Z., U.N., J.P., S.F., A.H., G.K., I.H., S.H.H., O.O., and D.I.. All authors compiled and edited the manuscript.

ACKNOWLEDGEMENTS
Financial support by the Deutsche Forschungsgemeinschaft (DFG) within FOR1738 (to DI, UN, OO, JP, and SHH) and SFB813 (to DI) is gratefully acknowledged. The FLI and IPTH are members of the Leibniz Association (WGL) and are financially supported by the Federal Government of Germany and the State of Thuringia. Financial support in part by Collaborative Research Centers SFB1181 (project no. A05) and the doctoral training program GRK1660 from the DFG (to SA, SF) are gratefully acknowledged.

DECLARATION OF INTERESTS
Authors declare no conflict of interest.

SUPPLEMENTAL INFORMATION
Supplemental Information includes five figures, seven tables and two videos and can be found with this article.

METHODS DETAILS

Recombinant protein expression

pET-28a (Novagen, Madison, Wisconsin, USA) was used as expression vector of the gene encoding 158 amino acids (long version) and 153 amino acids (truncated version, tr) of IL-36α and mutants, respectively, and was inserted into the NdeI/XhoI site. An N-terminal protein His_6 tag and the essential thrombin cleavage site between the tag and the gene-encoding sequence were introduced into the long versions. The procedure used leaves three additional amino acids (Gly-Ser-His) attached at the N-terminus of full-length IL-36α (161 amino acids). In contrast, a caspase-3 (DEVD) cleavage site was cloned into the vector before amino acid K5 of IL-36α in the truncated proteins. Following the BL21(DE3) *E. coli* (Novagen, Madison, Wisconsin, USA) transformation, cells were plated onto kanamycin including plates. Eventually a single colony was inoculated into kanamycin containing (50 µg/mL) Luria Bertani (LB) medium. After the colonies were grown up to an OD_{600nm} 0.7, the bacteria cultures were enlarged to 500 mL of LB medium. For NMR studies of wild-type full-length IL-36α and trIL-36α, the primary cultures were inoculated into $^{15}NH_4Cl$ and $^{13}C_6$-glucose containing M9 medium (500 mL). Protein expression was induced by 0.3 mM IPTG for 18 h at 18 °C. Subsequently a lysis buffer (50 mM Tris/HCl, 300 mM NaCl, 5 mM imidazole, 5 mM β-mercaptoethanol (pH 8)) was applied for cell lysis followed by French press and centrifuged at 10.000 × g. After lysis Ni-NTA agarose resin (GE Healthcare, Freiburg, Germany) was used for purification of the cell lysate. Upon washing with 5 mM and 10 mM imidazole-containing lysis buffer (10 column volumes each), the protein was eluted applying 0.25 M imidazole. Cleavage of the His_6 tag was performed at 4 °C overnight using 5 U/mg of thrombin (Sigma-Aldrich, Taufkirchen, Germany). In case of the truncated proteins, 1 mg of caspase-3 (produced in-house) was used to cleave 40 mg of trIL-36α overnight in dialysis buffer (50 mM HEPES, pH 7.4, 75 mM NaCl, 2 mM DTT) at 4 °C. This procedure leads to no additional overhang residues at the N-terminus. The overnight-cleaved protein was applied on a pre-equilibrated Ni-NTA column with overnight dialysis buffer, followed by elution with same dialysis buffer to collect remaining digested protein and leaving undigested protein bound to the column. Collected flow through was concentrated to 1-1.5 mL using a 3-kDa Amicon filter before injection onto a 16/60 Hiload S75 size exclusion chromatography column (GE Healthcare, Freiburg, Germany) that was pre-equilibrated with 20 mM Tris/HCl (full-length) or 20 mM HEPES (truncated), pH 7.4, 150 mM NaCl, 2 mM DTT. Protein fractions were combined, concentrated and the buffer was replaced to 20 mM sodium phosphate buffer (pH 6.9). Samples were either lyophilized or directly used for the further experiments.

SDS-PAGE

SDS-PAGE (gel electrophoresis) of the recombinantly expressed proteins was performed on tricine gels. 18% acrylamide/bis(acrylamide) with 5% cross-linking were used for the resolving gel, whereas the stacking gel contained 5% acrylamide/bis(acrylamide) with 3.3% cross-linking. Upon fixation with 5% glutaraldehyde (30 min) the gels were stained with colloidal Coomassie[43,44].

Peptide synthesis and purification

An EPS 221 peptide synthesizer (Intavis Bioanalytical Instruments AG, Cologne, Germany) was used for the synthesis of all presented peptides (**1-7**). using a standard Fmoc (N-(9-fluorenyl)methoxycarbonyl) protocol for automated solid-phase peptide synthesis and employing HBTU and HOBt as coupling reagents. Rink amide MBHA resin (0.53 mmol/g) served as polymer support. Peptide cleavage was performed adding 100 µL of reagent K (75 mg phenol, 25 µL ethandithiol, 50 µL thioanisol, 50 µL water) in 1 mL of TFA per 100 mg resin. Crude products were purified by semi-preparative RP-HPLC on a Shimadzu LC-8A

system equipped with a Knauer Eurospher 100 column (C18, 250 × 32 mm, 5 µm particle size, 100 Å pore size) using gradient elution with 0.1% TFA in water (eluent A) and 0.1% TFA in 90% acetonitrile/water (eluent B) as the mobile phases. Analytical HPLC on a Shimadzu LC-10AT system with a Vydac 218TP column (C18, 4.6 × 25 mm, 5 µm particle size, 300 Å pore size) was used to analyze peptide purity. The mobile phase consisted of 0.1% TFA in 100% water as eluent A and 0.1% TFA in acetonitrile as eluent B. Applied gradients for the individual peptides are listed in Supplementary table S3. Detection was at 220 nm in all cases[9–11].

Mass spectrometry

Molar masses of all peptides were detected with an LC-ESI micrOTOF-Q III system (Bruker Daltonics GmbH, Bremen, Germany) coupled to a Dionex Ultimate 3000 LC (ThermoFisher Scientific, Dreieich, Germany). An EC 100/2 Nucleoshell RP18 column (C18, 100 × 2 mm, 2.7 µm particle size, 90 Å pore size, Macherey-Nagel, Düren, Germany) was used prior to infection into the MS instrument. Mass spectra were analyzed using the Data Analysis 4.1 software (Bruker Daltonics GmbH, Bremen, Germany). Information about the molar mass of individual peptides can be found in the Supplementary table S3.

Amino acid analysis

Peptide content was determined by amino acid analysis applying an ion exchange chromatography system. Peptide hydrolysates (6 N HCl at 110 °C for 24 h) were analyzed using an Eppendorf Amino Acid Analyzer LC 3000. An external standard (Laborservice Onken GmbH, Gründau, Germany) was used for data evaluation. Expected results were obtained for all peptides with respect to amino acid composition. Peptide content (in %) was used to calculated concentrations of all peptides prepared and stored as lyophilized powders prior to the experiments.

Preparation of heme solution

If not stated otherwise, Fe(III)heme referred to as heme (1 mM) was dissolved in 30 mM NaOH and incubated for 30 minutes under the exclusion of light. The solution was further diluted in the buffer system required according to the respective experiment.

Surface plasmon resonance measurements

SPR measurements were performed on a Biacore T200 instrument (GE Healthcare Europe GmbH, Freiburg, Germany) at 25 °C. The running buffer was 10 mM HEPES (pH 7.4), 150 mM NaCl, 0.05% Tween 20. The proteins BSA (VWR Life Science AMRESCO, Germany), lysozyme (AppliChem GmbH, Darmstadt, Germany), IL-36α (protein expression), trIL-36α (R&D Systems, Minneapolis, MN, USA), trIL-36β (isoform 2, R&D Systems, Minneapolis, MN, USA) and trIL-36γ (R&D Systems, Minneapolis, MN, USA) were covalently immobilized by amine coupling on a CM5 sensor chip (GE Healthcare, Freiburg, Germany). Briefly, lysozyme was diluted to a final concentration of 2.5 µg/mL in acetate buffer (pH 7.0), and BSA was diluted to 2.5 µg/mL in acetate buffer (pH 5.0). trIL-36 α, trIL-36β, and trIL-36γ were diluted to 0.85 µg/mL in acetate buffer (pH 4.0). Subsequently, the proteins were separately injected at 10 µL/min on an EDC/NHS activated flow cell until immobilization levels of 1600 RU (lysozyme), 1050 RU (trIL-36α), 2900 RU (BSA), 937 RU (trIL-36β) and 320 RU (trIL-36γ) were achieved. An activated/deactivated flow cell was used for reference subtraction. For determination of K_D values and kinetic parameters, a titration series of five consecutive injections with increasing heme concentrations (0.08 µM, 0.31 µM, 1.25 µM, 5 µM, 20 µM, diluted in running buffer) was performed at a flow rate of 30 µL/min using a standard single-cycle kinetics method implemented in the Biacore T200 Control Software

(GE Healthcare). Afterwards, the surface was regenerated by two injections of 25 mM NaOH/500 mM NaCl. An injection series of running buffer for double referencing was subtracted from each curve. Data were globally fitted using the heterogeneous ligand analysis model.

UV/Vis spectroscopy

A Multiskan GO microplate spectrophotometer (ThermoFisher Scientific, Dreieich, Germany) was used for UV/Vis measurements. Heme and peptide solutions were prepared in 100 mM Hepes buffer (pH 7.0). IL-36 cytokines (~5 μM), dissolved in 20 mM sodium phosphate buffer (pH 6.9), were incubated with heme (0.2 to 40 μM) in the dark at room temperature for 60 minutes before UV/Vis spectra were measured at 300 to 600 nm. Protein concentrations were corrected using the calculated molar absorption coefficient at 280 nm. Peptides **1-7** (20 μM) were incubated with heme for 30 minutes in the dark at room temperature[9].

Fluorescence spectroscopy

All measurements were performed on a fluorescence spectrophotometer FP-8300 (Jasco, Tokyo, Japan). BSA (1 μM) and lysozyme (1 μM) were dissolved in PBS buffer (pH 7.4) and IL-36α variants (1 μM) in 20 mM sodium phosphate buffer (pH 6.9), were each dissolved in and incubated for 60 minutes with varying heme concentrations (0.1 - 16 μM) in the dark. Parameters were set to excitation at 306 nm, emission at 352 nm, bandwidth 10 nm (extinction) and 20 nm (emission)[21].

Resonance Raman spectroscopy

Resonance Raman spectroscopic measurements were conducted utilizing a Horiba Jobin-Yvon LabRam HR 800 Raman spectrometer (Horiba, Kyoto, Japan) equipped with a back-illuminated deep-depletion CCD detector (1024 × 256 pixels) cooled by liquid nitrogen. For excitation of Raman scattering, a Coherent Innova 300C ion laser using the krypton line at 413.1 nm was applied. The Raman system was connected to an Olympus BX41 upright microscope (Olympus, Tokyo, Japan) with a motorized XY microscope stage and a 20x objective (Olympus UPlanFL N, NA 0.50) which served to focus the incoming laser light onto the sample as well as for the collection of the 180° backscattered light. Aqueous solutions (phosphate buffered NaCl, pH 7.0) of heme (400 μM) and peptide or protein were equimolarly mixed. The heme solution used here was prepared using a protocol established in earlier studies[9]. The reaction mixture was incubated for 30 min (for peptides) or 60 min (for proteins) in the dark at room temperature and centrifuged to remove precipitant before measurement of the supernatant solution.

Circular dichroism (CD) spectroscopy

The secondary structure content of IL-36α was estimated using the algorithms CAPITO (CD Analysis and Plotting tool)[45] and K2D3[46]. CAPITO takes advantage of the available validated protein CD spectra in the Protein Circular Dichroism Data Bank (PCDDB) repository, while the K2D3 analysis is based on the k-nearest neighbors algorithm for pattern recognition. The wavelength range used for K2D3 was 190-240 nm. The data obtained from the programs mentioned is shown in Supplementary table S6.

NMR structure analysis

Solution NMR experiments were performed at 283 K on Bruker Avance III spectrometers with proton frequencies of 750 and 600 MHz. The IL-36α samples were dissolved in 20 mM phosphate buffer with 65 mM NaCl and 5% D_2O using the freeze-dried solid compound. For NMR studies of the heme-bound form, Ga(III)-protoporphyrin IX chloride (data not shown) and heme were used as obtained from Frontier Scientific (Logan, USA). Protein [^{1}H,^{15}N]-

HSQC spectra in the free and heme-bound state were recorded at concentrations of 100 µM for trIL-36α and of 140 µM for wild type IL-36α. NMR data were acquired and processed with Topspin (Bruker, Rheinstetten, Germany) and analyzed with XEASY[47]. Based on heteronuclear 3D NMR spectroscopy, an almost complete resonance assignment could be achieved[20]. Distance constraints were extracted from a NOESY spectra acquired with 120 ms mixing time. Upper limit distance constraints were calibrated according to their intensity in the NOESY spectrum. Cross peaks of vicinal and geminal protons were used as calibration reference. Torsion angle constraints were obtained from local conformational analysis with the FOUND module[48]. In addition, torsion angle constraints defining the allowed ϕ,ψ-regions in the Ramachandran map were included. The 20% of structures with the lowest CYANA target functions[49] were selected to represent the NMR solution structures. The figures were produced using MOLMOL[50].

Creation of IL-36α mutant structures

The structures of the seven IL-36α proteins mutants were created based on the NMR solution structure of IL-36α using the *Mutator* plugin of the VMD[51] program (version 1.9.3). Point mutations were iteratively introduced to the starting IL-36α NMR structure replacing Cys and Tyr residues by Ser and His and Pro residues by Ala. A single residue was mutated at each iteration and the resultant mutated structure was energy minimized by a simulated annealing energy minimization protocol using the Yasara (version 18.2.7)[52] molecular modeling and simulation suite. In this manner, the seven mutants of IL-36α namely Y108S, H109A, Y108SH109A, C136SP137A, Y108SC136SP137A, H109AC136SP137A and Y108SH109AC136SP137A were generated. All final mutant structures were energy minimized before being used for molecular docking and molecular dynamics (MD) simulations.

Molecular dynamics simulations

MD simulations were run using the MD macro in Yasara[53] (Yasara structure version 18.2.7)[21]. All simulations were run with a 2 fs time step using the AMBER99SB-ILDN force field[54]. Force field parameterization of the simulated system was done by the AutoSMILES method (http://www.yasara.org/autosmiles) implemented in Yasara. This entails parameter assignment for the protoporphyrin system using GAFF[55] and AM1-BCC[56] with Fe(III) vdW parameters taken from Li et al.[57] as reported previously[21]. The protein (or the heme-protein complex) was placed in the center of a cubic simulation cell with a distance of at least 15 Å from the edge of the box. The cell was filled with the 3 point model[58] of water with a physiological concentration of 0.9% NaCl. Periodic boundary conditions were used and a cut-off for long range was set at 8 Å. Long range coulomb interactions were accounted for by the particle-mesh Ewald[59] method. All simulations were run in the NPT ensemble at 298 K and the pressure maintained at 1 atm for 200 ns. Molecular graphics were produced using VMD and plots using Grace version 5.1.25 (http://plasma-gate.weizmann.ac.il/Grace/).

Molecular docking simulations

Molecular docking simulations were conducted using Yasara software[52] and the ensemble docking method[60] implemented in the program. A receptor ensemble of 20 high scoring side chain conformations at 298 K was created by the program on which the ligand heme (ChemSpider[61], 16739951) was docked 400 times. This resulted in 8,000 runs per docking experiment. The search space for docking H109 was narrowed to a 10 Å radius around H109, whereas the full structure of the protein was covered as the docking search space for all other runs. Results from docking runs were scored by predicted binding energies. A clustering method that employs a 5 Å heavy atom RMSD threshold between docked conformations was

used to sort the final set of docked complexes. The top five complexes ranked by predicted binding energies were subject to closer investigation.

Isolation of human fibroblast-like synoviocytes

Human fibroblast-like synoviocytes (FLS) were isolated from knee joints of rheumatoid arthritis patients obtained at the University Hospital Erlangen-Nuremberg[62]. All patients gave written informed consent, and their use for research was approved by the ethics committee of the University hospital Erlangen (ethic licenses 4013 and 4065). We confirm that all methods were performed in accordance with the relevant guidelines and regulations. Human RA FLS kept at 37 °C and 5% CO_2 in a humidified incubator upon isolation. They were cultured in RPMI and DMEM at a ratio of 1:5, supplemented with 50 U/mL penicillin, 50 µg/mL streptomycin, 0.2% amphotericin and 2% fetal bovine serum. Cells between passages 3 to 8 were used.

Stimulation of RA FLS with trIL-36α, mutants and heme

For stimulation experiments, human FLS from RA patients were seeded at a concentration of 100,000 cells/mL in 500 µL culture medium in a 48-well plate one day prior to the experiment. Before stimulation of FLS, heme was pre-incubated with trIL-36α or trIL-36α protein mutants with substituted amino acids in the proposed heme-binding site in medium for 1 h at room temperature in the dark. Herein, the concentration of trIL-36α or trIL-36α mutants was kept constant at 5.8 nM with varying ratios of IL-36α to heme (1:26 and 1:260, i.e. 0.15 µM and 1.5 µM). Cells were then incubated for either 5 min (western blot analysis of phosphorylation) or 24 h (qPCR and ELISA). Sample separation was performed by a reducing 2D gel electrophoresis (10% SDS polyacrylamide gel) and blotted to a nitrocellulose membrane by semi-dry transfer. Blocking was performed using 5% BSA/TBST for 1 h at room temperature, before the blots were incubated overnight at 4 °C with antibodies (rabbit anti-P-p38, rabbit anti-p38 and rabbit anti-GAPDH) from Cell Signaling Technology (Leiden, the Netherlands). As secondary antibody anti-rabbit HRP (Biozol, Eching, Germany) was applied. A Pierce™ ECL Western Blotting Substrate (Thermo Fisher Scientific, Dreieich, Germany) was used for detection according to the manufacturer's instruction. Western Blot images were acquired in the chemiluminescence-imager CELVIN® S (Biostep, Burkhardtsdorf, Germany) with the software SnapAndGo (Version 1.6.1). Protein detection parameter are: p38 (Exposure time 10 min, dynamic range 1 to 12,080), P-p38 (Exposure time 110 min, dynamic range 1 to 12,080) and GAPDH (Exposure time 6 min, dynamic range 1 – 12,080). Cell viability was analyzed using the AlamarBlue assay according to the manufacturer’s instruction (#741802, Invitrogen, Carlsbad, CA, USA), and absorbance was measured at 570 nm and 600 nm.

RNA, cDNA preparation and quantitative RT-PCR

For performing quantitative real-time PCR (qRT-PCR), RNA was isolated from FLS with peqGold TriFast (Peqlab, Erlangen, Germany), followed by first-strand cDNA synthesis using the MultiScribe™ MuLV reverse transcriptase (Applied Biosystems, Foster City, CA, USA), both according to manufacturer’s instruction. Relative gene expression was assessed by qRT-PCR using the Applied Biosystems 7500 fast-real-time-PCR System (Applied Biosystems, Foster City, CA, USA) with SYBR® Select Master Mix (ThermoFisher Scientific, Waltham, MA, USA) as detection method, according to the manufacturer’s manual. Samples and the housekeeping gene GAPDH as endogenous control were analyzed in duplicates. For evaluation, relative expression (ΔCt) and ΔΔCt method was utilized. Primers used were GAPDH (fwd 5’-TCCTGTTCGACAGTCAGCCGC-3’, rev 5’-

CGCCCAATACGACCAAATCCGT-3'), IL-6 (fwd 5'-AGAGCTGTGCAGATGAGTACAA-3', rev 5'-GCGCAGAATGAGATGAGTTGTC-3') and IL-8 (fwd 5'-AGCACCAGCCAACTCTCACT-3', rev 5'-CGTTAACTGCATCTGGCTGA-3').

Enzyme-linked immunosorbent assay (ELISA)
ELISAs were performed with DuoSet ELISA Kits (R&D Systems, Minneapolis, MN, USA) according to manufacturer's instructions, for which FLS cell culture supernatants were used undiluted. The optical density at 450 nm, with a wavelength correction set to 540 nm, was evaluated using the SpectraMax 190 ELISA-Reader and the Software Softmax Pro Version 3.0 (both Molecular Devices, Sunnyvale, CA, USA).

Bioinformatics
Values for sequence identity and similarity/homology were calculated with the SIAS webserver[SECRETARIA GENERAL DE CIENCIA, TECNOLOGIA E INNOVACION OF SPAIN]. Protein sequences for analysis and alignment were retrieved from Uniprot [63]. Alignments were carried out using the Clustal Omega webserver[22].

QUANTITATION AND STATSTICAL ANALYSIS
Statistical readout was performed using Graph Pad Pism 4.00 software (La Jolla, USA). Group differences were considered statistically significant with a p-value less than 0.05. Statistical parameters are reported in the figure legends.

DATA AND SOFTWARE AVAILABILITY
Atomic coordinates of IL-36α have been deposited in the Protein Data Bank (http://www.wwpdb.org/) under PDB: 6HPI.

REFERENCES

1. Dutra, F. F. & Bozza, M. T. Heme on innate immunity and inflammation. *Front. Pharmacol.* **5,** (2014).

2. Kühl, T. & Imhof, D. Regulatory FeII/III Heme: The Reconstruction of a Molecule's Biography. *ChemBioChem* **15,** 2024–2035 (2014).

3. Tang, X. D. *et al.* Haem can bind to and inhibit mammalian calcium-dependent Slo1 BK channels. *Nature* **425,** 531–535 (2003).

4. Atamna, H. & Frey, W. H. A role for heme in Alzheimer's disease: heme binds amyloid beta and has altered metabolism. *Proc. Natl. Acad. Sci. U. S. A.* **101,** 11153–11158 (2004).

5. Faller, M., Matsunaga, M., Yin, S., Loo, J. A. & Guo, F. Heme is involved in microRNA processing. *Nat. Struct. Mol. Biol.* **14,** 23–29 (2007).

6. Shen, J. *et al.* Iron metabolism regulates p53 signaling through direct Heme-p53 interaction and modulation of p53 localization, stability, and function. *Cell Rep.* **7,** 180–193 (2014).

7. Ogawa, K. *et al.* Heme mediates derepression of Maf recognition element through direct binding to transcription repressor Bach1. *EMBO J.* **20,** 2835–2843 (2001).

8. Kühl, T. *et al.* Determination of hemin-binding characteristics of proteins by a combinatorial peptide library approach. *ChemBioChem* **12,** 2846–2855 (2011).

9. Kühl, T. *et al.* Analysis of Fe(III) heme binding to cysteine-containing heme-regulatory motifs in proteins. *ACS Chem. Biol.* **8,** 1785–1793 (2013).

10. Brewitz, H. H. *et al.* Role of the chemical environment beyond the coordination site: Structural insight into Fe(III) protoporphyrin binding to cysteine-based heme-regulatory protein motifs. *ChemBioChem* **16,** 2216–2224 (2015).

11. Brewitz, H. H. *et al.* Heme interacts with histidine- and tyrosine-based protein motifs and inhibits enzymatic activity of chloramphenicol acetyltransferase from E. coli. *Biochim. Biophys. Acta - Gen. Subj.* **1860,** 1343–1353 (2016).

12. Dinarello, C. A. Immunological and inflammatory functions of the interleukin-1 family. *Annu. Rev. Immunol.* **27,** 519–550 (2009).

13. Towne, J. E. *et al.* Interleukin-36 (IL-36) ligands require processing for full agonist (IL-36α, IL-36β, and IL-36γ) or antagonist (IL-36Ra) activity. *J. Biol. Chem.* **286,** 42594–42602 (2011).

14. Henry, C. M. *et al.* Neutrophil-Derived Proteases Escalate Inflammation through Activation of IL-36 Family Cytokines. *Cell Rep.* **14,** 708–722 (2016).

15. Gabay, C. & Towne, J. E. Regulation and function of interleukin-36 cytokines in homeostasis and pathological conditions. *J. Leukoc. Biol.* **97,** 645–652 (2015).

16. Frey, S. *et al.* The novel cytokine interleukin-36α is expressed in psoriatic and rheumatoid arthritis synovium. *Ann. Rheum. Dis.* **72,** 1569–1574 (2013).

17. Towne, J. E., Garka, K. E., Renshaw, B. R., Virca, G. D. & Sims, J. E. Interleukin (IL)-1F6, IL-1F8, and IL-1F9 Signal Through IL-1Rrp2 and IL-1RAcP to Activate the Pathway Leading to NF-κB and MAPKs. *J. Biol. Chem.* **279,** 13677–13688 (2004).

18. Debets, R. *et al.* Two novel IL-1 family members, IL-1 delta and IL-1 epsilon, function as an antagonist and agonist of NF-kappa B activation through the orphan IL-1 receptor-related protein 2. *J. Immunol.* **167,** 1440–1446 (2001).

19. Khanskaya, I. *et al.* A Phase 1 Study of ANB019, an Anti-Interleukin-36-Receptor (IL-36R) Monoclonal Antibody, in Healthy Volunteers. *Eur. Acad. Allergy Clin. Immunol. Congr. - Poster* (2018).

20. Goradia, N. *et al.* (1)H, (13)C, and (15)N resonance assignments for the pro-inflammatory cytokine interleukin-36α. *Biomol. NMR Assign.* **10,** 329–333 (2016).

21. Peherstorfer, S. *et al.* Insights into mechanism and functional consequences of heme binding to hemolysin-activating lysine acyltransferase HlyC from Escherichia coli. *Biochim Biophys Acta* **1862,** 1964–1972 (2018).

22. Sievers, F. *et al.* Fast, scalable generation of high-quality protein multiple sequence alignments using Clustal Omega. *Mol. Syst. Biol.* **7,** 539 (2011).

23. Zhang, L. & Guarente, L. Heme binds to a short sequence that serves a regulatory

function in diverse proteins. *EMBO J.* **14,** 313–320 (1995).

24. Shelnutt, J. A., Satterlee, J. D. & Erman, J. E. Raman difference spectroscopy of heme-linked ionizations in cytochrome c peroxidase. *J. Biol. Chem.* **258,** 2168–2173 (1983).

25. Spiro, T. G. Resonance Raman spectroscopy as a probe of heme protein structure and dynamics. *Adv. Protein Chem.* **37,** 111–159 (1985).

26. Giacometti, G. M. & Giacometti, G. *Spectroscopic Techniques in Biophysics*. (2001).

27. Franzen, S., Bohn, B., Poyart, C. & Martin, J. L. Evidence for sub-picosecond heme doming in hemoglobin and myoglobin: a time-resolved resonance Raman comparison of carbonmonoxy and deoxy species. *Biochemistry* **34,** 1224–1237 (1995).

28. Murzin, A. G., Lesk, A. M. & Chothia, C. beta-Trefoil fold. Patterns of structure and sequence in the Kunitz inhibitors interleukins-1 beta and 1 alpha and fibroblast growth factors. *J. Mol. Biol.* **223,** 531–543 (1992).

29. Günther, S. & Sundberg, E. J. Molecular Determinants of Agonist and Antagonist Signaling through the IL-36 Receptor. *J. Immunol.* **193,** 921–30 (2014).

30. Caillet-Saguy, C. *et al.* Role of the iron axial ligands of heme carrier HasA in heme uptake and release. *J. Biol. Chem.* **287,** 26932–26943 (2012).

31. Wolff, N. *et al.* Histidine pK(a) shifts and changes of tautomeric states induced by the binding of gallium-protoporphyrin IX in the hemophore HasA(SM). *Protein Sci.* **11,** 757–765 (2002).

32. Wang, D. *et al.* Structural insights into the assembly and activation of IL-1β with its receptors. *Nat. Immunol.* **11,** 905–911 (2010).

33. Trott, O. & Olson, A. J. AutoDock Vina: improving the speed and accuracy of docking with a new scoring function, efficient optimization and multithreading. *J. Comput. Chem.* **31,** 445–461 (2010).

34. Figueiredo, R. T. *et al.* Characterization of heme as activator of toll-like receptor 4. *J. Biol. Chem.* **282,** 20221–20229 (2007).

35. Atamna, H. & Boyle, K. Amyloid-beta peptide binds with heme to form a peroxidase: relationship to the cytopathologies of Alzheimer's disease. *Proc. Natl. Acad. Sci. U. S. A.* **103,** 3381–3386 (2006).

36. Ghosh, C., Seal, M., Mukherjee, S. & Ghosh Dey, S. Alzheimer's Disease: A Heme–Abeta Perspective. *Acc. Chem. Res.* **48,** 2556–2564 (2015).

37. Wißbrock, A. *et al.* Synthesis and Evaluation of Amyloid β Derived and Amyloid β Independent Enhancers of the Peroxidase-like Activity of Heme. *J. Med. Chem.* **60,** 373–385 (2017).

38. Lu, N., Li, J., Tian, R. & Peng, Y. Key Roles for Tyrosine 10 in Abeta-Heme Complexes and Its Relevance to Oxidative Stress. *Chem. Res. Toxicol.* **28,** 365–372 (2015).

39. Immenschuh, S., Vijayan, V., Janciauskiene, S. & Gueler, F. Heme as a Target for Therapeutic Interventions. *Front. Pharmacol.* **8,** 146 (2017).

40. Reiter, C. D. *et al.* Cell-free hemoglobin limits nitric oxide bioavailability in sickle-cell disease. *Nat. Med.* **8,** 1383 (2002).

41. Zhang, L. Heme biology : the secret life of heme in regulating diverse biological processes. *World Sci. Singapore; Hackensack, NJ* (2011).

42. Roumenina, L. T. *et al.* Heme interacts with C1q and inhibits the classical complement pathway. *J. Biol. Chem.* **286,** 16459–16469 (2011).

43. Candiano, G. *et al.* Blue silver: A very sensitive colloidal Coomassie G-250 staining for proteome analysis. *Electrophoresis* **25,** 1327–1333 (2004).

44. Böhm, M. *et al.* Novel insights into structure and function of factor XIIIa-inhibitor tridegin. *J. Med. Chem.* **57,** 10355–10365 (2014).

45. Wiedemann, C., Bellstedt, P. & Görlach, M. CAPITO - A web server-based analysis and plotting tool for circular dichroism data. *Bioinformatics* **29,** 1750–1757 (2013).

46. Louis-Jeune, C., Andrade-Navarro, M. A. & Perez-Iratxeta, C. Prediction of protein secondary structure from circular dichroism using theoretically derived spectra. *Proteins. Struct. Funct. Bioinforma.* **80,** 374–381 (2012).

47. Bartels, C., Xia, T., Billeter, M., Guntert, P. & Wuthrich, K. The program XEASY for computer-supported NMR spectral analysis of biological macromolecules. *J Biomol NMR* **6,** 1–10 (1995).

48. Guntert, P., Billeter, M., Ohlenschlager, O., Brown, L. R. & Wuthrich, K. Conformational analysis of protein and nucleic acid fragments with the new grid search algorithm FOUND. *J Biomol NMR* **12,** 543–548 (1998).

49. Herrmann, T., Guntert, P. & Wuthrich, K. Protein NMR structure determination with automated NOE-identification in the NOESY spectra using the new software ATNOS. *J Biomol NMR* **24,** 171–189 (2002).

50. Koradi, R., Billeter, M. & Wüthrich, K. MOLMOL: A program for display and analysis of macromolecular structures. *J. Mol. Graph.* **14,** 51–55 (1996).

51. Humphrey, W., Dalke, A. & Schulten, K. VMD : Visual Molecular Dynamics. *J Mol Graph.* **14,** 33–38 (1996).

52. Krieger, E. & Vriend, G. YASARA View - molecular graphics for all devices - from smartphones to workstations. *Bioinformatics* **30,** 2981–2982 (2014).

53. Krieger, E. & Vriend, G. New ways to boost molecular dynamics simulations. *J. Comput. Chem.* **36,** 996–1007 (2015).

54. Lindorff-Larsen, K. *et al.* Improved side-chain torsion potentials for the Amber ff99SB protein force field. *Proteins Struct. Funct. Bioinforma.* **78,** 1950–1958 (2010).

55. Wang, J. M., Wolf, R. M., Caldwell, J. W., Kollman, P. a & Case, D. a. Development

and testing of a general amber force field. *J. Comput. Chem.* **25,** 1157–1174 (2004).

56. Jakalian, A., Jack, D. B. & Bayly, C. I. Fast, efficient generation of high-quality atomic charges. AM1-BCC model: II. Parameterization and validation. *J. Comput. Chem.* **23,** 1623–1641 (2002).

57. Li, P., Song, L. F. & Merz, K. M. Parameterization of highly charged metal ions using the 12-6-4 LJ-type nonbonded model in explicit water. *J. Phys. Chem. B* **119,** 883–895 (2015).

58. Jorgensen, W. L., Chandrasekhar, J., Madura, J. D., Impey, R. W. & Klein, M. L. Comparison of simple potential functions for simulating liquid water. *J. Chem. Phys.* **79,** 926–935 (1983).

59. Essmann, U. *et al.* A smooth particle mesh Ewald method. *J. Chem. Phys.* **103,** 8577–8593 (1995).

60. Novoa, E. M., De Pouplana, L. R., Barril, X. & Orozco, M. Ensemble docking from homology models. *J. Chem. Theory Comput.* **6,** 2547–2557 (2010).

61. Royal Society of Chemistry. ChemSpider. Search and Share Chemistry. *http://www.chemspider.com/Chemical-Structure.16739951.html, last accessed on 10th september, 2018.*

62. Zimmermann, T. *et al.* Isolation and characterization of rheumatoid arthritis synovial fibroblasts from primary culture - primary culture cells markedly differ from fourth-passage cells. *Arthritis Res.* **3,** 72–76 (2001).

63. Bateman, A. *et al.* UniProt: The universal protein knowledgebase. *Nucleic Acids Res.* **45,** D158–D169 (2017).

Supplementary Information

Structural insights into heme binding to IL-36α proinflammatory cytokine

Amelie Wißbrock[a,1], Nishit B. Goradia[b,1,2], Amit Kumar[b], Ajay Abisheck Paul George[a], Toni Kühl[a], Peter Bellstedt[c], Ramadurai Ramachandran[b], Patrick Hoffmann[d,e], Kerstin Galler[d,e], Jürgen Popp[e,f], Ute Neugebauer[d,e,f], Kornelia Hampel[g], Bastian Zimmermann[g], Susanne Adam[h], Maximilian Wiendl[h], Gerhard Krönke[h], Iqbal Hamza[i,j], Stefan H. Heinemann[k], Silke Frey[h], Axel J. Hueber[h], Oliver Ohlenschläger[b,*], and Diana Imhof[a,*],

[a]Pharmaceutical Biochemistry and Bioanalytics, Pharmaceutical Institute, University of Bonn, D-53121 Bonn, Germany;
[b]CS Protein Production, Leibniz Institute on Aging/Fritz Lipmann Institute, D-07745 Jena, Germany;
[c]Institute of Organic and Macromolecular Chemistry (IOMC), Friedrich Schiller University Jena, D-07743 Jena, Germany;
[d]Center for Sepsis Control and Care (CSCC), Jena University Hospital, D-07747 Jena, Germany;
[e]Leibniz Institute of Photonic Technology (Leibniz IPHT), D-07745 Jena, Germany;
[f]Institute of Physical Chemistry and Abbe Center of Photonics, Friedrich Schiller University Jena, D-07743 Jena, Germany;
[g]Biaffin GmbH & Co KG, D-34132 Kassel, Germany;
[h]Department of Internal Medicine 3 – Rheumatology and Immunology, University of Erlangen-Nürnberg (FAU) and University Hospital Erlangen, D-91054 Erlangen, Germany;
[i]Department of Animal & Avian Sciences, University of Maryland, College Park, MD 20742;
[j]Department of Cell Biology & Molecular Genetics, University of Maryland, College Park, MD 20742;
[k]Center for Molecular Biomedicine, Department of Biophysics, Friedrich Schiller University Jena and Jena University Hospital, D-07745 Jena, Germany;
[1]These authors contributed equally.
[2]Current address: European Molecular Biology Laboratory, D-22607 Hamburg, Germany.
*Correspondence: dimhof@uni-bonn.de, oliver.ohlenschlaeger@leibniz-fli.de

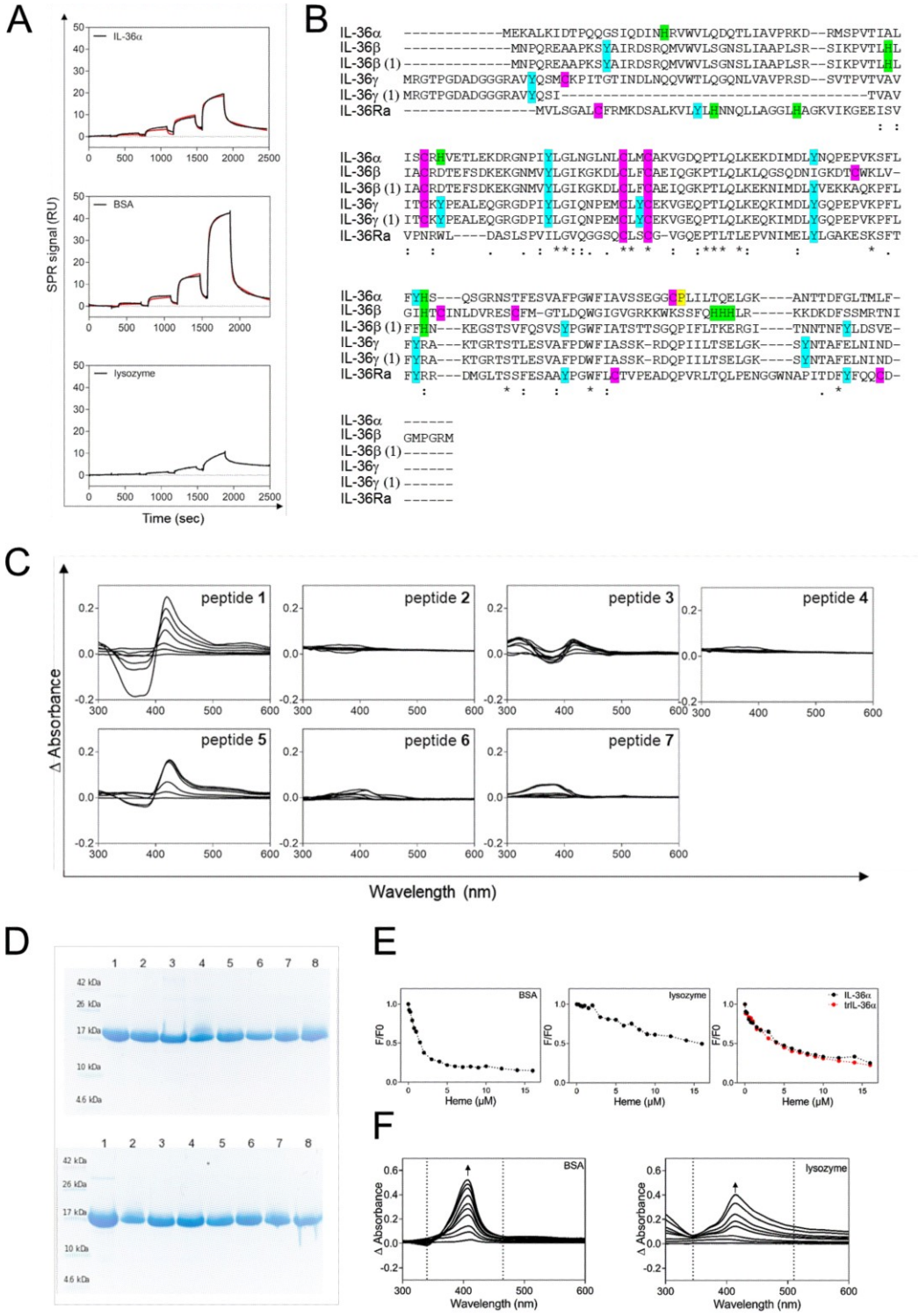

Figure S1. Spectroscopic studies on the formation of heme-IL-36α and derived heme-peptide complexes. (A) Surface plasmon resonance (SPR) spectra of heme-incubated full-length IL-36α and control proteins bovine serum albumin (BSA, *Bos taurus*) and lysozyme (*Gallus gallus*). Protein-complexes are in

black, whereas data fits are displayed in red. A K_D of 6 to 11 μM for the first heme interaction and 30 to 41 μM for a second binding event was determined for the positive control BSA, whereas it was not possible to determine the binding affinity of the negative control lysozyme due to weak signals. Lysozyme was thus considered as non-binder as earlier described (Shen et al., 2014). **(B)** Sequence alignment of IL-36α, β and γ (including all isoforms) and IL-36Ra by Clustal Omega (Sievers et al., 2011)**.** Potential heme-coordinating residues (Y, H, C) are marked in blue (Y), green (H), and purple (C). IL-36α is the only variant exhibiting a CP motif (P137 in yellow), a well-described HRM. **(C)** UV/Vis differential spectra for heme-incubated IL-36α-derived peptides **1-7**. Peptides **2**, and **4** (Cys-mutants), as well as **6** (Y108AH) and **7** (Y108AH109A) displayed no heme binding verifying the essential role of Cys in **2** and **4** for heme coordination, and for Tyr rather than His in **6** and **7**. Peptide **3** (Cys only) exhibited a maximum shift to ~319 nm and to ~416 nm, but heme-binding affinity could not be determined. Heme binding to peptide **1** (YH) revealed a UV/Vis band shift to ~415 nm and a K_D value of 4.48 ± 2.20 μM. Peptide **5** (YH109A) showed a UV/Vis band shift to ~418 nm and a K_D value of 2.29 ± 1.32 μM. A different binding mode of peptides **1** and **5** is visible from the diverging curve shape of the differential spectra indicating an involvement of Tyr and partially His in wild-type peptide **1**. This observation is supported by the loss of binding affinity of peptide **5** compared to peptide **1**. **(D)** SDS PAGE of IL-36α and protein mutants. Coomassie blue-stained 18% reducing gel of both, full-length and truncated wild-type and mutant IL-36α proteins. The proteins (left: full-length, right: truncated) are ordered as follows: 1) wild-type, 2) Y108S, 3) H109A, 4) C136SP137A, 5) Y108SH109A, 6) Y108SC136SP137A, 7) H109AC136SP137A, and 8) Y108SH109AC136SP137A. Molecular weight markers are indicated. **(E)** Fluorescence intensity of heme-incubated control proteins (BSA, lysozyme) as well as full-length and truncated IL-36α (λ_{ex} 306 nm, λ_{em} 352 nm). Heme-protein complex formation resulted in static quenching of the protein's intrinsic fluorescence leading to a detectable loss of fluorescence intensity following a non-linear decrease in contrast to dynamic quenching (Peherstorfer et al., 2018). As expected, lysozyme as the negative control only showed dynamic quenching with increasing heme concentration. The positive control BSA displayed a mixture of dynamic and static quenching detectable as a hyperbolic decay function upon incubation with heme. Thus, lysozyme was confirmed as non-binder, and BSA as heme-binding protein as reported earlier (Shen et al., 2014). For IL-36α a similar trend as found for BSA was observed. **(F)** Differential absorption spectra of heme-incubated (0-40 μM) BSA and lysozyme. A broad band as found for lysozyme hints at unspecific heme-protein interaction (Peherstorfer et al., 2018).

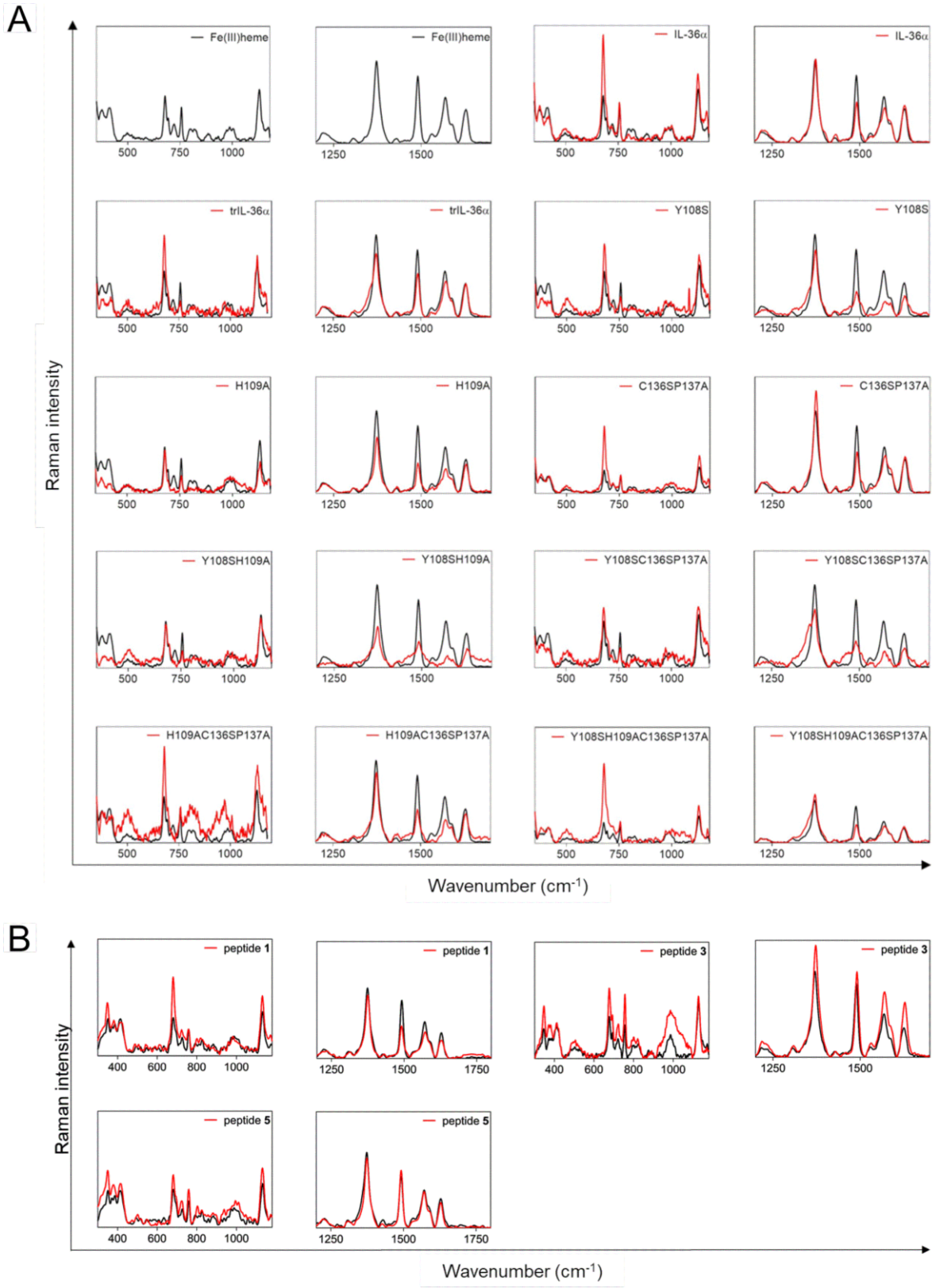
A
Fe(III)heme
IL-36α
trIL-36α
Y108S
H109A
C136SP137A
Y108SH109A
Y108SC136SP137A
H109AC136SP137A
Y108SH109AC136SP137A
Raman intensity
Wavenumber (cm-1)
B
peptide 1
peptide 3
peptide 5
Raman intensity
Wavenumber (cm-1)

Figure S2. Resonance Raman spectrosopcy of IL-36α, mutant proteins, and IL-36α-derived peptides. (A) Resonance Raman spectra of heme, wild-type (tr)IL-36α and IL-36α protein mutants. Lower (left) and higher (right) wavenumber fingerprint region with assignment of prominent normal mode frequencies ν_7 (681 cm^{-1}), ν_4 (1374 cm^{-1}), ν_3 (1492 cm^{-1}), ν_2 (1571 cm^{-1}) and ν_{10} (1628 cm^{-1}) for heme. Heme is displayed in black and the respective heme-protein spectra in red. To be able to obtain a detailed insight into the spectra of the lower wavenumbers an adapted y-axis scaling was applied. **(B)** Resonance Raman spectra of heme-incubated peptides **1**, **3** and **5**. Data anlaysis was performed as described in (G). Peptide **3** was measured in another experiment than the depicted spectra and the other complexes.

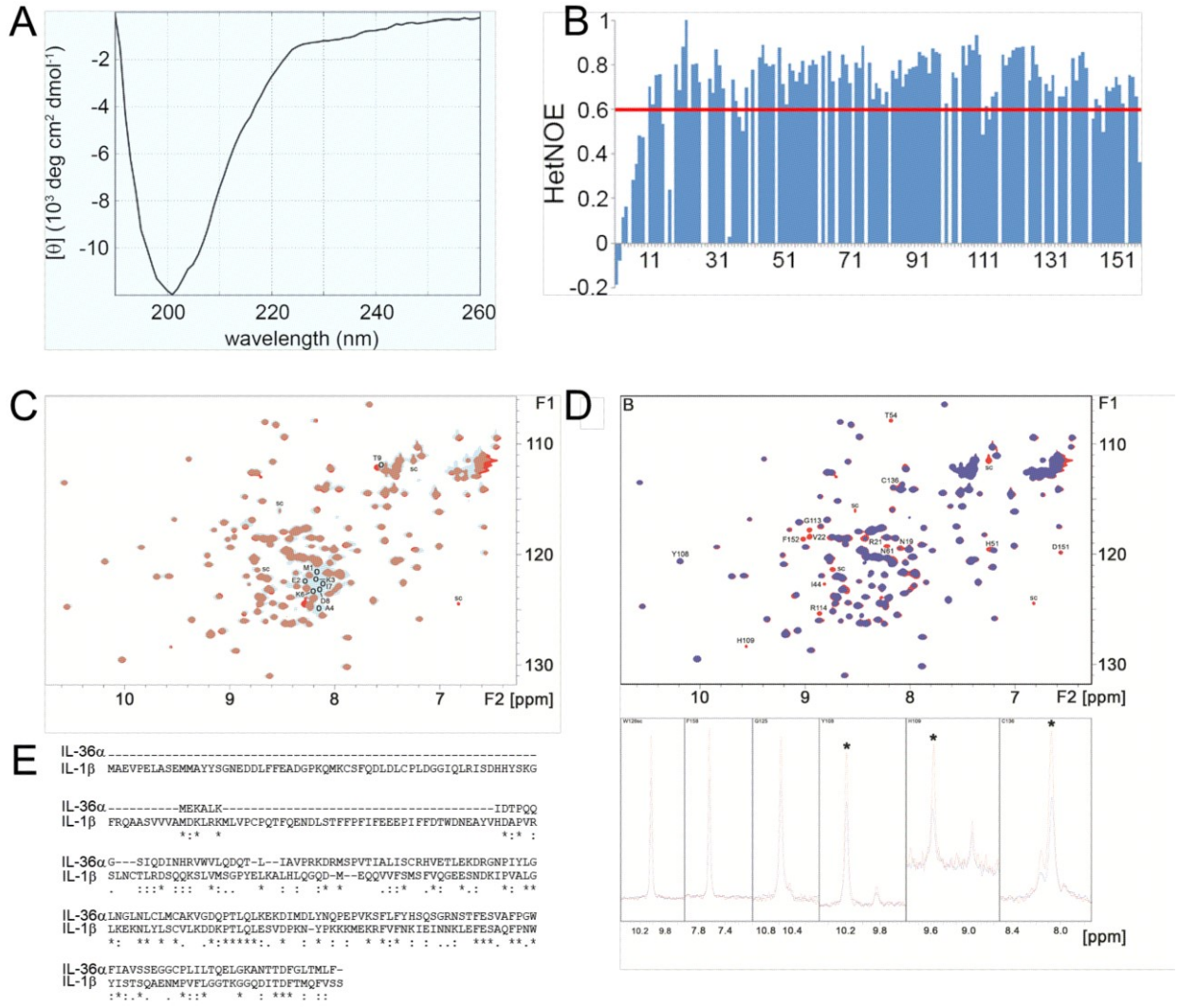

Figure S3. Structural analysis of IL-36α in free and heme-bound form. (A) The CD spectrum of IL-36α indicates a rather disordered structure as can be interpreted from the negative band at 203 nm. CD data was utilized to estimate the secondary structure content of IL-36α using the algorithms CAPITO (CD Analysis and Plotting tool) (Wiedemann et al., 2013) and K2D3 (Table S6) (Louis-Jeune and Andrade-Navarro, M A Perez-Iratxeta, 2012). Results of the prediction for wild-type IL-36α by both programs can be summarized as only a minor content of α-helix (~ 10%), between 20 and 35% β-sheet fold and a large fraction (~ 50-70%) of irregular structural elements.

(B) The {^{1}H,^{15}N} heteronuclear NOE data of IL-36α provides information about the motion of individual N-H bond vectors and thus the dynamics of the protein backbone. Values below 0.6 indicate an increased mobility. **(C)** Comparison of the [^{1}H,^{15}N]-HSQC spectra of full-length (cyan) and truncated IL-36α (red). Missing or shifted signals of the N-terminal residues in trIL-36α are indicated by black circles (sc ~ side chain signal). **(D)** Structural analysis of heme binding to trIL-36α. Top: Superposition of the [^{1}H,^{15}N]-HSQC spectra of trIL-36α in the free (red) and heme-bound state (blue). A drastic decrease in signal intensities is observed for residues N19, R21, V22, I44, H51, T54, N61, H109, G113, R114, D151, F152 (sc ~ side chain signal). Bottom: Moderate changes compared to e.g. H109 apply to Y108 and C136 (relevant cross peaks marked by *). For comparison of the uniform drop in signal intensities due to the solvent paramagnetic effect the traces of the binding-independent residues F158 and G125 as well as the side chain signal of W126 are given on the left. **(E)** Sequence alignment of IL-36α and IL-1β was performed using Clustal Omega (Sievers et al., 2011).

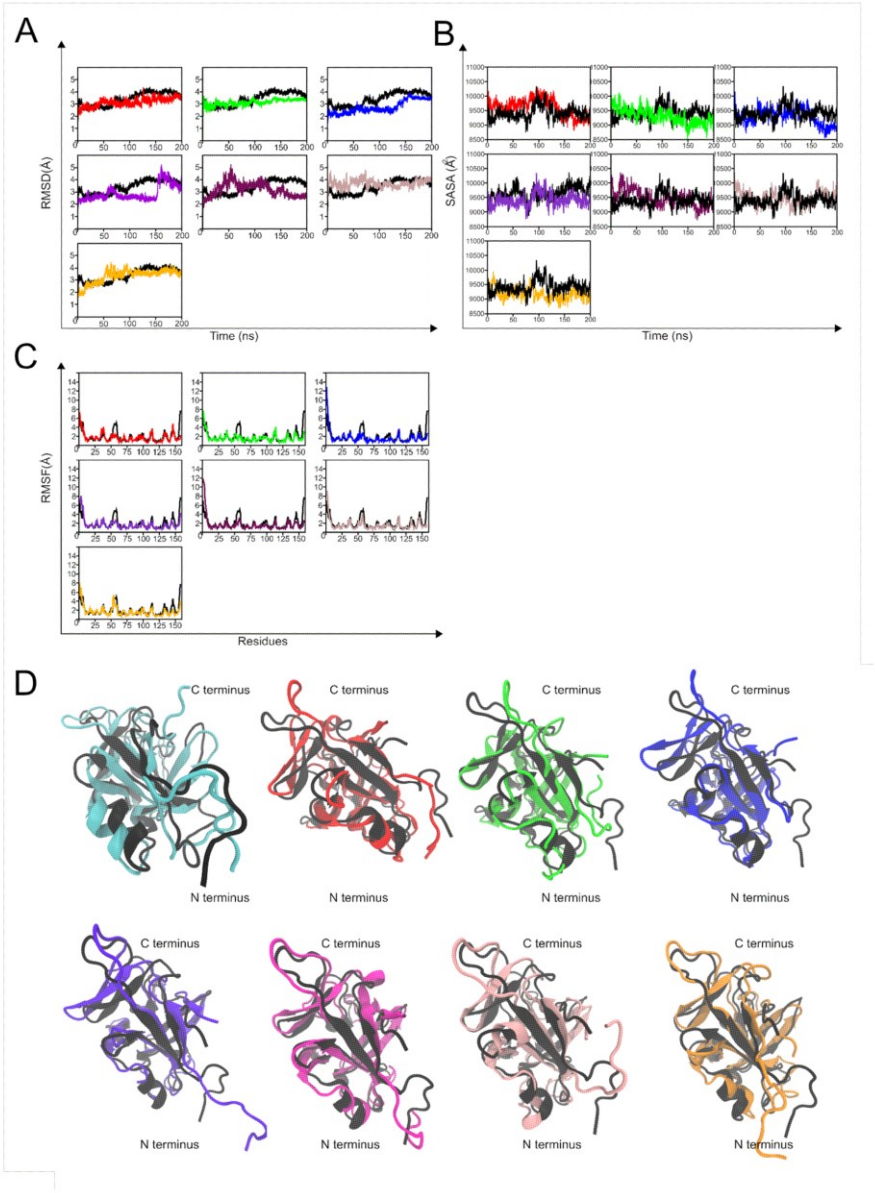

Figure S4. Computational studies on IL-36α wildtype and mutant proteins. Protein mutants in A-C are presented as follows: Y108S (red), H109A (green), Y108SH109A (blue), C136SP137A (indigo), Y108SC136SP137A (maroon), H109AC136SP137A mutant (brown) and Y108SH109AC136SP137A (orange). **(A)** Backbone RMSD (root mean square deviation) generated from the MD simulations. It is evident that both, the wild-type IL-36 and the mutants, reach sufficient equilibration at around 150 ns of simulation time. The average RMSD change of the wild-type IL-36α structure with reference to the NMR starting structure was 3.34 Å (Table S7). This structural deviation largely arises from the extreme fluctuations exhibited by the residues at both, the C- and N-terminal regions of the protein, as can be seen from the RMSF (root mean square fluctuation per residue) plots in **(B)**. The residues at the termini fluctuate at about 8 Å from their mean positions which has its consequent impact on the overall RMSD value. The conformational ensemble produced by the MD simulations are a suitable representation of the NMR ensemble of the protein given that the NMR ensemble contains structures that differ from each other by RMSD values up to 2.74 Å (data not shown). The disordered regions of the N-terminal region in the NMR ensemble are also seen in the conformations sampled in MD simulations and are quantified by the high RMSF values associated with them. **(C)** SASA (solvent accessible surface area) comparison between wild-type and mutant IL-36α structures show evolution of the SASA to lower values for the Y108SH109A mutant and higher values for the C136SP137A mutants and no significant deviation from the wild-type in the other mutants. This is a logical consequence of replacing residues with higher mean SASA values (46 Å2 for Y and 54 Å2 for H by ones with lower values (39 Å2 for S and 28 Å2 for A). The increase of SASA for the C136P137A mutants can also be explained similarily given that the mean SASA values for C (17 Å2) is much lower than that of S (39 Å2). The SASA values (Y-axis) start from 8500 onwards to avoid the visual obfuscation that arises from starting the plotting from 0. **(D)** Structural superimposition over Cα atoms of the NMR starting structure of IL-36α (black) and the final frame from the MD simulations of the IL-36α wild-type (cyan, A) and mutants Y108S (red), H109A (green), Y108SH109A (blue), C136SP137A (violet), Y108SC136SP137A (magenta), H109AC136SP137A (pink) and Y108SH109AC136SP137A (orange,). All structures are represented by the "new cartoon" style in VMD (Visual Molecular Dynamics) (Humphrey et al., 1996). MD simulations of the heme-bound complexes revealed that C136-mediated heme binding was a prerequisite for stable coordination of heme via Y108. As observed from the RMSF profiles, heme binding to C136 supported by P137 and other surrounding residues reduced the conformational flexibility of loops 6, 10, and some parts of loop 3 (Figures 3B, D). This binding-induced constraint has a dampening effect on the flexibility of the rest of the protein rendering it conformationally favorable for the binding event via Y108. Although heme coordination via Y108 is still observed upon loss of the CP motif in the docking experiment, MD simulations of the complex resulted in heme dislocation from the Y108 binding site into solution in about 5 ns of the simulation (***Movie S1***). With heme bound to C136 (e.g. wild-type IL-36α), however, the binding of the second heme molecule to Y108 is found to persist for a much longer period of time (~150 ns in 200 ns MD simulations) (***Movie S2***). To investigate coordination via the H109 residue, heme could be docked to the protein by narrowing down the docking search space to the vicinity of the H109 residue. However, MD simulations of these complexes revealed the dislocation of heme from the protein surface into solution almost instantaneously suggesting a lower preference of heme to bind via the H109 over Y108. Apart from heme binding via the proposed motifs, an additional heme interaction to the IL-36α surface was observed for all proteins investigated. This interplay was characterized by the Fe(III) ion found at a distance 2.42 Å from the oxygen atom of the S104 residue. This observation might explain heme binding to the Y108SH109AC136SP137A mutant as found by UV/Vis spectroscopy. It is suggested that this S104-mediated attachment of heme may have an influence on the protein by inducing a restraining effect on the protein's conformational flexibility. Although no coordinative interactions were observed, the electrostatic and hydrophobic interactions between heme and the protein surface at this interface may facilitate the surface attachment.

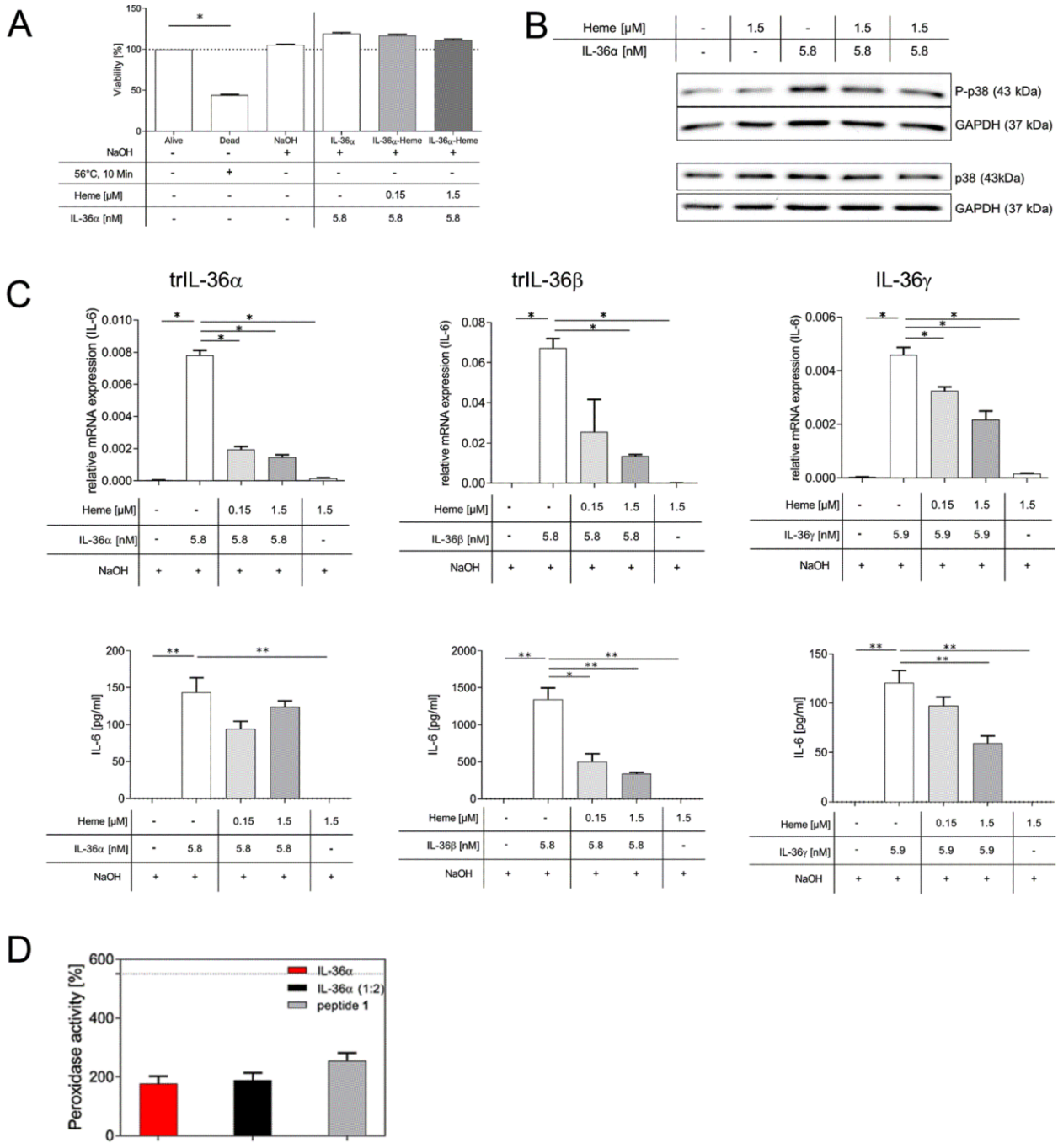

Figure S5. Biological testing of the agonistic trIL-36α family members. (A) Cell viability upon treatment of synovial fibroblast-like synoviocytes (FLS) from RA patients with trIL-36α, heme, and the trIL-36α-heme complex for 24 h. IL-36α and the respective agent were preincubated for 1 h prior to the addition to FLS. Cell viability was analyzed by the AlamarBlue assay according to the manufacturer's instruction (#741802, Invitrogen, Carlsbad, CA, USA), and absorbance was measured at 570 nm and 600 nm. Statistical analysis, only for samples with reduced cell viability compared to the alive control, was performed using Wilcoxon matched-pairs signed rank test with *$p < 0.05$. Values are means + SEM (n=6). **(B)** Impact of heme on IL-36α-induced intracellular signaling in FLS. FLS from RA patients were treated with varying

trIL-36α to heme ratios for 5 min. trIL-36α was preincubated with heme for 1 h prior to addition to the FLS. Samples were separated by a reducing 2D gel electrophoresis in a 10% SDS polyacrylamide gel and blotted to a nitrocellulose membrane by semi-dry transfer. After blocking in 5% BSA/TBST for 1 h at room temperature, the blots were incubated overnight at 4 °C using antibodies from Cell Signaling Technology (Leiden, the Netherlands), such as rabbit anti-P-p38, rabbit anti-p38 and rabbit anti-GAPDH. As secondary antibody anti-rabbit HRP (Biozol, Eching, Germany) was used. Detection was performed using Pierce™ ECL Western Blotting Substrate (Thermo Fisher Scientific, Dreieich, Germany) according to the manufacturer's instruction. Shown is one representative (of n=4) Western blot for phosphorylated p38 (P-p38) and p38 with respective GAPDH loading control. **(C)** Heme reduces trIL-36α, β, and γ-induced gene expression in FLS. FLS from RA patients were treated with varying ratios of recombinant human IL-36α, IL-36β, and IL-36γ (R&D Systems, Minneapolis, MN) to heme for 24 h. Left panel, relative mRNA expression of IL-6, normalized to GAPDH, analyzed by quantitative real-time PCR. Right panel, concentration of IL-6 in the cell culture supernatant measured by ELISA. Values are means + SEM (n=5). Statistical analysis was performed using Mann-Whitney test with $*p < 0.05$ and $**p < 0.01$. **(D)** Peroxidase-like activity (Atamna and Boyle, 2006; Atamna and Frey, 2004; Ghosh et al., 2015; Wißbrock et al., 2017) of heme-incubated IL-36α (1:1 and 1:2, protein:heme) and peptide **1**. No significant increase of the heme's peroxidase activity (100%) was observed upon complex formation with proteins and peptide, respectively, which is in agreement with the results obtained for the CP-based HRM on peptide level in previous studies (Wißbrock et al., 2017).

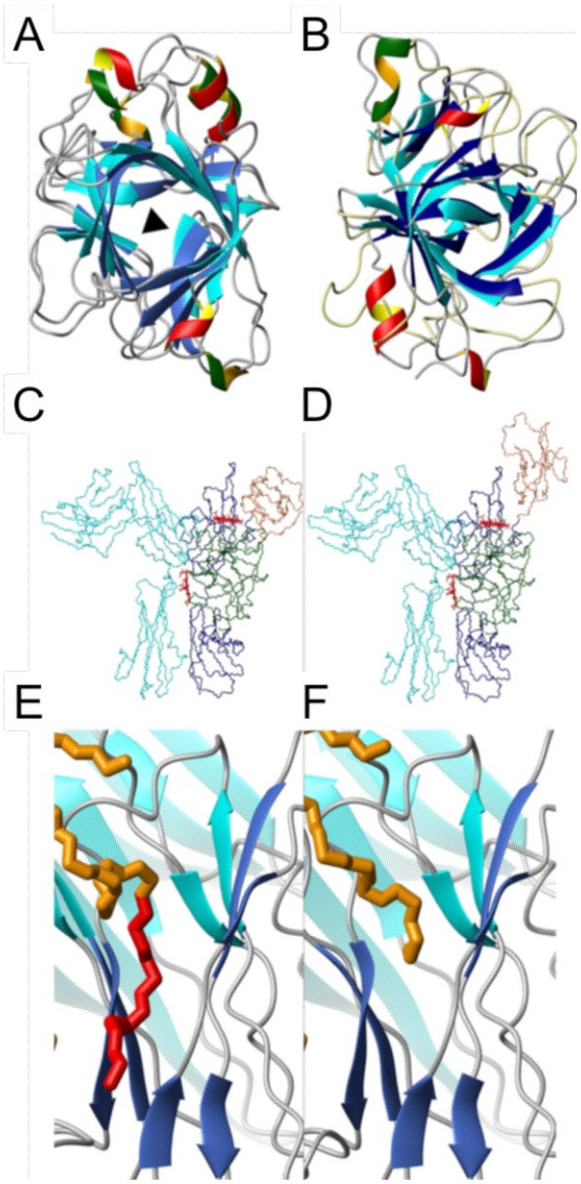

Figure S6. IL-36α structural comparison to IL-36γ and IL-1β as well as IL-36α superimposition with the IL-1β receptor. (A) Superimposition of the NMR structure of IL-36α and IL-36γ (PDB code: 4IZE). The NMR structure of IL-36α (β-strands cyan; helices red/yellow) and the X-ray structure of IL-36γ (β-strands navy; helices green/orange) are displayed. The trefoil pseudo-D3 symmetry axis is indicated by a black triangle. **(B)** Superimposition of the NMR structure of IL-36α and IL-1β (PDB code: 3O4O). The NMR-structure of IL-36α (β-strands cyan; helices red/yellow, backbone grey) and the X-ray structure of IL-1β (β-strands navy; helices green/orange; backbone khaki) are displayed. **(C)** Superimposition of the NMR solution structure of IL-36α with the IL-1β in the receptor complex (PDB code: 3O4O). **(C, D)** View of the full complex model. The wild-type N-terminal residues and the loop 3 (red) show steric clashes with IL-1RII domain-III and domain-I, respectively. **(E, F)** Truncation of the IL-36α sequence by the N-terminal five amino acids allows to resolve the steric interactions with two β-strands of IL-1RII (E) and to accommodate the flexible N-terminal stretch into a V-shaped cleft of IL-1RII domain-III (F). Rotation about

the torsion angle ϕ of Asp315 in IL-1RII leads to a repositioning of the full IL-1RII domain-I resolving van der Waals clashes with loop 3 of IL-36α. Coloring: IL-36α – green, IL-1RII domain-I – coral, IL-1RII domain-II and domain-III – navy, IL-1RAcP – cyan, IL-36α cysteine-136 – yellow, IL-36α loop 3 and N-terminal residues Met1-Leu5 – red, IL-1RII Asp315 C^{α} – magenta.

Table S1. Binding data of heme to full-length and trIL-36α, trIL-36β, trIL-36γ as well as IL-36α protein mutants. SPR, UV/Vis and resonance Raman spectroscopy were applied to the individual heme-incubated protein variants as required.

Protein	SPR K_{D1} [µM]	SPR K_{D2} [µM]	UV/Vis nUV K_{D1} [µM]	UV/Vis Soret K_{D2} [µM]	Raman coordination state
trIL-36α*	12.7 9.3	3.0 4.4	n.d.	n.d.	n.d.
trIL-36β*	10.0 13.9	4.1 3.7	n.d.	n.d.	n.d.
trIL-36γ*	8.9 15.9	5.3 4.1	n.d.	n.d.	n.d.
IL-36α	6.1 4.4	10.2 7.1	2.69 ± 1.15 ~369 nm	11.50 ± 3.06 ~416 nm	5c
Y108S	n.d.	n.d.	-	30.69 ± 7.49 ~418 nm	5c
H109A	n.d.	n.d.	0.77 ± 0.53 ~369 nm	10.35 ± 3.16 416 nm	5c
Y108SH109A	n.d.	n.d.	n.p.* ~368 nm	13.64 ± 4.69 ~420 nm	5c
C136SP137A	n.d.	n.d.	-	12.69 ± 4.43 ~415 nm	5c**
Y108SC136SP137A	n.d.	n.d.	-	15.17 ± 4.35 ~419 nm	5c
H109AC136SP137A	n.d.	n.d.	-	13.29 ± 3.12 ~417 nm	5c
Y108SH109AC136SP137A	n.d.	n.d.	-	14.23 ± 3.82 ~421 nm	5c**

K_D: dissociation constant, nUV: near UV, n.d.: not determined, n.p.: not possible, *Proteins for SPR studies were purchased from R&D systems (see materials). **Negligible indication of hexacoordination.

Table S2. Potential HRMs in IL-36α, IL-36β, and IL-36γ based on cysteine, histidine, or tyrosine as heme-coordination site. Probability for heme binding was evaluated based on the sequence composition, the location within the protein structure, and the net charge of the potential sequence stretches (Brewitz et al., 2015, 2016). Protein sequences were retrieved from Uniprot (Bateman et al., 2017).

No.	Position	Amino acid sequence	Net charge	Heme-binding potential
		IL-36α		
m1	H20	QDIN**H**RVWV	0/(+1)*	-
m2	C49	ALIS**C**R**H**VE	0/(+1)*	-
m3	H51	IS**C**R**H**VETL	0/(+1)*	-
m4	Y64	GNPI**Y**LGLN	0	-
m5	C73	GLNL**C**LM**C**A	0**	-
m6	C76	L**C**LM**C**AKVG	+1**	-
m7	Y96	IMDL**Y**NQPE	-2	-
m8	Y108	SFLF**YH**SQS	0/+1	+
m9	H109	FLF**YH**SQSG	0/+1	+
m10	C136	SEGG**CP**LIL	-1	+

		IL-36β (isoform 1)		
m1	Y12	APKS**Y**AIRD	+1	+
m2	H44	PVTL**H**LIA**C**	0/(+1)*	-
m3	C48	**H**LIA**C**RDTE	-1/(+0)*	-
m4	Y63	GNMV**Y**LGIK	+1	-
m5	C72	GKDL**C**LF**C**A	0	-
m6	C75	L**C**LF**C**AEIQ	-1	-
m7	C100	GKDT**C**WKLV	+1	+
m8	H107	LVGI**H**T**C**IN	0/(+1)*	-
m9	C109	GI**H**T**C**INLD	-1/(+0)*	-
m10	C118	VRES**C**FMGT	0	-
m11	H141	SSFQ**HHH**LR	+1/(+4)*	+
m12	H142	SFQ**HHH**LRK	+2/(+5)*	+
m13	H143	FQ**HHH**LRKK	+3/(+6)*	+
		IL-36β (isoform 2)		
		m1-m6 are identical to isoform 1 of IL-36β.		
m7	Y95	IMDL**Y**VEKK	0	-
m8	H108	FLFF**H**NKEG	0	+
m9	Y123	QSVS**Y**PGWF	0	-
m10	Y153	NTNF**Y**LDSV	-1	-
		IL-36γ (isoform 1)		
m1	Y16***	GRAV**Y**QSM**C**	+1	+
m2	C20	**Y**QSM**C**KPIT	+1	+
m3	C61	AVIT**C**K**Y**PE	0	-
m4	Y63	IT**C**K**Y**PEAL	0	-
m5	Y76	GDPI**Y**LGIQ	-1	-
m6	C85	NPEM**C**L**YC**E	-2	-
m7	Y87	EM**C**L**YC**EKV	-1	-
m8	C88	M**C**L**YC**EKVG	0	-
m9	Y108	IMDL**Y**GQPE	-2	-
m10	Y120	PFLF**Y**RAKT	+2	-
m11	Y159	LGKS**Y**NTAF	+1	+
		IL-36γ (isoform 2)		
m1	Y16***	GRAV**Y**QSIT	+1	+
m2	C26	AVIT**C**K**Y**PE	+1	+
m3	Y28	IT**C**K**Y**PEAL	0	-
m4	Y41	GDPI**Y**LGIQ	0	-
m5	C50	NPEM**C**L**YC**	-1	-
m6	Y52	NPEM**C**L**YC**E	-2	-
m7	C53	EM**C**L**YC**EKV	-1	-
m8	Y73	M**C**L**YC**EKVG	0	-
m9	Y85	IMDL**Y**GQPE	-2	-
m10	Y124	PFLF**Y**RAKT	+2	-
m11	Y164	LGKS**Y**NTAF	+1	+
		IL-36Ra		
m1	C8	SGAL**C**FRMK	+2	+
m2	Y20	LKVL**Y**L**H**NN	+1(+2*)	+
m3	H22	VL**Y**L**H**NNQL	0/(+1*)	+
m4	H32	AGGL**H**AGKV	+1	-
m5	C67	GGSQ**C**LS**C**G	0	-
m6	C70	Q**C**LS**C**GVGQ	0	-
m7	Y89	IMEL**Y**LGAK	0	-
m8	Y101	SFTF**Y**RRDM	+1	-
m9	Y116	ESAA**Y**PGWF	-1	-
m10	C122	GWFL**C**TVPEA	-1	-
m11	Y150	ITDF**Y**FQQ**C**	-1	-
m12	C154	**Y**FQQ**C**D	-1	-

m13	Y164	LGKS**Y**NTAF	+1	+

*Neutral charge if H involved as coordination site and is not considered as additional basic residue. **Cysteines alone were shown to be much less or ineffective for heme binding(Brewitz et al., 2015). ***Will be removed upon proteolytic truncation to achieve biological activity.

Table S3. Synthesized peptides and respective peptide mutants of potential HRMs derived from IL-36α. Peptides were synthesized via standard Fmoc-based solid phase peptide synthesis and subsequently analyzed by MS, HPLC, and TLC.

No.	Peptide sequence	M_w[a] (M_w theor.) [g/mol]	Preparative HPLC t_r [min]	Analytical HPLC t_r [min]	TLC R_f
1	FLFYHSQSG	542.77[a] (1083.51)	71.9[c]	20.4[e]	0.57[g] 0.71[h]
2	SEGGAPLIL	855.49[b] (854.49)	65.3[d]	20.6[f]	0.66[g] 0.73[h]
3	SEGGCALIL	861.43[b] (860.43)	62.9[d]	21.5[f]	0.57[g] 0.71[h]
4	SEGGAALIL	829.47[b] (828.47)	59.7[d]	20.5[f]	0.66[g] 0.73[h]
5	FLFYASQSG	1018.49[b] (1017.49)	83.3[c]	21.2[e]	0.66[g] 0.88[h]
6	FLFAHSQSG	496.75[a] (991.49)	66.4[c]	17.8[e]	0.51[g] 0.69[h]
7	FLFAASQSG	463.74[a] (925.47)	75.5[c]	19.2 [e]	0.61[g] 0.85[h]

Peptides were measured with LC-ESI-MS and peaks were detected as [a]$[M+2H]^{2+}$ or $[M+H]^{+}$. Semi-preparative RP-HPLC was applied for peptide purification using [c]0-50% eluent B (0.1% TFA in 90% acetonitrile, eluent A: 0.1% TFA in water) in 120 min and [d]10-60% eluent B in 120 min as gradients. Analytical HPLC was performed using [e]10-50% eluent B (0.1% TFA in acetonitrile, eluent A: 0.1% TFA in water) in 40 min and [f]10-40% eluent B in 30 min. For TLC the following systems were applied: [g]n-butanol/acetic acid/water (48:18:24, v/v) and [h]pyridine/ethyl acetate/acetic acid/water (5:5:1:3, v/v).

Table S4. Data of UV/Vis- and resonance Raman spectroscopy of IL-36α-derived peptides and respective mutants (**1-7**) in complex with heme. (For peptide sequences see Table S3.)

No.	K_D for UV/Vis [µM] (wavelength)	Raman coordination state
1	4.48 ± 2.20 (~415 nm)	5c(6c)
2	n.b.	-
3	n.d. (~319 nm, ~416 nm)	5c
4	n.b.	-
5	2.29 ± 1.32 (~418 nm)	5c
6	n.b.	-
7	n.b.	n.p.

K_D, dissociation constant; n.b. no binding; n.p., not possible; 5c, pentacoordinated; 6c, hexacoordinated.

Table S5. Structural statistics of the refined NMR solution structure of IL-36α.

Total distance restraints	4107
• intra (|i-j|=0)	350
• sequential / short (|i-j|=1)	1158
• medium (1<|i-j|<5)	767
• long range (|i-j|≥5)	1832
hydrogen bond	72
Target function [$Å^2$]	
after (before) energy minimization	4.13 (4.14)
AMBER physical energies [$kcal/mol^{-1}$]	
before energy minimization	-4526 ± 97
after energy minimization	-5812 ± 101
R.M.S.D. [Å]	
mean global r.m.s.d. values	
all heavy atom (residues 10-158)	1.52 ± 0.21
backbone (residues 10-158)	0.74 ± 0.12
Ramachandran plot [%]	
Residues in most favored regions	69.3
in additionally allowed regions	28.7
in generously allowed regions	1.9
in disallowed regions	0.1

Table S6. CD spectroscopy analysis of the secondary structure content of IL-36α and trIL-36α (6-158).

Protein	Analysis tool	α-helix	β-sheet	irregular
IL-36α	CAPITO	10-13%	30-35%	50-60%
IL-36α	K2D3	9.8%	19.7%	70.5%
trIL-36α	CAPITO	10-13%	32-37%	51-59%
trIL-36α	K2D3	8.5%	19.5%	72.0%

Table S7. Backbone RMSD based structural assessment of wild-type IL-36α and its mutants in a 200 ns MD simulation.

Protein	RMSD against model 1 of the NMR ensemble (Å)	RMSD against structure from MD equilibration (Å)
IL-36α	3.34 ± 0.52	2.516 ± 0.6
Y108S	3.06 ± 0.32	2.32 ± 0.56
H109A	3.11 ± 0.24	2.04 ± 0.65
Y108SH109A	2.75 ± 0.54	3.00 ± 1.18
C136SP137A	2.83 ± 0.61	2.63 ± 0.46
Y108SC136SP137A	3.17 ± 0.53	2.54 ± 0.82
H109AC136SP137A	3.67 ± 0.31	2.16 ± 0.5
Y108SH109AC136SP137A	3.30 ± 0.52	1.89 ± 0.67

RMSD of reference structure 1 w.r.t. NMR ensemble = 0.84 Å;

Movie Information

Movie S1: Heme binding to both C136 and Y108 residues on the surface of the IL-36α wild-type protein. The video is a screen recording of a fast-forwarded molecular dynamics trajectory. The video shows a simulation cell containing the IL-36α protein with two heme molecules bound to its surface as a result of molecular docking simulations. The protein is displayed in the cartoon style, colored gray. On the protein structure, the residues Y108, H109, and C136 are shown as sticks colored green, magenta, and yellow, respectively. Although the H109 residue does not participate in heme coordination, its orientation is relative to the Y108 residue. The heme molecule bound to the Y108 site is shown as red spheres, while the one bound to the C136 residue is shown as blue spheres. It can be clearly observed that both heme molecules stay bound to the surface of the protein.

Movie S2: Heme binding to the Y108 residue on the surface of the C136SP137A mutant of IL-36α. The video is a screen recording of a fast-forwarded molecular dynamics trajectory. The video shows simulation cell containing the C136SP137A mutant of IL-36α protein with a heme molecule bound to its surface as a result of molecular docking simulations. The protein is displayed in the cartoon style, colored gray. On the protein structure, the residues Y108 and H109 are shown as sticks colored green and magenta, respectively. Although the H109 residue does not participate in heme coordination, its orientation is relative to the Y108 residue. The heme molecule bound to the Y108 site is shown as red. It can be clearly observed that the heme molecule is quickly dislodged from its binding site on the Y108 residue and moves into the solution shortly after the simulation start. This video shows that in the absence heme binding to the C136 residue heme binding to the Y108 residue is short-lived.

2.4 ^{1}H, ^{13}C, and ^{15}N resonance assignments of the cytokine interleukin-36β isoform-2.

Authors: **Amit Kumar**, Amelie Wißbrock, Peter Bellstedt, Andras Lang, Ramadurai Ramachandran, Christoph Wiedemann, Diana Imhof & Oliver Ohlenschläger

Contributions: **AK contribution (85%)**
AK performed the experiments, prepared the samples, the, analyzed data and prepared figures for manuscript and PB, RR and CW helped in NMR data collection. AL evaluated the H bonding by temperature coefficient. OO wrote the manuscript. All the authors reviewed the manuscript. OO conceived the idea.

Status: Published in Biomolecular NMR Assignment (2019) 13: 155
https://doi.org/10.1007/s12104-018-09869-4

Summary: IL-36β cytokine is a member of IL-36 family and involved in the expression of other inflammatory mediators like chemokines, cytokines (IL-6, IL-8) and growth factors. Recent studies show their involvement in psoriasis, inflammation, rheumatoid arthritis and pregnancy. This manuscript reports the NMR resonance assignments for the backbone and sidechain atoms of Interleukin-36β isoform-2 (IL-36β). The manuscript is providing the bases for future determination of the NMR solution structure and mapping of the heme-binding motifs in IL-36β.

Biomolecular NMR Assignments (2019) 13:155–161
https://doi.org/10.1007/s12104-018-09869-4

ARTICLE

^{1}H, ^{13}C, and ^{15}N resonance assignments of the cytokine interleukin-36β isoform-2

Amit Kumar[1] · Amelie Wißbrock[4] · Peter Bellstedt[2] · Andras Lang[1] · Ramadurai Ramachandran[1] · Christoph Wiedemann[3] · Diana Imhof[4] · Oliver Ohlenschläger[1]

Received: 26 November 2018 / Accepted: 18 December 2018 / Published online: 13 February 2019
© Springer Nature B.V. 2019

Abstract
Interleukins are cytokines performing central tasks in the human immune system. Interleukin-36β (IL-36β) is a member of the interleukin-1 superfamily as are its homologues IL-36α and IL-36γ. All of them interact with a common receptor composed of IL-36R and IL-1R/acP. IL-36 cytokines can activate IL-36R to proliferation of CD4 + lymphocytes or stimulate M2 macrophages as potently as IL-1β. Within our efforts to study the structure–function relationship of the three interleukins IL-36α, IL-36β and IL-36γ by heteronuclear multidimensional NMR, we here report the ^{1}H, ^{13}C, and ^{15}N resonance assignments for the backbone and side chain nuclei of cytokine interleukin-36β isoform-2.

Keywords Resonance assignments · Heteronuclear NMR · Interleukin-36β · Interleukin-1 superfamily · Cytokines

Biological context

The interleukin (IL)-1 superfamily is a group of cytokines associated with pleiotropic effects on the innate and adaptive immune system (Sims and Smith 2010). IL-1 cytokines are discussed in the context of various autoimmune diseases, such as multiple sclerosis, type-1 diabetes, psoriasis, rheumatoid arthritis (RA), and inflammatory bowel disease (Kunz and Ibrahim 2009; Moudgil and Choubey 2011; O'Shea et al. 2002). The IL-1 family has recently been expanded by the new interleukin-36 subfamily, which consists of three agonistic members, namely IL-36α, IL-36β and IL-36γ, and the natural antagonist IL-36Ra (Smith et al. 2000). These cytokines signal through the same heterodimeric receptor complex, consisting of interleukin-1 receptor-like 2 (IL-1Rrp2) and the co-receptor IL-1R accessory protein (IL-1RacP) (Towne et al. 2004). Recruitment of the accessory protein is essential for successful signaling. Receptor binding triggers an intracellular signalling cascade involving several proteins such as the kinases JNK, and ERK1/2, and the transcription factor NF-κB (Debets et al. 2001; Towne et al. 2004). Truncation of the IL-36 cytokines is required to generate the active proteins (Towne et al. 2011). Recent studies suggest that neutrophil-derived cathepsin G and elastase can cleave IL-36α, whereas only cathepsin G can process IL-36β, and elastase and proteinase-3 are able to truncate IL-36γ (Henry et al. 2016). IL-36s are primarily found in the skin and other epithelial tissues, in the esophagus, the brain, the lung, and the gut (Gabay and Towne 2015). Moreover, IL-36 cytokines appear to be of particular importance in psoriasis (Towne and Sims 2012). Thus, altered IL-36 expression levels were found in lesional psoriasis skin (Blumberg et al. 2007; Debets et al. 2001; Towne and Sims 2012). Moreover, reduced levels of IL-36Ra and dysfunctional IL-36Ra species have been associated with generalised pustular psoriasis, an extremely aggressive and life-threatening form of psoriasis (Boehner et al. 2018; Farooq et al. 2013; Kanazawa et al. 2013; Marrakchi et al. 2011; Renert-Yuval et al. 2014; Sugiura et al.

In memory of Frank Große.

✉ Oliver Ohlenschläger
oliver.ohlenschlaeger@leibniz-fli.de

1 Leibniz Institute on Aging – Fritz Lipmann Institute, Beutenbergstr. 11, 07745 Jena, Germany

2 Faculty of Chemistry and Earth Sciences, Friedrich Schiller University, Humboldtstr. 10, 07743 Jena, Germany

3 Institute of Biochemistry and Biotechnology, Martin Luther University Halle-Wittenberg, Kurt-Mothes-Str. 3a, 06120 Halle/Saale, Germany

4 Pharmaceutical Biochemistry and Bioanalytics, Pharmaceutical Institute, University of Bonn, An der Immenburg 4, 53121 Bonn, Germany

2012; Tauber et al. 2016). An antibody (ANB019; AnaptysBio) is currently in clinical trials, which is tested for two forms of psoriasis, i.e., generalised pustular psoriasis, and palmo-plantar pustular psoriasis. A role of IL-36 cytokines in other inflammatory diseases, among them inflammatory arthritis and Crohn's disease, is currently under investigation (Hahn et al. 2017).

The protein structures of the family members IL-36α, IL-36γ, and IL-36Ra (murine) have previously been solved (Dunn et al. 2003; Goradia et al. 2016; Gunther and Sundberg 2014). All proteins share the characteristic IL-1 β-trefoil structure, consisting of 12 β-sheets connected via 11 loops or turns (Dunn et al. 2003; Goradia et al. 2016; Gunther and Sundberg 2014). Human IL-36β displays 45.2% sequence identity with IL-36α and 43.6% with IL-36γ (Clustal2.1) and comes with two isoforms differing in amino acid composition from residues 88 onwards. Thereby, isoform-1 consists of 164 amino acids while isoform-2 is shorter by seven residues (157 a.a.). Both isoforms of IL-36β contain a propeptide sequence of four amino acids (MNPQ) which was omitted in our study. We here present the NMR assignments of the cytokine IL-36β-2 as a basis for biomolecular and functional studies of the interleukin-36 subfamily.

Methods and experiments

Protein expression and purification

The pET45b vector containing the gene of the IL-36β isoform-2 protein was obtained from the Martin laboratory, Dublin. A caspase-3 (DEVD) site was cloned before Arg-5 in the IL-36β-2 protein sequence. The recombinant IL-36β-2 protein expression and purification was modified from a protocol in the literature (Clancy et al. 2016). The constructs were transformed in BL21 DE3 RIL (codon) *E. coli* cells and plated onto ampicillin plates. A single colony from the plates was inoculated into 100 mL of Luria Bertani (LB) medium containing 50 µg/mL ampicillin and chloramphenicol. This primary culture was inoculated into 500 mL of M9 medium-containing labelled $^{15}NH_4Cl$ (1 gL^{-1}) and $^{13}C_6$-glucose (3 gL^{-1}). Protein expression was induced at an OD600nm of 0.7 by adding 0.5 mM IPTG (isopropyl-1-thio-D-galactopyranoside). After 18 h growth at 18 °C the cells were homogenised in a lysis buffer containing 50 mM Tris/HCl, 300 mM NaCl, 5 mM imidazole and 5 mM β-mercaptoethanol (pH 7.2), lysed with the French press and then centrifuged at 10,000*g*. The clear cell lysate was applied to Ni–NTA agarose resin and allowed to flow with gravity. The resin was washed with ten column volumes each of 5 mM and 10 mM imidazole containing lysis buffer and the purified protein was eluted with 250 mM imidazole. The His_6 tag was cleaved from the protein by addition of 1 mg caspase-3 (produced in house) for 40 mg of IL-36β-2 protein in dialysis buffer (50 mM HEPES, 75 mM NaCl, and 2 mM DTT, pH 7.4) at 4 °C overnight, leaving no additional residue at the N-terminus. The cleaved protein was then loaded on the Ni–NTA column, pre-equilibrated with dialysis buffer. Undigested IL-36β-2 and caspase-3 protein were bound on the Ni–NTA column and the digested IL-36β-2 protein was collected in flow through. Remaining digested protein was eluted using the same dialysis buffer. Digested protein was concentrated to 1 mL using a 3-kDa Vivaspin filter (Sartorius) and injected onto a 16/60 HiLoad S75 size exclusion chromatography column (GE Healthcare). The fractions of the IL-36β-2 were pooled together, concentrated, and the buffer was exchanged into 20 mM sodium phosphate buffer, pH 7.2. The concentration was measured using UV/Vis spectroscopy. The final concentration of the protein samples for NMR experiments was about 1 mM.

NMR spectroscopy

NMR experiments for the ^1H, ^{15}N and ^{13}C chemical shift assignments were acquired at 293 K in 20 mM sodium phosphate pH 7.2 (90% H_2O/10%D_2O) on Bruker 600 and 700 MHz Avance III spectrometers. The chemical shifts for the backbone atoms were assigned from HNCO, HNCA (Kay et al. 1990), HN(CO)CA (Bax and Ikura 1991), HN(CA)CO (Clubb et al. 1992), HNCACB (Wittekind and Mueller 1993) and HNHA experiments (Vuister and Bax 1993). Side chain assignments were obtained from HSQC, (H)CC(CO)NH, H(CCO)NH (Grzesiek and Bax 1993), NOESY-HSQC (Bax et al. 1990) and HCCH-TOCSY spectra (Kay et al. 1993). The spectra were processed using TOPSPIN v.3.5 and analysed with CCPNmr Analysis (Vranken et al. 2005).

Structure prediction

In order to obtain a prediction of the secondary structure element composition of IL-36β-2 the chemical shift data was analysed with the program CSI v.3.0 (Hafsa et al. 2015).

Extent of assignments and data deposition

The [^1H,^{15}N]-HSQC (Fig. 1) of IL-36β-2 displayed well dispersed signals allowing assignment of 98% of the backbone ^1H and ^{15}N resonances of the non-proline residues. 100% of the $^1H^\alpha/^{13}C^\alpha$ and 97% of the $^{13}C'$ backbone chemical shifts have been assigned employing HNCACB, HNHA, HNCO, HNCACO and [^1H,^{13}C]-HSQC spectra. 100% assignments for the β-proton and β-carbon resonances could be determined. For aliphatic residues, 98% of the $^1H^\gamma$, 82% of the $^{13}C^\gamma$, 86% of the $^1H^\delta$, 71% of the $^{13}C^\delta$, 64% of the $^1H^\varepsilon$ and

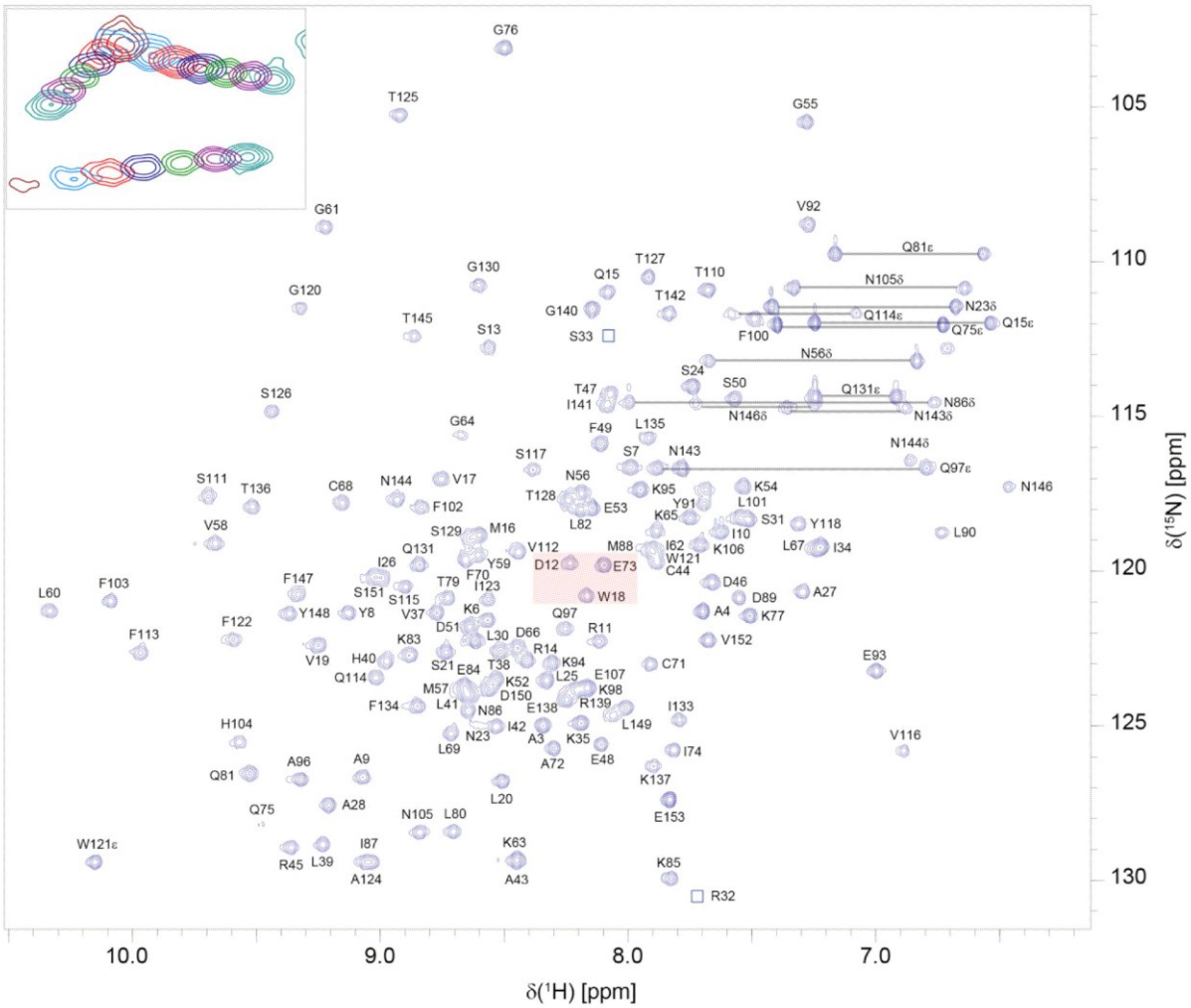

Fig. 1 [^{1}H, ^{15}N]-HSQC spectrum of ^{15}N-labelled IL-36β-2 at pH 7.2, 293 K collected using a 600 MHz spectrometer equipped with a cryoprobe. The peak assignments for backbone amides are annotated. Non-degenerate protons of the side chain amino groups are connected by a shaded line. Squares are indicating positions of amides at a lower intensity level. The inset is the magnification of red shaded area of the spectrum with peaks corresponding to residues D12; E73; W18. H^N and N chemical shifts are correlated at different temperatures (brown: 278 K; royal: 283 K; red: 288 K; navy: 293 K; green: 298 K; purple: 303 K; cyan: 308 K). Note the entirely different shifts of the three peaks not only in rate but also in orientation

46% of the $^{13}C^{\varepsilon}$ have been assigned.[1] In addition, 78% and 44% of N^{δ} and N^{ε} nitrogens could be assigned. Missing assignments mainly correspond to the imino groups of the chain termini and of two residues (Gly108, Ser109) for which N/H cross peaks in the [^{1}H, ^{15}N]-HSQC spectrum could not be identified. The methionine ε-nuclei were tentatively assigned on the basis of NOE cross peaks from the methyl groups to neighbouring residues.

IL-36β-2 is characterised by a number of non-canonical chemical shifts with lower ppm values than empirically expected and also extending into the negative ppm scale. Unusual negative chemical shifts were e.g., observed for side chains atoms of residues Ile10, Leu60, Leu90, Val116 and Ile133. Most of the 21 residues strongly affected are either charged or are located in positions +1 and −1 to an aromatic amino acid.

The CSI predictions obtained via the CSI web server (CSI-3.0 webserver at http://csi3.wishartlab.com; Fig. 2) show that IL-36β-2 consists mainly of a β-sheet composition. 12 β-strands of 2–6 residues in length supplemented by only

[1] CCPNmr derived numbers for the γ/δ/ε-positions include aromatic residues for which currently no assignment was attempted.

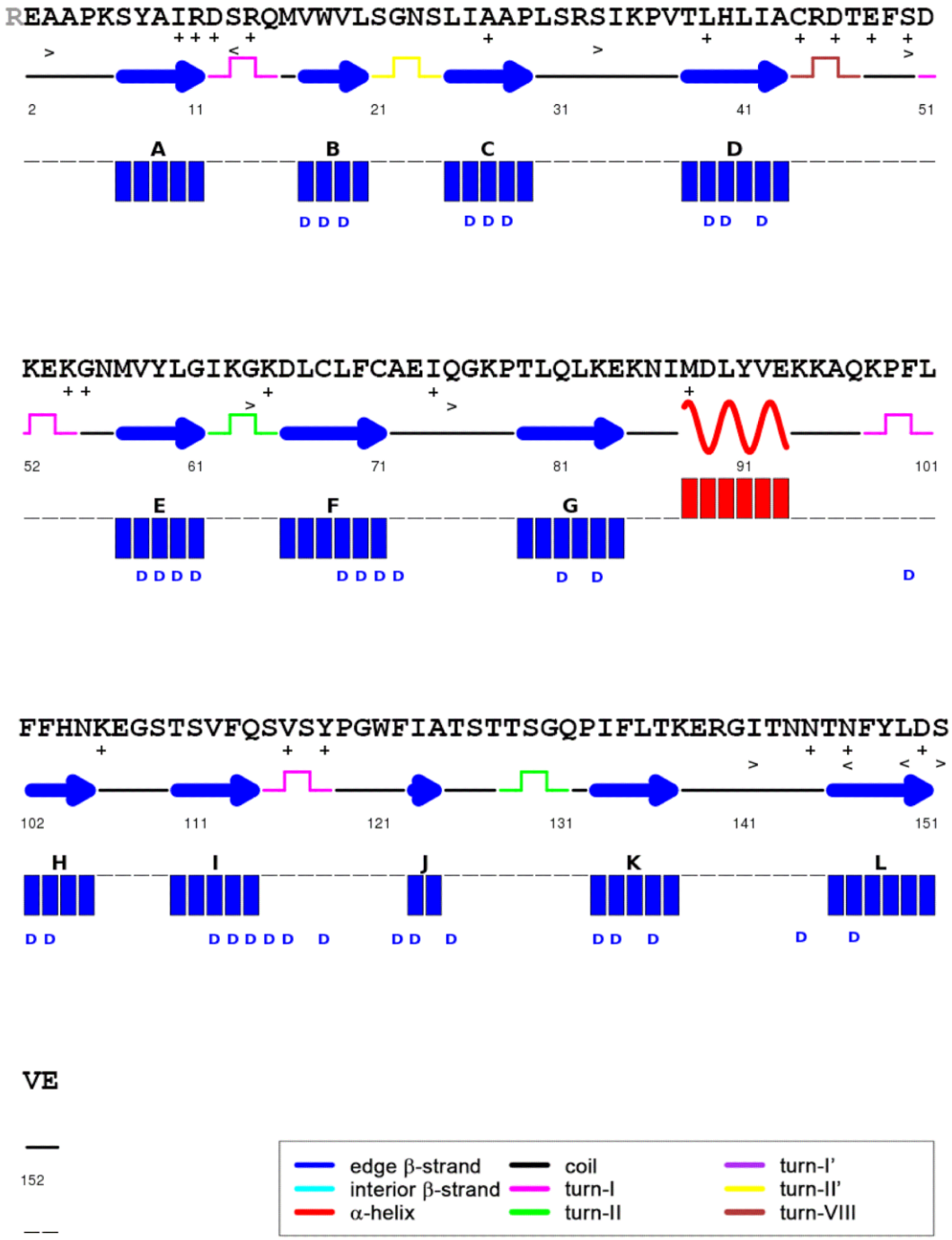

Fig. 2 Chemical shift analysis using the CSI-3.0 web server for IL-36β-2. Main secondary structure elements are coloured in blue for β-strands and red for α-helices. Colours of further structure elements predicted for IL-36β-2 are detailed in the inset box. β-strands (A–L) are labelled above the CSI bars and amino acids displaying a slow H/D exchange are indicated by a 'D' below the CSI bars. Residues with positive H^N coefficients are marked by '+'. Residues showing line broadening at low or high temperatures are marked by '<' or '>', respectively

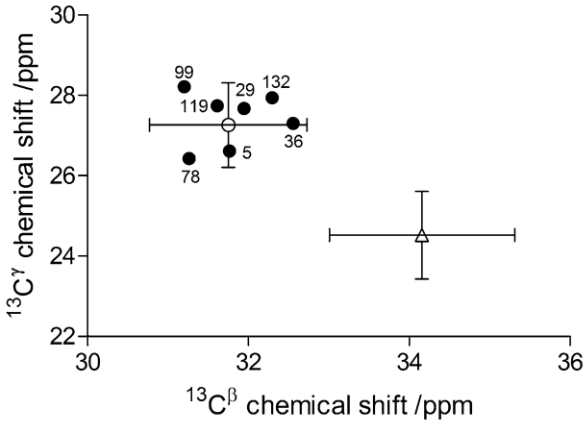

Fig. 3 Proline $^{13}C^{\beta}$ and $^{13}C^{\gamma}$ chemical shift analysis for IL-36β-2. Filled circles correspond to the chemical shifts characteristics of the numbered amino acids. The open circle indicates the location of the mean for a trans conformation, while the open triangle locates at the center of the conformational area indicative for a *cis* proline (Schubert et al. 2002) (standard deviation area shown as error bars)

one short α-helical element of two turns are predicted. The CSI predictions for IL-36β-2 coincide with the homology-related positions of the β-strands and α-helical substructures observed in the NMR solution structure of IL-36α (Goradia et al. 2016) and the X-ray structure of IL-36γ. Analysis of the chemical shifts for the *cis*/*trans* conformation distribution of proline peptide bonds (Fig. 3) according to the method of (Schubert et al. 2002) revealed that all prolines were predicted to display a *trans* conformation.

The ^{1}H, ^{13}C and ^{15}N chemical shifts of IL-36β-2 have been deposited in the BioMagResBank (BMRB) under the Accession Number 27688.

Evaluation of H bonding by temperature coefficients and D_2O exchange measurements

Monitored via [^{1}H, ^{15}N]-HSQC spectra, D_2O exchange of H^N is unsuccessful for several residues even after three times of lyophilisation suggesting that there are proton donors of strong or buried H bonds inaccessible for water exchange (e.g., residues W18, H40, F113, Y118, F134, F147). Many of these IL-36β-2 residues are expected to be located in antiparallel β-strands of pleated sheets, namely the better defined strands B/C, D/E, H/I, J/K pair of strands. Some β-turns and small loops also have protections against water exchange, e.g., between strands E–F, F–G and I–J or between G–H and K–L, respectively. Although most of these residues are hydrophobic, several are polar or even charged ones, a fact that alone would not explain their solvent inaccessible behaviour. In order to identify if these residues are exchange protected by H bonding, knowing also that most of these are presumably residents in H bonded strands or helices, H^N temperature coefficients were determined by collecting a series of [^{1}H, ^{15}N]-HSQC spectra referenced to DSS between 5 and 35 °C in 5 degree steps (see insert in Fig. 1). Interestingly, some residues are beyond detection by line broadening at low temperatures (S13, N146 and L149) or high temperatures (A3, S33, S50, G64, Q75, I141 and S151) only. All these residues are located in β-turns or loops, except the three at the last β-strand (N146, L149 and S151), which implies its temperature induced unfolding.

It is reported that residues having H^N temperature coefficients larger (i.e., less negative) than −4.6 ppb/K (Cierpicki and Otlewski 2001; Cierpicki et al. 2002) are predicted to be involved in H bonding but this low cut-off line gives some false positive hits. In IL-36β-2, there are several residues where positive H^N coefficients are observed such as I10, R11, D12, R14, A27, L39, C44, D46, E48, S50, K54, G55, K65, I74, M88, K106, V116, Y118, N144, N146 or D150. Some of these have a significant upfield H^N shift, which might be due to the ring current effect of the nearby -FLFF-site or the sequential aromatics. In contrast, two other residues (L39 and N144) have downfield-shifted H^N with a positive temperature coefficient indicating a structural resistance against thermal disturbance. Analysis of the IL-36α structure (PDB code 6HPI) reveals that it might be Y8 and F147, respectively, that produce the structural stabilisation. In contrast to this, helix resident and, thus, H bonded amide protons, although having considerable upfield shifts do have negative coefficients. The aromatic effect (Daley et al. 2004) has a major contribution on chemical shifts and hence could also affect the temperature coefficients. As the H^N and N coefficients show generally positive correlation for most residues, ring effects might also be determined by the presence of largely anti-correlated H^N and N values. Such residues are E48 (3.59; −75.96), F49 (−14.61; 37.60) and D51 (−13.26; 5.80), and F49 is presumably the one that contributes to this aromatic effect. If such chemical shift deviations (either up- or downfield) from random coil values are also taken into account and correlated with the temperature coefficients, according to (Andersen et al. 1997), the plot might highlight H bonding amide protons, i.e., values fall under the red cut-off line (Fig. 4, red line with the equation: $y = -1.8 \times -4.1$) [taken from Andersen et al. (1997)]. As several non-exchangeable proton values (red diamonds) are also found above the cut-off line, H bonding is not or not the only parameter that contributes to protection against water exchange in the cytokine IL-36β-2.

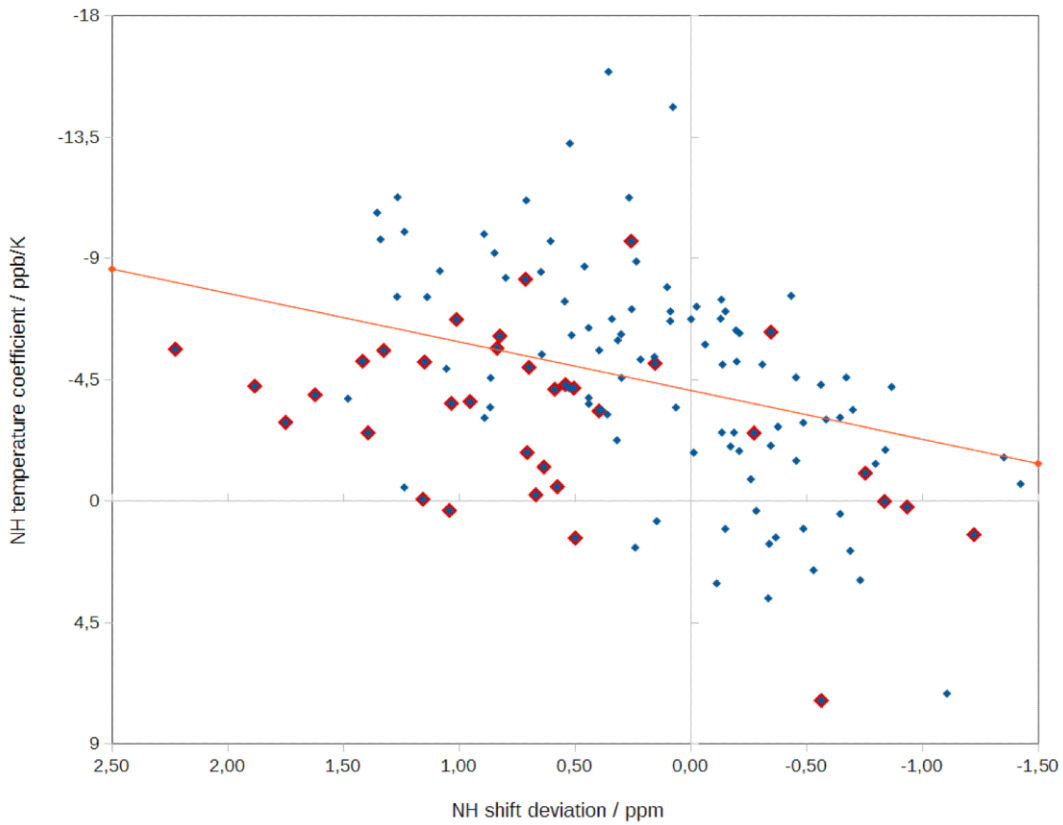

Fig. 4 Correlated values of NH temperature coefficients (ppb/K) and NH shift deviations from temperature corrected random coil values at 278 K determined for IL-36β-2 (blue diamonds). Therefore, downfield shifted amide protons are placed on the left side whereas upfield shifted ones are on the right side of the graph. Large red diamonds are values of residues that are protected against water exchange. Red line defined by equation $y = -1.8 \times -4.1$ represents a cut-off line expected to be a border between H bonding (below line) and no H bonding (above line) amide groups. Random coil values and the cut-off line are taken from Andersen et al. (1997)

Acknowledgements Financial support by the Deutsche Forschungsgemeinschaft (DFG) within FOR 1738 (to D.I. and O.O.) is gratefully acknowledged. The FLI is a member of the Leibniz Association (WGL) and is financially supported by the Federal Government of Germany and the State of Thuringia. We thank Prof. Seamus Martin, Smurfit Institute of Genetics, Trinity College Dublin, Ireland for providing the IL-36β plasmid.

References

Andersen NH, Neidigh JW, Harris SM, Lee GM, Liu Z, Tong H (1997) Extracting information from the temperature gradients of polypeptide NH chemical shifts. J Am Chem Soc 119:8547–8561

Bax A, Ikura M (1991) An efficient 3D NMR technique for correlating the proton and 15N backbone amide resonances with the alpha-carbon of the preceding residue in uniformly 15N/13C enriched proteins. J Biomol NMR 1:99–104

Bax A, Ikura M, Kay LE, Torchia DA, Tschudin R (1990) Comparison of different modes of two-dimensional reverse-correlation NMR for the study of proteins. J Magn Reson 86:304–318

Blumberg H et al (2007) Opposing activities of two novel members of the IL-1 ligand family regulate skin inflammation. J Exp Med 204:2603–2614

Boehner A, Navarini AA, Eyerich K (2018) Generalized pustular psoriasis—a model disease for specific targeted immunotherapy, systematic review. Exp Dermatol 27:1067–1077

Cierpicki T, Otlewski J (2001) Amide proton temperature coefficients as hydrogen bond indicators in proteins. J Biomol NMR 21:249–261

Cierpicki T, Zhukov I, Byrd RA, Otlewski J (2002) Hydrogen bonds in human ubiquitin reflected in temperature coefficients of amide protons. J Magn Reson 157:178–180

Clancy DM, Henry CM, Davidovich PB, Sullivan GP, Belotcerkovskaya E, Martin SJ (2016) Production of biologically active IL-36 family cytokines through insertion of N-terminal caspase cleavage motifs. FEBS Open Bio 6:338–348

Clubb RT, Thanabal V, Wagner G (1992) A constant-time 3-Dimensional triple-resonance pulse scheme to correlate intraresidue H-1(N), N-15, and C-13′ chemical-shifts in N-15-C-13-labeled proteins. J Magn Reson 97:213–217

Daley ME, Graether SP, Sykes BD (2004) Hydrogen bonding on the ice-binding face of a beta-helical antifreeze protein

indicated by amide proton NMR chemical shifts. Biochemistry 43:13012–13017

Debets R et al (2001) Two novel IL-1 family members, IL-1 delta and IL-1 epsilon, function as an antagonist and agonist of NF-kappa B activation through the orphan IL-1 receptor-related protein 2. J Immunol 167:1440–1446

Dunn EF, Gay NJ, Bristow AF, Gearing DP, O'Neill LA, Pei XY (2003) High-resolution structure of murine interleukin 1 homologue IL-1F5 reveals unique loop conformations for receptor binding specificity. Biochemistry 42:10938–10944

Farooq M et al (2013) Mutation analysis of the IL36RN gene in 14 Japanese patients with generalized pustular psoriasis. Hum Mutat 34:176–183

Gabay C, Towne JE (2015) Regulation and function of interleukin-36 cytokines in homeostasis and pathological conditions. J Leukoc Biol 97:645–652

Goradia N, Wissbrock A, Wiedemann C, Bordusa F, Ramachandran R, Imhof D, Ohlenschlager O (2016) (1)H, (13)C, and (15)N resonance assignments for the pro-inflammatory cytokine interleukin-36alpha. Biomol NMR Assign 10:329–333

Grzesiek S, Bax A (1993) Amino acid type determination in the sequential assignment procedure of uniformly 13C/15N-enriched proteins. J Biomol NMR 3:185–204

Gunther S, Sundberg EJ (2014) Molecular determinants of agonist and antagonist signaling through the IL-36 receptor. J Immunol 193:921–930

Hafsa NE, Arndt D, Wishart DS (2015) CSI 3.0: a web server for identifying secondary and super-secondary structure in proteins using NMR chemical shifts. Nucleic Acids Res 43:W370–W377

Hahn M, Frey S, Hueber AJ (2017) The novel interleukin-1 cytokine family members in inflammatory diseases. Curr Opin Rheumatol 29:208–213

Henry CM, Sullivan GP, Clancy DM, Afonina IS, Kulms D, Martin SJ (2016) Neutrophil-Derived Proteases Escalate Inflammation through Activation of IL-36 Family Cytokines. Cell Rep 14:708–722

Kanazawa N, Nakamura T, Mikita N, Furukawa F (2013) Novel IL36RN mutation in a Japanese case of early onset generalized pustular psoriasis. J Dermatol 40:749–751

Kay LE, Ikura M, Tschudin R, Bax A (1990) 3-Dimensional triple-resonance NMR-spectroscopy of isotopically enriched proteins. J Magn Reson 89:496–514

Kay LE, Guang-Yi X, Singer AU, Muhandiram DR, Forman-Kay JD (1993) A gradient-enhanced HCCH-TOCSY experiment for recording side-chain 1H and 13C correlations in H2O samples for proteins. J Magn Reson B 101:333–337

Kunz M, Ibrahim SM (2009) Cytokines and cytokine profiles in human autoimmune diseases and animal models of autoimmunity. Mediators Inflamm 2009:979258

Marrakchi S et al (2011) Interleukin-36-receptor antagonist deficiency and generalized pustular psoriasis. N Engl J Med 365:620–628

Moudgil KD, Choubey D (2011) Cytokines in autoimmunity: role in induction, regulation, and treatment. J Interferon Cytokine Res 31:695–703

O'Shea JJ, Ma A, Lipsky P (2002) Cytokines and autoimmunity. Nat Rev Immunol 2:37–45

Renert-Yuval Y, Horev L, Babay S, Tams S, Ramot Y, Zlotogorski A, Molho-Pessach V (2014) IL36RN mutation causing generalized pustular psoriasis in a Palestinian patient. Int J Dermatol 53:866–868

Schubert M, Labudde D, Oschkinat H, Schmieder P (2002) A software tool for the prediction of Xaa-Pro peptide bond conformations in proteins based on 13C chemical shift statistics. J Biomol NMR 24:149–154

Sims JE, Smith DE (2010) The IL-1 family: regulators of immunity. Nat Rev Immunol 10:89–102

Smith DE, Renshaw BR, Ketchem RR, Kubin M, Garka KE, Sims JE (2000) Four new members expand the interleukin-1 superfamily. J Biol Chem 275:1169–1175

Sugiura K, Takeichi T, Kono M, Ogawa Y, Shimoyama Y, Muro Y, Akiyama M (2012) A novel IL36RN/IL1F5 homozygous nonsense mutation, p.Arg10X, in a Japanese patient with adult-onset generalized pustular psoriasis. Br J Dermatol 167:699–701

Tauber M et al (2016) IL36RN mutations affect protein expression and function: a basis for genotype-phenotype correlation in pustular diseases. J Invest Dermatol 136:1811–1819

Towne JE, Sims JE (2012) IL-36 in psoriasis. Curr Opin Pharmacol 12:486–490

Towne JE, Garka KE, Renshaw BR, Virca GD, Sims JE (2004) Interleukin (IL)-1F6, IL-1F8, and IL-1F9 signal through IL-1Rrp2 and IL-1RAcP to activate the pathway leading to NF-kappaB and MAPKs. J Biol Chem 279:13677–13688

Towne JE, Renshaw BR, Douangpanya J, Lipsky BP, Shen M, Gabel CA, Sims JE (2011) Interleukin-36 (IL-36) ligands require processing for full agonist (IL-36alpha, IL-36beta, and IL-36gamma) or antagonist (IL-36Ra) activity. J Biol Chem 286:42594–42602

Vranken WF et al (2005) The CCPN data model for NMR spectroscopy: development of a software pipeline. Proteins 59:687–696

Vuister GW, Bax A (1993) Quantitative J correlation—a new approach for measuring homonuclear 3-Bond J(H(N)H(Alpha) coupling-constants in N-15-enriched proteins. J Am Chem Soc 115:7772–7777

Wittekind M, Mueller L (1993) HNCACB: a high-sensitivity 3D NMR experiment to correlate amide proton and nitrogen resonances with the alpha-carbon and beta-carbon resonances in proteins. J Magn Reson B 101:201–205

Publisher's Note Springer Nature remains neutral with regard to jurisdictional claims in published maps and institutional affiliations.

3 Further results

In this section data will be presented in continuation of the studies described in **publication 4**.

3.1 HRMs investigations of IL-36β and IL-36γ

3.1.1 Protein expression and purification of recombinant IL-36β and IL-36γ

The expression and purification protocol for IL-36β protein has been described in **publication 4**. The synthesized IL-36γ gene containing a caspase-3 site (DEVD) was obtained from Eurofins Genomics. The IL-36γ gene was further sub-cloned into the pET28a vector between NdeI and XhoI restriction sites and its sequence was confirmed with DNA sequencing. The pET28a_IL-36γ plasmid was transformed into the BL21(DE3) competent *E. coli* cells. One colony was inoculated into 250 ml Luria Bertani (LB) medium and allowed to grow at 37 °C until optical density ($O.D_{600nm}$) reached 1.4. Cells were spun down at 5000 r.p.m. and LB supernatant was discarded. Cells were resuspended in M9 medium containing $^{15}NH_4Cl$ and $^{13}C_6$-glucose for the ^{15}N and ^{13}C labeling of protein. Cells were allowed to acclimatize in M9 medium for 15 minutes before the IPTG (isopropyl-1-thio-D-galactopyranoside) induction. Cells were induced with 0.6 mM IPTG and transferred into an 18 °C incubator shaker for overnight expression. Expressed cells were spun down at 5000 r.p.m. and resuspended in a lysis buffer containing 50 mM Tris/HCl, 300 mM NaCl, 5 mM imidazole and 5 mM β-mercaptoethanol (pH 8), followed by three rounds of lysis with the French press. Lysed cells were centrifuged at 7500 r.p.m. at 4 °C. The clear supernatant of cell lysate was applied to a pre-equilibrated Ni-NTA agarose resin with lysis buffer and allowed to flow with the gravity. The resin was washed with 10 column volumes each of lysis buffer and wash buffer containing 10 mM. Ultimately, the protein was eluted with elution buffer containing 0.25 M imidazole. The eluted protein was dialyzed overnight at 4 °C in dialysis buffer containing Hepes 50 mM, 75 mM NaCl, 2 mM DTT (pH 7.4) to remove the N-terminal His tag using in-house expressed caspase-3 protein (40:1). Next day, the digested protein was passed through the pre-equilibrated (using dialysis buffer) Ni-NTA agarose resin to bind the remaining undigested IL-36γ protein and caspase-3 protein. This mixture was allowed to flow with the gravity and the flow through containing digested protein was collected. Remaining digested protein was collected with the same dialysis buffer. All the digested protein was concentrated to 1 ml using a 3-kDa amicon filter and injected on a size exclusion chromatography column (GE Healthcare) 16/60 Hiload S75. The fractions containing pure IL-36γ were pooled together and concentrated using a 3-kDa amicon filter. Later the protein was dialyzed into 20 mM sodium phosphate buffer, pH 7.2 for the further experiments. The final protein was either used directly for experiments or lyophilized for later use.

3.1.2 Circular Dichroism (CD) spectroscopy of IL-36β and IL-36γ

CD spectroscopy was initially employed to obtain a preliminary idea about the conformation or secondary structure elements in the IL-36β and IL-36γ proteins. The CD spectrum of proteins in the far ultraviolet region can usefully disclose information about secondary structure elements. The method has many advantages such as smaller amount of protein required, label free samples and fast result about secondary structure. Usually, a 218 nm negative band represents the β sheet structure while a band around 197 nm indicates a random coil structure in a protein. A Jasco J-710 spectropolarimeter with Peltier thermostat was used to obtain the far UV range (260 nm-190 nm) spectrum of both the proteins. A 1-mm pathlength cuvette was used containing 15 µM of each protein sample. The protein was kept at 20 ± 0.3 °C temperature at a 20 nm/min scan speed, bandwidth of 1.0 nm with a 1.0 nm of resolution and 4 seconds of response time.

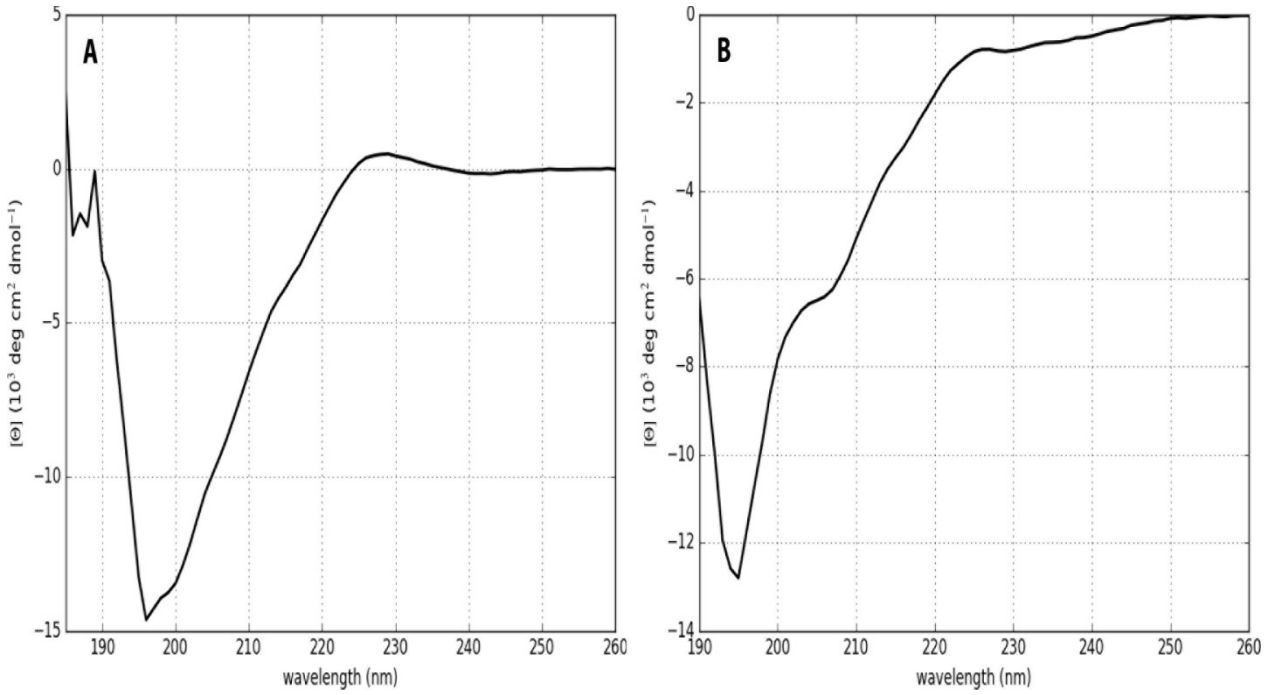

Figure 14: The CD spectra of (A) IL-36β and (B) IL-36γ in the far UV range.

Obtained CD data was further analyzed using two online secondary structure prediction servers, CAPITO (CD Analysis and Plotting Tool) [169] and BeStSel (Beta Structure Selection) [170]. The CAPITO algorithm utilizes the existing validated CD spectra from the Protein Circular Dichroism Data Bank (PCDB) while BeStSel takes an advantage of already available structures in the Protein Data Bank (PDB) and the CATH- protein structure classification database. Analyzed data can be seen in table 3 below.

Table 3: Secondary structure element analysis of IL-36β and IL-36γ

Protein	Server	α-helix	β-sheet	Irregular
IL-36β	CAPITO	31	54	15
	BeStSel	12.4	62.2	25.4
IL-36γ	CAPITO	32	53	14
	BeStSel	12.4	62.2	25.4
	X-ray	12	45	

When comparing the results with the secondary structure content of the X-ray structure of IL-36γ as comparison standard BeStSel gives a more correct estimation of the α-helix while CAPITO more correctly describes the β-sheet content. The CD analysis shows that the generated constructs IL-36β and IL-36γ basically display the same content of α-helix and β-sheet content.

3.1.3 NMR solution structure of the IL-36β protein

For the calculation of the NMR solution structure of IL-36β nuclear Overhauser enhancement distances (NOE) and torsion angle constraints were used. Three-dimensional [^{1}H, ^{1}H, ^{15}N]-NOESY-HSQC and [^{1}H, ^{1}H, ^{13}C]-NOESY-HSQC experiments were used to extract NOE-derived distance restraints, spectra were recorded at 20 °C using 1 mM ^{1}H, ^{13}C, ^{15}N labeled IL-36β protein samples prepared in 90% H_2O 10% D_2O and 100% D_2O, respectively. The Varian 900 MHz NMR system equipped with 5mm triple resonance cryo-probes. Referencing of C and N was performed via indirect chemical shift referencing. Processing of spectra was performed using TOPSPIN V2.2 (Bruker software) and for NOE assignment the CCPNmr analysis tool [171] was used.

The preliminary structure of IL-36β was generated using CYANA 3.98.5 [172], [173] where a total of 9225 unambiguous distance restraints (3955 ^{15}N-NOE and 5270 ^{13}C-NOE) were employed in the calculations. From 100 structures started with random angle distributions the best 20 solutions were selected for further energy minimization using two programs firstly OPAL [174] and secondly SYBYL (Certara St.Louis, US). The energy statistics of the final ensemble of 20 energy-minimized structures (Figure 28 in discussion) are shown in table 4.

Table 4: Energies of best IL-36β molecule

Bond Stretching Energy	26.928
Angle Bending Energy	210.642
Torsional Energy	163.445
Improper Torsional Energy	4.111
1-4 van der Waals Energy	268.817
van der Waals Energy	-963.745
H-Bond Energy	0.000
Total	-289.803 kcals/mol

The inspection of the initial NMR solution structure of IL-36β displays the typical β-trefoil fold similar to those found for other cytokines in the IL-1 family [175], [176]. Detailed structural comparisons are shown in the discussion section.

3.1.4 UV/Visible spectroscopy of heme with IL-36β and IL-36γ

As mentioned previously, heme shows a characteristic Soret band shift upon protein interaction in UV/Vis spectroscopy [177]. The Cary series UV/Vis spectrophotometer of Agilent technologies was employed for the measurement in the range of 250 nm to 800 nm using a 1-cm pathlength cuvette. A heme stock solution of 4 mM was prepared in 0.2 N NaOH solution and titrated against 5 µM of IL-36β and IL-36γ in 20 mM sodium phosphate buffer (pH 7.2) in equimolar concentration.

The UV/Vis spectra of the heme-IL-36β complex shows the Soret band shift towards 420 nm while the heme-IL-36γ exhibits a Soret band shift towards 370 nm which corresponds to hexa- and penta-coordination, respectively (Figure 15).

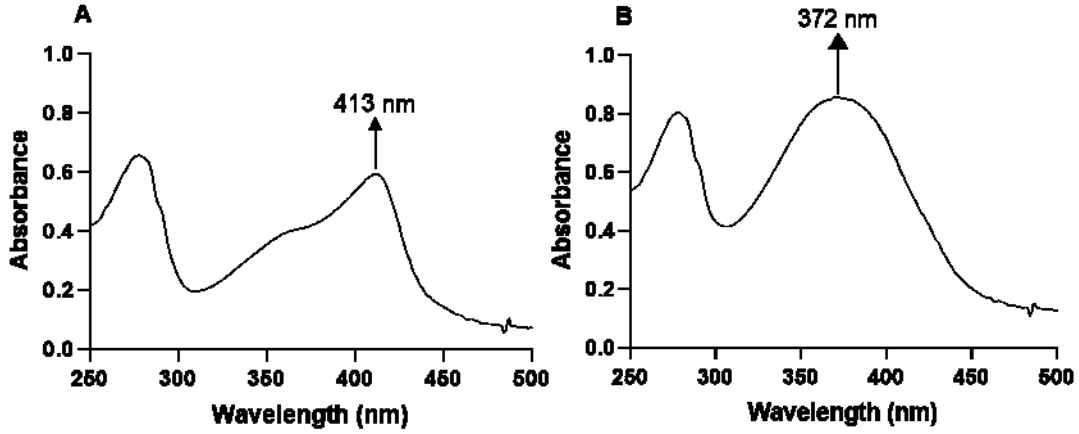

Figure 15: The UV/Visible spectroscopy absorbance spectra: (A) IL-36β-heme and (B) IL-36γ-heme complex

3.1.5 Resonance Raman spectroscopy of IL-36β-heme complex

A Horiba Jobin-Yvon LabRam HR 800 Raman spectrometer (Horiba, Kyoto, Japan) was used to obtain information on the heme coordination pattern in the IL-36β-heme complex. This device was equipped with a back-illuminated deep-depletion CCD detector (1024 × 256 pixels) cooled using liquid nitrogen. A Coherent Innova 300C ion laser was applied through the krypton line at 413.1 nm for excitation of Raman scattering. An Olympus BX41 upright microscope (Olympus, Tokyo, Japan) was connected to this Raman assembly to focus the incoming laser light onto the sample and also to collect the 180° backscattered light using a motorized XY microscope stage and a 20x objective (Olympus UPlanFL N, NA 0.50). The phosphate buffered NaCl, pH 7.0 was used for the preparation of the heme sample (400 µM) and the heme-protein sample in equimolar concentration (400 µM). The heme solution used here was prepared as described in **publication 3**. The heme-protein reaction mix was incubated at room temperature for 60 min in the dark and centrifuged before the measurement to remove any precipitant in the solution.

The 413 nm wavelength was applied to excite the heme moiety alone or heme-protein complex to gather the information of two spectral regions 1) Lower wavenumber region 2) Higher wavenumber region at a spectral center of 750 and 1400 cm^{-1}. The moderately increased band ν_7 and decreased band ν_3 around 1492 cm^{-1} indicated the penta-coordination pattern in the protein-heme complex [178]–[181]. In general, the Raman spectra showed IL-36β to bind to heme predominately in a penta-coordinated complex (Figure 16).

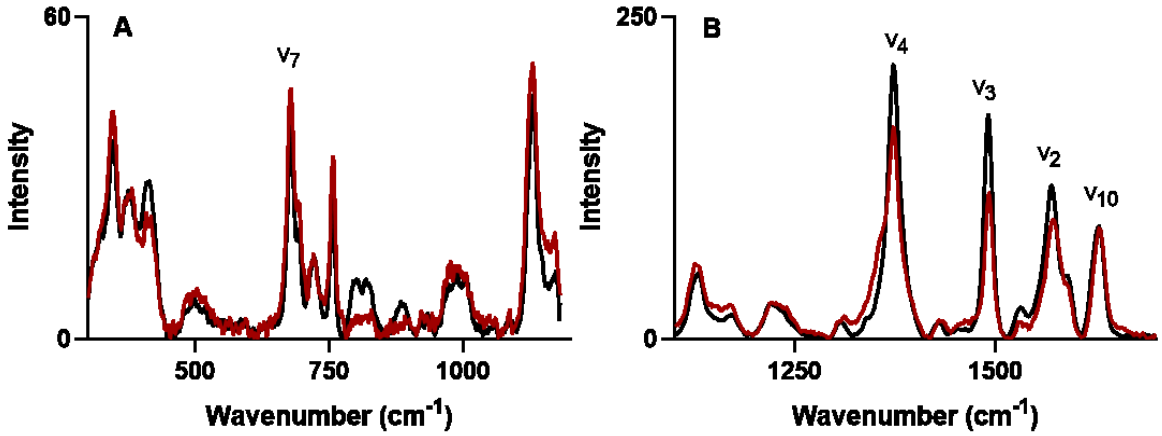

Figure 16: Superimposed resonance Raman spectra of IL-36β-heme complex (red) and heme (black). (A) Lower wavenumber region (B) High wavenumber region with frequencies indicated

3.1.6 NMR spectroscopy of IL-36β and IL-36γ protein (wild type and mutant proteins) with heme

The [^{1}H,^{15}N]-HSQC experiment was used for the monitoring of IL-36β and IL-36γ protein interaction with heme. The 4 mM heme solution was prepared in 0.2 N NaOH and 100 µM of protein dissolved in 20 mM sodium phosphate buffer, pH 7.2, at 20 °C for these measurements.

3.1.7 IL-36β interaction with heme

The IL-36β protein sample (100 µM) was measured alone and with the addition of 50 µM of heme. Upon addition of heme no chemical shift changes were observed, only selected residues intensities were either attenuated or completely disappeared (G130, Q131, S126, A28 and side chain of N56) (Figure 17). These residues were mapped on the initial IL-36β structure which revealed the effect of heme at two sites. To determine the exact heme-binding motifs we decided to produce protein mutants. Using site directed mutagenesis with complementary primers in total six mutant IL-36β proteins (H104A, Q131V, Q131E, Q131G, P132G and N56G) were produced in same way as described for wild type for NMR mapping experiments.

Interestingly, inspection of the NMR spectra revealed that the previously speculated heme binding at H104 which corresponds to H109 in IL-36α seemed not to be affected compared to effects at other residues (Figure 18). This was further confirmed as the H104A mutant showed heme binding similar to that observed for the wild type IL-36β protein. Q131V mutants were created which resulted in heme binding as in the wild type protein. This suggests that the valine in the Q131V mutant might mediate an interaction with heme. To test this theory of an interaction via valine in Q131V we created two mutants: 1) a Q131E mutant which shares a sterically similar side chain structure with glutamine and 2) a Q131G mutant which lacks a sidechain. The Q131E mutant also showed heme binding which was not as prominent as in wild type and in the Q131V mutant. An effect could be still seen at G130 and N56δ (side chain) while the Q131G mutant abolished most of signal changes characteristic for heme binding except at N56δ (side chain) (Figure 18). This suggests that heme binding can also be mediated by side chain interactions of Gln, Val, Asp and Asn. To check the contribution of N56 we created a N56G mutant which resulted in abolition of heme binding even at the Q131 residues (Figure 18). Thus, it might be possible that heme binding at N56 favors the binding at Q131P132 site.

In order to check a supporting role of P132 we created the P132G mutant which showed the less intensity reduction upon heme binding as compared to wild type which suggests that heme binding effects were reduced (Figure 18). This confirms the supporting role of P132 in heme binding at Q131 as in the CP motif as shown in IL-36α (**publication 3**). This

evidence clearly supports heme binding in Il-36β at Q131P132 as well as N56. The result is in also accordance with the observation of SPR studies that two molecules of heme bind to one molecule of protein.

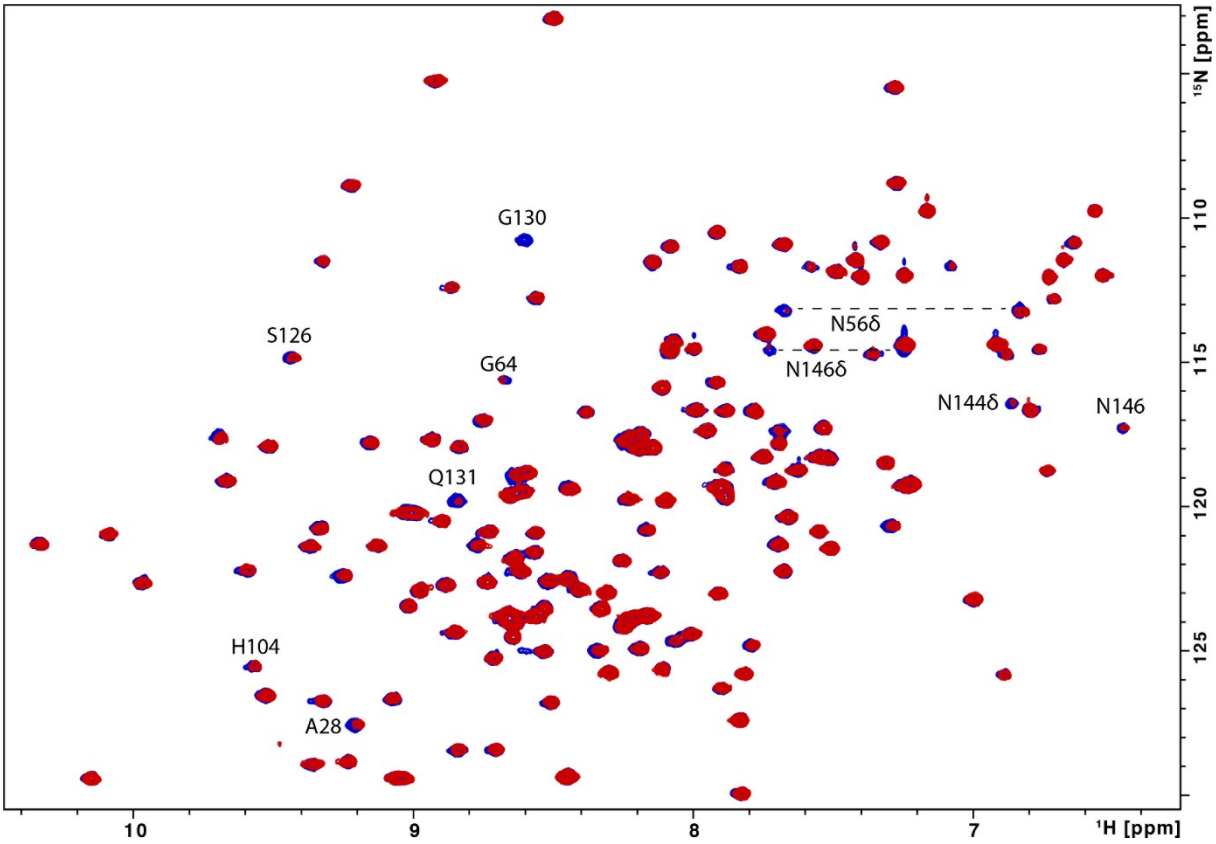

***Figure 17**: Superimposition of the [¹H,¹⁵N]-HSQC spectrum of 100 μM IL-36β protein without (blue) and with 50 μM heme (red). Affected residues are indicated.*

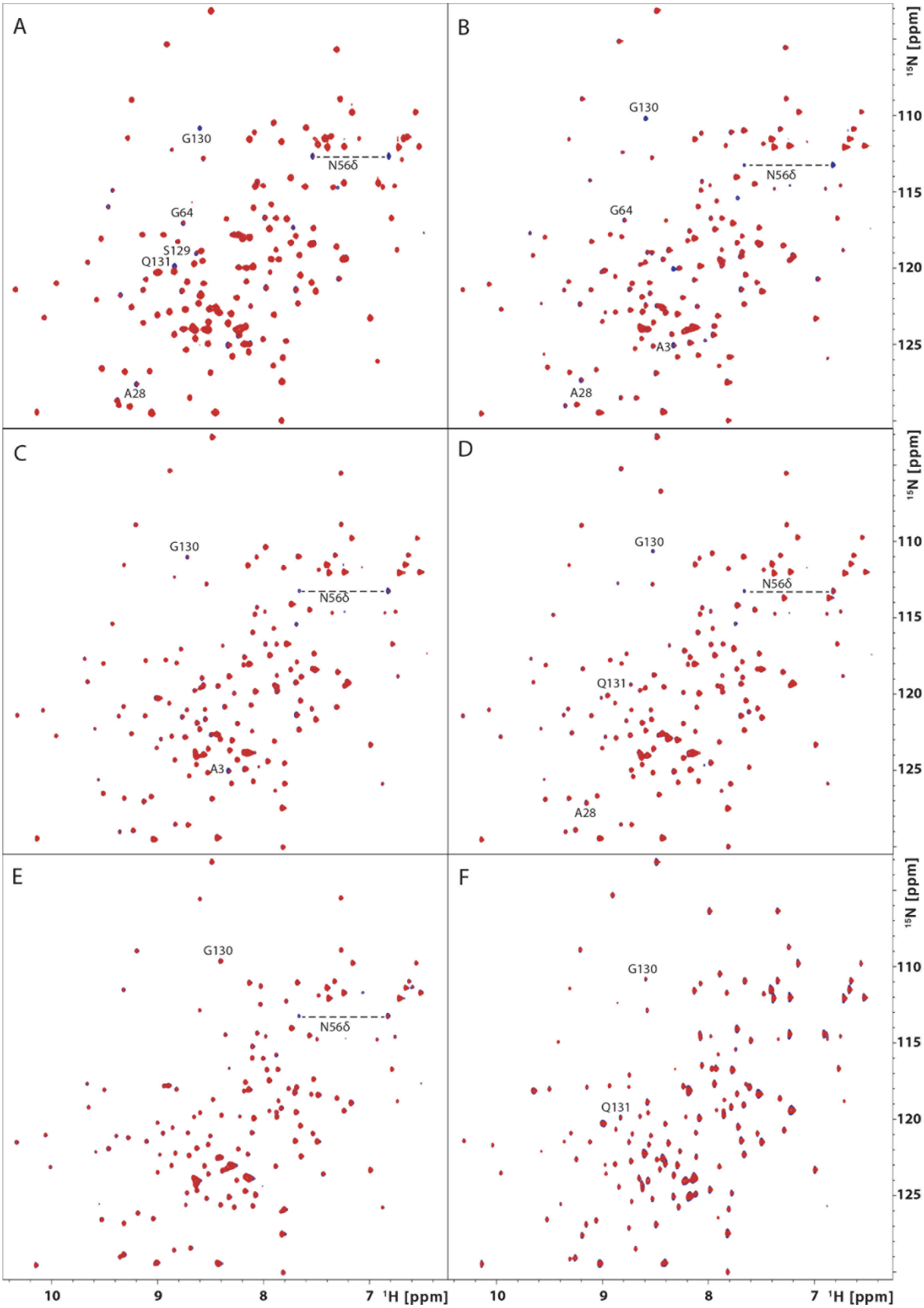

Figure 18: *Superimposition of the [^{1}H,^{15}N]-HSQC spectrum of 100 µM IL-36β mutant proteins without (blue) and with 50 µM heme (red) (A) H104A, (B) Q131V, (C) Q131E, (D) P132G, (E) Q131G, (F) N56G.*

3.1.8 IL-36γ interaction with heme

To obtain a complete overview of heme binding in the IL-36 family we performed also NMR measurements with IL-36γ. [^{1}H,^{15}N]-HSQC spectra of IL-36γ (100 µM) were acquired with and without the of heme addition. Consistent with IL-36β no chemical shift changes were observed upon 50 µM heme addition. However, again reduction of some peak intensities was observed (Figure 20). As mentioned previously the X-ray structure of IL-36γ is already available (PDB code 4IZE) which allowed a mapping without undergoing a complete NMR structural analysis. A mutation strategy was used to uncover the HRMs in IL-36γ without performing an extensive NMR resonance assignment. The mutant proteins of IL-36γ were prepared after examining its X-ray structure and taking into account its close sequence similarity with the IL-36β protein (Figure 19).

```
IL-36β_IF2_HUMAN  -------------------------MNPQREAAPKSYAIRDSRQMVWVLSGNSLIAAPL 34
IL-36γ_IF1_HUMAN  -MRGTPGD------------ADGGGRAVYQSMCKPITGTINDLNQQVWTLQGQNLVAVPR 47

IL-36β_IF2_HUMAN  SRSIKPVTLHLIACRDTEFSDKEKGNMVYLGIKGKDLCLFCAEIQGKPTLQLKEKNIMDL 94
IL-36γ_IF1_HUMAN  SDSVTPVTVAVITCKYPEALEQGRGDPIYLGIQNPEMCLYCEKVGEQPTLQLKEQKIMDL 107

IL-36β_IF2_HUMAN  YVEKKAQKPFLFFHNKEGSTSVFQSVSYPGWFIATSTTSGQPIFLTKERGITNNTNFYLD 154
IL-36γ_IF1_HUMAN  YGQPEPVKPFLFYRAKTGRTSTLESVAFPDWFIASSK-RDQPIILTSELGKSYNTAFELN 166

IL-36β_IF2_HUMAN  SVE 157
IL-36γ_IF1_HUMAN  IND 169
```

***Figure 19**: Sequence alignment of IL-36β and IL-36γ showed 43% sequence identity (Clustal 2.1). Suggested heme-binding sites marked in color.*

Mutants Q130V, Q130E, Q130G and D56G were created. These mutant proteins upon heme addition showed a similar behavior to the mutant proteins produced for IL-36β (Figure 21). Q130V and Q130E mutants display a higher intensity reduction and more residues were affected as compared to the Q130G mutant. This suggests Q130 as the one possible heme binding site as observed for IL-36β. The IL-36β has N56 as second heme binding site whereas in IL-36γ at this position resides a D56 residue. To test if this aspartate residue has the potential for heme binding, a D56G mutant was created. This mutant showed an intensity reduction at few residues and similar to the IL-36β N56G mutant almost abolished the heme binding of the whole molecule (Figure 21). Again, the possible explanation for this observation could be the same as in IL-36β where binding at the D56 site favors the binding of heme at the Q130P131 motif. This evidence suggests the possible

role of Q130P131 and D56 in heme binding which coincide with the SPR results of two heme molecules binding to one molecule of IL-36γ. The most affected residues are marked by an arrow in figure 21 and are further discussed later in this discussion section.

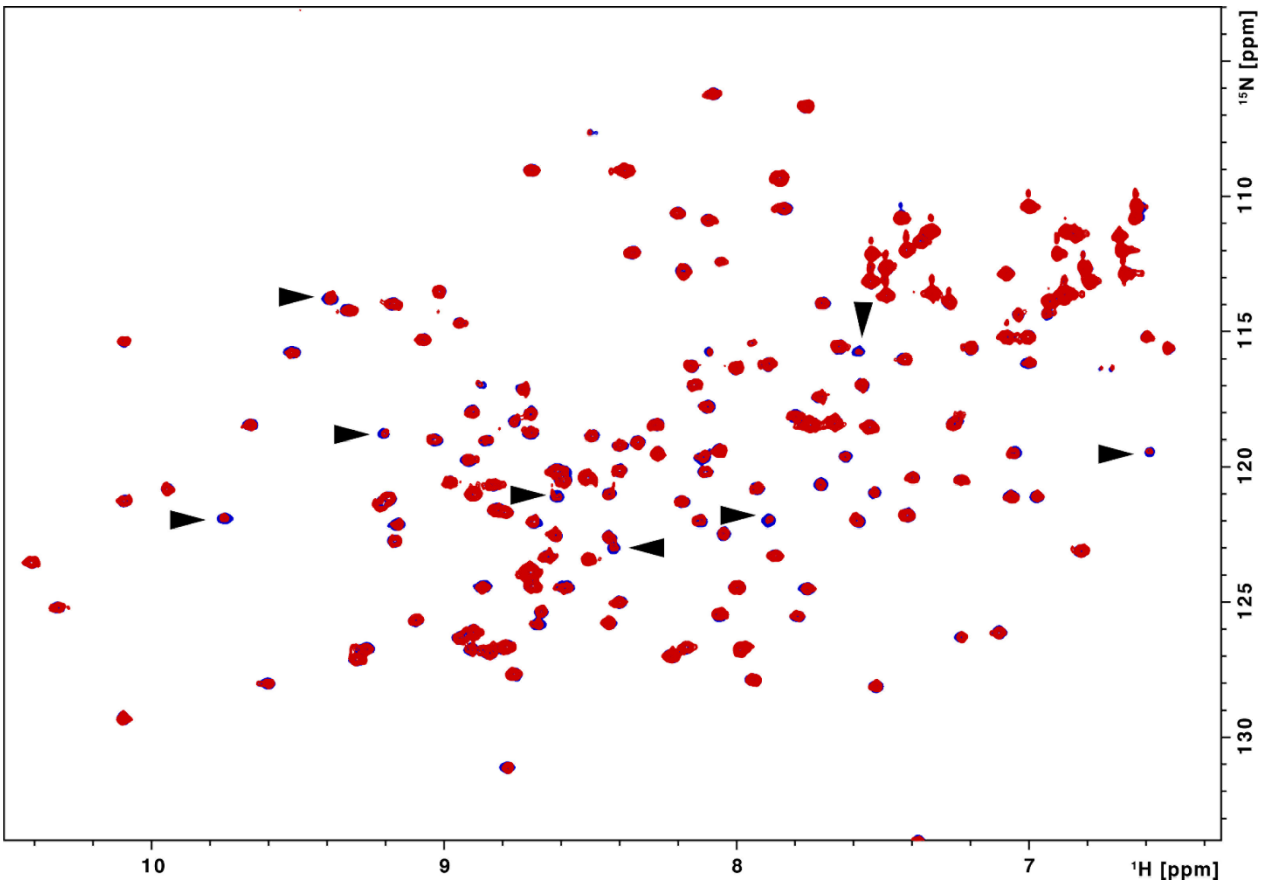

***Figure 20**: Superimposition of the [^{1}H,^{15}N]-HSQC spectrum of 100 µM IL-36γ protein without (blue) and with 50 µM heme (red). Strong intensity reductions can be seen at the marked (arrow) affected residues*

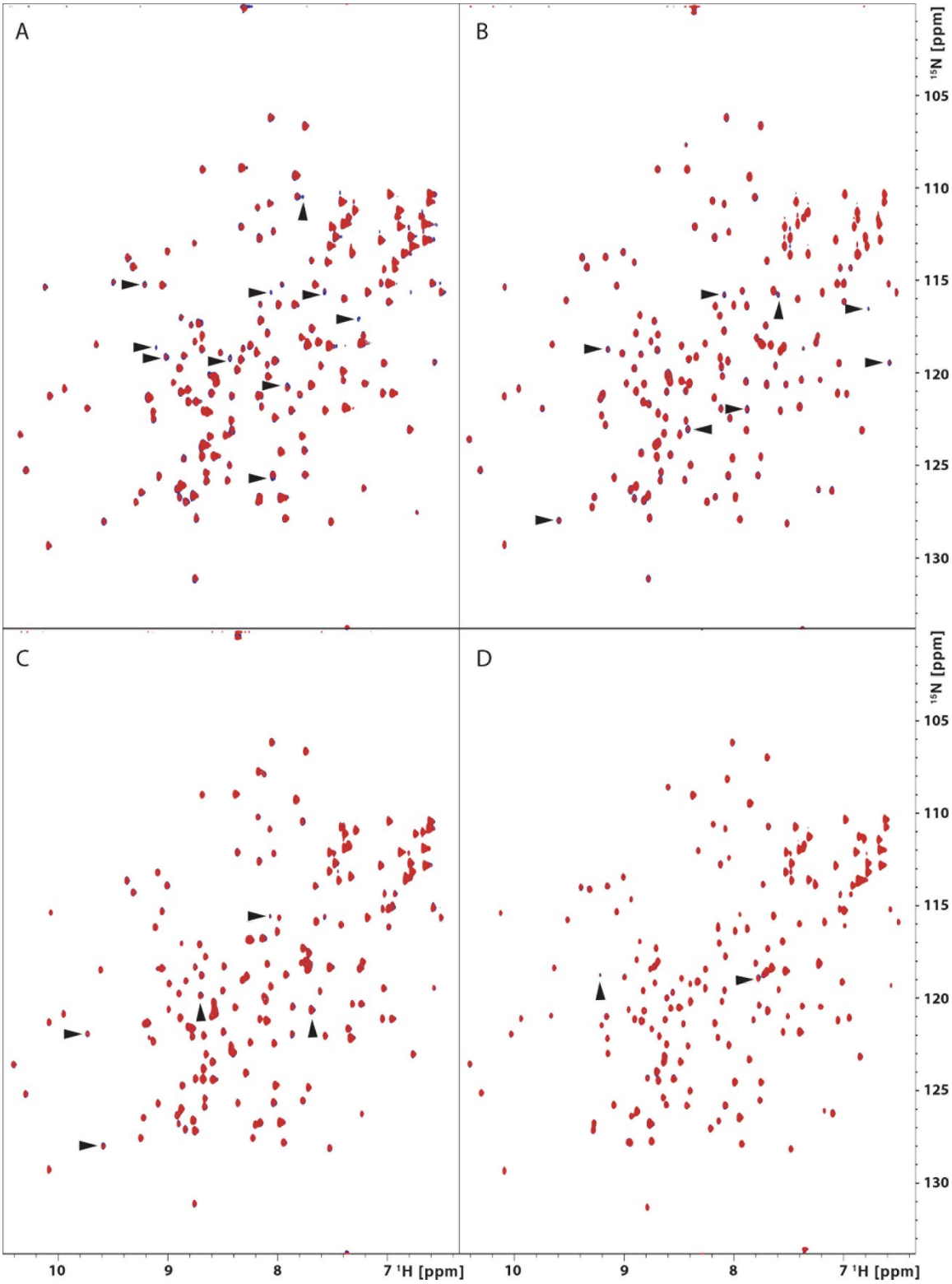

Figure 21: *Superimposition of the [^{1}H,^{15}N]-HSQC spectrum of 100 µM IL-36γ mutant proteins without (blue) and with 50 µM heme (red) (A) Q130V, (B) Q130E, (C) Q130G, (D) D56G. Most affected residues are marked with arrow.*

4 Discussion

In the last two decades the regulatory or signaling role of heme came under light in different biological processes where heme binds transiently to HRMs in proteins. Although a classification of HRMs has been proposed in the last years based on the case where an iron moiety in heme directly binds to cysteine, histidine, tyrosine [80], not all HRMs have been identified. In this study we have gained evidence that not only the central iron atom of heme but also propionate side chains can mediate a binding to amino acid residues through electrostatic or other weak interactions. These new identified HRMs will add knowledge to the growing structural HRMs classification and help to understand yet unidentified heme regulated proteins in biological processes.

4.1 N-terminus of the intrinsically disordered region (IDPR) of human cystathionine-β-synthase (CBS) (Publication 1)

The human CBS enzyme belongs to the large family of PLP dependent enzymes (EC 4.2.1.22), which is involved in the first step of the transsulfuration pathway thereby converting toxic homocysteine to cystathione. It is the only unique PLP-containing enzyme that has heme as a second cofactor. Deficiency or mutation of this enzyme leads to homocystinuria, an inherited disease. Characterized by elevated levels of toxic homocysteine in blood plasma this leads to many fatal pathological conditions in the cardiovascular, ocular, skeletal, and central nervous system e.g. in neural tube defects, cardiovascular diseases and Alzheimer's disease [182]–[184].

CBS has an N-terminal canonical heme binding domain followed by a catalytic core, which is conserved in most proteins of this class of organisms, and a C-terminal regulatory domain (**Publication 1,** Figure 1). For the first time, in **publication 1** we have shown that apart from canonical (covalently) heme binding at C52 and H65, heme also interacts transiently to a CP motif consisting of C15P16 and H22 via hexa-coordination. This allows heme to act via a second independent heme-binding site and this transient interaction of heme constitutes for approximately 30% of the enzyme activity. This effect was shown using a CBS protein activity assay on wild-type CBS and its mutant proteins. A series of NMR and UV/Vis spectroscopy experiments have been performed to structurally define this transient heme interaction.

4.1.1 Production of CBS (1-40 amino acids) protein

The N-terminal region of CBS (amino acids 1-40) responsible for the gain in enzyme activity mentioned above is intrinsically disordered as deduced from our NMR studies and supported by the absence of this stretch in X-ray structures. IDPs are prone to proteolytic cleavage during expression and purification [185]–[187]. To obtain the stable CBS (1-40) region, a fusion approach with the streptococcal protein GB1 was used. GB1 is the commonly

used tag to improve the solubility of small peptide and proteins. This tag is inert in nature and does not interfere with its fusion partner. Additionally, it also lacks cysteine and histidine as binding residues for heme interactions which was further confirmed by NMR experiments performed on GB1 alone with heme that proved no interaction. A NMR assignment experiment (3D HNN) performed on $_{GB1}$CBS(1-40) also revealed that the assignment of CBS can be easily performed without being hindered by spectral overlap of GB1 fusion protein peaks (**Publication 1,** Figure S1). The GB1 signals were mostly filtered out during the 3D HNN NMR experiment because the free induction decay (FID) signals of the rigid structured GB1 domain die fast, while the flexible nature of CBS(1-40) results in longer lasting FID and recordable signals (Figure 22). Thus, a spectral overlap problem of the fusion tag can be avoided without the need of complex and time-consuming segmental unlabeling techniques [188], [189].

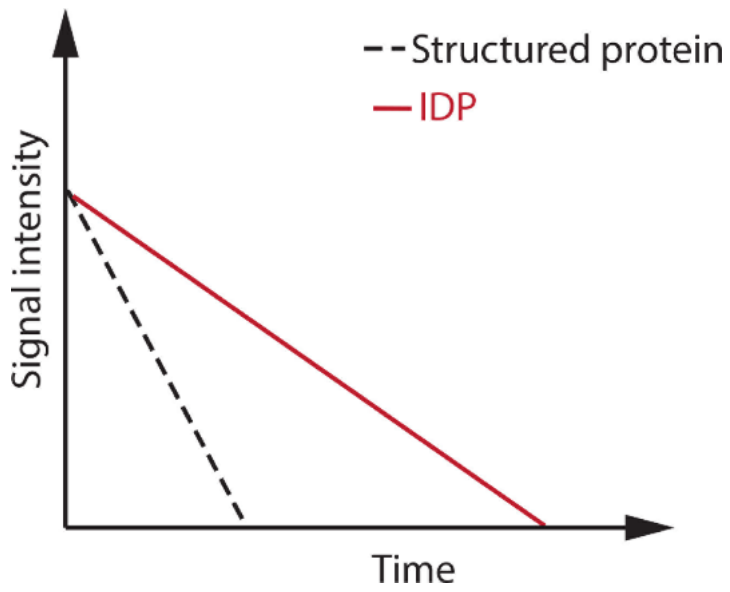

Figure 22: *Diagrammatic representation of FID and relaxation time in structured and intrinsically disordered proteins (IDPs)*

4.1.2 Heme-$_{GB1}$CBS(1-40) interaction studies

After obtaining stable $_{GB1}$CBS(1-40) we have used the conventional 2D NMR [^{1}H,^{15}N]-HSQC experiment (protein finger printing) for monitoring of the heme interaction. The resulting spectra showed no chemical shift changes, only a reduction of peaks intensities was observed with the maximum reduction at C15 and surrounding residues (T13, G14, C15, H17, R18, S19, H22, S23). This indicated the spatial proximity of paramagnetic iron (heme) to these residues and was in agreement with the Soret band shift near 420 nm in UV/Vis spectroscopy. This 420-nm shift indicates the protein binds to heme in hexa-coordinated geometry (Figure 23). We have also observed similar intensity reductions upon binding experiments with diamagnetic Ga-PPIX, which is a substitute of paramagnetic Fe-PPIX

(**Publication** 1, Figure 5b). This explains that Fe-PPIX has not only a paramagnetic relaxation effect (PRE) but also exerts an exchange contribution upon heme binding. The effect of Fe-PPIX PRE can be seen up to ~ 12 Ångstrom (Å) [190] explaining the maximum intensity reduction at C15 to H22 where heme binds as well as residues apart from this site (S3, Q40) with a reduced effect (**Publication 1** Figure S3). This is in accordance with Clore et al. who have defined transient protein-DNA interactions with lifetimes spanning nanoseconds to milliseconds using PRE effects [191], [192]. The single point mutation at C15 leads to abolition of heme binding in [^{1}H,^{15}N]-HSQC spectra. Again, this is in agreement with UV/Vis spectroscopy, which shows no Soret band maxima at 370 nm or 420 nm. This underlines the involvement of C15 in transient heme binding in a hexa-coordinated complex together with H22 as other axial ligand site. The involvement of H17 can be excluded due to insufficient residue spacing to form a hexa-coordination loop. However, the point mutation at H22 shows no significant intensity reduction in the [^{1}H,^{15}N]-HSQC spectra upon heme addition, while UV/Vis spectra displays a Soret band at 370 nm. This suggest that heme binds to C15 very weakly or the rate of exchange between heme-bound and free $_{GB1}$CBS(1-40) is not in a favorable range on the PRE time scale [80], [191], [192]. In general, heme binds to CBS(1-40) peptide via C15 and H22. Thereby, the peptide undergoes a conformational change to form a hexa-coordinated complex. This is reflected and further supported by an enzymatic assay done on the CBS(1-413) and CBS(1-413)_C15S mutant proteins which shows that the mutant protein has approx. 30% less activity than the wild type. The same type of activity reduction was observed by Oliveriusová upon deletion of CBS(1-39) residues (Oliveriusová, Kery, Maclean & Kraus, 2002) and several other studies also pointed out the importance of heme in activity of CBS enzyme [142], [148].

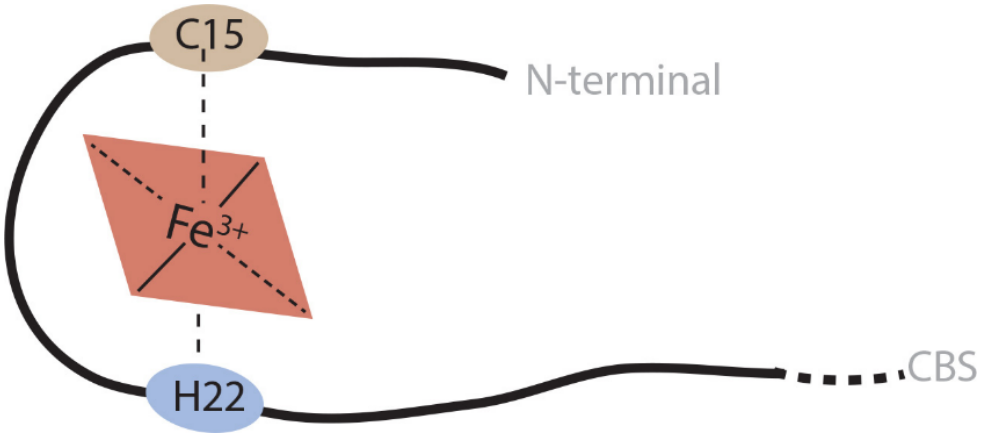

***Figure 23**: Cartoon illustration of CBS(1-40) forming hexa-coordination through cysteine 15 and histidine 22 with the central iron atom of heme*

This flexible N-terminus peptide either act as second independent transient heme binding site apart from the canonical covalent heme binding site or its flexible nature make it as a heme scavenger for canonical heme binding site as depicted in (Figure 24). This

$_{GB1}$CBS(1-40) study also stresses that we need to consider the complete molecule for full functional description as during X-ray studies often these flexible or disordered regions which can serve as potential interaction sites are eliminated from molecules of interest to facilitate the crystallization.

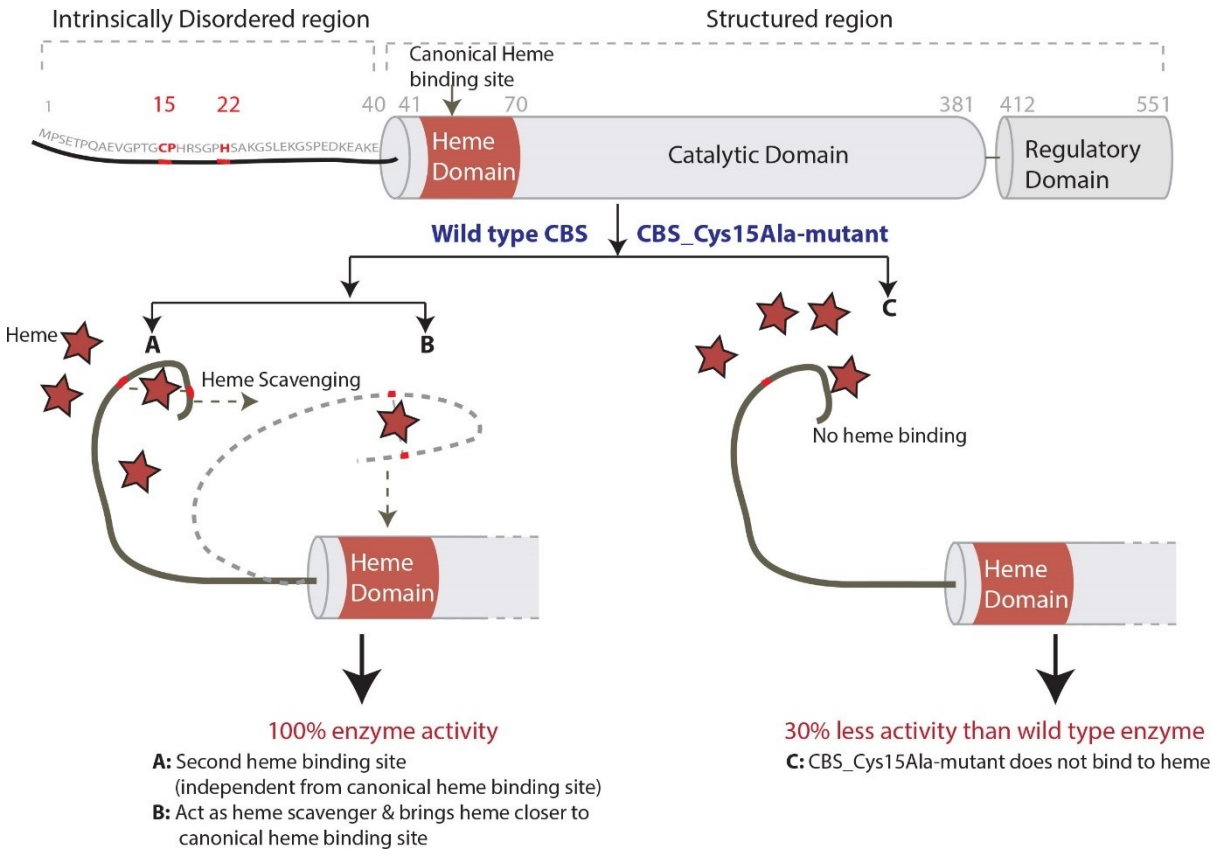

***Figure 24**: Cartoon illustration of CBS showing the possible role of the N-terminus (1-40) in context of heme*

4.2 Development of a NMR pulse to study intrinsically disordered protein (IDP)-heme interaction (Publication 2)

The growing number of reports of functionally relevant IDP in the last two decades made NMR spectroscopist to develop new pulse programs to study IDP systems at atomic level. The classical two dimensional [^{1}H,^{15}N]-HSQC experiment is often used to map protein-ligand interactions and we initially also employed this approach for protein-heme interaction studies. However, it became clear that this experiment has some limitations at physiological temperatures and pH, where signals start disappearing due to increased amide proton exchange and limitations in sensitivity. Often protein-heme interactions studied by [^{1}H,^{15}N]-HSQC experiments mirror only the effect of heme on the protein backbone while the more solvent exposed side chains could provide better interaction data.

For instance, we found that the H22L mutant protein of $_{GB1}$CBS(1-40) shows heme binding in UV/Vis spectroscopy but failed to reflect this feature in the [^{1}H,^{15}N]-HSQC experiments. This instigated us to further develop a NMR experiment to probe IDP-heme interaction more reliably as demonstrated in **publication 2.**

The newly modified HCBCACON is a side-chain experiment that yields the information of involved side chains upon heme interaction. Here we have exploited the ability of IDPs to provide better inter-residue $^{15}N_i{}^{13}CO_{i-1}$ chemical shift correlations than intra-residue spectra to generate better spectral dispersion and achieve resonance assignment [152], [153]. These $^{15}N_i{}^{13}CO_{i-1}$ chemical shift correlation spectra were generated by excitation of side chains and detecting either ^{13}CO or H$^{\alpha}$ (Figure 25). This ^{13}CO detection allows a simple 2D experiment and, therefore, can be carried out in less time. The heme binding experiment carried out using this protocol on $_{GB1}$CBS(1-40) shows similar residues affected like [^{1}H,^{15}N]-HSQC experiment. In addition, measurements can be done at physiological temperature (37 °C) and also provide information about proline residues which is missing in [^{1}H,^{15}N]-HSQC experiments. This information is especially crucial when studying heme interactions with CP motifs. An additional advantage of this ^{13}CO experiment is that in cases where IDP-heme interaction studies were carried out with GB1 fusion protein tag at 10 °C, it can reduce the large portion of signals originating from the GB1 tag which leads to less spectral crowding and unambiguous mapping of the interaction. These studies can also be performed using the HCBCACO experiment [193] but the ^{13}CO-detected HCBCACON experiment displays a better resolution. The experiment conducted on $_{GB1}$CBS(1-40)_H22L finally shows the heme interaction and sensitivity advancement over the [^{1}H,^{15}N]-HSQC experiment and confirms the UV/Vis study. However, at elevated temperature signals from the GB1 tag start appearing because of the increased molecular tumbling rate and less relaxation losses of signals. Nevertheless, in cases where the interaction does not lead to chemical shift changes it still provides a useful mapping approach even under spectral crowding.

To solve the spectral crowding problem and to obtain more sensitivity, the second H$^{\alpha}$ detection method came to view. This approach employs the same HCBCACON experimental protocol to detect the H$^{\alpha}$ because protons are the most sensitive nuclei compared to C and N, instead of ^{13}CO. This H$^{\alpha}$ detection was implemented as a 3D experiment, which is more time consuming. However, utilizing the non-uniform sampling technique (REF) allows to compensate for the extended 3D measurement time. Unlike the [^{1}H,^{15}N]-HSQC experiment, elevated temperature favors this experiment since increased molecular motion leads to increased relaxation times and thus a better signal to noise ratio. Improved sensitivity and spectral resolution were demonstrated using this approach not only on $_{GB1}$CBS(1-40) but also on its mutants. The C15 mutants shows no heme binding, while H22 mutants shows heme binding which was in accordance with the UV/Vis

spectroscopy and proves the improved sensitivity of this experiment over the [^{1}H,^{15}N]-HSQC experiment. The additional advantage of this experiment is that it can also be run as 2D if the system has good H^{α}_{i-1}-$^{15}N_{i}$ and $^{13}CO_{i-1}$-$^{1}H_{i-1}$ dispersion and that not only the protein-heme but other protein-ligands interaction can also be mapped in few hours.

In total, H^{α} detection using the HCBCACON experimental protocol can be used as a robust complimentary approach over conventional [^{1}H,^{15}N]-HSQC and ^{13}CO-based experiments [194] at lower or physiological temperature. Initial measurements (data not shown) suggest that this experiment can also be used to study protein-heme interaction under molecular crowding (which might better mimic conditions in the cellular environment).

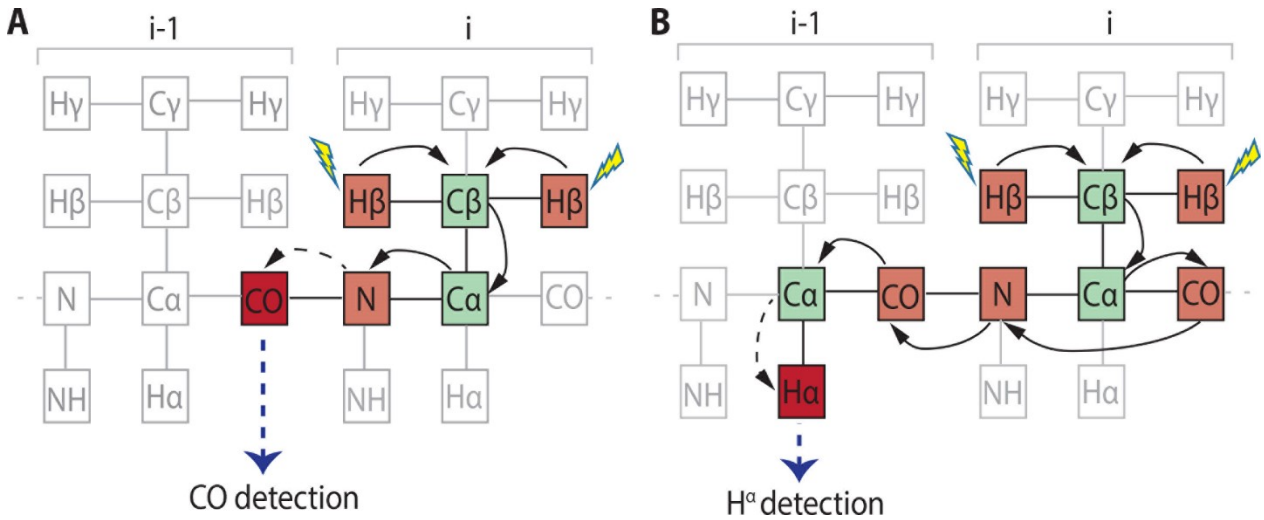

Advantages:

- Good sensitivity to detect IDP-heme interactions and applicable with GB1 fusion tag
- Can be carried out at physiological temperature (37 °C) and provides proline resonance information
- Interaction can be map in few hours
- Can be run as 3D for improved resolution
- Can be used for other IDP-ligand interactions

***Figure 25**: Signal transfer scheme of HCBCACON experiment in protein, starting excitation of H^{β} and detecting at the end (A) CO (B) H^{α} detection. Mentioned several advantages of HCBCACON over [^{1}H,^{15}N]-HSQC experiment.*

4.3 Interleukin-36α (IL-36α) and its interaction with heme (Publication 3)

IL-36α is a second protein derived from the peptide-heme interaction studies as a potential heme binder. As shown in **publication 3**, IL-36 family members (α, β, γ) bind to heme. Surface plasmon resonance (SPR) and biological tests confirmed the binding of heme. However, a detailed study has been performed only on IL-36α in this **publication 3**.

Initial UV/Vis experiments on nona-peptides resembling the CP sequence part of this protein showed heme binding at CP and YH, which made us to further investigate it at protein level. The UV/Vis study on IL-36α displayed Soret band shifts at 370 nm and 420 nm, which reflected the binding of two heme molecules. This was in accordance with the SPR measurements, which also showed a biphasic heme interaction. UV/Vis experiments done with only protoporphyrin IX (PPIX) showed no effect on the IL-36α molecule confirming the importance of iron for this interaction. Seven mutants were created to further confirm the involvement of CP and YH residues in heme binding: Y108S, H109A, C136SP137A, Y108SH109A, Y108SC136SP137A, H109AC136SP137A and Y108SH109AC136SP137A The UV/Vis of the Y108S mutant resulted in loss of the 370-nm shift and a reduced affinity was observed for heme, while the H109A mutant behaved like the wild type with the presence of both 370- and 420-nm Soret shifts. However, only minor differences in heme affinity were observed which might be explained by a supporting role of H109 in binding of heme at Y108. The C136SP137A mutant shows a loss of the 370-nm shift confirming the involvement of CP in heme binding. This is further supported by the results of the Y108SC136SP137A, H109AC136SP137A and Y108SH109AC136SP137A mutants.

The loss of ~ 370-nm shift in case of Y108S mutant has not been fully understood. The UV/Vis band around 420 nm in all Y108S mutants showed unusual broadening, which might indicate the unspecific or less specific binding of heme as shown in earlier studies [48], [195]. Involvement of the C136P137 and Y108H109 was clear where P137 and H109 have a supporting role in heme binding. The heme dissociation constant determined by SPR and UV/Vis spectroscopy reveals that one heme molecule binds at C136P137 with high affinity, while another heme molecule binds at Y108H109 with low affinity.

Raman spectroscopy provided further insight into the geometry of bound heme with the IL-36α protein. The wild-type IL-36α-heme complex and its mutant proteins exhibit a dominant presence of penta-coordination except the mutant C136SP137A and Y108SH109AC136SP137A additionally shows the negligible indication of heme complex.

4.3.1 NMR spectroscopy of IL-36α-heme interaction

NMR experiments performed on the full-length and truncated IL-36α show that there were no spectral changes upon truncation of the pro-peptide. Binding of heme results in no

chemical shift changes. However, for both Ga-PPIX and Fe-PPIX, an intensity reduction at selected residues was observed. Mapping of these affected residues on the NMR derived IL-36α solution structure reveals the presence of these residues in the vicinity of positions C136P137 and Y108. This suggests the C136P137 motif as coordination site for one heme molecule and attenuation of, e.g., H109 shows the binding of another heme molecule at Y108 which is in accordance with the UV/Vis study of the mutants. Molecular dynamics (MD) simulations and molecular docking of heme performed on the IL-36α NMR solution structure showed that the stereoelectronic conditions for binding of heme at C136 and Y108 are fulfilled, additionally supporting our experimental data.

4.3.2 Docking of IL-36α structure on its cognate receptor

The NMR study performed on full-length and truncated IL-36α indicated no major changes of the overall structure upon heme binding. Docking of the IL-36α structure on its cognate receptor complex (IL-1 receptor, PDB code 3O4O) showed that the presence of the first five N-terminal residues in full length IL-36α hindered the association with the receptor complex. After cleavage of these five residues, the shorter N-terminal section could be fully accommodated in a molecular cleft thus promoting association with the receptor. This explains very well the need for N-terminal processing of the IL-36α pro-peptide for a full activation of its molecular function as previously reported in literature [161].

4.3.3 Negative regulation of IL-36α-mediated signal transduction

In vivo studies performed on synovial fibroblast-like synoviocyte (FLS) cells from rheumatoid arthritis (RA) patients (data communicated from Hueber group at Erlangen University Hospital) showed the impact of IL-36α-heme complex on its signaling. In normal conditions, IL-36α binds to its receptor (IL-36R) and stimulates the expression of IL-6 and IL-8 cytokines. Pathological conditions [4], [39], [196] where severe hemolysis leads to a drastic increase in heme concentration (20 to 350 µM) can abrogate the IL-36α signaling. There, binding of heme with IL-36α leads to disabled association with the receptor, which in turn is not able to stimulate the expression of IL-6 and IL-8 proinflammatory cytokines (Figure 26). The same study performed on all truncated IL-36α mutant proteins showed that either the mutation leads to complete loss of activity or that the mutated residues were critical for binding to the receptor complex except C136SP137A mutant. The C136SP137A mutant showed relatively less but still activity compared to the wild type, suggesting a potential role of the Y108H109 motif in heme association and functional signaling.

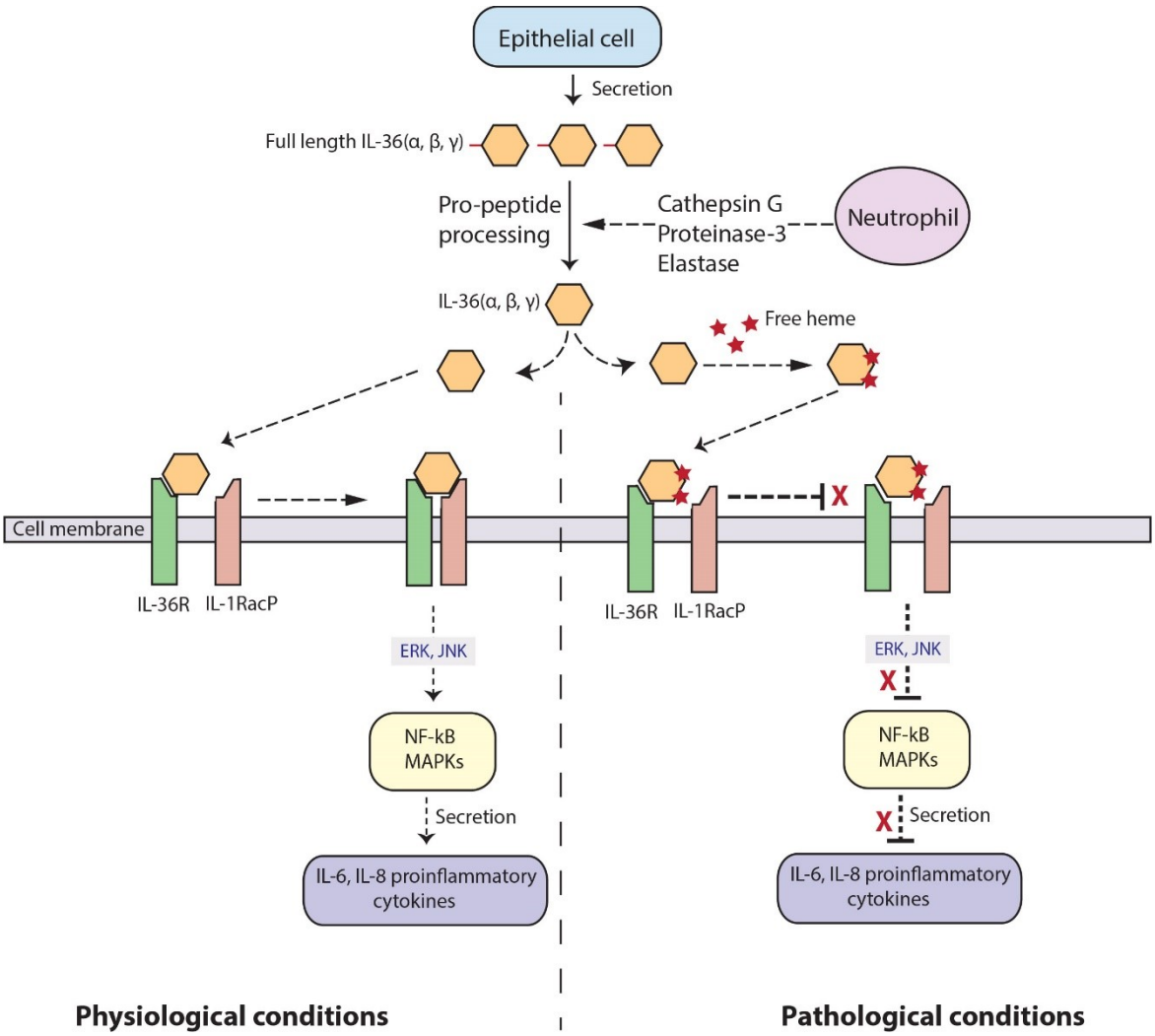

Figure 26: Possible scenarios of IL-36 mediated signaling in normal and pathological conditions (presence of heme)

4.4 Interaction of heme with interleukin-36β (IL-36β) and interleukin-36γ (IL-36γ) (Publication 4 & further results)

As mentioned previously these two cytokines are also a part of the IL-36 family and during SPR and biological studies also their heme binding capacity was revealed. Sequence alignment of all three cytokines (IL-36α, IL-36β and IL-36γ) reveals that the heme binding CP motif is uniquely present in the IL-36α while in IL-36β and IL-36γ CP is replaced by QP. The second heme binding site in IL-36α was located at Y108H109, interestingly histidine is present in IL-36β while tyrosine is conserved in IL-36γ at same position in IL-36α. We speculated that heme might be interacting with QP, Y, H amino acids in IL-36β and IL-36γ as shown in Figure 27. Apart from these residues several other potential heme-binding amino acids are also present in all three members.

```
IL-36α_HUMAN      -------------------------MEKALKIDTPQQGSIQDINHRVWVLQDQTLIAVPR 35
IL-36β_IF2_HUMAN  -------------------------MNPQREAAPKSYAIRDSRQMVWVLSGNSLIAAPL 34
IL-36γ_IF1_HUMAN  -MRGTPGD------------ADGGGRAVYQSMCKPITGTINDLNQQVWTLQGQNLVAVPR 47

IL-36α_HUMAN      KDRMSPVTIALISCRHVETLEKDRGNPIYLGLNGLNLCLMCAKVGDQPTLQLKEKDIMDL 95
IL-36β_IF2_HUMAN  SRSIKPVTLHLIACRDTEFSDKEKGNMVYLGIKGKDLCLFCAEIQGKPTLQLKEKNIMDL 94
IL-36γ_IF1_HUMAN  SDSVTPVTVAVITCKYPEALEQGRGDPIYLGIQNPEMCLYCEKVGEQPTLQLKEQKIMDL 107

IL-36α_HUMAN      YNQPEPVKSFLFYHSQSGRNSTFESVAFPGWFIAVSSEGGCPLILTQELGKANTTDFGLT 155
IL-36β_IF2_HUMAN  YVEKKAQKPFLFFHNKEGSTSVFQSVSYPGWFIATSTTSGQPIFLTKERGITNNTNFYLD 154
IL-36γ_IF1_HUMAN  YGQPEPVKPFLFYRAKTGRTSTLESVAFPDWFIASSK-RDQPIILTSELGKSYNTAFELN 166

IL-36α_HUMAN      MLF 158
IL-36β_IF2_HUMAN  SVE 157
IL-36γ_IF1_HUMAN  IND 169
```

***Figure 27**: Sequence alignment of all three members of IL-36 family cytokines. Suggested heme-binding sites marked in color.*

4.4.1 Secondary structure elements in IL-36β and IL-36γ

Before performing the detailed NMR based structure determination the simple far UV CD spectroscopy was used to get an idea about the secondary structure elements of IL-36β. The CD spectra of IL-36β showed a high composition of β-sheet as analyzed through CAPITO and BeStel which in accordance with the predicted secondary structure content from NMR data by the CSI program as discussed in **publication 4**. The program CSI uses the backbone chemical shift assignments of the respective protein to calculate the secondary structure information [197], [198]. Comparison of the IL-36α NMR solution structure and the X-ray structure of IL-36γ with the predicted CSI results of the homologous IL-36β revealed that the location of secondary structure elements in all proteins coincides. The chemical shift of all the prolines present in IL-36β revealed an all-trans conformations. A result which has been also observed for IL-36α [199]. In addition, the D_2O exchange study on IL-36β gives additional evidence for the presence of β-sheet arrangements as predicted by CD and CSI since many of the residues failed to exchange after three times of D_2O lyophilization. This suggests the locations of these residues are inaccessible or buried and reveals the position of β-strands (**Publication 4** figure2). In the NMR literature [200], [201] it was reported that a temperature coefficient study can also be used to locate secondary structure elements. The temperature coefficients of IL-36β as described in **publication 4** also suggest that some of the affected residues are located on the H-bonded strands or helices. Finally, the CD spectroscopy results of IL-36γ are matching well with the secondary structure content derived from the analysis of the X-ray structure.

4.4.2 NMR solution structure of the IL-36β protein

An initial 3D NMR solution structure of IL36-β was calculated employing the program CYANA 3.98.5 and a set of distance restraints based on the initially assigned ^{15}N-NOE and ^{13}C-NOE cross peaks. The best 20 of 100 calculated structures with lowest target function were chosen and further relaxed by energy minimization using the OPAL and SYBYL. The

final ensemble of 20 structures has a low root mean square deviation (RMSD) value for the backbone atoms of 0.52 Å.

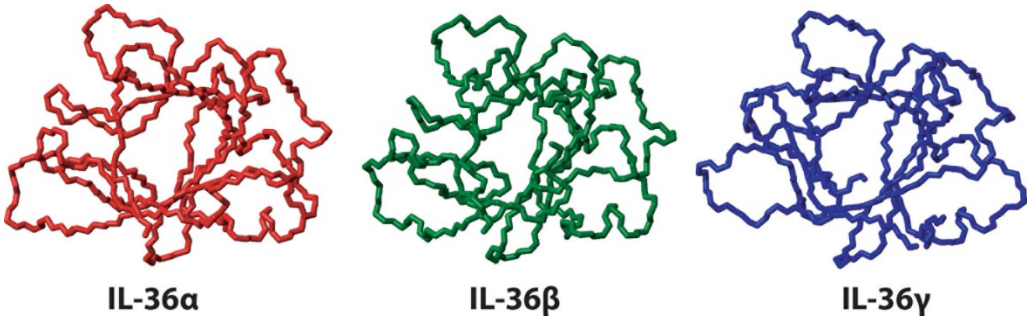

***Figure 28**: Backbone structure of all three members of IL-36 family (prepared in Mol Mol)*

The preliminary NMR solution structure exhibits the typical β-trefoil fold symmetry like observed for the IL-36α NMR solution structure and the IL-36γ X-ray structure with ~27% of identity shares among them. For visual comparison Figure 28 shows the backbone of all three IL-36α, IL-36β, IL-36γ structures in parallel. It becomes obvious that the overall fold for all three members are highly similar and contains almost same distribution of β-strands and α-helical elements.

4.4.3 Heme interaction study of IL-36β and IL-36γ using NMR spectroscopy

The [^{1}H,^{15}N]-HSQC spectra were used for the monitoring of IL-36β and IL-36γ interaction with heme. The spectra displayed no chemical shift changes in residues position only intensity reductions were noticed at special positions. The affected residues were mapped on the preliminary IL-36β structure showing that residues around Q131P132 and N56 residues (Figure 29) were affected. The NMR studies performed on the wild type IL-36β and Q131V, Q131E, N56G mutants suggest that the heme is interacting with the side chains of this molecule. The wild type IL-36β has Q131P132 as a first heme binding site while N56 acts as secondary binding site. It has been shown that amino acids containing nitrogen atoms in the side chain like lysine, asparagine [202] with its amide group and in rare cases an amino group of proline [203], [204] can act as a axial ligand or interact with the propionate groups as shown in (Figure 30). This is also in accordance with Raman spectroscopy showing penta-coordination and supports our experimental studies. One study reported that often hydrophobic amino acids like valine, leucine, isoleucine and alanine are frequently found close to the proximal or distal side of heme where they can interact with non-polar propionate groups through hydrophobic interactions [4], [205]. Our study suggests that the two methyl groups of valine in the Q131V mutant are able to interact with propionate groups of heme through weak hydrophobic interactions. The effect of heme in the Q131E mutant was less pronounced as compared to Q131V and wild type IL-36β which indicates that the negatively charged COO^{-} group of the glutamate in the Q131E

mutant might be directly interacting with the iron ($Fe^{2+/3+}$) atom of heme through even weaker electrostatic or ionic interactions. As reported earlier not only hydrophobic but also electrostatic interactions are possible interactions between heme and a protein through hydrogen bonds or weaker salt bridges [4]. These conditions also apply to the IL-36γ and its mutant proteins where Q130 is the first heme binding site interacting through amide side chain. In addition, the second heme interaction site D56 might be interacting through weaker electrostatic interactions (Figure with structure). This is further supported by SPR data where one heme molecule binds relatively stronger than a second site in both IL-36β and IL-36γ molecules (Publication 3, TableS1). The functional aspects of the interaction of these proteins with heme have been illustrated previously in figure 26 with IL-36α.

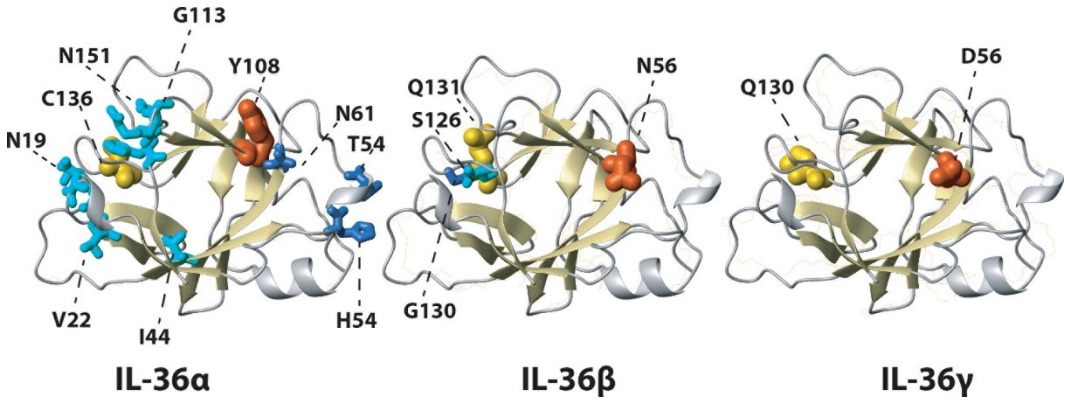

***Figure 29**: Affected residues upon heme addition indicated in IL-36 family members with blue color while heme-binding sites marked in orange and khaki*

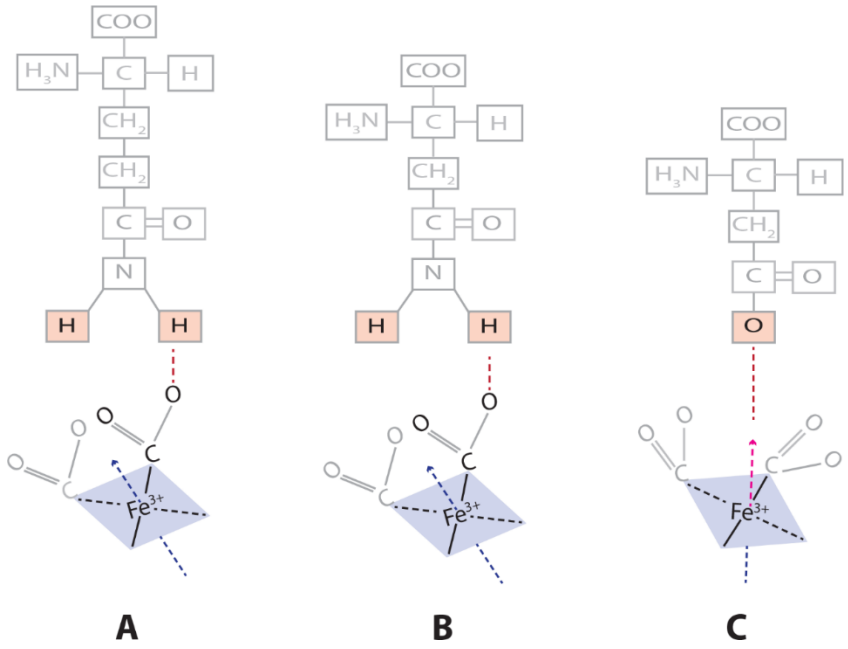

***Figure 30**: Possible interaction (Red) of heme propionate group with (A) Glutamine (B) Asparagine and (C) Aspartate directly interacting with iron atom*

In conclusion, to our knowledge for the first time through these in vitro studies we are unraveling that glutamine and asparagine can also act as an axial ligand for transient heme binding. This adds further potential residues beside the previously reported cysteine, histidine, tyrosine, methionine to the interaction repertoire. While the latter are known as canonical binding sites for the central iron atom, aspartate, valine and glutamate can interact to propionate side chains.

5 Future Prospects

5.1 Human cystathionine-β-synthase (CBS) interaction with heme

The study performed in this thesis revealed the role of transient heme interaction for the enzymatic activity of CBS. Deficiency in this enzyme or loss of function is responsible for a disease called homocystinuria. Many pharmacological studies have been performed to restore the function of this enzyme caused by pathological mutations [206]–[208]. To consider this new transient heme binding functional aspects to further explore the activity of this enzyme could strengthen these strategies. One study already suggested δ-aminolevulinic acid (δ-ALA), a heme precursor, with other small osmolytes were able to restore 30% activity of 14 pathogenic CBS mutants [206]. In addition, CBS is also responsible for the production of 95% of hydrogen sulfide (H2S) in brain which is recently recognized as signaling molecule and to have implications in cardiovascular and nervous systems [137], [209], [210].

5.2 Development of a NMR pulse sequence to map intrinsically disordered protein (IDP)-heme interactions

The developed new NMR approach is more sensitive and can help in discovering yet unknown heme-binding proteins along with the traditional NMR methods. NMR mapping applications have been used in pharmaceutical studies since 1976 [211] and witnessed the identification of a number of drugs and inhibitors [212]–[215]. The presented method can similarly be used for mapping of IDP-ligand interactions in pharmacological drug discoveries, e.g for small molecules in the fragment based drug discovery approaches where the interaction is too weak to be detected through biochemical or biophysical assays like ELISA and fluorescence resonance energy transfer (FRET) [216], [217].

5.3 The Interleukin-36 family cytokine interaction with heme

A detailed study of IL-36α has been presented involving the determination of its NMR solution structure and its interaction via biophysical techniques like Raman, UV/Visible spectroscopy. However, further investigation of this interaction in in vivo and mouse studies could give more insight for its involvement in the diseases psoriasis and rheumatoid arthritis.

Within this thesis a preliminary structure of IL-36β is presented. Although the final refined NMR solution structure of IL-36β has still to be calculated it already allowed to define the heme interaction sites and to compare the structural features with other members of this family. The interaction of heme with these cytokine class should be considered by the growing number of reports on IL-36 family members and their involvement in inflammation, rheumatoid arthritis, inflammation and latest involvement during pregnancy which could give further insight at biological level [165].

5.4 Development of heme sensors

There has been a number of reports in the last decade on development of heme sensors [218]–[221].During many pathological conditions like Malaria, sub arachnoid hemorrhage labile heme is accumulated in the body and exerts toxicity for the cells. It is important to characterize this labile heme for the therapeutic developments [218], [222]. This study would be beneficial to create heme sensors based upon the structural information obtained from how heme binds transiently to proteins or what is modulating the binding affinity. So it might contribute not only to determine the heme in pathological conditions but also to uncover the poorly understood nature of heme trafficking in organisms [219], [223].

5.5 Heme induced polyreactivity in antibodies

Immunoglobulins are a new class of molecules which has been seen interacting with heme in the last few years [224]. Antibodies are the second most abundant molecules circulating in plasma after the albumin. It has been seen that heme can induce polyreactivity in immunoglobulins (IgG, IgM, IgE etc.) which resulted in new specific binding properties and thereby diversifies the antibodies functions [106], [225]. One study shows that heme induced polyreactivity helped in neutralization of Japanese Encephalitis viruses [226] while other indicates its potential in cancer therapeutics [227]. At the structural level very few information is available on how heme binds in the variable region of antibodies and induces polyreactivity. Knowledge obtained from the present study can be applied on designing a strategy to find the heme-binding motifs in antibodies and to elucidate the molecular dynamics changes of antibodies upon heme interaction. This could help in designing antibodies delivering drugs or could contribute to develop heme scavenging antibodies to prevent the deadly effect of heme on cells.

6 Conclusion

We have validated the knowledge obtained from previous peptide-heme interaction studies at protein level. During this study we have shown the structural details upon heme interaction to intrinsically disordered proteins as well as structured globular proteins. Transient interaction of heme to the intrinsically disordered N-terminus of the CBS protein revealed the involvement of heme in the activity of this enzyme as well as possible conformational changes in structure upon heme interaction. It also emphasizes the probable role of these disordered regions in signaling.

The study performed on interleukin-36 family members shows that among the family members different kinds of heme regulatory motifs (HRMs) are involved in heme binding with different affinity. We also shed the light at structural level on how N-terminal processing of pro-peptides in these cytokines leads to full activation. In vitro studies on these cytokines unravelled new types of HRMs for the first time with possible interaction through propionate groups of heme with side chains of residues in these HRMs. Thus, this study contributes more details to the growing classes of HRMs and adds some aspects for the determination of yet unknown transient heme-binding proteins. This study also adds with the IL-36 proteins three new structured proteins and with CBS1-40 an intrinsically disordered protein to the growing number of transiently heme-interacting proteins.

7 References

[1] I. Moura ', G. Fauque *, ', J. Legall3, A. V Xavier', J. J. G. Moura', and J. J. G. Moura, "Characterization of the cytochrome system of a nitrogen-fixing strain of a sulfate-reducing bacterium: Desulfovibrio desuZjiuricans strain Berre-Eau," 1987.

[2] T. Yagi, "Purification and properties of cytochrome c-553, an electron acceptor for formate dehydrogenase of Desulfovibrio vulgaris, Miyazaki," *Biochim. Biophys. Acta - Bioenerg.*, vol. 548, no. 1, pp. 96–105, Oct. 1979.

[3] Y. Higuchi, K. Inaka, N. Yasuoka, and T. Yagi, "Isolation and crystallization of high molecular weight cytochrome from Desulfovibrio valgaris Hildenborough," *Biochim. Biophys. Acta - Protein Struct. Mol. Enzymol.*, vol. 911, no. 3, pp. 341–348, Feb. 1987.

[4] L. Zhang, *Heme Biology : the Secret Life of Heme in Regulating Diverse Biological Processes*. 2011.

[5] K. E. Anderson, S. Sassa, D. F. Bishop, and R. J. Desnick, "Chapter 124: Disorders of Heme Biosynthesis : X-Linked Sideroblastic Anemia and the Porphyrias," *The Online Metabolic and Molecular Bases of Inherited Disease*, 2014. .

[6] A. A. Khan and J. G. Quigley, "Control of intracellular heme levels: Heme transporters and heme oxygenases," *Biochim. Biophys. Acta - Mol. Cell Res.*, vol. 1813, no. 5, pp. 668–682, May 2011.

[7] P. Lunetti *et al.*, "Characterization of Human and Yeast Mitochondrial Glycine Carriers with Implications for Heme Biosynthesis and Anemia.," *J. Biol. Chem.*, vol. 291, no. 38, pp. 19746–59, Sep. 2016.

[8] F. Palmieri, "The mitochondrial transporter family SLC25: Identification, properties and physiopathology," *Molecular Aspects of Medicine*. 2013.

[9] D. L. Guernsey *et al.*, "Mutations in mitochondrial carrier family gene SLC25A38 cause nonsyndromic autosomal recessive congenital sideroblastic anemia," *Nat. Genet.*, 2009.

[10] R. S. Ajioka, J. D. Phillips, and J. P. Kushner, "Biosynthesis of heme in mammals," *Biochim. Biophys. Acta - Mol. Cell Res.*, vol. 1763, no. 7, pp. 723–736, Jul. 2006.

[11] S. Taketani, H. Kohno, T. Furukawa, and R. Tokunaga, "Involvement of peripheral-type benzodiazepine receptors in the intracellular transport of heme and porphyrins," *J. Biochem.*, 1995.

[12] P. Casellas, S. Galiegue, and A. S. Basile, "Peripheral benzodiazepine receptors and mitochondrial function," *Neurochem. Int.*, 2002.

[13] S. R. Karr and H. A. Dailey, " The synthesis of murine ferrochelatase in vitro and in vivo ," *Biochem. J.*, 2015.

[14] S. Taketani, Y. Adachi, and Y. Nakahashi, "Regulation of the expression of human ferrochelatase by intracellular iron levels," *Eur. J. Biochem.*, 2000.

[15] C. H. Flowers, B. S. Skikne, A. M. Covell, and J. D. Cook, "The clinical measurement of serum transferrin receptor," *J Lab Clin Med*, 1989.

[16] M. D. Knutson, "Iron transport proteins: Gateways of cellular and systemic iron

homeostasis.," *J. Biol. Chem.*, vol. 292, no. 31, pp. 12735–12743, Aug. 2017.

[17] R. S. Ohgami *et al.*, "Identification of a ferrireductase required for efficient transferrin-dependent iron uptake in erythroid cells," *Nat. Genet.*, 2005.

[18] M. Tabuchi, T. Yoshimori, K. Yamaguchi, T. Yoshida, and F. Kishi, "Human NRAMP2/DMT1, Which Mediates Iron Transport across Endosomal Membranes, Is Localized to Late Endosomes and Lysosomes in HEp-2 Cells," *J. Biol. Chem.*, vol. 275, no. 29, pp. 22220–22228, Jul. 2000.

[19] G. C. Shaw *et al.*, "Mitoferrin is essential for erythroid iron assimilation," *Nature*, 2006.

[20] P. N. Paradkar, K. B. Zumbrennen, B. H. Paw, D. M. Ward, and J. Kaplan, "Regulation of Mitochondrial Iron Import through Differential Turnover of Mitoferrin 1 and Mitoferrin 2," *Mol. Cell. Biol.*, 2008.

[21] W. Chen, H. A. Dailey, and B. H. Paw, "Ferrochelatase forms an oligomeric complex with mitoferrin-1 and Abcb10 for erythroid heme biosynthesis," *Blood*, 2010.

[22] L. Tang *et al.*, "Human mitochondrial ATP-binding cassette transporter ABCB10 is required for efficient red blood cell development," *Br. J. Haematol.*, vol. 157, no. 1, pp. 151–154, Apr. 2012.

[23] W. Chen *et al.*, "Abcb10 physically interacts with mitoferrin-1 (Slc25a37) to enhance its stability and function in the erythroid mitochondria," *Proc. Natl. Acad. Sci.*, 2009.

[24] D. Chiabrando *et al.*, "The mitochondrial heme exporter FLVCR1b mediates erythroid differentiation," *J. Clin. Invest.*, 2012.

[25] S. B. Keel *et al.*, "A heme export protein is required for red blood cell differentiation and iron homeostasis," *Science (80-.).*, 2008.

[26] M. Knutson and M. Wessling-Resnick, "Iron metabolism in the reticuloendothelial system," *Critical Reviews in Biochemistry and Molecular Biology*. 2003.

[27] A. Smith and W. T. Morgan, "Haem transport to the liver by haemopexin. Receptor-mediated uptake with recycling of the protein," *Biochem. J.*, 2015.

[28] P. R. Sinclair, W. J. Bement, N. Gorman, H. H. Liem, A. W. Wolkoff, and U. Muller-Eberhard, "Effect of serum proteins on haem uptake and metabolism in primary cultures of liver cells," *Biochem. J.*, 2015.

[29] M. Kristiansen *et al.*, "Identification of the haemoglobin scavenger receptor," *Nature*, 2001.

[30] C. A. Schaer, G. Schoedon, A. Imhof, M. O. Kurrer, and D. J. Schaer, "Constitutive endocytosis of CD163 mediates hemoglobin-heme uptake and determines the noninflammatory and protective transcriptional response of macrophages to hemoglobin," *Circ. Res.*, 2006.

[31] D. J. Schaer *et al.*, "CD163 is the macrophage scavenger receptor for native and chemically modified hemoglobins in the absence of haptoglobin," *Blood*, 2006.

[32] A. Etzerodt, M. Kjolby, M. J. Nielsen, M. Maniecki, P. Svendsen, and S. K. Moestrup, "Plasma Clearance of Hemoglobin and Haptoglobin in Mice and Effect of CD163 Gene Targeting Disruption," *Antioxid. Redox Signal.*, 2012.

[33] V. Hvidberg, M. B. Maniecki, C. Jacobsen, P. Højrup, H. J. Møller, and S. K. Moestrup, "Identification of the receptor scavenging hemopexin-heme complexes," *Blood*, 2005.

[34] C. White *et al.*, "HRG1 is essential for heme transport from the phagolysosome of macrophages during erythrophagocytosis," *Cell Metab.*, 2013.

[35] S. Searle *et al.*, "Localisation of Nramp1 in macrophages: modulation with activation and infection.," *J. Cell Sci.*, 1998.

[36] S. Vidal, A. M. Belouchi, M. Cellier, B. Beatty, and P. Gros, "Cloning and characterization of a second human NRAMP gene on chromosome 12q13," *Mamm. Genome*, 1995.

[37] J. Martínez-Barnetche *et al.*, "Cloning and functional characterization of the Anopheles albimanus DMT1/NRAMP homolog: Implications in iron metabolism in mosquitoes," *Insect Biochem. Mol. Biol.*, 2007.

[38] Y. Gottlieb, M. Truman, L. A. Cohen, Y. Leichtmann-Bardoogo, and E. G. Meyron-Holtz, "Endoplasmic reticulum anchored heme-oxygenase 1 faces the cytosol," *Haematologica*, 2012.

[39] S. Immenschuh, V. Vijayan, S. Janciauskiene, and F. Gueler, "Heme as a Target for Therapeutic Interventions.," *Front. Pharmacol.*, vol. 8, p. 146, 2017.

[40] M. D. Maines, "THE HEME OXYGENASE SYSTEM:A Regulator of Second Messenger Gases," *Annu. Rev. Pharmacol. Toxicol.*, vol. 37, no. 1, pp. 517–554, Apr. 1997.

[41] G. Balla *et al.*, "Ferritin: a cytoprotective antioxidant strategem of endothelium.," *J. Biol. Chem.*, vol. 267, no. 25, pp. 18148–53, Sep. 1992.

[42] J. Muñoz-Sánchez and M. E. Chánez-Cárdenas, "A Review on Hemeoxygenase-2: Focus on Cellular Protection and Oxygen Response," *Oxid. Med. Cell. Longev.*, 2014.

[43] R. Zakhary, S. P. Gaine, J. L. Dinerman, M. Ruat, N. A. Flavahan, and S. H. Snyder, "Heme oxygenase 2: endothelial and neuronal localization and role in endothelium-dependent relaxation.," *Proc. Natl. Acad. Sci. U. S. A.*, vol. 93, no. 2, pp. 795–8, Jan. 1996.

[44] P. J. Kemp, "Hemeoxygenase-2 as an O2 sensor in K+ channel-dependent chemotransduction," *Biochem. Biophys. Res. Commun.*, vol. 338, no. 1, pp. 648–652, Dec. 2005.

[45] L. E. Otterbein *et al.*, "Carbon monoxide has anti-inflammatory effects involving the mitogen- activated protein kinase pathway," *Nat. Med.*, 2000.

[46] G. Kikuchi, T. Yoshida, and M. Noguchi, "Heme oxygenase and heme degradation," *Biochemical and Biophysical Research Communications*. 2005.

[47] R. Tenhunen, H. S. Marver, and R. Schmid, "The enzymatic conversion of heme to bilirubin by microsomal heme oxygenase.," *Proc. Natl. Acad. Sci.*, 2006.

[48] F. Zsila, T. Juhász, S. Bősze, K. Horváti, and T. Beke-Somfai, "Hemin and bile pigments are the secondary structure regulators of intrinsically disordered antimicrobial peptides," *Chirality*, vol. 30, no. 2, pp. 195–205, Feb. 2017.

[49] M. Miksanova *et al.*, "Characterization of heme-regulated eIF2α kinase: Roles of the N-terminal domain in the oligomeric state, heme binding, catalysis, and inhibition,"

Biochemistry, 2006.

[50] J. F. Clark, M. Reilly, and F. R. Sharp, "Oxidation of bilirubin produces compounds that cause prolonged vasospasm of rat cerebral vessels: A contributor to subarachnoid hemorrhage-induced vasospasm," *J. Cereb. Blood Flow Metab.*, vol. 22, no. 4, pp. 472–478, 2002.

[51] G. J. Pyne-Geithman *et al.*, "Bilirubin production and oxidation in CSF of patients with cerebral vasospasm after subarachnoid hemorrhage," *J. Cereb. Blood Flow Metab.*, 2005.

[52] M. Ritter, S. Neupane, R. A. Seidel, C. Steinbeck, and G. Pohnert, "In vivo and in vitro identification of Z-BOX C - a new bilirubin oxidation end product.," *Org. Biomol. Chem.*, vol. 16, no. 19, pp. 3553–3555, 2018.

[53] M. A. Lyons *et al.*, "Increase of metabolic activity and disruption of normal contractile protein distribution by bilirubin oxidation products in vascular smooth-muscle cells," *J. Neurosurg.*, 2009.

[54] S. Hou, R. Xu, J. F. Clark, W. L. Wurster, S. H. Heinemann, and T. Hoshi, "Bilirubin Oxidation End Products Directly Alter K^+ Channels Important in the Regulation of Vascular Tone," *J. Cereb. Blood Flow Metab.*, vol. 31, no. 1, pp. 102–112, Jan. 2011.

[55] P. Sabanci *et al.*, "Effect of Visible Light on Vasospasticity of Post–Subarachnoid Hemorrhage Cerebrospinal Fluid," *J. Neurol. Surg. Part A Cent. Eur. Neurosurg.*, vol. 78, no. 06, pp. 548–555, Nov. 2017.

[56] J. T. Lathrop and M. P. Timko, "Regulation by heme of mitochondrial protein transport through a conserved amino acid motif.," *Science*, vol. 259, no. 5094, pp. 522–5, Jan. 1993.

[57] T. Li, H. L. Bonkovsky, and J. T. Guo, "Structural analysis of heme proteins: Implication for design and prediction," in *2010 IEEE International Conference on Bioinformatics and Biomedicine Workshops, BIBMW 2010*, 2010.

[58] S. Schneider, J. Marles-Wright, K. H. Sharp, and M. Paoli, "Diversity and conservation of interactions for binding heme in b-type heme proteins," *Natural Product Reports*. 2007.

[59] M. Yamamoto, N. Hayashi, and G. Kikuchi, "Translational inhibition by heme of the synthesis of hepatic delta-aminolevulinate synthase in a cell-free system.," *Biochem. Biophys. Res. Commun.*, vol. 115, no. 1, pp. 225–31, Aug. 1983.

[60] S. Hira, T. Tomita, T. Matsui, K. Igarashi, and M. Ikeda-Saito, *Bach1, a heme-dependent transcription factor, reveals presence of multiple heme binding sites with distinct coordination structure*, vol. 59, no. 8. 2007, pp. 542–551.

[61] J. Sun *et al.*, "Hemoprotein Bach1 regulates enhancer availability of heme oxygenase-1 gene.," *EMBO J.*, vol. 21, no. 19, pp. 5216–24, Oct. 2002.

[62] K. Furuyama, K. Kaneko, and P. D. Vargas V., "Heme as a Magnificent Molecule with Multiple Missions: Heme Determines Its Own Fate and Governs Cellular Homeostasis," *Tohoku J. Exp. Med.*, vol. 213, no. 1, pp. 1–16, Sep. 2007.

[63] W. K. McCoubrey, T. J. Huang, and M. D. Maines, "Heme oxygenase-2 is a hemoprotein and binds heme through heme regulatory motifs that are not involved in heme catalysis," *J. Biol. Chem.*, vol. 272, no. 19, pp. 12568–12574, May 1997.

[64] H. Ishikawa *et al.*, "Involvement of heme regulatory motif in heme-mediated ubiquitination and degradation of IRP2," *Mol. Cell*, 2005.

[65] L. S. Goessling, D. P. Mascotti, and R. E. Thach, "Involvement of heme in the degradation of iron-regulatory protein 2," *J. Biol. Chem.*, 1998.

[66] X. D. Tang, R. Xu, M. F. Reynolds, M. L. Garcia, S. H. Heinemann, and T. Hoshi, "Haem can bind to and inhibit mammalian calcium-dependent Slo1 BK channels," *Nature*, 2003.

[67] N. Sahoo *et al.*, "Heme impairs the ball-and-chain inactivation of potassium channels," *Proc. Natl. Acad. Sci.*, 2013.

[68] M. J. Burton *et al.*, "A heme-binding domain controls regulation of ATP-dependent potassium channels," *Proc. Natl. Acad. Sci.*, 2016.

[69] S. Raghuram *et al.*, "Identification of heme as the ligand for the orphan nuclear receptors REV-ERBα and REV-ERBβ," *Nat. Struct. Mol. Biol.*, 2007.

[70] J. Yang *et al.*, "A Novel Heme-Regulatory Motif Mediates Heme-Dependent Degradation of the Circadian Factor Period 2," *Mol. Cell. Biol.*, 2008.

[71] M. V. Airola, J. Du, J. H. Dawson, and B. R. Crane, "Heme binding to the mammalian circadian clock protein period 2 is nonspecific," *Biochemistry*, 2010.

[72] M. Faller, M. Matsunaga, S. Yin, J. A. Loo, and F. Guo, "Heme is involved in microRNA processing," *Nat. Struct. Mol. Biol.*, vol. 14, no. 1, pp. 23–29, Jan. 2007.

[73] J. Shen *et al.*, "Iron metabolism regulates p53 signaling through direct Heme-p53 interaction and modulation of p53 localization, stability, and function," *Cell Rep.*, 2014.

[74] E. Y. Hayden, P. Kaur, T. L. Williams, H. Matsui, S. R. Yeh, and D. L. Rousseau, "Heme Stabilization of α-Synuclein Oligomers during Amyloid Fibril Formation," *Biochemistry*, 2015.

[75] D. Howlett, P. Cutler, S. Heales, and P. Camilleri, "Hemin and related porphyrins inhibit β-amyloid aggregation," *FEBS Lett.*, 1997.

[76] H. Atamna, "Heme binding to Amyloid-β peptide: Mechanistic role in Alzheimer's disease," *Journal of Alzheimer's Disease*. 2006.

[77] H. Atamna and K. Boyle, "Amyloid-beta peptide binds with heme to form a peroxidase: Relationship to the cytopathologies of Alzheimer's disease," *Proc. Natl. Acad. Sci.*, 2006.

[78] J. A. Westberg, J. Jiang, and L. C. Andersson, "Stanniocalcin 1 binds hemin through a partially conserved heme regulatory motif," *Biochem. Biophys. Res. Commun.*, 2011.

[79] J. Jiang, J. A. Westberg, and L. C. Andersson, "Stanniocalcin 2, forms a complex with heme oxygenase 1, binds hemin and is a heat shock protein," *Biochem. Biophys. Res. Commun.*, 2012.

[80] A. Kumar *et al.*, "Heme interaction of the intrinsically disordered N-terminal peptide segment of human cystathionine-β-synthase," *Sci. Rep.*, 2018.

[81] X. Yao, P. Balamurugan, A. Arvey, C. Leslie, and L. Zhang, "Heme controls the regulation of protein tyrosine kinases Jak2 and Src.," *Biochem. Biophys. Res. Commun.*, vol. 403, no. 1, pp.

30–5, Dec. 2010.

[82] X. Yao, P. Balamurugan, A. Arvey, C. Leslie, and L. Zhang, "Heme controls the regulation of protein tyrosine kinases Jak2 and Src," *Biochem. Biophys. Res. Commun.*, vol. 403, no. 1, pp. 30–35, Dec. 2010.

[83] R. Pancsa and P. Tompa, "Structural disorder in eukaryotes.," *PLoS One*, vol. 7, no. 4, p. e34687, 2012.

[84] P. Tompa, "Intrinsically disordered proteins: a 10-year recap," *Trends Biochem. Sci.*, vol. 37, no. 12, pp. 509–516, Dec. 2012.

[85] P. Radivojac, L. M. Iakoucheva, C. J. Oldfield, Z. Obradovic, V. N. Uversky, and A. K. Dunker, "Intrinsic Disorder and Functional Proteomics," *Biophys. J.*, vol. 92, no. 5, pp. 1439–1456, Mar. 2007.

[86] J. C. Hansen, X. Lu, E. D. Ross, and R. W. Woody, "Intrinsic Protein Disorder, Amino Acid Composition, and Histone Terminal Domains," *J. Biol. Chem.*, vol. 281, no. 4, pp. 1853–1856, Jan. 2006.

[87] P. Tompa, *Structure and function of intrinsically disordered proteins*. 2009.

[88] L. M. Iakoucheva, C. J. Brown, J. D. Lawson, Z. Obradović, and A. K. Dunker, "Intrinsic Disorder in Cell-signaling and Cancer-associated Proteins," *J. Mol. Biol.*, vol. 323, no. 3, pp. 573–584, Oct. 2002.

[89] A. Campen, R. M. Williams, C. J. Brown, J. Meng, V. N. Uversky, and A. K. Dunker, "TOP-IDP-scale: a new amino acid scale measuring propensity for intrinsic disorder.," *Protein Pept. Lett.*, vol. 15, no. 9, pp. 956–63, 2008.

[90] H. J. Dyson and P. E. Wright, "Coupling of folding and binding for unstructured proteins.," *Curr. Opin. Struct. Biol.*, vol. 12, no. 1, pp. 54–60, Feb. 2002.

[91] G. T. Heller, F. A. Aprile, and M. Vendruscolo, "Methods of probing the interactions between small molecules and disordered proteins.," *Cell. Mol. Life Sci.*, vol. 74, no. 17, pp. 3225–3243, 2017.

[92] M. Yamamoto, N. Hayashi, and G. Kikuchi, "Evidence for the transcriptional inhibition by heme of the synthesis of δ-aminolevulinate synthase in rat liver," *Biochem. Biophys. Res. Commun.*, 1982.

[93] N. Hayashi, M. Terasawa, and G. Kikuchi, "Immunochemical studies of the turnover of delta-aminolevulinate synthase in rat liver mitochondria and the effect of hemin on it.," *J. Biochem.*, vol. 88, no. 4, pp. 921–6, Oct. 1980.

[94] H. Munakata *et al.*, "Role of the heme regulatory motif in the heme-mediated inhibition of mitochondrial import of 5-aminolevulinate synthase," *J. Biochem.*, 2004.

[95] N. Wang, S. Gottesman, M. C. Willingham, M. M. Gottesman, and M. R. Maurizi, "A human mitochondrial ATP-dependent protease that is highly homologous to bacterial Lon protease.," *Proc. Natl. Acad. Sci.*, 2006.

[96] S. G. Kang *et al.*, "Functional proteolytic complexes of the human mitochondrial ATP-dependent protease, hClpXP," *J. Biol. Chem.*, 2002.

[97] Y. Kubota, K. Nomura, Y. Katoh, R. Yamashita, K. Kaneko, and K. Furuyama, "Novel mechanisms for heme-dependent degradation of ALAS1 protein as a component of negative feedback regulation of heme biosynthesis," *J. Biol. Chem.*, 2016.

[98] Q. Tian, T. Li, W. Hou, J. Zheng, L. W. Schrum, and H. L. Bonkovsky, "Lon peptidase 1 (LONP1)-dependent breakdown of mitochondrial 5-aminolevulinic acid synthase protein by heme in human liver cells.," *J. Biol. Chem.*, vol. 286, no. 30, pp. 26424–30, Jul. 2011.

[99] T. Kitamuro *et al.*, "Bach1 Functions as a Hypoxia-inducible Repressor for the Heme Oxygenase-1 Gene in Human Cells," *J. Biol. Chem.*, vol. 278, no. 11, pp. 9125–9133, Mar. 2003.

[100] S. M. Mense and L. Zhang, "Heme: a versatile signaling molecule controlling the activities of diverse regulators ranging from transcription factors to MAP kinases," *Cell Res.*, vol. 16, no. 8, pp. 681–692, Aug. 2006.

[101] K. Ogawa *et al.*, "Heme mediates derepression of Maf recognition element through direct binding to transcription repressor Bach1," *EMBO J.*, 2001.

[102] H. Suzuki *et al.*, "Heme regulates gene expression by triggering Crm1-dependent nuclear export of Bach1," *EMBO J.*, 2004.

[103] H. Suzuki, S. Tashiro, J. Sun, H. Doi, S. Satomi, and K. Igarashi, "Cadmium induces nuclear export of Bach1, a transcriptional repressor of heme oxygenase-1 gene.," *J. Biol. Chem.*, 2003.

[104] M. Watanabe-Matsui *et al.*, "Heme regulates B-cell differentiation, antibody class switch, and heme oxygenase-1 expression in B cells as a ligand of Bach2," *Blood*, 2011.

[105] K. Igarashi and M. Watanabe-Matsui, "Wearing Red for Signaling: The Heme-Bach Axis in Heme Metabolism, Oxidative Stress Response and Iron Immunology," *Tohoku J. Exp. Med.*, vol. 232, no. 4, pp. 229–253, 2014.

[106] J. D. Dimitrov *et al.*, "Antibodies use heme as a cofactor 1 ANTIBODIES USE HEME AS A COFACTOR TO EXTEND THEIR PATHOGEN ELIMINATION ACTIVITY AND TO ACQUIRE NEW EFFECTOR FUNCTIONS *," 2007.

[107] S. J. Parsons and J. T. Parsons, "Src family kinases, key regulators of signal transduction," *Oncogene*, vol. 23, no. 48, pp. 7906–7909, Oct. 2004.

[108] R. Roskoski, "Src protein–tyrosine kinase structure and regulation," *Biochem. Biophys. Res. Commun.*, vol. 324, no. 4, pp. 1155–1164, Nov. 2004.

[109] R. Roskoski, "Src protein-tyrosine kinase structure, mechanism, and small molecule inhibitors," *Pharmacol. Res.*, vol. 94, pp. 9–25, Apr. 2015.

[110] M. Guarino, *Src signaling in cancer invasion*, vol. 223, no. 1. p. n/a-n/a.

[111] K. Fizazi, "The role of Src in prostate cancer," *Annals of Oncology*. 2007.

[112] R. J. Salmond, A. Filby, I. Qureshi, S. Caserta, and R. Zamoyska, "T-cell receptor proximal signaling via the Src-family kinases, Lck and Fyn, influences T-cell activation, differentiation, and tolerance," *Immunol. Rev.*, 2009.

[113] B. Seliger, C. Massa, B. Rini, J. Ko, and J. Finke, "Antitumour and immune-adjuvant activities of protein-tyrosine kinase inhibitors," *Trends in Molecular Medicine*. 2010.

[114] S. Li, "Src kinase signaling in leukaemia.," *Int. J. Biochem. Cell Biol.*, vol. 39, no. 7–8, pp. 1483–8, 2007.

[115] T. J. Boggon and M. J. Eck, "Structure and regulation of Src family kinases," *Oncogene*. 2004.

[116] J. Araujo and C. Logothetis, "Targeting Src signaling in metastatic bone disease," *Int. J. Cancer*, 2009.

[117] V. G. Brunton and M. C. Frame, "Src and focal adhesion kinase as therapeutic targets in cancer," *Current Opinion in Pharmacology*. 2008.

[118] J. A. Cooper and H. Qian, "A mechanism for Src kinase-dependent signaling by noncatalytic receptors," *Biochemistry*, 2008.

[119] J. de Groot and V. Milano, "Improving the prognosis for patients with glioblastoma: The rationale for targeting Src," *Journal of Neuro-Oncology*. 2009.

[120] R. S. Finn, "Targeting Src in breast cancer," *Annals of Oncology*. 2008.

[121] E. Ingley, "Src family kinases: Regulation of their activities, levels and identification of new pathways," *Biochimica et Biophysica Acta - Proteins and Proteomics*. 2008.

[122] J. M. Bradshaw, "The Src, Syk, and Tec family kinases: Distinct types of molecular switches," *Cellular Signalling*. 2010.

[123] C. H. M. Jamieson *et al.*, "The JAK2 V617F mutation occurs in hematopoietic stem cells in polycythemia vera and predisposes toward erythroid differentiation," *Proc. Natl. Acad. Sci.*, 2006.

[124] N. Kröger *et al.*, "Monitoring of the JAK2-V617F mutation by highly sensitive quantitative real-time PCR after allogeneic stem cell transplantation in patients with myelofibrosis," *Blood*, 2007.

[125] R. Zhao *et al.*, "Identification of an acquired JAK2 mutation in polycythemia vera," *J. Biol. Chem.*, 2005.

[126] Z. Li, S. Xing, S. Wang, W. T. Ho, and Z. J. Zhao, "Characterization of a Highly effective protein substrate for analysis of JAK2V617F Activity," *Exp. Hematol.*, 2007.

[127] Z. Li *et al.*, "Erlotinib effectively inhibits JAK2V617F activity and polycythemia vera cell growth," *J. Biol. Chem.*, 2007.

[128] P. Mossuz *et al.*, "Proteomic study of the impact of the JAK2–V617F mutation on the phenotype of essential thrombocythemia," *Exp. Hematol.*, vol. 36, no. 12, pp. 1642–1647, Dec. 2008.

[129] R. J. Olsen, C. H. Dunphy, D. P. O'Malley, L. Rice, A. A. Ewton, and C. C. Chang, "The implication of identifying JAK2V617F in myeloproliferative neoplasms and myelodysplastic syndromes with bone marrow fibrosis," *J. Hematop.*, 2008.

[130] D. M. Williams, A. H. Kim, O. Rogers, J. L. Spivak, and A. R. Moliterno, "Phenotypic variations and new mutations in JAK2 V617F-negative polycythemia vera, erythrocytosis, and idiopathic myelofibrosis," *Exp. Hematol.*, 2007.

[131] S. Xing *et al.*, "Transgenic expression of JAK2 V617F causes myeloproliferative disorders in

mice," *Blood*, 2008.

[132] X. Xu *et al.*, "JAK2V617F: Prevalence in a large Chinese hospital population," *Blood*, 2007.

[133] R. Zhao, X. Fu, L. Teng, Q. Li, and Z. J. Zhao, "Blocking the Function of Tyrosine Phosphatase SHP-2 by Targeting Its Src Homology 2 Domains," *J. Biol. Chem.*, vol. 278, no. 44, pp. 42893–42898, Oct. 2003.

[134] E. W. Miles and J. P. Kraus, "Cystathionine β-Synthase: Structure, Function, Regulation, and Location of Homocystinuria-causing Mutations," *J. Biol. Chem.*, vol. 279, no. 29, pp. 29871–29874, Jul. 2004.

[135] R. Banerjee and C. Zou, "Redox regulation and reaction mechanism of human cystathionine-β-synthase: a PLP-dependent hemesensor protein," *Arch. Biochem. Biophys.*, vol. 433, no. 1, pp. 144–156, Jan. 2005.

[136] M. R. Hellmich, C. Coletta, C. Chao, and C. Szabo, "The Therapeutic Potential of Cystathionine β-Synthetase/Hydrogen Sulfide Inhibition in Cancer," *Antioxid. Redox Signal.*, vol. 22, no. 5, pp. 424–448, Feb. 2015.

[137] B. L. Predmore, D. J. Lefer, and G. Gojon, "Hydrogen Sulfide in Biochemistry and Medicine," *Antioxid. Redox Signal.*, 2012.

[138] D. A. Dickinson and H. J. Forman, "Glutathione in defense and signaling: lessons from a small thiol.," *Ann. N. Y. Acad. Sci.*, vol. 973, pp. 488–504, Nov. 2002.

[139] N. A. J. Carson, D. C. Cusworth, C. E. Dent, C. M. B. Field, D. W. Neill, and R. G. Westall, "Homocystinuria: A new inborn error of Metabolism associated with Mental Deficiency," *Arch. Dis. Child.*, vol. 38, no. 201, pp. 425–436, Oct. 1963.

[140] S. P. Stabler, J. Lindenbaum, D. G. Savage, and R. H. Allen, "Elevation of serum cystathionine levels in patients with cobalamin and folate deficiency.," *Blood*, 1993.

[141] S. Harvey Mudd; Harvey L. Levy; Jan P. Kraus, "Disorders of Transsulfuration | The Online Metabolic and Molecular Bases of Inherited Disease | OMMBID | McGraw-Hill Medical," 2001. [Online]. Available: https://ommbid.mhmedical.com/content.aspx?bookid=971&sectionid=62675596&jumpsectionid=62675603. [Accessed: 09-May-2019].

[142] V. Kery, G. Bukovska, and J. P. Kraus, "Transsulfuration depends on heme in addition to pyridoxal 5???-phosphate: Cystathionine ??-synthase is a heme protein," *J. Biol. Chem.*, 1994.

[143] ‡ Vladimir Kery, ‡ Loelle Poneleit, § Jeffrey D. Meyer, § and Mark C. Manning, and ‡ Jan P. Kraus, "Binding of Pyridoxal 5'-Phosphate to the Heme Protein Human Cystathionine β-Synthase†," 1999.

[144] A. L. Pey, T. Majtan, J. M. Sanchez-Ruiz, and J. P. Kraus, "Human cystathionine β-synthase (CBS) contains two classes of binding sites for *S* -adenosylmethionine (SAM): complex regulation of CBS activity and stability by SAM," *Biochem. J.*, vol. 449, no. 1, pp. 109–121, Jan. 2013.

[145] J. Ereño-Orbea, T. Majtan, I. Oyenarte, J. P. Kraus, and L. A. Martínez-Cruz, "Structural insight into the molecular mechanism of allosteric activation of human cystathionine β-synthase by *S* -adenosylmethionine," *Proc. Natl. Acad. Sci.*, vol. 111, no. 37, pp. E3845–E3852, Sep. 2014.

[146] R. Banerjee, R. Evande, O. Kabil, S. Ojha, and S. Taoka, "Reaction mechanism and regulation of cystathionine beta-synthase.," *Biochim. Biophys. Acta*, vol. 1647, no. 1–2, pp. 30–5, Apr. 2003.

[147] T. Majtan, L. R. Singh, L. Wang, W. D. Kruger, and J. P. Kraus, "Active cystathionine beta-synthase can be expressed in heme-free systems in the presence of metal-substituted porphyrins or a chemical chaperone.," *J. Biol. Chem.*, vol. 283, no. 50, pp. 34588–95, Dec. 2008.

[148] S. Ojha, J. Wu, R. LoBrutto, and R. Banerjee, "Effects of heme ligand mutations including a pathogenic variant, H65R, on the properties of human cystathionine β-synthase," *Biochemistry*, 2002.

[149] J. Oliveriusová, V. Kery, K. N. Maclean, and J. P. Kraus, "Deletion Mutagenesis of Human Cystathionine β-Synthase," *J. Biol. Chem.*, vol. 277, no. 50, pp. 48386–48394, Dec. 2002.

[150] H. H. Brewitz *et al.*, "Heme interacts with histidine- and tyrosine-based protein motifs and inhibits enzymatic activity of chloramphenicol acetyltransferase from Escherichia coli," *Biochim. Biophys. Acta - Gen. Subj.*, vol. 1860, no. 6, pp. 1343–1353, Jun. 2016.

[151] T. Kühl *et al.*, "Analysis of Fe(III) Heme Binding to Cysteine-Containing Heme-Regulatory Motifs in Proteins," *ACS Chem. Biol.*, vol. 8, no. 8, pp. 1785–1793, Aug. 2013.

[152] J. Nováček, L. Žídek, and V. Sklenář, "Toward optimal-resolution NMR of intrinsically disordered proteins," *J. Magn. Reson.*, vol. 241, pp. 41–52, Apr. 2014.

[153] W. Bermel, M. Bruix, I. C. Felli, V. Kumar M. V., R. Pierattelli, and S. Serrano, "Improving the chemical shift dispersion of multidimensional NMR spectra of intrinsically disordered proteins," *J. Biomol. NMR*, vol. 55, no. 3, pp. 231–237, Mar. 2013.

[154] J. E. Sims and D. E. Smith, "The IL-1 family: regulators of immunity," *Nat. Rev. Immunol.*, vol. 10, no. 2, pp. 89–102, Feb. 2010.

[155] C. Dinarello *et al.*, "IL-1 family nomenclature," *Nat. Immunol.*, 2010.

[156] J. E. Sims *et al.*, "A new nomenclature for IL-1-family genes," *Trends in Immunology*. 2001.

[157] E. Y. Bassoy, J. E. Towne, and C. Gabay, "Regulation and function of interleukin-36 cytokines," *Immunol. Rev.*, vol. 281, no. 1, pp. 169–178, Jan. 2018.

[158] A. Torales-Cardeña *et al.*, "Cross Talk between Proliferative, Angiogenic, and Cellular Mechanisms Orchestred by HIF-1 α in Psoriasis," *Mediators Inflamm.*, vol. 2015, pp. 1–11, 2015.

[159] J. E. Towne, K. E. Garka, B. R. Renshaw, G. D. Virca, and J. E. Sims, "Interleukin (IL)-1F6, IL-1F8, and IL-1F9 Signal through IL-1Rrp2 and IL-1RAcP to Activate the Pathway Leading to NF-κB and MAPKs," *J. Biol. Chem.*, vol. 279, no. 14, pp. 13677–13688, Apr. 2004.

[160] D. E. Smith, B. R. Renshaw, R. R. Ketchem, M. Kubin, K. E. Garka, and J. E. Sims, "Four New Members Expand the Interleukin-1 Superfamily," *J. Biol. Chem.*, vol. 275, no. 2, pp. 1169–1175, Jan. 2000.

[161] J. E. Towne *et al.*, "Interleukin-36 (IL-36) Ligands Require Processing for Full Agonist (IL-36α, IL-36β, and IL-36γ) or Antagonist (IL-36Ra) Activity," *J. Biol. Chem.*, vol. 286, no. 49, pp. 42594–42602, Dec. 2011.

[162] C. M. Henry, G. P. Sullivan, D. M. Clancy, I. S. Afonina, D. Kulms, and S. J. Martin, "Neutrophil-Derived Proteases Escalate Inflammation through Activation of IL-36 Family Cytokines," *Cell Rep.*, 2016.

[163] R. Debets *et al.*, "Two novel IL-1 family members, IL-1 delta and IL-1 epsilon, function as an antagonist and agonist of NF-kappa B activation through the orphan IL-1 receptor-related protein 2.," *J. Immunol.*, vol. 167, no. 3, pp. 1440–6, Aug. 2001.

[164] A. Menter *et al.*, "Guidelines of care for the management of psoriasis and psoriatic arthritis," *J. Am. Acad. Dermatol.*, vol. 58, no. 5, pp. 826–850, May 2008.

[165] J. M. Murrieta-Coxca, S. Rodríguez-Martínez, M. E. Cancino-Diaz, U. R. Markert, R. R. Favaro, and D. M. Morales-Prieto, "IL-36 Cytokines: Regulators of Inflammatory Responses and Their Emerging Role in Immunology of Reproduction.," *Int. J. Mol. Sci.*, vol. 20, no. 7, Apr. 2019.

[166] S. Vigne *et al.*, "IL-36R ligands are potent regulators of dendritic and T cells," *Blood*, 2011.

[167] R. T. Chustz *et al.*, "Regulation and function of the IL-1 family cytokine IL-1F9 in human bronchial epithelial cells," *Am. J. Respir. Cell Mol. Biol.*, 2011.

[168] X. Wang *et al.*, "IL-36γ Transforms the Tumor Microenvironment and Promotes Type 1 Lymphocyte-Mediated Antitumor Immune Responses," *Cancer Cell*, 2015.

[169] C. Wiedemann, P. Bellstedt, and M. Görlach, "CAPITO - A web server-based analysis and plotting tool for circular dichroism data," *Bioinformatics*, 2013.

[170] A. Micsonai *et al.*, "BeStSel: A web server for accurate protein secondary structure prediction and fold recognition from the circular dichroism spectra," *Nucleic Acids Res.*, 2018.

[171] W. F. Vranken *et al.*, "The CCPN data model for NMR spectroscopy: development of a software pipeline.," *Proteins*, vol. 59, no. 4, pp. 687–96, Jun. 2005.

[172] T. Herrmann, P. Güntert, and K. Wüthrich, "Protein NMR structure determination with automated NOE assignment using the new software CANDID and the torsion angle dynamics algorithm DYANA.," *J. Mol. Biol.*, vol. 319, no. 1, pp. 209–27, May 2002.

[173] P. Güntert, C. Mumenthaler, and K. Wüthrich, "Torsion angle dynamics for NMR structure calculation with the new program Dyana," *J. Mol. Biol.*, vol. 273, no. 1, pp. 283–298, Oct. 1997.

[174] P. Luginbühl, P. Güntert, M. Billeter, and K. Wüthrich, "The new program OPAL for molecular dynamics simulations and energy refinements of biological macromolecules," *J. Biomol. NMR*, vol. 8, no. 2, pp. 136–146, Sep. 1996.

[175] A. G. Murzin, A. M. Lesk, and C. Chothia, "beta-Trefoil fold. Patterns of structure and sequence in the Kunitz inhibitors interleukins-1 beta and 1 alpha and fibroblast growth factors.," *J. Mol. Biol.*, vol. 223, no. 2, pp. 531–43, Jan. 1992.

[176] S. Günther and E. J. Sundberg, "Molecular Determinants of Agonist and Antagonist Signaling through the IL-36 Receptor," *J. Immunol.*, vol. 193, no. 2, pp. 921–930, Jul. 2014.

[177] B. J. Goodfellow, J. S. Dias, G. C. Ferreira, P. Henklein, V. Wray, and A. L. Macedo, "The solution structure and heme binding of the presequence of murine 5-aminolevulinate

synthase.," *FEBS Lett.*, vol. 505, no. 2, pp. 325–31, Sep. 2001.

[178] T. G. Spiro, "Resonance Raman Spectroscopy as a Probe of Heme Protein Structure and Dynamics," *Adv. Protein Chem.*, 1985.

[179] M. Abe, T. Kitagawa, and Y. Kyogoku, "Resonance Raman spectra of octaethylporphyrinato-Ni(II) and meso-deuterated and 15N substituted derivatives. II. A normal coordinate analysis," *J. Chem. Phys.*, 1978.

[180] G. M. Giacometti, G., Giacometti, "IOS Press," 2001, p. 296.

[181] H. H. Brewitz *et al.*, "Role of the Chemical Environment beyond the Coordination Site: Structural Insight into FeIII Protoporphyrin Binding to Cysteine-Based Heme-Regulatory Protein Motifs," *ChemBioChem*, 2015.

[182] H. Refsum, P. M. Ueland, O. Nygård, and S. E. Vollset, "HOMOCYSTEINE AND CARDIOVASCULAR DISEASE," 1998.

[183] R. Clarke, A. D. Smith, K. A. Jobst, H. Refsum, L. Sutton, and P. M. Ueland, "Folate, vitamin B12, and serum total homocysteine levels in confirmed Alzheimer disease," *Arch. Neurol.*, 1998.

[184] J. L. Mills *et al.*, "Homocysteine metabolism in pregnancies complicated by neural-tube defects.," *Lancet (London, England)*, vol. 345, no. 8943, pp. 149–51, Jan. 1995.

[185] S. P. Graether, "Troubleshooting Guide to Expressing Intrinsically Disordered Proteins for Use in NMR Experiments.," *Front. Mol. Biosci.*, vol. 5, p. 118, 2018.

[186] P. Tsvetkov, N. Reuven, C. Prives, and Y. Shaul, "Susceptibility of p53 Unstructured N Terminus to 20 S Proteasomal Degradation Programs the Stress Response," *J. Biol. Chem.*, vol. 284, no. 39, pp. 26234–26242, Sep. 2009.

[187] S. Prakash, L. Tian, K. S. Ratliff, R. E. Lehotzky, and A. Matouschek, "An unstructured initiation site is required for efficient proteasome-mediated degradation," *Nat. Struct. Mol. Biol.*, vol. 11, no. 9, pp. 830–837, Sep. 2004.

[188] P. Zhou and G. Wagner, "Overcoming the solubility limit with solubility-enhancement tags: Successful applications in biomolecular NMR studies," *Journal of Biomolecular NMR*. 2010.

[189] H. Kobayashi *et al.*, "Segmental isotope labeling of proteins for NMR structural study using a protein S tag for higher expression and solubility," *J. Biomol. NMR*, 2012.

[190] I. Bertini, K. S. McGreevy, and G. Parigi, *NMR of Biomolecules: Towards Mechanistic Systems Biology*. 2012.

[191] G. M. Clore, "Seeing the invisible by paramagnetic and diamagnetic NMR," *Biochem. Soc. Trans.*, vol. 41, no. 6, pp. 1343–1354, Dec. 2013.

[192] N. J. Anthis and G. M. Clore, "Visualizing transient dark states by NMR spectroscopy," *Q. Rev. Biophys.*, vol. 48, no. 1, pp. 35–116, Feb. 2015.

[193] T. Madl, I. C. Felli, I. Bertini, and M. Sattler, "Structural Analysis of Protein Interfaces from 13C Direct-Detected Paramagnetic Relaxation Enhancements," 2010.

[194] J. Lopez, R. Schneider, F.-X. Cantrelle, I. Huvent, and G. Lippens, "Studying Intrinsically

Disordered Proteins under True In Vivo Conditions by Combined Cross-Polarization and Carbonyl-Detection NMR Spectroscopy," *Angew. Chemie Int. Ed.*, vol. 55, no. 26, pp. 7418–7422, Jun. 2016.

[195] S. Peherstorfer *et al.*, "Insights into mechanism and functional consequences of heme binding to hemolysin-activating lysine acyltransferase HlyC from Escherichia coli.," *Biochim. Biophys. acta. Gen. Subj.*, vol. 1862, no. 9, pp. 1964–1972, 2018.

[196] C. D. Reiter *et al.*, "Cell-free hemoglobin limits nitric oxide bioavailability in sickle-cell disease," *Nat. Med.*, vol. 8, no. 12, pp. 1383–1389, Dec. 2002.

[197] N. E. Hafsa, D. Arndt, and D. S. Wishart, "CSI 3.0: a web server for identifying secondary and super-secondary structure in proteins using NMR chemical shifts," *Nucleic Acids Res.*, vol. 43, no. W1, pp. W370–W377, Jul. 2015.

[198] D. S. Wishart, B. D. Sykes, and F. M. Richards, "The chemical shift index: a fast and simple method for the assignment of protein secondary structure through NMR spectroscopy," *Biochemistry*, vol. 31, no. 6, pp. 1647–1651, Feb. 1992.

[199] N. Goradia *et al.*, "H, 13 C, and 15 N resonance assignments for the pro-inflammatory cytokine interleukin-36a," *Biomol. NMR Assign.*, vol. 10, pp. 329–333, 2016.

[200] T. Cierpicki, I. Zhukov, R. A. Byrd, and J. Otlewski, "Hydrogen Bonds in Human Ubiquitin Reflected in Temperature Coefficients of Amide Protons," *J. Magn. Reson.*, vol. 157, no. 2, pp. 178–180, Aug. 2002.

[201] T. Cierpicki and J. Otlewski, "Amide proton temperature coefficients as hydrogen bond indicators in proteins," *J. Biomol. NMR*, vol. 21, no. 3, pp. 249–261, 2001.

[202] D. Leys, K. Backers, T. E. Meyer, W. R. Hagen, M. A. Cusanovich, and J. J. Van Beeumen, "Crystal structures of an oxygen-binding cytochrome c from Rhodobacter sphaeroides," *J. Biol. Chem.*, 2000.

[203] H. Youn *et al.*, "The Heme Pocket Afforded by Gly117 Is Crucial for Proper Heme Ligation and Activity of CooA," *J. Biol. Chem.*, 2001.

[204] W. N. Lanzilotta, D. J. Schuller, M. V. Thorsteinsson, R. L. Kerby, G. P. Roberts, and T. L. Poulos, "Structure of the CO sensing transcription activator CooA," *Nat. Struct. Biol.*, 2000.

[205] M. Paoli, J. Marles-Wright, and A. Smith, "Structure–Function Relationships in Heme-Proteins," *DNA Cell Biol.*, 2002.

[206] J. Kopecká, J. Krijt, K. Raková, and V. Kožich, "Restoring assembly and activity of cystathionine β-synthase mutants by ligands and chemical chaperones.," *J. Inherit. Metab. Dis.*, vol. 34, no. 1, pp. 39–48, Feb. 2011.

[207] T. Majtan *et al.*, "Potential Pharmacological Chaperones for Cystathionine Beta-Synthase-Deficient Homocystinuria," in *Handbook of experimental pharmacology*, vol. 245, 2017, pp. 345–383.

[208] T. Majtan, A. L. Pey, J. Ereño-Orbea, L. A. Martínez-Cruz, and J. P. Kraus, "Targeting Cystathionine Beta-Synthase Misfolding in Homocystinuria by Small Ligands: State of the Art and Future Directions.," *Curr. Drug Targets*, vol. 17, no. 13, pp. 1455–70, 2016.

[209] Y. Han, Q. Shang, J. Yao, and Y. Ji, "Hydrogen sulfide: a gaseous signaling molecule

modulates tissue homeostasis: implications in ophthalmic diseases," *Cell Death Dis.*, vol. 10, no. 4, p. 293, Apr. 2019.

[210] Y. Zhang *et al.*, "Hydrogen Sulfide, the Next Potent Preventive and Therapeutic Agent in Aging and Age-Associated Diseases," *Mol. Cell. Biol.*, vol. 33, no. 6, pp. 1104–1113, Mar. 2013.

[211] D. M. Rackham, "Recent applications of quantitative nuclear magnetic resonance spectroscopy in pharmaceutical research," *Talanta*, vol. 23, no. 4, pp. 269–274, Apr. 1976.

[212] W. Jahnke *et al.*, "Binding or Bending: Distinction of Allosteric Abl Kinase Agonists from Antagonists by an NMR-Based Conformational Assay," *J. Am. Chem. Soc.*, vol. 132, no. 20, pp. 7043–7048, May 2010.

[213] L. Kategaya *et al.*, "USP7 small-molecule inhibitors interfere with ubiquitin binding," *Nature*, vol. 550, no. 7677, pp. 534–538, Oct. 2017.

[214] J. R. Pritz *et al.*, "Allosteric sensitization of proapoptotic BAX," *Nat. Chem. Biol.*, vol. 13, no. 9, pp. 961–967, Sep. 2017.

[215] A. A. Wylie *et al.*, "The allosteric inhibitor ABL001 enables dual targeting of BCR–ABL1," *Nature*, vol. 543, no. 7647, pp. 733–737, Mar. 2017.

[216] M. Congreve, R. Carr, C. Murray, and H. Jhoti, "A 'rule of three' for fragment-based lead discovery?," *Drug Discov. Today*, vol. 8, no. 19, pp. 876–7, Oct. 2003.

[217] C. Fernández and W. Jahnke, "New approaches for NMR screening in drug discovery," *Drug Discov. Today Technol.*, vol. 1, no. 3, pp. 277–283, Dec. 2004.

[218] J. R. Abshire, C. J. Rowlands, S. M. Ganesan, P. T. C. So, and J. C. Niles, "Quantification of labile heme in live malaria parasites using a genetically encoded biosensor," 2017.

[219] D. A. Hanna *et al.*, "Heme dynamics and trafficking factors revealed by genetically encoded fluorescent heme sensors.," *Proc. Natl. Acad. Sci. U. S. A.*, vol. 113, no. 27, pp. 7539–44, Jul. 2016.

[220] Y. Song *et al.*, "A Genetically Encoded FRET Sensor for Intracellular Heme," *ACS Chem. Biol.*, vol. 10, no. 7, pp. 1610–1615, Jul. 2015.

[221] S. Takeda, N. Kamiya, and T. Nagamune, "A novel protein-based heme sensor consisting of green fluorescent protein and apocytochrome b(562).," *Anal. Biochem.*, vol. 317, no. 1, pp. 116–9, Jun. 2003.

[222] Z. Gouveia *et al.*, "Characterization of plasma labile heme in hemolytic conditions," *FEBS J.*, vol. 284, no. 19, pp. 3278–3301, Oct. 2017.

[223] R. K. Donegan, C. M. Moore, D. A. Hanna, and A. R. Reddi, "Handling heme: The mechanisms underlying the movement of heme within and between cells," *Free Radic. Biol. Med.*, vol. 133, pp. 88–100, 2019.

[224] J. A. McIntyre, "The appearance and disappearance of antiphospholipid autoantibodies subsequent to oxidation-reduction reactions," in *Thrombosis Research*, 2004.

[225] L. T. Roumenina, J. Rayes, S. Lacroix-Desmazes, and J. D. Dimitrov, "Heme: Modulator of Plasma Systems in Hemolytic Diseases," *Trends Mol. Med.*, vol. 22, no. 3, pp. 200–213, Mar. 2016.

[226] N. Gupta *et al.*, "Neutralization of Japanese Encephalitis Virus by heme-induced broadly reactive human monoclonal antibody," *Sci. Rep.*, vol. 5, no. 1, p. 16248, Dec. 2015.

[227] J. A. McIntyre and and W. P. Faulk, "Autoantibody potential of cancer therapeutic monoclonal antibodies," *Int. J. Cancer*, p. NA-NA, 2010.

8 Declaration of honour

I hereby declare that:

1) I am familiar with the present course of examination for doctoral research studies (Promotionsordnung) at the Faculty of Biological Sciences, Friedrich Schiller University Jena, Germany.
2) I have conducted the research and written the presented dissertation myself. All the collaboration, additional assistance, personal communication and tools have acknowledged in the work.
3) No doctoral consultant assistance has been utilized and no third parties have either directly or indirectly received any monetary benefits from me or with submitted thesis.
4) I have not submitted the dissertation as an examination paper for a state or other academic examination.
5) I have not submitted the same dissertation or similar dissertation to any other university.

Jena, June 24, 2019 ----------

Amit Kumar

9 Acknowledgement

Work joyfully and peacefully, knowing that right thoughts and right efforts inevitably bring about right results. ---- *James Allen*

This thesis brings me to the end of my journey to Ph.D. and I would like to thank all the people who helped me during this adventures journey.

I would like to sincerely acknowledge DFG for providing funding to conduct my research under research group FOR 1738 (OH 86/3-2).

I would like to express my heartfelt gratitude to my supervisor **Dr. Oliver Ohlenschläger** who gave me an opportunity to work under his supervision, guidance on this project. Thanks to your constant support even during some tough times during the project and I owe you a big thanks for familiarizing me to NMR spectroscopy data analysis and finally after three years I feel comfortable with NMR. I would also like thanks for giving me tips and suggestion to travel around in Europe. This project would not have been possible without you and thanks for believing in me.

I would like to specially thanks **Dr. Ramadurai Ramachandran** for my continues support during this journey. Thanks for teaching me how to use NMR spectrometer and designing new NMR pulse sequence for one of my papers. I would also like to thank for those encouraging talks, when we walk from lab to home.

I would like to thank **Dr. Mathias Görlach** for being one of my Ph.D. thesis committee members. I am grateful for his helpful discussion during the meetings and reviewing my thesis. Thanks for being patient with my questions. Danke schön from the peptide bond who has now grown to full structured/IDP protein. 😃

I would like to express my gratitude to **Prof. Stefan Heinemann** for being my university supervisor and one of the members of my Ph.D. committee. Thanks for all the helpful discussions and reviewing my thesis. I remember our HHDP retreat to Dresden when you taught us some presentation skills and they were very helpful to improve my presentation skills. Thanks for the HHDP (FOR1738) consortium and being an inspiration to me.

I would like to say thousands of thanks to **Sabine Häfner** for keeping a friendly, positive environment in the lab and also thanks to **Georg Peiter** for his help in resolving computer problems. Thankful to both of you for teaching me some German. Tausend Dank. 😊

I would like to expand my thanks to **Dr. Andreas Lang, Dr. Peter Bellstedt, Dr. Christoph Wiedemann, Friedike Pielenz** for helping me with NMR data collection and also to **Prof. Diana Imhof** and **Amelie Wißbrock** for the collaboration.

A big thanks to my previous lab members in India who helped me start my scientific career.

My sincere gratitude to **Dr. Claudia Müller** and **Cornelia Meyerrose** for helping me with all the administrative things and settlement in Germany.

Finally, but importantly I thanks to my parents, sister, brother and awesome friends for their encouragement and constant support.

-Amit Kumar